Optical Coherence Tomography for the Assessment of Skin Adaptation to Repetitive Mechanical Stress

Eric C Swanson

A dissertation
submitted in partial fulfillment of the
requirements for the degree of

Doctor of Philosophy

University of Washington
2019

Reading Committee:
Joan E Sanders, Chair
Janna L Friedly
Ruikang K Wang

Program Authorized to Offer Degree:
Bioengineering

University of Washington

Abstract

Optical Coherence Tomography for the Assessment of Skin Adaptation to Repetitive Mechanical Stress

Eric Swanson

Chair of the Supervisory Committee:
Joan Sanders
Bioengineering

Skin breakdown is a problem that affects many individuals with lower limb loss. Breakdown is caused most commonly by repetitive mechanical stresses that are imposed on the residual limb at its interface with the prosthetic socket. Skin can adapt to become more tolerant to these stresses, thus reducing the risk of breakdown, yet little is understood about this phenomenon and no methods exist for objectively determining if skin has become more load tolerant. These factors have limited the ability of clinicians to more fully understand the health of their patients' skin and they have limited the ability of researchers to develop improved rehabilitation strategies and therapeutics to enhance the load tolerance of skin. At the root of these needs is the lack of understanding of how skin adapts to mechanical stress. In order to develop a better understanding, new methods are needed that can safely and accurately probe the cutaneous physiology of individuals with lower limb loss. The objective of this dissertation was to develop noninvasive methods to assess the structure and function of skin and then to determine the utility of the developed tools for the investigation of skin adaptation in individuals with lower limb loss.

In Aim 1, novel noninvasive techniques were developed to measure key structural and functional features of the cutaneous microvasculature that may be involved in skin adaptation. In Aim 2, these tools were introduced to investigate skin adaptation to mechanical stress on eight able-bodied participants who wore a modified below-knee prosthetic socket for two weeks. Study results demonstrated good repeatability of the OCT-based measurement methods with the exception of some features. No statistically significant differences were found in any of the OCT measurements taken at different time points throughout the study or between the test site and a location-matched control site on the contralateral limb. It is believed that the limb skin was not stressed enough to induce adaptation in the participants. In Aim 3, a case study of three participants with unilateral transtibial limb loss was performed to investigate the skin of chronically-stressed regions of the residual limb using the measurement methods developed in Aim 1. Measurements were compared between a highly stressed region of the residual limb and a location-matched site on the intact contralateral limb. Notable differences in functional and structural characteristics of the microvasculature were found between the two limbs for each study participant and between the residual limbs of all study participants. The epidermis was also thicker in the residual limb versus the contralateral limb for all participants, a difference that was statistically significant. Taken together, this thesis introduced new noninvasive methods for investigating skin adaptation in users of lower limb prostheses, highlighted advantages and limitations related to the developed methods, and identified potential biomarkers for skin adaptation that are worth further investigation.

TABLE OF CONTENTS

LIST OF FIGURES

LIST OF TABLES

ABBREVIATIONS

a.u.	Arbitrary Unit(s)
DAQ	Data Acquisition Device
DEJ	Dermal-Epidermal Junction
FSPT	Fitzpatrick Skin Phototype
FSR	Force Sensing Resistor
LDF	Laser Doppler Flowmetry
LDPI	Laser Doppler Perfusion Imaging
LSCI	Laser Speckle Contrast Imaging
LVDT	Linear Variable Differential Transformers
MFCL	Medicare Functional Classification Level
NO	Nitric Oxide
NPUAP	National Pressure Ulcer Advisory Panel
OCT	Optical Coherence Tomography
OCTA	Optical Coherence Tomography Angiography
PTB	Patellar Tendon Bearing (Socket Style)
RH	Reactive Hyperemia
ROI	Region of Interest
SMC	Smooth Muscle Cell
TSB	Total Surface Bearing (Socket Style)
VAD	Vessel Area Density

Chapter 1. INTRODUCTION

1.1 PROBLEM STATEMENT

Skin breakdown is a problem that affects as many as 63% of individuals with a lower limb amputation at least once in their lifetime [1]. The skin of the residual limb is subjected to extensive mechanical stresses at its interface with the prosthetic socket, especially during weight-bearing activities. Skin breakdown comes in many forms. Commonly breakdown occurs when the skin is mechanically stressed above its tolerable stress level leading to a mechanical failure of skin structures or cell death due to an obstructed nutrient supply. Breakdown results in pain and reduced socket use, thereby limiting mobility and decreasing the ability to carry out normal daily activities.

Skin breakdown can develop through multiple pathways. The pathway is determined by the combination of compressive, shear, and tensile stresses applied as well as the static or dynamic nature of the stresses [2]. Though the underlying physiology involved in prosthesis-induced skin breakdown is complex and not well-studied, some key contributing factors have been identified from an extensive body of research investigating pressure ulcers. The two primary mechanisms of pressure ulcer formation are tissue ischemia and cellular deformation [3]. In the tissue ischemia pathway, blood flow to the tissue is occluded which leads to altered cellular metabolism and a buildup of harmful metabolic byproducts. In the deformation pathway, cell membranes are mechanically damaged by high magnitude mechanical strains. The effects of mechanical stress accumulate during bouts of loading, and if the skin is not given sufficient time to recover to a normal metabolic state and to repair damaged cells, skin breakdown will occur [4,5].

When biological tissue is mechanically stressed below its breakdown threshold it can adapt to become more resistant to the imposed stress [6]. This principle is employed during a period of post-amputation rehabilitation known as “prosthetic training,” when weight-bearing activity using a prosthesis is gradually introduced over a period of several weeks. If executed successfully, this process allows the residual limb tissues to adapt into a more load tolerant state without suffering skin breakdown or other detrimental health effects. Eventually, by continuing to increase prosthesis wear time, the limb can withstand full-day weight-bearing activities, provided other comorbidities do not prevent it.

Despite its important role in preventing skin breakdown, little is understood about the changes that take place within the skin that enable it to become more load tolerant and, as such, there are currently no methods for objectively determining if skin has become more load tolerant. Instead, prosthetic clinical practice relies on subjective measures such as visual assessment and palpation to determine skin load tolerance and to progress patients through periods when adaptation is desired. Additionally, there are no evidence-based methods available for enhancing the load tolerance of skin. There is a need to provide clinicians with objective tools to monitor the load tolerance state of their patients' skin. There is also a need to provide clinicians and users of prosthetic devices with more effective methods of adapting skin so that it can better resist breakdown. **At the root of these needs is a lack of understanding of skin adaptation to mechanical stress. In order to develop a better understanding, new methods are needed that can safely and accurately probe the cutaneous physiology of individuals with lower limb loss.**

1.2 SPECIFIC AIMS

The goal of this dissertation was to investigate skin adaptation to repetitive mechanical stress as it relates to users of transtibial prosthetic sockets. Specifically, this work sought to determine if changes occurred within the cutaneous microvasculature that could provide insights into the physiology of skin adaptation or that could be used as biomarkers to monitor the progression of adaptation. The microvasculature of the skin represents an important target of study related to adaptation because of the critical role these vessels have in supplying nutrients to the tissue and in facilitating tissue recovery from mechanical stress [7]. Ample blood supply is required to maintain normal metabolic processes within tissue and to restore normal processes following ischemic stress. Additionally, as a mediator of the inflammatory process, the microvasculature has an important role in coordinating tissue repair after damage has occurred via the deformation breakdown pathway [8]. Without fully resolving these issues, more extensive tissue damage can develop. Importantly for this work, the cutaneous microvasculature can be imaged and measured noninvasively using Optical Coherence Tomography (OCT) [9].

The objective of this dissertation was to develop noninvasive OCT-based methods to measure structural and functional features of the cutaneous microvasculature. Once developed, these methods were used to investigate skin adaptation in able-bodied participants whose skin was induced to adapt to a modified prosthetic socket for two weeks

and in individuals with limb loss who had used a prosthetic limb for several years. The specific aims of this work were as follows:

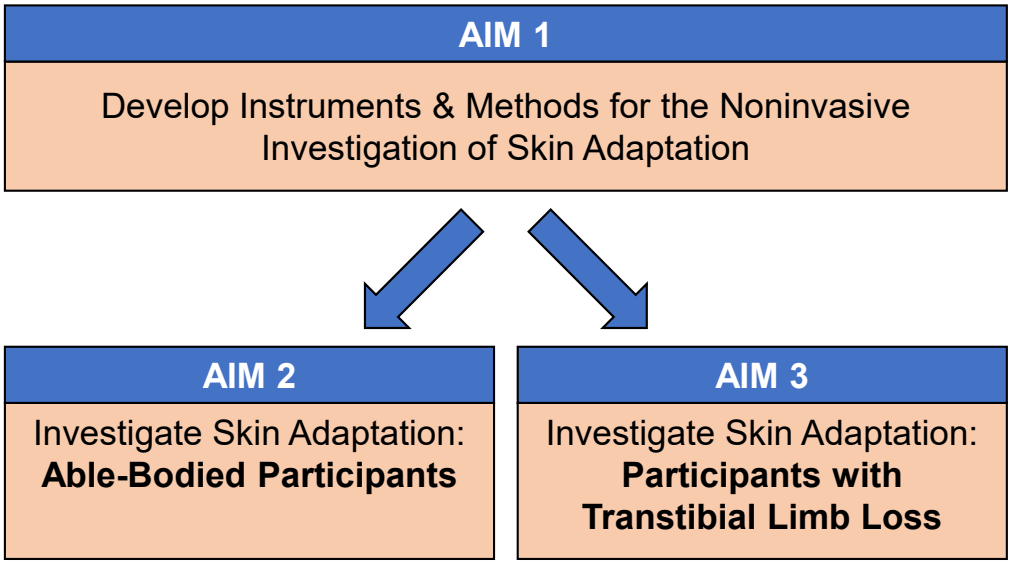

Figure 1.1. Summary of study aims.

1.2.1 *Aim 1: Instrumentation and Methods Development*

In Aim 1, three instruments and three test methods were developed to enable the noninvasive investigation of cutaneous microvascular structure and function. A Maximum Dilation Test was developed to visualize and quantify **vessel structure**. The test used a skin heating device to induce a repeatable vascular state followed by OCT imaging. A Reactive Hyperemia (RH) Test was developed to measure **microvascular function**. A loading device applied cyclic compressive and shear stress modeled after interface stresses within the prosthetic sockets of individuals with transtibial limb loss. The RH response that was induced in the cutaneous microvasculature by this stress application was then measured by quantifying the blood flow in time-series OCT images. A modified transtibial prosthesis (an "Able-Bodied Socket") was designed for use in Aim 2. The socket was used to stress the skin of an intact lower limb similarly to the limb-socket interface stresses experienced in a transtibial socket in order to develop a model to study mechanically-induced lower limb skin adaptation in able-bodied participants. A Load Tolerance Test was also developed for use in Aim 2 to determine if the skin of able-bodied participants had adapted into a more load tolerant state after wearing the Able-Bodied Socket. The test was based on the clinical assessment for load tolerance, which is to monitor the duration the skin redness following a period of walking while wearing the prosthesis. The test developed in this aim applied a cyclic

compressive and shear stress followed by the collection of photographs which were later randomized and assessed by a blinded clinical expert for redness.

1.2.2 *Aim 2: Investigate Skin Adaptation that is Induced in Able-Bodied Participants*

In a repeated-measures observational study we investigated microvascular adaptations to mechanical stress in eight able-bodied participants whose lower limb skin was mechanically stressed by a modified prosthetic socket for two weeks. Sockets were molded specifically to match each participant's lower limb. Standard prosthetic socket shape capture and fabrication techniques were employed, and the distal end of the socket was removed to allow the foot to pass through. Participants' limbs were suspended slightly by the socket, thus partially offloading the foot and allowing stresses to act through the surfaces of the limb similar to the interface stresses of a transtibial prosthetic socket. Participants followed a wear schedule that resembled a prosthetic training program used to introduce a prosthetic socket for the first time after an amputation. Wear times increased from 15 minutes on the first day to 7 hours by day 14. The OCT-based microvascular tests developed in Aim 1 were used to capture cutaneous microvascular structure and function at three time points: (1) prior to wearing the socket, (2) after one week of socket wear time, and (3) after the completion of the two-week wear program. Skin measurements at a highly-loaded region within the socket—the test region of interest (ROI)—were compared longitudinally between these three time points and were also compared to measurements taken at a location-matched control ROI on the unloaded contralateral limb.

Participants wore the sockets for the entire two-week period without any reports of skin problems or other complications. Measurements of cutaneous vascular function demonstrated that a RH response was reliably induced in the study participants, however no statistically significant differences in RH peak vessel area density (VAD), RH time-to-peak, or RH recovery time were found between the test limb and control limb or between the three time points. Measurements of vessel structure using the Maximum Dilation Test demonstrated good repeatability of the imaging location throughout the course of the study. No statistically significant differences were found in measurements of vessel density, vessel count, and mean vessel diameter between time points or test versus control ROI. A small increase in epidermal thickness was demonstrated at the test ROI after wearing the socket for two weeks, however this difference was not statistically significant. It is believed that the lack of statistically significant differences was largely due to the test limb not

being stressed enough to induce measurable adaptation. This was further supported by pressures measurements taken at the limb-socket interface throughout the study, which suggested that the pressure at the ROI was much lower than pressures typically seen in transtibial prosthetic sockets.

This study introduced new noninvasive techniques to investigate skin adaptation to mechanical stress. The results highlighted the utility of these methods as well as their current limitations. If the key limitations are addressed, these methods have the potential to provide valuable insight into the function and structure of the cutaneous microvasculature that previously could not be attained noninvasively.

1.2.3 *Aim 3: Investigate Skin Adaptation in Participants with Transtibial Limb Loss*

In a case-study of three participants with unilateral transtibial limb loss we studied the skin in a chronically-stressed region of the residual limb using the OCT-based test methods developed in Aim 1. These measurements were compared to measurements taken at a location-matched skin site on the intact contralateral limb. Individuals without recurring skin breakdown issues at the ROI were used to increase the likelihood that any differences identified would be indicative of skin that had adapted into a more load tolerant state, thus increasing the likelihood that any differences seen could be interpreted as potential markers of adaptation.

Differences in functional and structural characteristics of the microvasculature were found between the residual limb and contralateral limb for each study participant and between the residual limbs of all study participants. The RH Test demonstrated a larger magnitude vascular response and a faster RH time-to-peak in two of the three participants. The Maximum Dilation Test demonstrated a greater vessel density in two of three participants due to both a greater vessel count and larger vessel diameters. Epidermal thickness was also greater in the residual limb versus the contralateral limb for all participants, which was a statistically significant difference.

This study demonstrated the utility of two novel OCT imaging techniques for investigating skin adaptation in users of lower limb prostheses and highlighted potential biomarkers for skin adaptation that are worth investigating further.

1.3 Hypothesized Microvascular Adaptations to Mechanical Stress

While several potential biomarkers for skin adaptation were evaluated when analyzing the data collected during Aim 2 and 3, we hypothesized that three specific microvascular adaptations would

be measured when comparing skin that had adapted to mechanical stress versus unstressed skin. These physiological changes were hypothesized due to existing literature support for these adaptations given the stimuli present in skin subjected to prosthetic interface stresses.

1.3.1 *1. Vessel Count Will Increase as Skin Adapts to Prosthetic Socket Interface Stresses.*

Increasing the number of vessels within the tissue may result in a more extensive network of vessels through which blood could perfuse through during or following an applied mechanical stress. This could create more conduits to circumvent occluded vascular regions, lessening negative effects downstream, and could enable more efficient reperfusion of tissue following occlusive events. Known cues for angiogenesis are present during occlusive tissue stress, namely tissue hypoxia which leads to an increased expression of pro-angiogenic signaling factors such as vascular endothelial growth factor (VEGF) and hypoxia inducible factors (HIFs) [10].

1.3.2 *2. Reactive Hyperemia Time-to-Peak Will Become Faster as Skin Adapts to Prosthetic Socket Interface Stresses.*

Reactive hyperemia is a protective mechanism of the microvasculature that counteracts periods of ischemia to help tissue to recover quickly from potentially dangerous bouts of reduced nutrients, namely oxygen [11]. We hypothesized that chronically, dynamically loaded skin would adapt such that blood flow recovery from bouts of ischemia would become more rapid. Thus, the microvasculature of adapted skin would exhibit a faster RH time-to-peak. A more rapid RH time-to-peak is a physiological change that would indicate that the tissue more rapidly reperfuses with blood following an occlusive event.

1.3.3 *3. RH Recovery Time to Baseline Will Become Shorter as Skin Adapts to Prosthetic Socket Interface Stresses.*

We hypothesized that RH recovery to baseline would become more rapid as skin adapted to repetitive mechanical stresses. RH recovery time is largely dictated by the magnitude and duration of stress the tissue receives and the ability of the tissue to recover from the effects of the stress [5,12]. We expected that a shorter recovery time following a prescribed stress application would be facilitated by structural and functional adaptations in the vasculature and extracellular matrix of skin to make it more resistant to the stress.

Chapter 2. BACKGROUND AND SIGNIFICANCE

2.1 SIGNIFICANCE

There are approximately 1 million individuals living in the United States with a lower limb amputation [13]. Between 36-63% of people with lower limb loss experience skin breakdown issues at least once in their lifetime [1,14,15]. Clinically, skin breakdown presents in many forms (Figure 2.1), most of which involve failure of the protective epidermal barrier, and a majority of which are mechanically induced from the limb's interaction with the prosthetic socket. Skin damage is painful and frustrating for prosthetic users and commonly results in limited or suspended prosthesis use, thus impacting their mobility and ability to perform normal daily activities. Without proper care skin breakdown can lead to more proximal revision amputations [16].

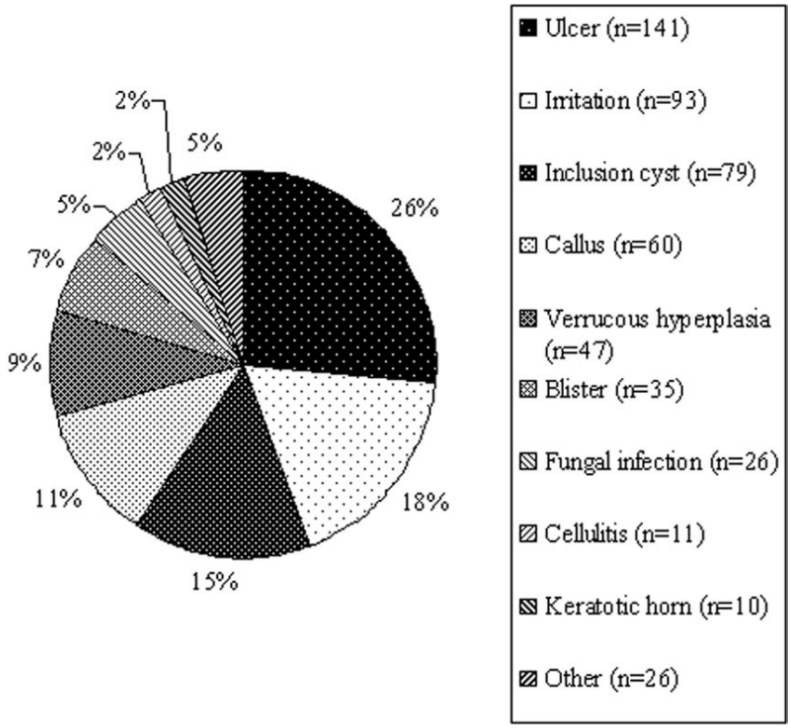

Figure 2.1. Skin problems experienced by lower limb prosthetic users. From [17].

Unlike the skin at the bottom of the foot, lower limb skin is not well-suited to handle weight-bearing loads which occur when wearing a prosthetic socket in daily life. Figure 2.2 described the anatomy of a transtibial amputation, typical prosthetic system components, and regions of the limb that are usually highly loaded within the prosthetic socket. Interface stresses

include static and dynamic combinations of pressure, shear, and friction [18]. Skin breakdown occurs when the skin is mechanically stressed above its current tolerable level for the given stress type. This is discussed in further detail in Section 2.3 below.

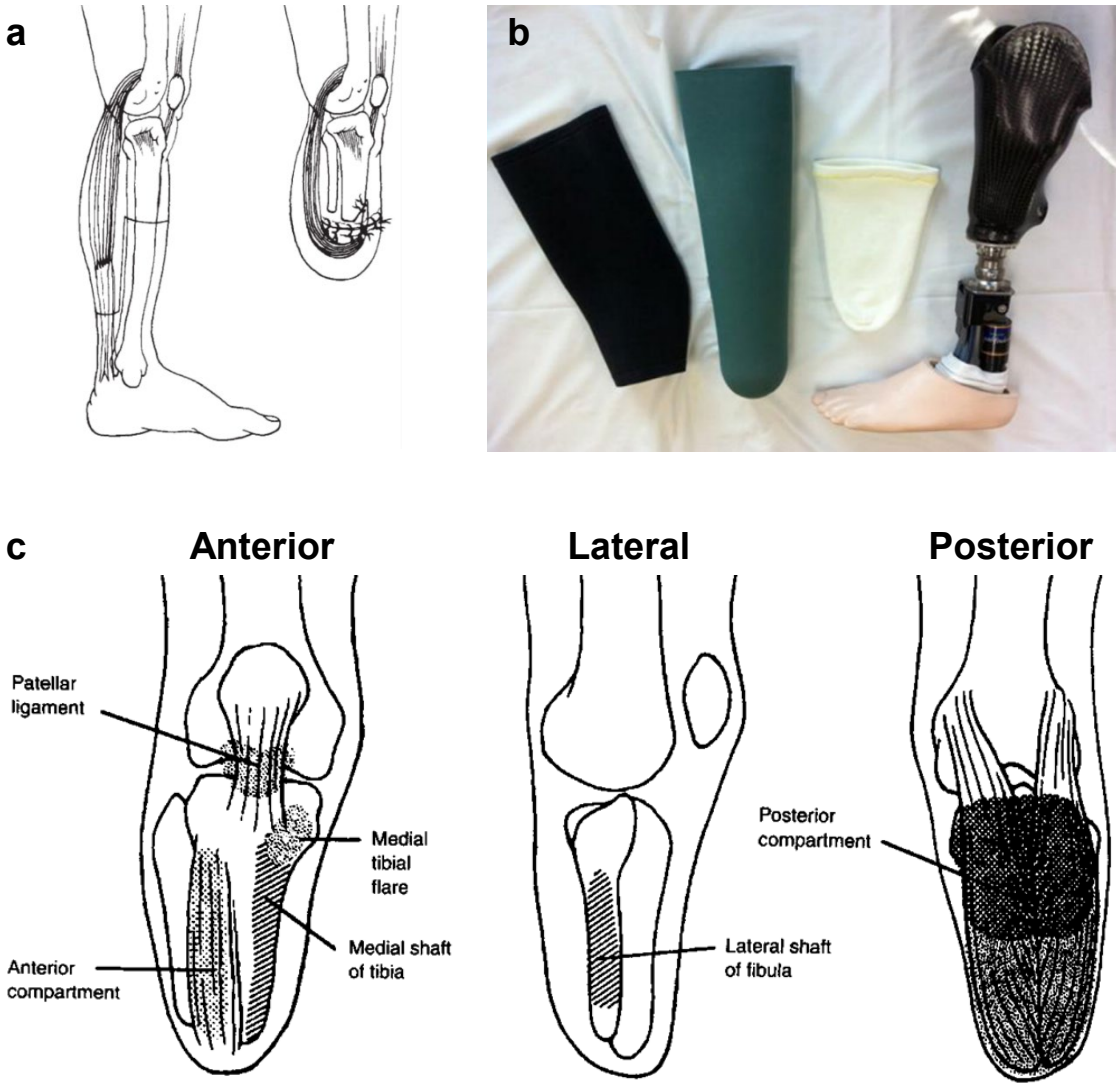

Figure 2.2. Transtibial residual limb anatomy and prosthetic system. (a) Basic anatomy of the posterior flap surgical technique for transtibial amputation. From [19]. (b) Common transtibial prosthetic system components. From left to right: exterior suspension sleeve (less common), gel liner, prosthetic sock, and socket. From [16]. (c) Transtibial residual limb with common high-load regions indicated. Adapted from [20].

Research in the Sanders Lab focuses on transtibial limb loss, versus transfemoral, because there are more individuals with transtibial limb loss, and these individuals also tend to experience more difficulty with skin breakdown largely due to the shape and tissue composition of the residual limb resulting in higher compressive and shear stresses acting through the skin.

Though the limb skin was not designed to withstand the interface stresses of the prosthetic socket, it can adapt to become more resistant to breakdown. When biological tissue is mechanically stressed below its breakdown stress threshold it can adapt to become more resistant to imposed stress [6]. Skin adaptation has been demonstrated in runners' feet becoming less susceptible to breakdown following frequent training [21] and physiological changes occurring in the fingers of guitar players enabling increased tolerance to their interaction with the instrument's strings [22]. This concept is demonstrated during the post-amputation rehabilitation process known as "prosthetic training," when prosthesis use is gradually introduced to allow the residual limb tissues to adapt into a more load tolerant state until it can eventually withstand full-day weight-bearing activities [23].

Despite its important role in preventing skin breakdown, little is known about the physiological changes that occur during skin adaptation to prosthetic use. As such, milestones of the prosthetic training period are difficult to standardize and measure, which results in a process that can be inefficient and/or lead to skin breakdown [24,25]. Long time users of transtibial prosthetic devices face similar challenges due to variable limb-socket interface stresses that occur when changes to the prosthetic device are made or due to short and long term limb volume fluctuations [26–28]. Increasing loading too quickly in poorly adapted areas leads to skin breakdown [25].

Additionally, because of this gap in knowledge, no methods have been developed for enhancing the load tolerance of skin aside from gradually increasing prosthesis use. If therapeutic interventions existed to better prepare the limb skin for its first interaction with the prosthesis, they could significantly increase efficiency through the prosthetic training program and reduce the incidence of skin breakdown as well. For example, if an intervention could create targeted regions of load tolerant skin prior to the start of prosthetic training, the load could be reduced at more sensitive sites such as the surgical suture site which would lessen the risk of breakdown in at-risk area early on in the prosthetic training process.

There is a need for a better understanding of the physiology of skin adaptation and for the development of tools that can measure these changes. A tool that could measure indicators of adaptation could enable researchers to develop therapeutics to enhance the load tolerance of skin and to more scientifically evaluate prosthetic rehabilitation programs. The development of a tool that could be used clinically to assess adaptation would enable more efficient transitions through prosthetic training and prosthetic device alterations, with fewer incidents of skin breakdown.

2.2 Skin Structure and Microcirculation Overview

2.2.1 *Structure & Function of Skin Layers [29]*

The skin is divided into 3 main layers: the epidermis, the dermis, and the subcutis (Figure 2.3). Skin thickness is generally between 2-4 mm, though the total thickness and thickness of each layer vary significantly among locations on the body.

The **epidermis** is the main protective barrier of the skin. This layer is comprised mainly of keratinocytes that pack together to form four layers: basal layer, spinous layer, granular layer, and cornified layer (stratum corneum). The most external layer of the epidermis is the stratum corneum, which is comprised of densely packed keratinocytes whose keratin filaments have become tightly bonded with those of surrounding cells, thus creating a rigid protective structure. Keratinocytes in the basal layer migrate to the stratum corneum within approximately two weeks where they usually reside for another two weeks until they are eventually sloughed away from the skin's surface. The basal layer of epidermal cells is strongly attached via hemidesmosome adhesion molecules to the basement membrane which separates the epidermis and dermis. This interface is also known as the dermal-epidermal junction (DEJ).

The protective barrier function of skin is achieved largely in the stratum corneum. Strongly bonded anucleate cornified cells are surrounded by intercellular lipid membranes, creating a semi-permeable barrier that prevents percutaneous penetration of external substances [30]. The mechanical strength of the epidermis results from a tightly bonded network of keratin filaments that forms as keratinocytes migrate into the stratum corneum and also by strong desmosome attachments between viable keratinocytes below the stratum corneum. These strong connections enable the epidermis to be particularly resistant to shear stresses acting on the surface of the skin.

The epidermis is generally between 0.06-0.10 mm thick, except for the palms of the hands and soles of the feet which are approximately 0.6 mm due to a much thicker stratum corneum, making these surfaces especially well-suited to friction and shear stress. The epidermis is avascular and receives nutrients from capillaries that extend near the DEJ.

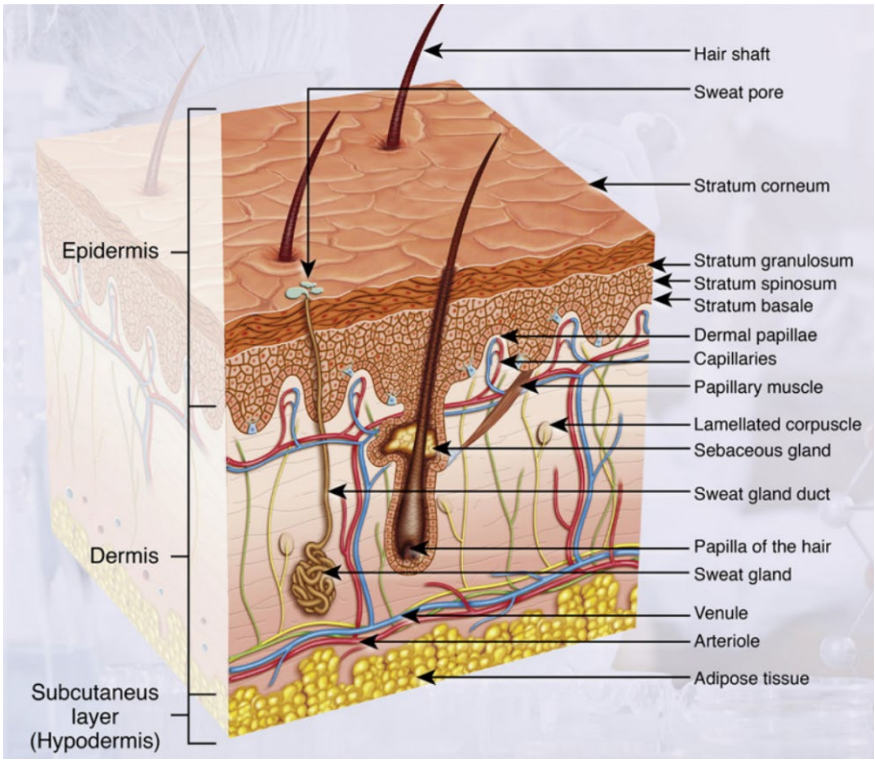

Figure 2.3. Diagram of skin anatomy. Of note are the three may skin layers: epidermis, dermis, and subcutaneous layer; and the two microvascular plexuses: the papillary and subpapillary plexus. From [31].

The **dermis** provides skin with much of its mechanical strength and elasticity, contains blood vessels that supply nutrients to the tissue, and is an active site of inflammatory and immune responses. It is comprised of a superficial papillary dermis and deeper reticular dermis.

Collagen is the main structural component within the dermis. It is a fibrous protein that packs together to form long fibrils (50-200 nm in diameter) which bundle to form larger fibers (<10 μm in papillary layer, increasing to >50 μm in the reticular layer) [32,33]. Type I collagen makes up approximately 75% of the dermis dry tissue weight and 80-85% of all collagen. Type I collagen forms fibers that are typically longer than those of type II. Type I fibrils have greater tensile strength. Type III collagen is present surrounding blood vessels in the skin [32].

Elastic fibers make up less than 10% of the dermis fibers and consist of elastic microfibers and amorphous matrix. Elastin comprises most of the amorphous matrix component and imparts much of skin's elasticity. Elastic fibers can be stretched up to 100% their relaxed length and are distributed throughout the dermis and are anchored to the basement membrane at the DEJ. In the papillary dermis, the fibers are largely oriented perpendicular to the DEJ and in the reticular dermis they are oriented parallel to it. Elastic fibers allow skin to recover its initial shape following a deformation.

Additional proteins are present in the extracellular matrix and are commonly referred to as "ground substance." These proteins include glycosaminoglycans, proteoglycans, and glycoproteins. They make up only 0.1-0.3% dry weight of skin, but they help to retain water molecules in the skin, providing skin with turgidity and hydration.

The primary cells that reside within the dermis are fibroblasts, resident macrophages, mast cells, and dermal dendrocytes. The latter 3 cells originate in bone marrow and travel to dermis through the blood stream. When activated, these cells serve critical roles in healing, tissue remodeling, and infection prevention. Fibroblasts are the most abundant cell within the dermis. Their key role is to maintain and remodel the extracellular matrix. Fibroblasts respond to chemical and mechanical stimuli to mediate degradation and synthesis of structural proteins, namely collagen and elastin.

The papillary dermis contains a loose network of type I and type III collagen and elastin fibers running perpendicular to skin surface, making it a more compliant layer than the reticular dermis. This layer contains many capillaries and is densely populated with immune cells. As such, it is an active layer for protecting the skin from infection and for healing tissue damage.

The reticular dermis contains much denser collagen and elastin networks that run parallel to the skin's surface, structurally supporting the skin against potentially deforming mechanical stresses. Collagen is laid down in layers resembling a basket weave pattern, and layers are usually perpendicularly oriented to each other, which imparts tensile strength in all directions, though some anisotropy is still exhibited [34]. There is also a higher ratio of type I to type III collagen in the reticular layer, which also contributes to greater mechanical strength. The reticular dermis contains larger vessels, very few capillaries, and a lower cell density than the papillary layer.

The **subcutaneous layer** consists mainly of adipose tissue. Though this layer does not provide much structural support it does provide additional stress distribution, thermal insulation for the body, and energy reserves for surrounding tissues.

2.2.2 *The Cutaneous Microvasculature [35]*

The cutaneous microvasculature is organized into two main sections: the papillary plexus and the subpapillary plexus, each running approximately parallel to the skin's surface (Figure 2.3). The **papillary plexus** is situated just beneath the DEJ and consists of a dense network of terminal arterioles, arterial and venous capillaries, and post-capillary venules. This plexus is the main site of nutrient exchange in the tissue, is a key mediator of the inflammatory response, and is a significant mediator of vascular resistance and therefore blood flow within the skin. This vessel network also serves as a thermal radiator for the body, though the thermal regulation process is thought to be orchestrated by vessels within the subpapillary plexus. Due to the density of vessels in the papillary plexus and the critical functions they perform, these vessels comprise the majority of what is considered the cutaneous microcirculation.

Blood enters the plexus through ascending arterioles from the subpapillary plexus and flows from terminal arterioles to capillaries then post-capillary venules. Blood returns to the subpapillary plexus via descending post-capillary venules. These vessels contain valves to prevent backflow into the vascular bed. Anastomoses are direct connections between arterioles and venules that dilate to allow blood to surpass capillary loops. They are highly innervated with an inner diameter between 10-150 μm, wall thickness of 40-60 μm, and are typically 200-500 μm in length. Anastomoses are dense within glabrous skin—hairless skin on the sole of the foot and palms—but they are sparse in non-glabrous skin, such as on the leg [36].

Arterioles in the papillary plexus have diameters of approximately 17-26 μm and are a highly active feature of the microvasculature. Arterioles consist of a layer of endothelial cells surrounded by a thin elastic lamina beneath two layers of smooth muscle cells. The vessel is surrounded by a thin layer of basement membrane composed of extracellular matrix fibers, namely collagen, laminin, and fibrillin. Dilation and constriction of these vessels occurs frequently and thus these vessels serve as mediators of vascular resistance and blood flow throughout the tissue bed.

Capillaries are the primary site of nutrient exchange in the skin. In the skin, capillaries form loops that typically ascend into the papillae of the dermis, close to the DEJ, and have diameters of approximately 4-12 μm. When blood is actively flowing through capillaries they can expand to the diameter of red blood cells, which are 6-8 μm [37]. Capillaries are composed of a single layer of endothelial cells and do not contain smooth muscle cells. Instead, they are surrounded by pericytes and veil cells. Pericytes are contractile cells that are thinner and have fewer myofilaments than smooth muscle cells. Pericytes have some contractile ability, though largely insignificant in comparison to regulation that is mediated by arterioles. Veil cells, which are fibroblast-like in appearance, are dispersed in the extravascular space, but their role is largely unknown. Capillaries do not contribute to active regulation of blood flow and passively change dilation state based on the interluminal pressure gradient. The structure of capillary loops throughout the body is similar, though their density is largely heterogeneous and can vary.

Venules in the papillary plexus have diameters of approximately 8-35 μm and function as the main site of inflammation activity. Inflammatory cells migrate to these vessels and can be exchanged into the tissue. They are the most abundant vessel in the papillary plexus. Venules are similar to capillaries in structure, but larger, with two to three layers of pericytes, and a multi-laminated basement membrane. Venules are mostly passive vessels and thus do not contribute significantly to microcirculation autoregulation. Some have mild myogenic response to pressure decreases, but the response is weak and limited.

The **subpapillary plexus** is situated in the lower third of the dermis. This plexus has a key role in thermoregulation for the body. These vessels supply blood to the papillary plexus in addition to hair bulbs and sweat glands. Arterioles and venules in this plexus have diameters of 34-50 μm and arise from muscular vessels in the subcutaneous layer. Arterioles have four to five layers of smooth muscle cells and collagen fibers that encircle the endothelial cell layer. Venules here have four to five layers of pericytes.

2.2.3 *Cutaneous Lymphatic Vessels [38]*

Lymphatic vessels in the dermis help regulate extracellular fluid balance and remove debris and some cells, such as macrophages. The vessels are comprised of endothelial cells surrounded by a basement membrane that is linked to the extracellular matrix via elastic oxytalan fibers. The fibers are linked such that when fluid pressure builds up in the tissue, as in the case of edema, the vessels

are passively opened allowing surrounding fluid and particles to enter. Materials are then transported when the vessels are compressed, primarily through mechanical muscle pump action. Many substances that are too large to reabsorb into blood vessels, such as macromolecules and immune cells, can only be removed from the tissue through the lymphatic system. Valves are present in the lymphatic lumen which prevent retrograde flow. Lymphatic vessels in the papillary dermis can be as large as 60 μm in diameter.

2.2.4 *Post-Occlusive Reactive Hyperemia*

Significance and background. Post-Occlusive Reactive Hyperemia (RH) is a protective mechanism of the skin's microvasculature that is characterized by an increase in blood flow, above normal resting levels, following a vascular occlusion. It is an important phenomenon to consider in the study of lower body residual limbs because the tissues experience repetitive periods of occlusive stress followed by rest periods where full or partial blood flow can return. A properly functioning RH response that can restore nutrients to the skin and resolve accumulating stressors is critical to maintaining skin health. RH is used by researchers to investigate microvascular function [39].

Studies of RH in the early 1900's used a tourniquet or pressure cuff to occlude forearm blood flow and measured the blood flow using plethysmography, temperature measurements, and visual documentation of skin redness [40]. The RH response occurs in most vessels throughout the body, and is largely mediated by endothelial and smooth muscle cells in arterioles [41]. The phenomenon has been studied extensively in multiple animal and human models—both *in vivo* and *ex vivo*—and in many different vascular beds. The mechanisms associated with the response are not fully understood, but many factors have been elucidated, and many of the key mechanisms of RH have been consistent regardless of the model used [39,42].

Physiology of RH. The RH response results from events that occur both during and after an occlusion and it is locally medicated through several mechanisms (Figure 2.6). The initial stimuli that are sensed include (1) hypoxia, (2) a change in vessel transmural pressure, and (3) mechanical deformation. The RH response is largely mediated by arterioles since their multi-layered smooth muscle exterior can be modulated to induce vasodilation and vasoconstriction, whereas other vessels in the microvasculature are more passive elements.

Hypoxia is the key stimulus that initiates RH. Hypoxia occurs in tissue when the blood supplying the tissue is reduced, in this case due to blood flow occlusion. As a result of hypoxia, cells enter an altered metabolic state. Cells require oxygen for normal, aerobic metabolism. Without oxygen, metabolism occurs through an anaerobic pathway and produces a different set of metabolic byproducts, chiefly lactic acid and protons (H^+). If allowed to build up, these byproducts lower the pH in the tissue, which can lead to many complications in the tissue, including cell death. The endothelial cells that line the vascular lumen respond to accumulating anaerobic byproducts by initiating the production of several vasodilators. The most widely studied and demonstrated of these is nitric oxide (NO). NO diffuses readily between cells and through cell membranes, acting on smooth muscle cells (SMCs) through a cyclic guanosine monophosphate-dependent pathway, to induce their relaxation, thereby causing vessel dilation [43]. Studies have shown this hypoxia-induced metabolic pathway is the most significant contributor to the RH response. For example, blood taken from ischemic tissue and infused into non-ischemic tissue causes hyperemia [42].

Vascular smooth muscle cells respond to **changes in transmural pressure**—the difference between intraluminal and external pressures—that occurs due to reduction of blood pressure within the vessel. Transmural pressure decreases downstream of an occlusion, resulting in SMC relaxation. When the mechanical stress is removed, SMCs are initially in a relaxed state, thus dilating vessels. Changes in transmural pressure are sensed by the cell membranes of SMCs. This induces membrane depolarization which triggers Voltage-Gated Ca^{2+} Channels allowing Ca^{2+} to enter/exit the cell, thus modulating contraction/relaxation. This mechanism of vasodilation has been demonstrated *in vivo* and *in vitro*, including studies on isolated vessel networks, individual vessels, and individual myocytes [41].

Studies have also shown that **mechanical deformation** directly contributes to the initiation of the RH response. When an imposed shear stress causes deformation of endothelial cells, the cell membranes can become strained enough to mechanically open ion channels allowing cellular K^+ release and Ca^{2+} entry, which leads to NO production [43]. Studies have also found a neuronal role in the development of the RH response, but there are conflicting beliefs as to how much this contributes to the overall response [39,44].

Following the removal of the occlusive stress, several other mechanisms contribute to the RH response, some promoting the continued vasodilation and others counteracting it. Since the half-life of NO and many other vasodilators is only a few seconds, it is likely that the initial

production of vasodilators during the occlusive event is not sufficient to sustain the response. The continued production of vasodilators by endothelial cells in response to **shear stress** from the newly introduced blood flow is a key mechanism that enables sustained vasodilation [45,46]. It has also been hypothesized that endothelial cells continue to produce vasodilators in response to metabolic byproducts that remain in the tissue, since they are not washed out immediately after blood flow returns [47].

SMCs contract during reperfusion, partially counteracting the immediate influx of blood. This occurs via a similar mechanism to that which induces their dilation during occlusion. During RH, as blood flow reenters arterioles, transmural pressure increases, causing SMC depolarization, which elicits Ca^{2+} influx and induces contraction. Although this mechanism slightly counteracts the RH response, it is thought that this contractile mechanism is initially impaired due to depletion of cellular energy reserves during the period of mechanical deformation of the occlusive stress [5].

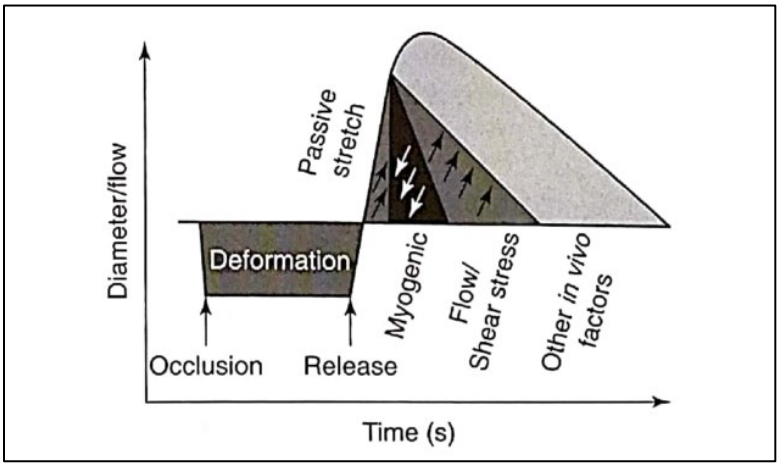

Figure 2.4. Proposed factors and phases of the RH response. From [48].

Accumulation of RH factors. If normal blood flow is not fully restored prior to a subsequent occlusive stress, it has been shown that RH factors can accumulate and intensify the RH subsequent response. This is an important phenomenon to consider when studying the skin of lower limb prosthetic users, since this phenomenon will likely come into play if normal blood flow is not restored between rests in between bouts of loading. Thorfinn *et al.*, demonstrated this *in vivo* by measuring the RH response to sitting pressures in human buttock skin with four load cycles of either short 3 minutes or long 15 minutes. The study measured RH during 5-minute rests in

between cycles. Peak RH following longer loads progressively got larger, whereas shorter loads were able to fully recover and did not accumulate (Figure 2.5) [5].

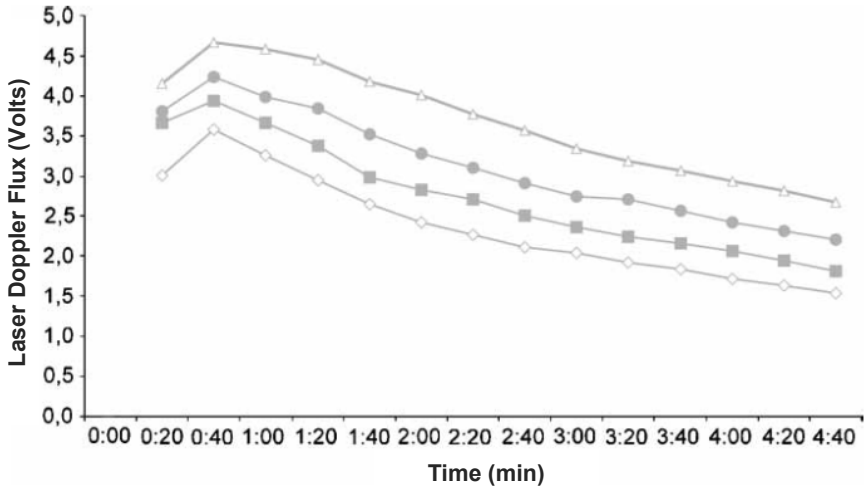

Figure 2.5. Demonstration of the accumulative effects of RH. RH following 4 cycles of 15-minute pressure application is shown. Rests between loads were 5 minutes. Diamonds = cycle 1, squares = cycle 2, circles = cycle 3, triangles = cycle 4. From [5].

The factors that result in accumulation of RH response are not fully known, however it is likely a combination of: accumulated metabolic byproducts that have not been removed from the tissue; a delayed cellular recovery to a normal metabolic state; additional tissue damage incurred during reperfusion (called ischemia-reperfusion injury), delayed repair of cell membranes from deformation or chemical damage; and altered contraction of SMCs due to reduced energy stores of that were not able to recover.

Based on prior studies that have demonstrated the accumulative effect of RH, it is feasible that regions of skin which experience high interface stresses within the socket receive stress magnitudes larger than the commonly accepted occlusive stress—typically around 12 kPa [49,50]—for times similar to those reported to cause a RH response. Even in cases of dynamic loading, where unloading may occur during periods such as swing phase of the gait cycle or when shifting weight over to the intact limb during standing, the unloaded durations are far less than those commonly reported to achieve recovery back to a stable baseline state in the microcirculation

of the skin, as evidenced by the Thorfinn *et al.* study described above. For these reasons, it is reasonable to expect that similar physiology occurs in the skin of a transtibial residual limb as it does in these studies where an accumulative RH response has been shown.

RH curve features. Investigating the RH response in stressed skin is of interest because it provides an indication of how the tissue, specifically the microvasculature, responds to an imposed stress. The RH response can be modulated in various ways depending on the stress that the tissue experiences. Several features of the PORH curve are of interest because of the physiology they represent and the role they play in assisting in tissue recovery. A key concept in RH literature is that occlusion creates an "oxygen debt" and the RH response can be thought of as an "oxygen debt repayment". As such, the duration and magnitude of the RH response is generally considered to be indicative of this debt repayment [11]. The key features of the RH curve that are relevant to this dissertation are described below and illustrated in (Figure 2.6).

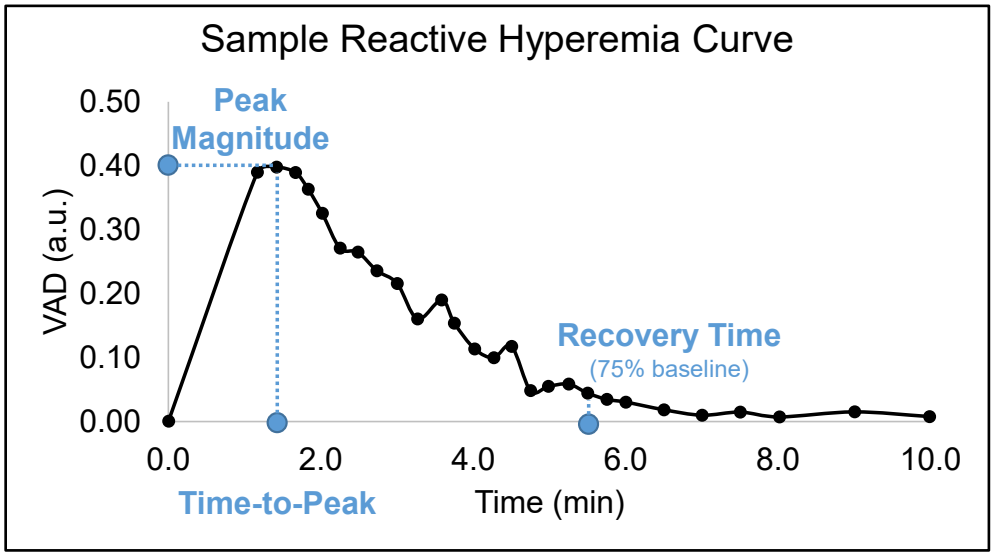

Figure 2.6. Sample RH curve with key features indicated.

RH Peak Magnitude. The peak magnitude that RH reaches indicates the point of maximal blood flow during the response and is dictated by the extent to which vessels have been stimulated to dilate. RH peak magnitude increases with increases in duration [5,12] and magnitude [12,51,52] of an applied occlusive mechanical stress.

RH Time-to-Peak. The RH time-to-peak represents the time that it takes the microvasculature to reach its maximal point during the RH response. Studies reporting RH time-to-peak are sparse and those that exist have conflicting results. Sanders *et al.* reported a case study demonstration of RH using thermal measurements of human skin and demonstrated a general trend of longer times-to-peak as pressure was increased and as shear was added. In the study mentioned previously by Thorfinn *et al.* that used sitting pressures and Laser Doppler Imaging, a longer time-to-peak was found following 15 minutes of loading versus 5 minutes; however, time-to-peak was unchanged between repeat 15-minute loading sessions, despite a significant increase in blood flow with each cycle due to accumulating stress factors (Figure 2.5) [5]. Importantly, RH time-to-peak is longer in individuals who are at risk for skin breakdown. A study by Meijer *et al.* using 109 nursing home patients, demonstrated that a longer RH time-to-peak correlated with individuals that eventually developed pressure ulcers [53]. Studies have also shown that visibly injured tissue has been shown to have a longer duration RH time-to-peak [54].

RH Recovery Time. RH recovery back to baseline blood flow is of interest because it provides an indication of how quickly tissue can recover to a normal vascular state following a mechanical stress. This measure is relevant to prosthetics clinical practice, which uses the duration skin redness following an imposed load as an indicator of how well the tissue tolerated the load [25,55]. This skin redness is due to capillaries in the papillary plexus filling with blood. RH recovery time is dependent on the duration and magnitude of an imposed stress [12]. Similar to RH peak magnitude, RH recovery time increases with increasing stress duration and magnitude. One study found that injured tissue both with and without visible signs of injury from an occlusive load, demonstrated a longer duration RH recovery time [54]. Since a full recovery to baseline can take long to achieve, in practice a percentage of recovery from the peak to the baseline may be more useful. The sample RH curve in Figure 2.6 uses a 75% recovery.

2.3 Physiology of Skin Breakdown in the Transtibial Residual Limb

Clinically, skin breakdown presents in many forms, most of which are defined by a failure of the protective epidermal barrier. Mechanically induced breakdown commonly seen in individuals with a lower limb amputation includes blisters, abrasions, folliculitis, deep tissue injuries, and pressure sores [56,57].

The type of breakdown that occurs in skin depends on the nature of the mechanical stress imposed on the tissue. The three main stresses present at the limb-socket interface are pressure, shear, and tension (Figure 2.7) [23]. **Pressure** results from a load being applied normal to the skin's surface. The main pathological conditions that can result from this are pressure ulcers and deep tissue injuries. These types of injury have been studied extensively in relation to static loads, due to the prevalence of hospital-acquired pressure injuries or in individuals with spinal cord injury. Though both forms of pressure injury were previously considered "pressure ulcers," in 2016 the National Pressure Ulcer Advisory Panel (NPUAP) separated the two due to mounting evidence that pressure breakdown can elicit superficial ulcers in the skin or ulcers beginning deeper in the muscle, as in the case of deep tissue injuries [58]. Studies have demonstrated that when an imposed mechanical load is applied normal to the skin, deep tissue injuries are more common due to large stress concentrations that occur in muscle over bone. When shear is included, these effects may act more superficially, resulting in pressure ulcer damage within the skin [59,60].

The mechanism of pressure breakdown is multi-factorial and involves a combination of ischemic damage, ischemia-reperfusion injury, lymphatic occlusion, and cellular deformation. Tissue ischemia results in a lack of oxygen and glucose supplied to cells, which shifts the cellular metabolism into a state of anaerobic glycosylation. This leads to the production of byproducts that can become harmful if allowed to accumulate in the tissue—namely lactic acid. The accumulation decreases the pH of the extracellular environment, which damages cell membranes, disrupting normal cell processes, such as membrane ion transport. If the pH is decreased low enough, cell death via apoptosis can be triggered [61]. Ischemia-reperfusion injury is a cellular injury that occurs because reactive oxygen species precursors accumulate during ischemia and become activated into highly reactive oxygen species once oxygen is reintroduced. These substances react with cell membranes and damage cellular DNA [62]. Deformation damage is caused by high strains acting on cells that disrupts cell membranes and cytoskeletons. Damage by this pathway occurs more rapidly compared to the other pressure-related pathways [3]. Minor damage to cell

membranes can be repaired by the cell, however large strains may induce cell membrane rupture and rapid necrotic cell death. Lymphatic occlusion prevents the removal of wastes, such as lactic acid that accumulate during hypoxia and debris that collects from damaged cells. Occlusion of lymphatic vessels occurs at smaller stress magnitudes than for blood vessels. The most harmful of these pressure ulcer contributors are believed to be the ischemic and deformation pathways, as described by Stekelenburg *et al.* (Figure 2.8) [61].

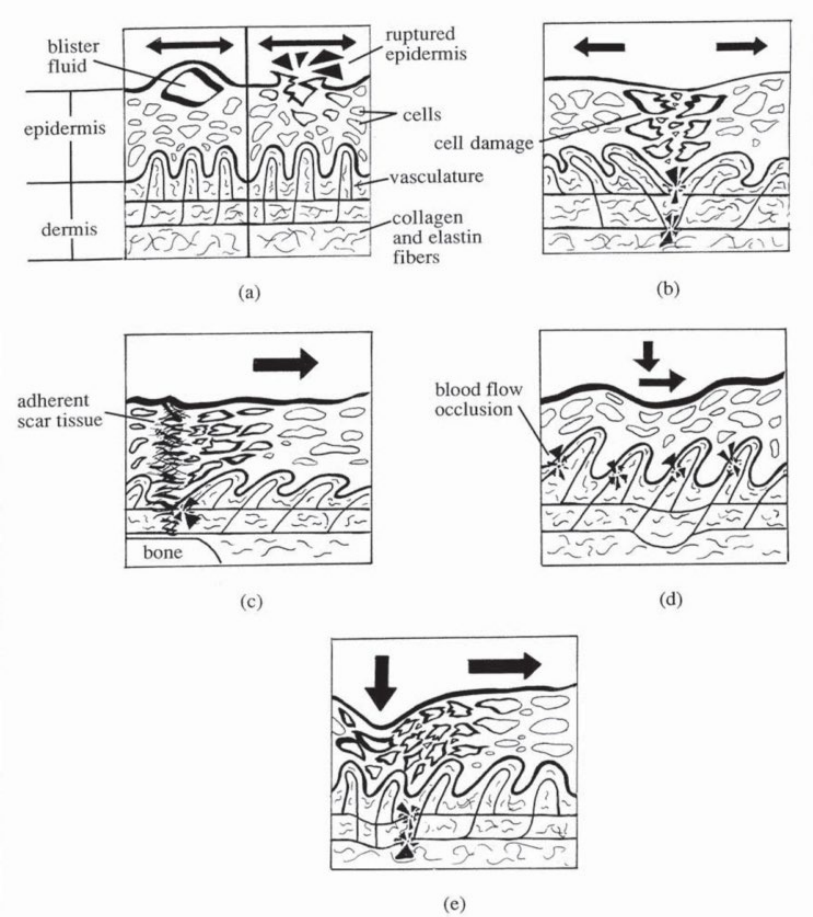

Figure 2.7. Mechanisms of mechanical skin breakdown. From [2]. (a) (left) Shear stress can result in blister formation in the epidermis or (right) abrasion of the superficial layers of cells. (b) Opposing shear induce tension in skin, which can cause cellular damage and vessel occlusion. (c) Shear stress opposing adherent tissue also induces tension within the skin, resulting in tension injury mechanics. (d) Combinations of normal and shear stress can occlude blood vessels leading to ischemia-related injuries. Cellular deformation injuries may also be induced. (e) Shear acting adjacent to a normal stress results in tension and pressure effects.

Even though pressure ulcer research typically studies the effects of static loads of 30 minutes or more, which may not accurately represent the dynamic loading that occurs within the transtibial prosthetic socket, it is likely that similar pathways are involved. For one, as these studies have demonstrated, the mechanisms that lead to clinical skin breakdown are accumulative. If damage is not given a sufficient recovery period between bouts of stress, an accumulative effect is expected to occur. Therefore, in the case of mechanical stress imposed on the residual limb, if a highly stressed region of skin is not given sufficient time to fully recover from the effects of ischemia and deformation—either through shifting body position to relieve stress in the region or during periods of doffing—then the effects may accumulate to levels demonstrated in pressure ulcer studies. This would likely result from altered metabolic conditions not fully resolving, cell membrane damage not being fully repaired, and/or the inflammatory process remaining activated and continuing to inflict secondary harm on the tissue.

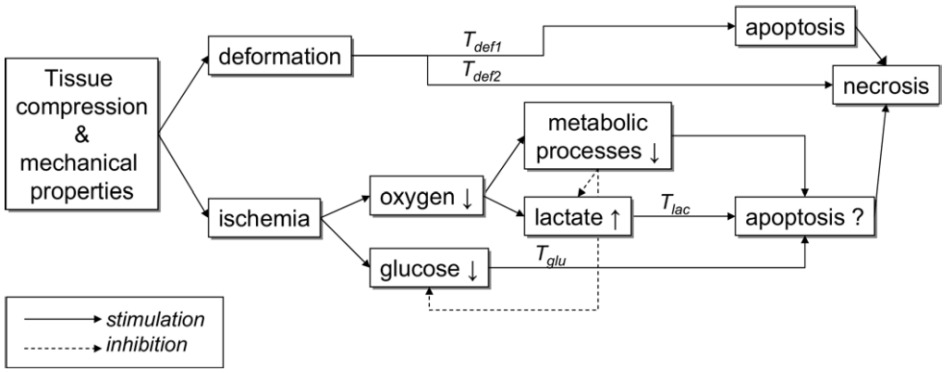

Figure 2.8. Proposed key mechanisms leading to pressure-induced breakdown. From [61]. The compression imposed and the mechanical properties of the tissue will determine the relative contribution of ischemia and deformation experienced. If T_{def1} is reached programmed cell death through apoptosis will occur. If T_{def2} is reached, immediate cell death is reached. The ischemia pathway results in decreases in oxygen and glucose and altered metabolic processes leading to the accumulation of lactate. Slowed metabolic processes reduce the buildup of lactate and glucose. When lactate concentration rises above T_{lac} or glucose levels fall below T_{glu}, cell death occurs, likely through apoptosis.

One study that demonstrated the accumulative effect of pressure injury was a study by Peirce *et al.* which induced pressure injuries in rat skin by compressing it between an implanted

plate and a magnet at 6.7 kPa [4]. Researchers observed tissue damage by measuring the amount of necrotic tissue, decreases in blood flow due to capillary plugging, and leukocyte infiltration into the tissue. In one of their experiments, the number of load cycles per day was varied using cycles of two-hour pressure separated by 30-minute rest periods, for five total days. Tissue damage was significantly more severe with 10 load cycles per day versus five cycles per day. In another experiment, five load cycles of one hour with a 30-minute rest period were used and the number of days compared was 1, 2, and 3. Accumulated tissue damage increased as more daily load protocols occurred. These data suggest that not only was a 30-minute rest period not enough to recover from the damage incurred by one or two hours of low magnitude pressure, but a 24-hour rest period was not sufficient to fully recover from the daily load protocol.

The connection between skin breakdown due to static pressure and dynamic loading similar to that experienced by a transtibial residual limb was further supported by Sanders *et al.* using a porcine model and a cyclic compression and shear stress application [63]. Compression and shear magnitudes were varied, and stress was applied 10 minutes at a time for up to 40 minutes. Skin breakdown occurred more often in tests that used larger magnitude pressure and shear, as measured by clinical visual classification. Histologically, the damaged tissue exhibited signs of inflammation such as leukocyte extravasation into the tissue, edema within the tissue and surrounding vessels. In extreme cases extravasation of red blood cells was seen. These observations are consistent with those seen during pressure ulcer studies.

Shear occurs when a force is applied in the plane of the skin's surface. When this force is large enough in comparison to the normal force and coefficient of friction between the two surfaces, displacement occurs between the two layers. This can result in abrasion breakdown, in which the top layers of the epidermis become removed. Shear stress that acts through the tissue can contribute to multiple different breakdown pathways. For one, blister formation can occur within the epidermis or at the DEJ and can be fluid filled or blood filled if the blister occurs in a vascular layer. Shear has also been shown to contribute significantly to vascular occlusion and is therefore implicated in the pressure injury pathways as well, as described above. Bennet *et al.* measured the effects of pressure and pressure-with-shear on blood flow on the human palm and demonstrated that the pressure required to achieve occlusion was nearly halved when at least 10 kPa shear was present [64].

In the transtibial prosthetic socket ***tension*** commonly occurs in regions of skin when shear force is acting to deform the tissue in opposing directions, as can occur at the tibial crest in a transtibial prosthetic socket, or when a shear stress is applied next to an area of adherent tissue. Tension causes cellular deformation and can occlude blood vessels. Thus, tension may contribute to ischemic damage and/or cellular deformation damage through disruption of cell membranes and cytoskeleton proteins. If tension induces failure of the epidermis such that an open wound is created, this is known as a skin tear. Skin tears are more common in older populations and can have a secondary effect of separation of the epidermis from the dermis or the separation of both layers from the subcutaneous layer [65].

According to the NPUAP guidelines, early tissue breakdown is commonly indicated by the prolonged presence of erythema—or skin redness [58]. Erythema is caused by red blood cells filling the capillaries of the skin, which occurs when the vessels have become activated. This occurs normally in the skin during hyperemia but may also indicate an inflammatory response within the tissue, particularly if the erythema lasts for several minutes. Non-blanchable erythema is erythema that does not go away by applying pressure to the tissue, indicating extravasation of red blood cells into the tissue has occurred.

2.4 Skin Adaptation to Mechanical Stress: Current State of Knowledge

It is commonly accepted that tissue adapts to an applied stress in a manner that opposes the stress (Figure 2.9) [6,66]. This principal is applied to muscle during weight training, to the cardiovascular system during exercise training, and to bone and tendon during many rehabilitation programs. Though research on skin adaptation is limited, studies have highlighted that skin adaptations to stress can result in altered cellular composition, microvascular structure, and extracellular matrix remodeling.

In an early study on skin adaptation, Jagoda *et al.* highlighted the effects of skin adaptation by showing that experienced runners' feet suffered fewer skin breakdown events than the feet of inexperienced runners in the same training program. This suggests that the experienced runners had previously built up a tolerance to the loading [21].

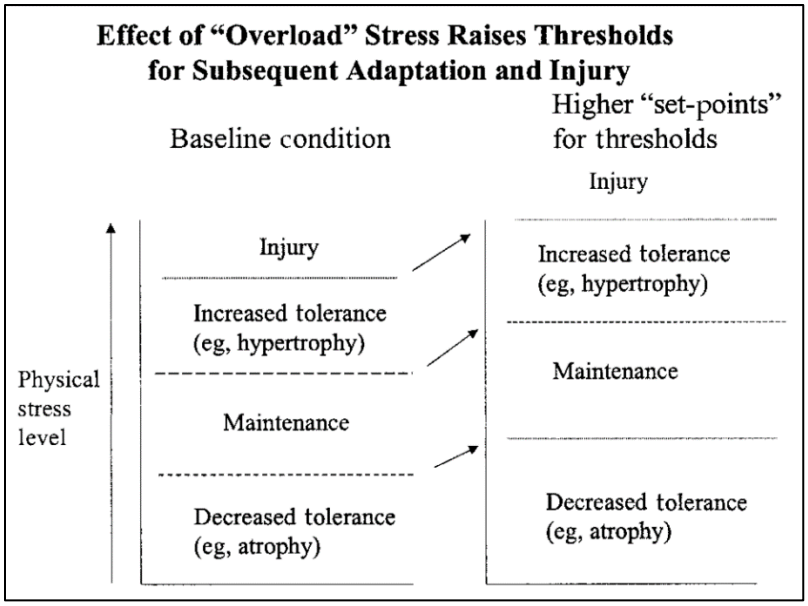

Figure 2.9. Tissue adaptation conceptualized through the Physical Stress Theory. From [6]. If stress is imposed on tissue above its current "maintenance" threshold but below the "injury" threshold then increased tolerance can occur, resulting in a rise in the stress thresholds.

The largest body of research probing the physiology of skin adaptation is in the field of skin expansion—a technique used in plastic surgery to induce skin growth. Skin expansion involves applying a mostly tensional stress to the skin to stimulate proliferation of skin cells and extracellular matrix. It has commonly been achieved by using an expandable air-filled pocked implanted beneath the dermis, but mechanisms that stretch the skin externally have also been used. Animal and human models, both *in vivo* and *ex vivo*, have been used to study the physiological changes that occur during this procedure, and have demonstrated increases in the number of vessels in the tissue, increased vessel diameters, increased epidermal thickness, and increased collagen fiber alignment [67–72]. Pietramaggiori *et al*. showed that applying tension to rat ears increased epidermal thickness and induced vascular remodeling [73]. Vascular remodeling was evidenced by increases in vessel diameters and in epidermal cell proliferation compared to sham ears. Vessel diameters increased by 30% after only eight hours of cyclic tension (two hours on, one hour off). Continuous static tension increased vessel diameters by 60% on day two and by 100% on day four. Also using a rat model, Chin *et al*. applied one or four hours of static or cyclic tension for two days and found that vessel numbers in the papillary plexus had increased by 2.5- to 3.5-fold compared to internal controls for all load profiles tested (Figure 2.10) [74]. Real-time PCR indicated an

increased expression of hypoxia induced factor 1α (HIF-1α) which is known to stimulate angiogenesis, suggesting a key stimulus to the vessel number increase was the hypoxic environment induced in the tissue during the stress application. Furthermore, it was demonstrated that cyclic loading, which consisted of two minutes loaded followed by one minute unloaded, induced larger increases in vessel number and HIF-1α, suggesting that cyclic loading may be more beneficial for stimulating vessel growth.

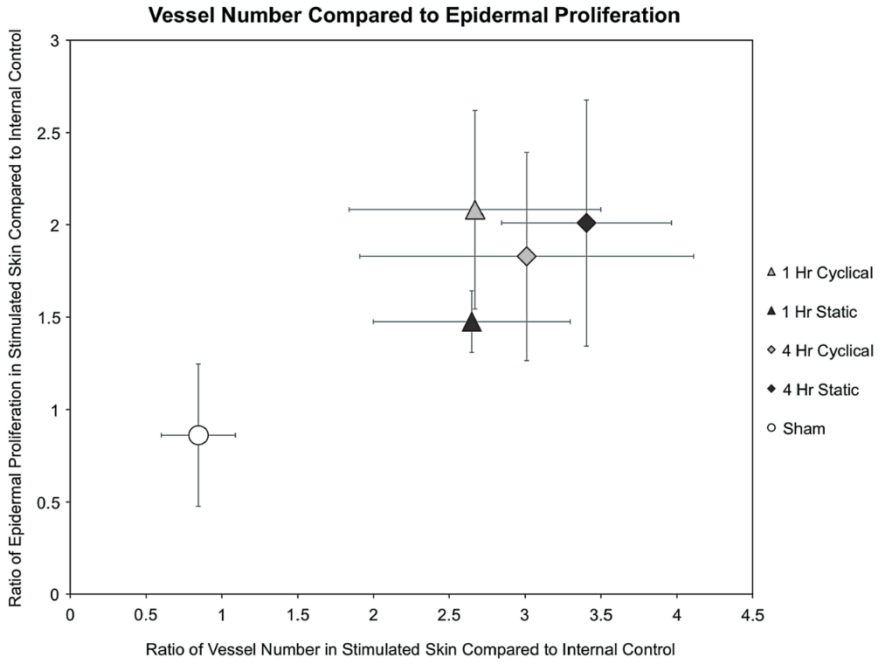

Figure 2.10. Skin adaptation to tension. Vessel number and epidermal cell proliferation in rat skin following a two-day loading period, each are displayed as a ratio compared to an unstressed internal control location. Significant increases in vessel number were demonstrated in all loading protocols tested. From [74].

Though the general principles of skin adapting to an imposed stress can be translated to research on residual limb skin, the physiology is expected to be different considering the key stresses involved are dynamic compression and shear. The only skin adaptation studies that have used skin stresses relevant to interface stresses between the lower limb and prosthetic socket have been carried out previously by Sanders *et al*. In one study, researchers investigated skin adaptation using a porcine model and a daily 1-hour protocol of cyclic compressive and shear stress for four weeks [75]. Following the 4 weeks, collagen fibril diameters increased, though the overall collagen content did not change. The diameters in the upper 1/3 of the dermis increased most significantly

with some increase in the middle 1/3 and no difference in the deepest 1/3. In another study, four days of a similar protocol using a porcine skin explant model was not enough to significantly increase diameters, though increased collagen degradation, which is the hypothesized initial step of collagen remodeling, had already begun [76].

Research on exercise training has highlighted the ability of the vasculature to adapt functionally and structurally to frequent bouts of elevated blood flow. Green *et al.* demonstrated adaptations in cutaneous perfusion capability in response to repeated skin heating [77]. Following four weeks of repetitive forearm heating, 30 minutes per day and three sessions per week, a significant increase in cutaneous blood flow during heating was demonstrated. A slight increase was seen after eight weeks; however, it was not statistically significant improvement over the four-week values. This change was not seen in an arm which was subjected to the same heating program but had a pressure cuff applied to ensure blood flow was maintained at baseline values. This suggests that a key mechanism for stimulating adaptation is an increase in shear stress on endothelial cells lining vessels. As described in a 2017 review by Green *et al*., both functional and structural adaptations have been demonstrated, including increased vessel diameters and a faster and larger RH response following occlusions [78]. Though the stress conditions in these studies were different than the case of a transtibial residual limb, they provide evidence that vessels can adapt given the appropriate stimulus.

2.5 Optical Coherence Tomography

2.5.1 *Summary*

Optical Coherence Tomography (OCT) is a noninvasive imaging technique that was used in this dissertation to visualize the cutaneous microvasculature and quantify structural and functional characteristics that may be involved in skin adaptation. OCT was chosen over other imaging and blood flow measurement techniques because it is the only method currently available to image vessel structure and thus obtain measurements of vessel density, vessel count, and vessel diameter, and to also enable rapid enough measurements to capture the RH response following a stress application.

2.5.2 *OCT Principles*

OCT is a noninvasive technique that can produce three-dimensional images of biological tissue by detecting light signals backscattered from internal tissue structures. OCT provides structural images of skin to a depth of 2 mm with a resolution as fine as 1 to 10 µm.

The OCT technique is analogous to an optical version of Ultrasound. It operates using the basic principal of low coherence interferometry. A light source produces a beam of light that passes through a beam splitter which directs one beam toward a reference mirror and another beam toward the sample to be imaged. The backscattered signal from the sample beam is combined with the beam sent to the reference mirror to a create an interference pattern whose maximum intensity represents optical path length matching of the two arms. By using a low coherent light source and scanning the reference mirror location, the path length can be matched with the tissue-backscattered beam at different depths within the tissue to obtain depth imaging. Modern OCT systems accomplish this more rapidly by using multiple wavelengths of light and resolving depth information using a Fourier transform, rather than mechanically scanning a mirror (Figure 2.11). These systems are known as Fourier Domain OCT systems. The system used here, is a specific type of Fourier Domain OCT system known as Swept Source OCT (Figure 2.12), wherein multiple wavelengths of coherent, narrow bandwidth light are rapidly scanned at each location. This can be accomplished much faster than by a mechanically scanning mirror.

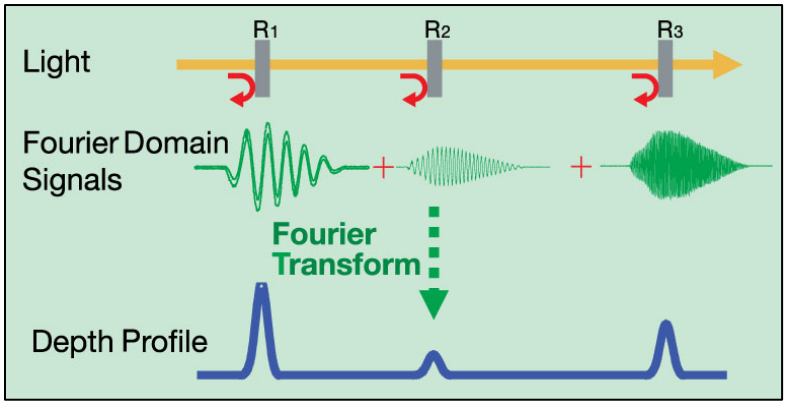

Figure 2.11. Fourier Domain OCT A-scan creation. Interference patterns measured by the detector correspond to different depth locations in the sample. From [79].

A single OCT depth scan produces a single vector of values, known as an A-scan (or A-line), that represents the depth information at a single axial location. Two-dimensional slices, known as B-scans, are created by using mirrors to translate the sample beam in a transverse direction through the tissue. Three-dimensional images are formed by scanning in a perpendicular transverse direction, essentially collecting a series of side-by-side B-scans. The wavelength of light used for biological tissue is typically centered near 1300 nm wavelength to maximize penetration depth into the tissue.

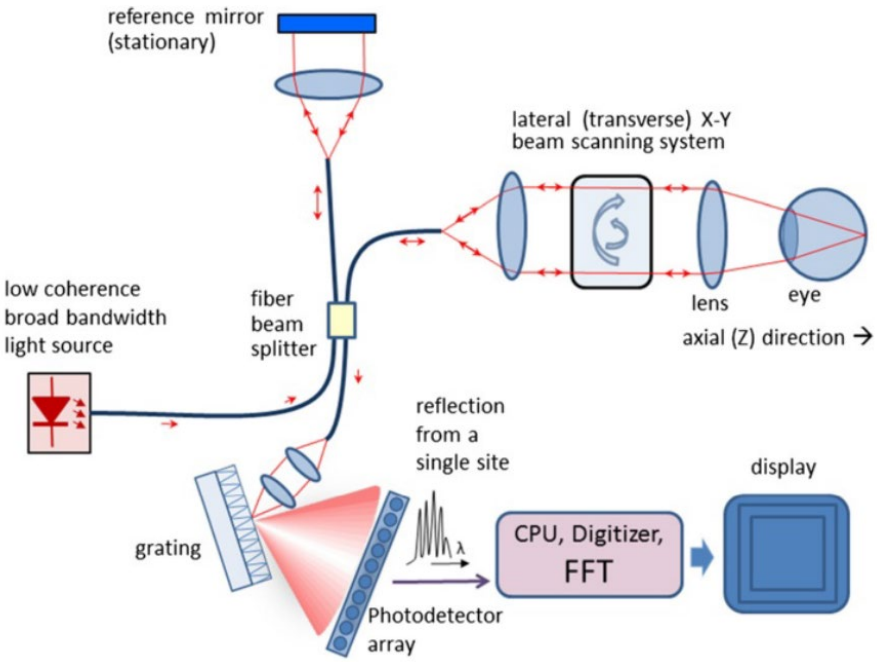

Figure 2.12. Swept Source OCT system diagram. A tunable laser source that sweeps multiple wavelengths is split to a reference arm and a sample arm, which in this example is the eye. Scanner mirrors in the OCT probe scan in transverse directions (x and y). Depth information (z) is obtained using a Fast Fourier Transform (FFT). From [80].

2.5.3 *OCT Angiography [9,81]*

Through a slightly modified image acquisition method and specialized post-processing steps, OCT can also be used to image vascular networks within a region of tissue. This method is called OCT Angiography (OCTA). To identify the vasculature, red blood cells travelling through the tissue are used as a contrast agent against static tissue. Repeat cross-sectional B-scans are taken at a single location and are compared over time. Within this set of repeat scans, pixels corresponding to

regions of static tissue maintain a consistent intensity value over time, whereas pixels in locations where red blood cells intermittently pass through (i.e. vessels with flowing blood) vary in intensity. This variance in intensity is used to determine where blood is flowing. While many different methods have been employed to compose OCTA images, a common technique is called Speckle Variance OCT. This method measures changes in speckle pattern by comparing each pixel location across repeat B-scans and calculating the variance in intensity. Pixels locations with higher variance indicate movement, in this case blood flow. The Speckle Variance equation is shown here:

$$Flow_{SV}(x,z) = \frac{1}{N}\sum_{i=1}^{N}\left(I_i(x,z) - I_{mean}(x,z)\right)^2 \quad (2.1)$$

The variables *(x,z)* represent the x and z coordinates of a single pixel location in both the image being evaluated and the final speckle variance image; N is the number of B-scan repeats; I_i is the current B-scan being evaluated and I_{mean} is a single two-dimensional image where each *(x,z)* pixel is the mean of all of the pixels in the B-scan set.

In this dissertation we have chosen to use a modified version of Speckle Variance OCT, known as High-Sensitivity Speckle Variance OCT [82]. This method enhances the signal-to-noise ratio of vessels by comparing each consecutive B-scan repeat with the previous B-scan, rather than combining all scans into a single mean intensity scan. This method is particularly well-suited for skin imaging because it reduces artifacts caused by bulk tissue motion. Most OCTA methods rely on movement within the tissue (of red blood cells) to identify vessels. Thus, when the tissue itself moves, the cross-sections that are being compared move from one B-scan repetition to the next, and the entirety of the tissue within that cross-section is incorrectly identified as a vessel. Bulk tissue motion is a common issue for skin OCTA since it is difficult to eliminate skin motion in live subjects. Even motion due to the pulse temporarily expanding the tissue can lead to severe motion artifacts that have the potential to impair images and subsequent vessel quantification. High-Sensitivity Speckle Variance OCT reduces this effect by reducing the time between images that are compared, thus reducing the distance the tissue travels between images. The High-Sensitivity Speckle Variance equation is shown here:

$$Flow_{SVHS}(x,z) = \frac{1}{(N-1)}\sum_{i=1}^{(N-1)}\left(I_i(x,z) - I_{i+1}(x,z)\right)^2 \quad (2.2)$$

As with the standard Speckle Variance calculation, the variables (x,z) represent the x and z coordinates of a single pixel location in both the image being evaluated and the final OCTA image; N is the number of B-scan repeats; I_i is the current B-scan being evaluated.

2.5.4 *Rationale for Using OCT to Investigate Skin Adaptation*

Though other methods are available for measuring structural and functional aspects of the cutaneous vasculature, OCT is the only method that can noninvasively measure the targets of interest in support of the central hypotheses of the present study: vessel count, vessel diameters, and time-series blood flow measurements during RH. Reliable noninvasive approaches must be used in order to investigate these properties *in vivo*. Although biopsy has been the gold standard in skin adaptation studies thus far, it is not feasible for use in humans who rely on a prosthetic device for mobility since any injury to the skin will likely preclude continued use of the prosthetic socket or lead to further damage. Furthermore, damaging the skin through taking a biopsy makes it impossible to study adaptation of those sites over time.

The desired measurements involve vessels within the highly active papillary plexus, which is approximately 1-2 mm below the skin's surface. To image vessels and measure of vessel count and vessel diameter the following features must be resolved: arterioles and venules (8-35 μm), and capillaries (6-12 μm with red blood cells present) [35].

OCT is well-suited to image the cutaneous microvasculature because it offers a depth and resolution balance that match these depth and resolution needs. Noninvasive methods such as Computed Tomography, Magnetic Resonance Imaging, and High-Frequency Ultrasound demonstrate good imaging depth, but at a maximum resolution of 100 μm they cannot meet the resolution needs of this study. Others have analyzed the skin using various forms of Confocal Microscopy [83] and Multiphoton Tomography [84–86]. While they provide sufficient resolution, their maximum imaging depth is only 200 μm.

While other methods exist for noninvasively measuring the functionality of vascular beds in the skin, none offer vessel images which would allow measurement of diameters and vessel count and none provide depth information, making it difficult to pinpoint which vessels are dominating the response. Some of these methods include Laser Doppler Flowmetry, Laser Doppler Imaging, Infrared (Thermal) Imaging, Laser Speckle Contrast Imaging, and Transcutaneous Oxygen Pressure. Allen and Howell provide an extensive review of these techniques [87]. These

methods have been used to study various aspects of the RH response, however they only provide a single “flux” measurement for a given volume of skin, that is often overwhelmed by flow through larger vessels below the papillary plexus [88]. Using OCT, a depth range can be specified, to ensure the same vessel region is used for each measurement. Additionally, these other methods do not provide information regarding number of vessels or diameters.

Chapter 3. AIM 1: INSTRUMENTATION AND TEST METHOD DEVELOPMENT

3.1 ABSTRACT

Instruments and methods were developed to enable the study of key structural and functional microvascular features that may be involved in skin adaptation. These instruments and methods were developed for use in Aim 2 and 3 of this dissertation. They include the following:

Instruments

3.2.1 OCT Imaging and Processing Methods. *Used in Aim 2 & 3.* A commercial OCT system was modified for use in the Reactive Hyperemia and Maximum Dilation Tests, described below. Post-processing methods were developed to improve image reliability and enable quantification of key vascular parameters.

3.2.2 Biaxial Load Applicator. *Used in Aim 2 & 3.* A device was developed to apply a controllable cyclic compression and shear stress to stimulate a cutaneous microvascular response in the Reactive Hyperemia and Load Tolerance Tests.

3.3.3 Able-Bodied Socket. *Used in Aim 2.* A modified transtibial prosthetic device was designed to induce skin adaptation in an adaptation model using individuals without limb loss.

Test Methods

3.2.4 Reactive Hyperemia Test. *Used in Aim 2 & 3.* A test was developed to assess cutaneous microvascular function by applying a controlled mechanical stress using the Biaxial Load Applicator and quantifying the vascular response using OCT imaging.

3.2.5 Maximum Dilation Test. *Used in Aim 2 & 3.* A test was developed to assess cutaneous microvascular structure by locally heating the skin to induce maximal vessel dilation and filling. OCT images were then captured.

3.2.6 Load Tolerance Test. *Used in Aim 2.* A test was developed to assess skin's ability to tolerate mechanical stress. The test was based on the current clinical standard of assessing redness duration after it is loaded. This was used in Aim 2 to determine if two weeks wearing the Able-Bodied Socket made the skin more load tolerant.

3.2 INSTRUMENT DEVELOPMENT

Three instruments were developed for use in future aims.

3.2.1 *OCT Imaging and Processing Methods*

Rationale. A commercially available Optical Coherence Tomography (OCT) imaging system was modified and image processing techniques were developed to enable (1) time-series measurement of blood flow during a reactive hyperemia (RH) functional assessment and (2) to obtain structural images of the vasculature at maximum dilation induced by heating. The vessels of interest in this study—arterioles, venules, and capillaries in the papillary plexus of the microvasculature—cannot be visualized and measured noninvasively by any other current imaging or measurement method available.

Image capture. The imaging system was a Swept-Source OCT system (OCS1310V1, Thorlabs Inc., Newton, NJ, USA) [89], with a central wavelength of 1300 nm and a 100 nm bandwidth. The system could acquire A-scans at 100 kHz. The lateral resolution (x & y, transverse directions), based on the focusing optics, was 20 μm. Axial (z, depth) resolution is based on the spectral bandwidth of the light source which has been measured at 12 μm in water and 16 μm in air. Despite this resolution limitation, depth pixels were captured every 5.6 μm. The system consistently achieved an imaging depth of approximately 1 mm below the skin's surface. Though OCT is capable of higher resolution images, our resolution was limited by our lens selection, which was chosen due to its wider focal depth range. A wider focal depth range was necessary to enable consistent measurements of the vasculature since small changes in focal depth are expected when imaging live human subjects, and small changes in focus can lead to altered vessel diameters or the potential exclusion of out-of-focus vessels.

Three-dimensional structural OCT images were captured and vascular images, also known as OCT Angiography (OCTA) images, were obtained using the High-Sensitivity Speckle Variance OCT method described in Section 2.5.3. Unless otherwise noted, all image post-processing methods, including High-Sensitivity Speckle Variance, were performed using MATLAB (MATLAB R2016b, MathWorks, Inc., Natick, Massachusetts). The specific image capture parameters that were used are described in the RH Test and Maximum Dilation Test sections below (3.3.1 and 3.3.2, respectively).

It is believed that, using these OCTA methods, the vessels that were imaged in this study include most of the arterioles and venules in the papillary plexus and some capillaries. As demonstrated by Wang *et al.*, even when vessel diameters are smaller than the documented resolution limit of the optics of a system, they can often still be imaged by OCT because the movement of red blood cells can still perturb the incident light enough to produce a change in the backscattered light [90]. Choi *et al.* demonstrated OCTA imaging of nailfold capillaries using a similar OCT system to the one used in the present study [91]. Furthermore, a similar OCT system was validated using microfluidic flow phantom and demonstrated the ability to image flow in the smallest channel tested, which was 15 μm wide [92].

En face image construction. The OCTA images that were collected were analyzed most commonly in a two-dimensional projected view known as "*en face"* images. This view was analogous to looking down into the tissue from above the tissue surface, if the non-vessel tissue was translucent. This was done so the data could be more easily visualized and interpreted and because OCTA images commonly have a shadow effect that extends below the vessel and causes vessel diameters in the depth-direction to appear stretched larger than they are. In the current study, *en face* images were constructed using a maximum intensity projection method. In the three-dimensional OCTA image, every depth vector (i.e. every A-line) was reduced only to its 10 largest pixel intensity values. Each vector was then compressed into a single pixel value for that A-line by taking the mean of the intensities of those 10 pixels. Basic OCT *en face* image construction is summarized in Figure 3.1 and more detailed processing steps are shown in Figure 3.2, and described further in the following sections.

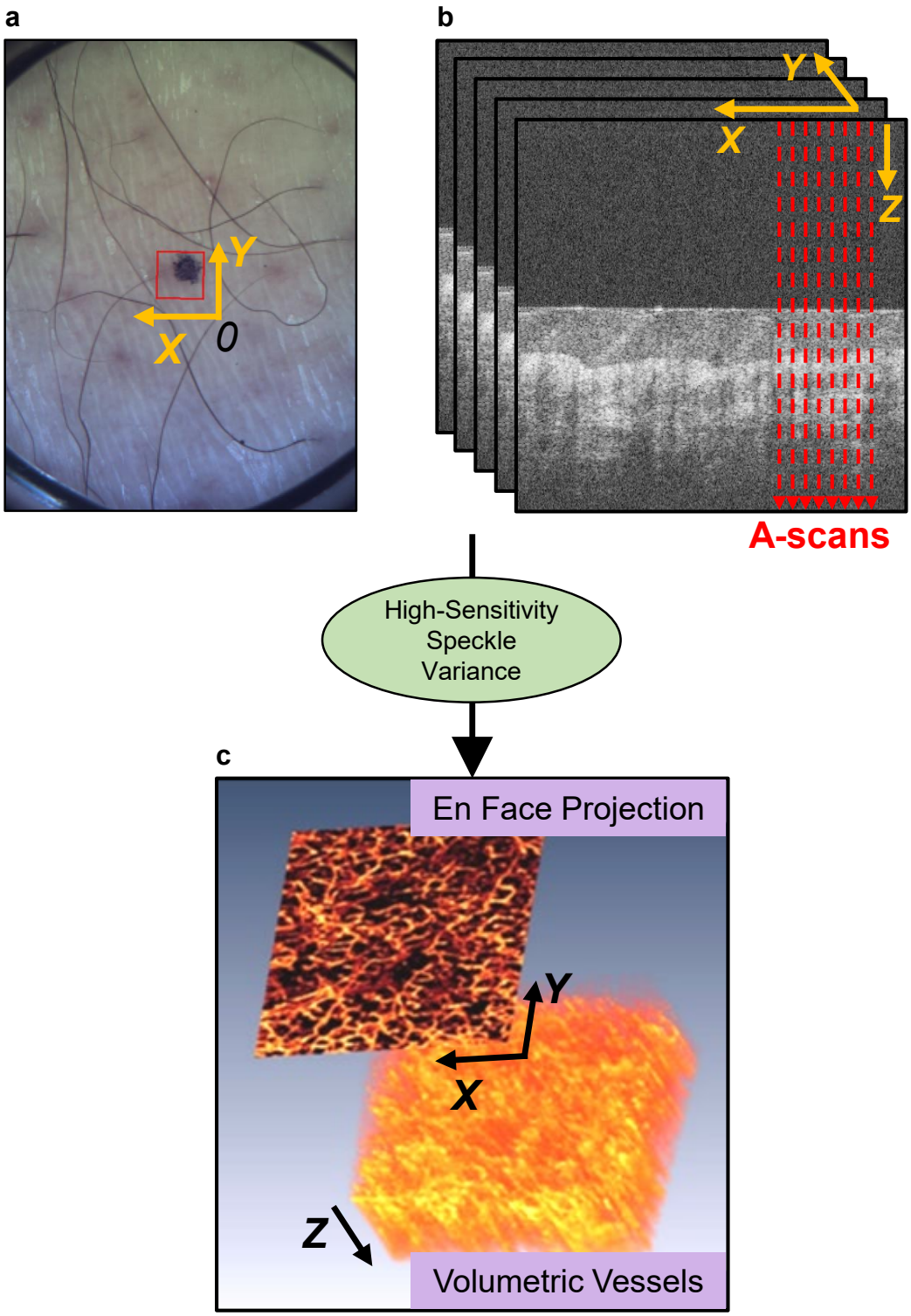

Figure 3.1. OCT image formation. (a) Field-of-view to be imaged in the skin. (b) Structural image B-scan cross-sections are captured. (c) After High-Sensitivity Speckle Variance, a volumetric OCTA vessel image is created, followed by an *en face* image via maximum intensity projection.

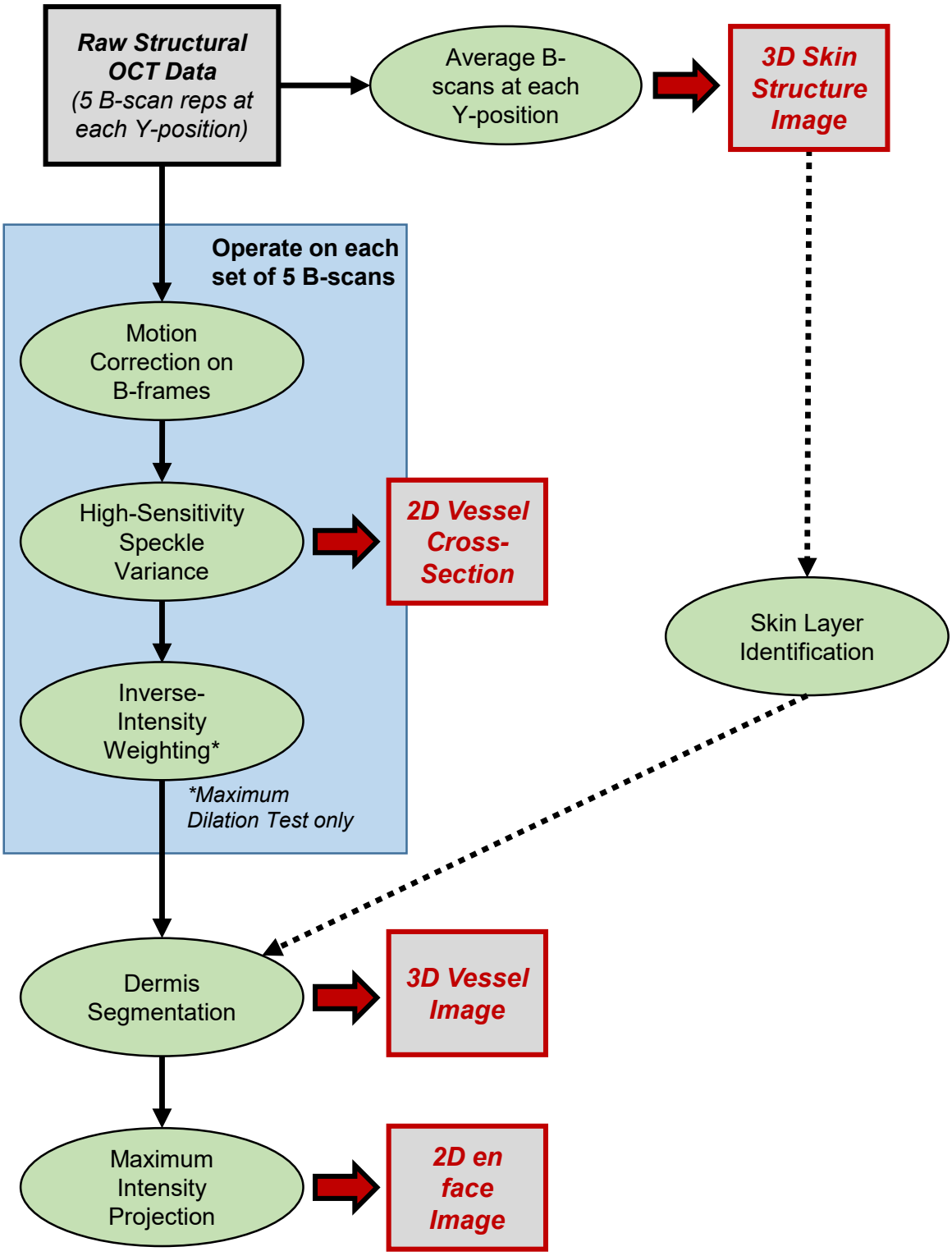

Figure 3.2. OCT image processing flow.

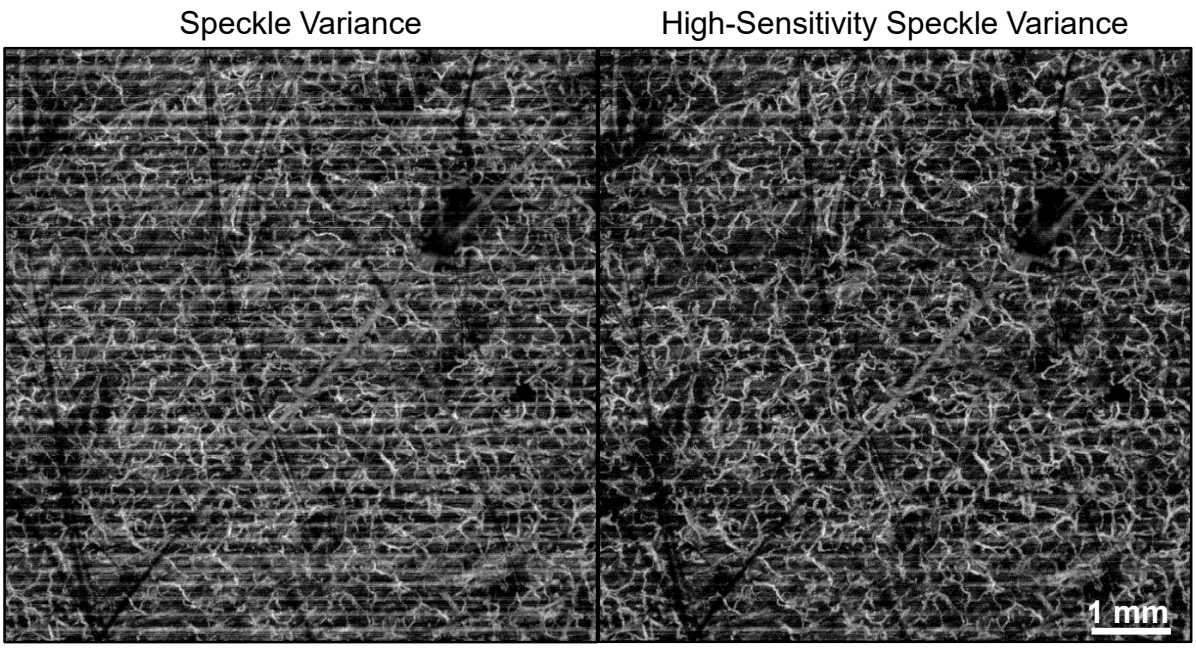

Figure 3.3. High-Sensitivity Speckle Variance. The High-Sensitivity version significantly reduced motion artifacts.

Motion artifact removal. OCTA is extremely sensitive to bulk tissue motion, which is of concern when imaging the skin of live human participants. Even small movements caused by the blood pumping into the tissue of interest or by the heart beating can cause disruptive noise in images. Since OCTA relies on comparing the difference between pixel values at each pixel location across five repeat B-scans, when bulk tissue movement occurs, and entire B-scan is identified as "a vessel." Since B-scan repetitions are taken very rapidly, tissue motion generally lasts for many groups of B-scans in the y-direction, which results in thick, bright horizontal lines across the image. High-Sensitivity Speckle Variance produced images with far less motion artifact than the standard Speckle Variance method. This is mainly because it compares consecutive images rather than comparing all five images in a B-scan set together (see Section 2.5.3 for more detail). An example of the improvement seen using the High-Sensitivity version is shown in Figure 3.3.

While High-Sensitivity Speckle Variance reduces this issue, in our study this was often not enough to remove motion artifacts to the point where they would not impact vessel quantification. As such, we used a couple of additional strategies to reduce motion artifacts in the images.

First, prior to identifying vessel images in a cross-section location, all B-scan repetitions at that location were registered to each other using a cross-correlation motion correction technique. Each correction was performed on one image at a time and began by up-sampling each image by

a factor of ten using a bicubic interpolation to achieve subpixel registration. The normalized cross-correlation matrix of the two up-sampled images was then computed and the second of the two images was translated to the location of peak correlation. The images were then down-sampled back to their starting resolution.

Image segmentation. Next, after the three-dimensional vessel image was created, the vasculature was segmented from the rest of the volume by automatically identifying the dermal-epidermal junction (DEJ) and keeping only pixels from the dermal layer. By analyzing only data from a specific depth window we were able to leverage a key advantage that OCT has over other measurement methods, which was to ensure the same volume of tissue was being analyzed with each measurement.

In many cases, segmenting away the epidermis also provided a secondary benefit of further reducing motion artifacts in the images. In OCT images of skin structure, the epidermis is usually comprised of high intensity pixels, therefore when motion occurs these pixels generate high-intensity noise in the OCTA images. By removing these pixels from the image, we were often able to marginally reduce motion-related noise without losing any vessel information since the epidermis is avascular.

While the DEJ can usually be identified visually in each B-scan, it would not have been feasible to perform this operation manually given the large amount of data that was generated in this study. A program was developed to perform this automatically in MATLAB based on methods described previously by Cobb *et al.* [93]. The automatic segmentation program was comprised of two parts: first the skin surface was found, then the DEJ was identified. The program worked on one A-line at a time from the structural OCT image (Figure 3.4). To find the skin surface we leveraged the drastic difference in pixel intensity between the external medium (air or mineral oil) and the stratum corneum at the skin's surface. First, the A-line vector was smoothed using a Gaussian filter. A differentiation-based weighting was then applied to each pixel as a moving window filter. For each pixel-of-interest, a vector of [-1 -1 -2 -3] was multiplied by the intensity values of the four pixels superficial to the pixel-of-interest and a vector of [3 2 1 1] was multiplied by the four pixels below the pixel-of-interest. The pixel-of-interest then became the sum of these eight individual products. This step was performed on every pixel in the A-line vector. Since a transition of low intensity to high intensity was expected at the stratum corneum, any negative numbers (indicating a decrease in pixel value with depth) were then set to zero. Each value of this

vector was then squared to amplify the signal. The index of the maximum value of this final squared-differentiation vector was then chosen as the skin surface depth for that A-line. A check was also performed to verify the intensity of the pixels just below the identified surface index did not correspond to low, background intensity pixels. This prevented artifacts such as hairs from being incorrectly identified as the skin surface. This process was performed on every A-line in the volumetric image, generating a two-dimensional matrix which represented the surface. A 10-pixel by 10-pixel median filter was applied to the surface to smooth the result and remove outliers.

Identification of the DEJ followed a similar process except the search on each A-line began five pixels below the identified skin surface for that A-line. Since the DEJ usually appears as a thin band of high intensity pixels just below a lower-intensity band in the epidermis, the index of the maximum value of the squared-differentiation vector was selected as the DEJ depth. This was performed on every A-line below the skin surface, creating a two-dimensional matrix of DEJ indexes. This matrix was smoothed using a 10 x 10 pixel median filter to remove any outliers.

To ensure no vessels were removed from the data, segmentation began 10 pixels above the identified DEJ. The depths retained were 125 pixels (approximately 0.70 mm) for the RH Test and 150 pixels (approximately 0.84 mm) for the Maximum Dilation Test. These depths were chosen since these depths were usually near the imaging depth limit of the given optical setups for each test.

Noise reduction and depth-compensation using inverse-intensity weighting. For the Maximum Dilation Test, OCTA images were further improved using a pixel weighting scheme based on the inverse of the intensity values in the structural OCT. The method is described in detail below. To summarize, every voxel in the three-dimensional OCTA images was divided by intensity of that voxel location in the structural OCT image. This method significantly reduced overall noise in the OCTA image, including motion-induced noise because most of the noise that existed in the images came from regions of high pixel intensities, such as tissue regions surrounding vessels in the superficial papillary dermis. The method also acted as a form of depth-compensation to increase intensity in deeper vessels that were otherwise too faint to be visualized or quantified. An example image is shown in Figure 3.6.

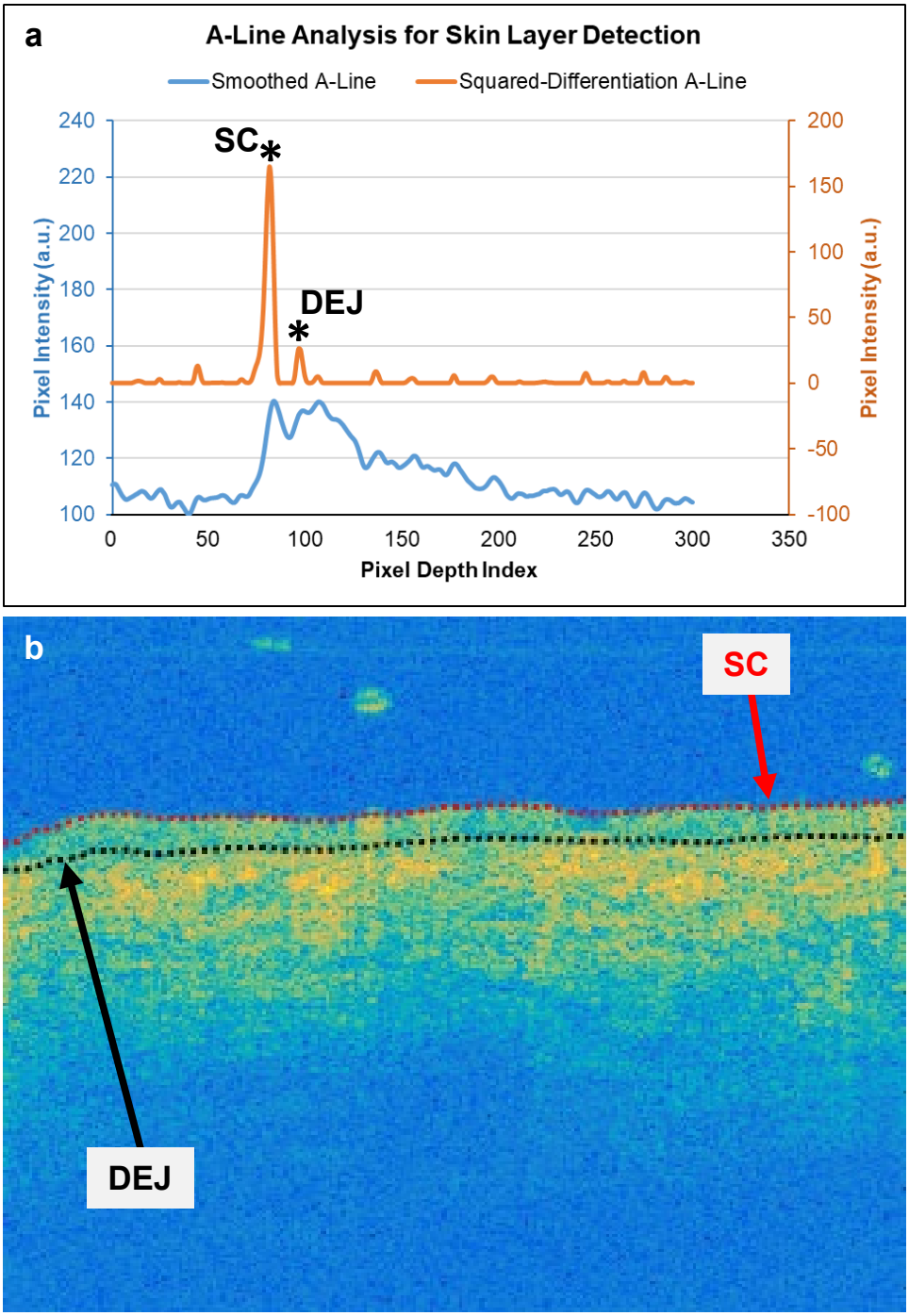

Figure 3.4. Skin layer segmentation. (a) Example of A-line processing for skin layer detection used in vessel segmentation. Representative data of a single A-line, including the associated squared-differentiation plot of the A-line used to select skin layer locations. (b) Detected layers plotted on top of structural OCT B-scan. SC = Stratum Corneum (skin surface), DEJ = Dermal-Epidermal Junction.

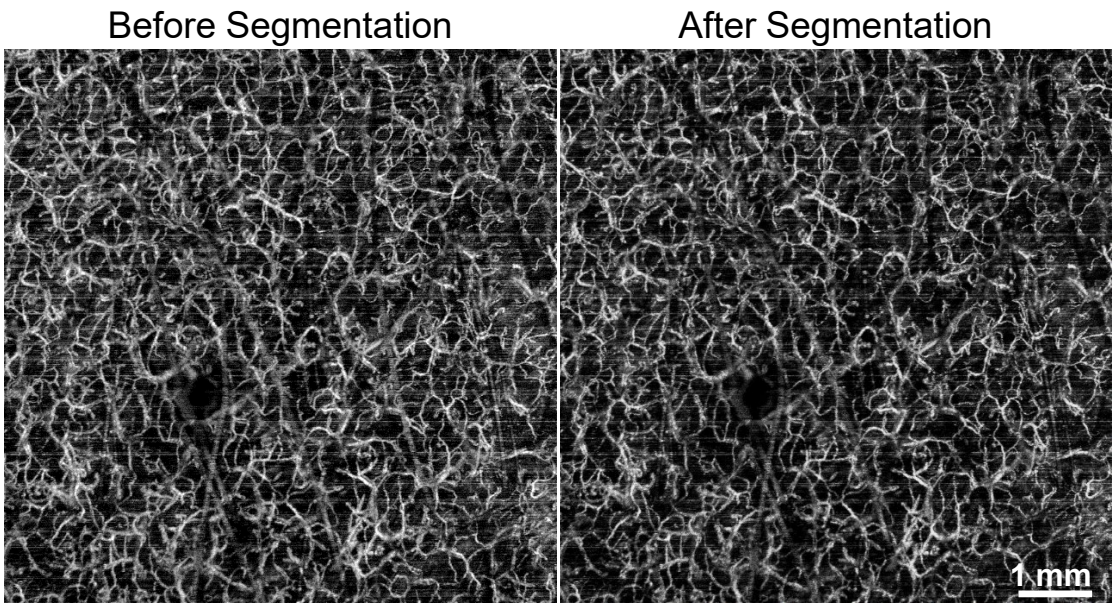

Figure 3.5. Result of layer segmentation. Segmentation slightly reduced motion artifact lines and hair artifacts in OCTA *en face* images.

This step was performed on every OCTA B-scan immediately following High-Sensitivity Speckle Variance. First, a single structural B-scan was created (I_{mean}) by taking the mean of all five B-scan repeats in a set. Next, a background noise threshold was determined. Pixels in the OCTA B-scan were set to zero if the corresponding pixel location in the mean structural B-scan (I_{mean}) was below the noise threshold. This was done to avoid amplifying background noise in subsequent steps. Then, each pixel location in the OCTA B-scan was divided by the intensity of the corresponding pixel in the mean structural B-scan (I_{mean}). This method was not optimized for the RH Test images, though it is possible that doing so would also improve the image quality and provide slightly more accurate results for that test. The inverse-intensity weighting equation that was used in the present study is shown here:

$$OCTA(x,y,z) = \begin{cases} \frac{SVHS(x,y,z)}{I_{mean}(x,y,z) \times W} & if\ I_{mean}(x,y,z) \geq T_{noise} \\ 0 & if\ I_{mean}(x,y,z) < T_{noise} \end{cases} \quad (2.3)$$

In the equation above, *OCTA(x,y,z)* represents a voxel in the final three-dimensional OCTA image while *SVHS(x,y,z)* is the high-sensitivity speckle variance voxel before the weighting is applied. $I_{mean}(x,y,z)$ is a three-dimensional volume of OCT intensity (structural) image where each

cross-section (y-dimension) is the mean of the five B-scan repeats taken at that y-location. W is a weighting factor and T_{noise} is the noise threshold, both chosen empirically.

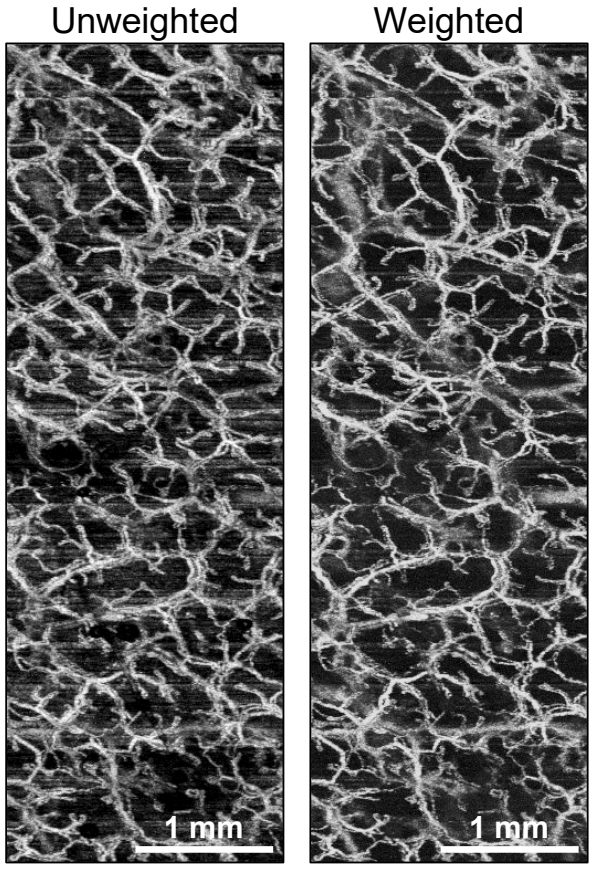

Figure 3.6. Inverse-intensity weighting. Representative image shown without and with inverse-intensity weighting applied. Weighting reduces background noise and motion artifacts and increases the intensity of deeper vessels.

OCT vessel quantification. The key OCT measurements used in the current study include vessel area density (VAD), vessel count, and mean vessel diameter. The post-processing steps used to obtain these measurements are described here and summarized in Figure 3.7.

Before calculating the measurements, the two-dimensional *en face* image was binarized. The images were pre-processed for binarization by applying a median filter. Median filters are a common image processing technique used to reduce noise in an image while preserving edge features. The median filter used here set each pixel to the median value of all neighboring pixels in a 3-pixel by 3-pixel area. From there, a binarization threshold was determined manually for each data set as the value which appeared to most accurately retain the vessel data while eliminating a majority of background noise and motion artifacts. All pixels whose intensity value was greater

than or equal to the threshold value were set to 1 and all pixels less than this value were set to 0. All pixels set to one were considered part of the vessel, and all pixels set to zero were considered non-vessel tissue (Figure 3.8a-b).

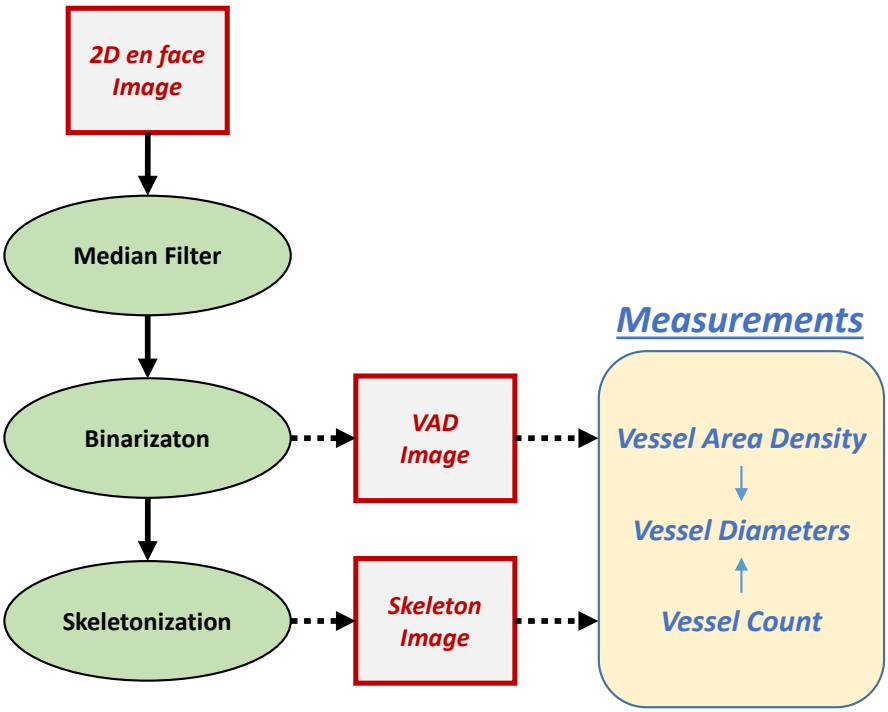

Figure 3.7. OCT image quantification flow chart.

Skeletonization was then performed by reducing each vessel into a single pixel width, placed at the centerline of the vessel. Skeletonization is a common image processing technique that works by considering a group of "1" pixels as an "object" and then removing the boundaries of the object until a single pixel width is remaining (Figure 3.8c-d).

Prior to quantification of Maximum Dilation Test images, the *en face* image was visually assessed and if artifacts were identified (usually hair or motion artifacts) the region surrounding the artifact was removed. The removed pixels were thus not quantified falsely as vessels. The key calculations used to represent this information were "density" measurements that were divided by the total number of active pixels. Since any removed pixels were also removed from the active pixel count the removal of these pixels did not falsely decrease the measurements. Artifacts in RH images were handled on a case-by-case basis and were usually left in the image because the RH trend did not appear disturbed.

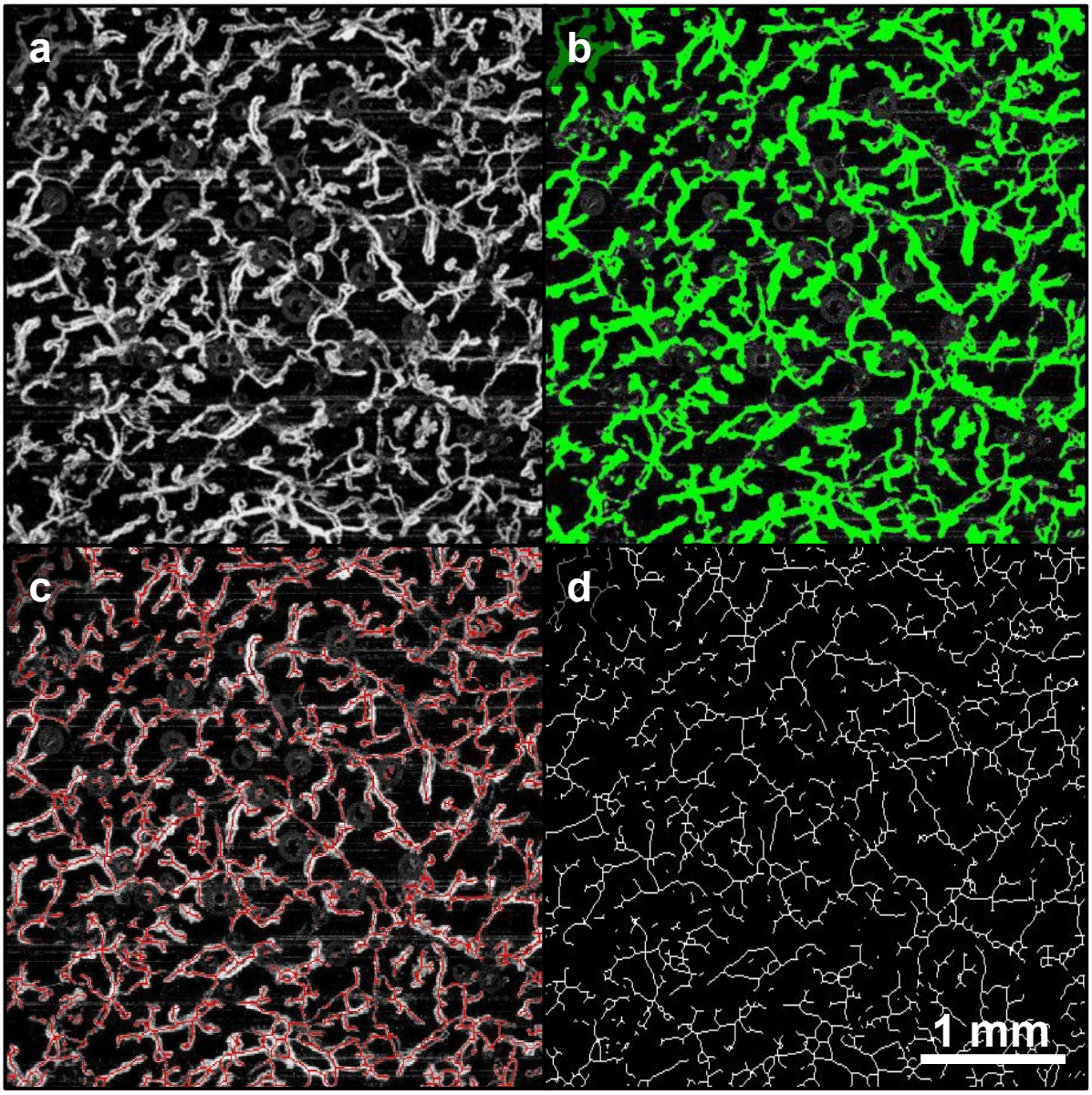

Figure 3.8. OCT image post-processing of *en face* vessel images. (a) *En face* image. (b) VAD image (green) created by binarization of *en face* image. (c) Skeleton image (red) overlaid on *en face* image (grayscale). (d) Skeleton image.

Vessel Area Density (VAD). VAD was used to quantify the amount of blood flowing in the image. VAD represents the overall perfusion in the vascular bed within the three-dimensional volume being imaged. It is important to note that VAD is not a direct measure of blood flow, but rather an estimate of the total amount of flowing blood in the tissue bed that is imaged. VAD was calculated from the binarized *en face* images by counting the total number of vessel pixels (1's) and dividing by the total number of pixels

in the image [82]. VAD was the primary measurement used in the RH Test for quantifying the vasculature's response over time.

Vessel Count (i.e. Skeleton Density). Vessel count was quantified for images in the Maximum Dilation Test to determine if vessel structure differences existed between images. The calculation was performed on skeletonized *en face* images (Figure 3.8d). The total number of skeletonized vessel pixels were counted and divided by the total number of pixels in the image to give the "skeleton density" [94]. Skeleton density was used rather than using the absolute skeleton pixel count since small differences in image sizes often existed. These potential differences were caused by small differences in overlap of the four Maximum Dilation image segments or if sections were removed due to the presence of artifacts such as hair. The term "vessel count" is used in this dissertation to simplify the interpretation of this calculation, but more accurately this measurement represents "vessel length density" in an image.

Mean Vessel Diameter. In Maximum Dilation Test *en face* images, the mean vessel diameter was estimated by combining VAD and vessel count measurements. First, since images were oversampled in the x-direction (B-scan) versus the y-direction (C-scan), the *en face* image was up-sampled in the y-direction using a bicubic interpolation so that both dimensions contained pixels which each represented 8 μm. The image was split into a grid where each grid box was a square with side length 50 pixels (40 μm). Then, within each grid box, the mean vessel diameter was calculated as the VAD in the box divided by the vessel count. The final mean vessel diameter reported was the mean of the individual grid box mean vessel diameters.

Measurement of pressure application during imaging. In the current study, an OCT imaging probe was modified to measure the pressure that the probe applied to the skin during imaging (Figure 3.9). One challenge with using OCT imaging to measure cutaneous blood flow is that, while the imaging method itself can be non-contact, in order to minimize motion artifacts there must be a connection between the skin surface and the OCT imaging probe, and some pressure must be applied. It is known that applying pressure to the skin can alter blood flow, which would have influenced the measurements collected in this study. Thus, a method was needed to make pressure application consistent between images and to minimize that pressure as much as possible.

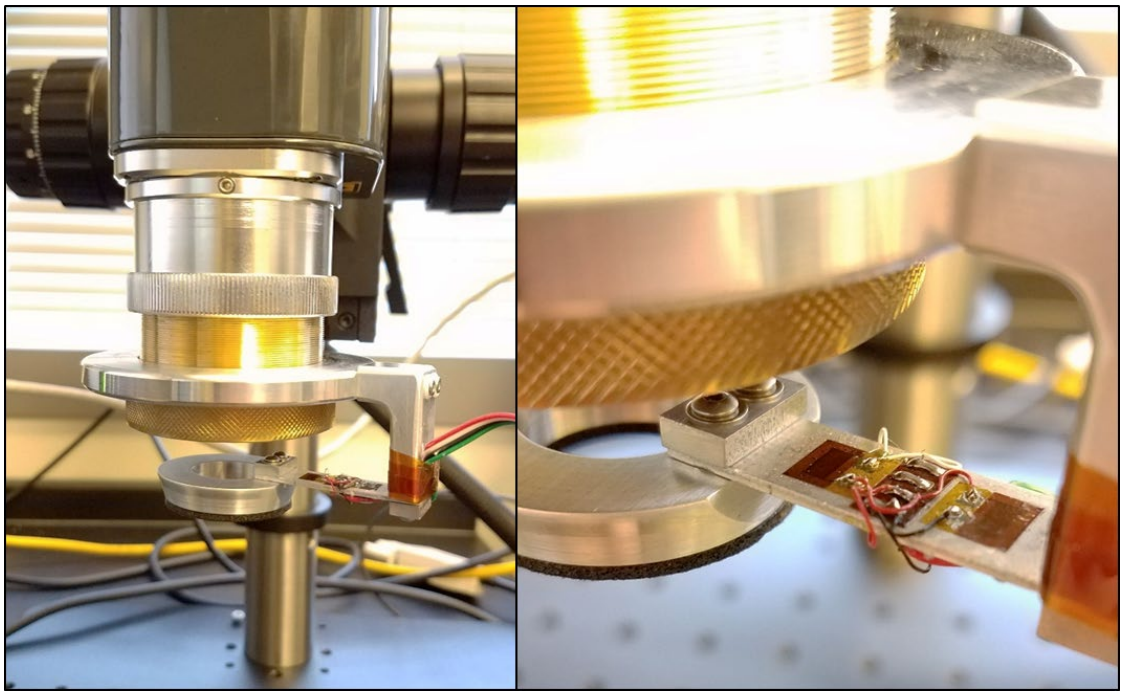

Figure 3.9. OCT pressure measurement adapter. Strain gages on a horizontal beam measured the force applied by the OCT probe during imaging. Pressure was calculated using the known skin contact surface area.

A custom machined aluminum contact probe and OCT-adapter were created which used strain gages to measure deflection of a horizontal beam. The contact probe was open in the center (ID: 18 mm, OD: 30 mm), which further reduced the risk that pressure applied would alter blood flow in the region being imaged since the largest images were 7.4 x 7.4 mm centered at the center of the contact probe ring. A thin foam ring similar to prosthetic interface materials was adhered to the skin-interface to improve pressure distribution over the ring's surface.

The device was calibrated to report force (N), and pressure was calculated using the known contact surface area of the probe. The strain gages interfaced with a strain gage module on the controller also used for the Biaxial Load Applicator (Section 3.2.2) (compactRIO-9030, National Instruments, Austin, TX, USA). The pressure applied was visualized in real-time during imaging using a custom LabVIEW program.

By monitoring the applied pressure in real time, the OCT operator made sure the pressure applied during imaging remained below 4.5 kPa. Goossens *et al.* showed that pressure applied to the sacrum of healthy individuals reduced blood flow by approximately 20% at 4.6 kPa, increasing to full cut-off at 11.6 kPa [95]. Holloway *et al.* showed that of 4-20 kPa decreased cutaneous blood

flow nearly proportionally to the pressure applied, but no changes occurred between 1.3-4 kPa [49]. Preliminary tests showed that decreasing the pressure much lower than 4 kPa often resulted in a loss of contact when small movements of the participant's limb occurred. Since the studies by Goossens *et al.* and Holloway *et al.* measured the effect of pressure applied directly to the area where blood flow was being measured and the device used in the present study applied pressure outside of the imaging area, 4.5 kPa was chosen as the pressure to not exceed during imaging.

The device was characterized through a series of tests. Sensitivity and linearity were assessed through calibration using hanging calibration weights. Repeatability and drift were assessed using repeat calibration tests followed by loaded drift tests. Beam resonant frequency was determined through a resonance test, initiated by tapping the end of the probe and capturing the oscillating frequency in the strain gages. A thermal test was used to test the effect of temperature increases like those which could occur when used near the human body or the skin heater device. The tests confirmed that the measurement: was linear; did not display significant drift; the sensitivity enabled measurements accurate to <0.1 N; and the measurements were not significantly impacted by temperature. These tests, including results, are described further in Appendix D.

Devices for OCT probe placement. Methods for OCT probe placement were improved by incorporating new components into the probe setup. These improvements were necessary for the current study to enable more efficient imaging and more reliable measurements. While both OCT tests benefited from these improvements, the changes were largely implemented for the RH Test to enable faster imaging as well as pressure and focus adjustments during the RH response. Frequent focus adjustments were required in the RH Test largely because the skin surface was often indented following the load application, and as the skin recovered from this deformation the OCT focal depth would change. Thus, by adjusting the focal depth relative to the OCT probe throughout the imaging process, we were able to maintain the same focal depth within the tissue throughout the test.

An articulated arm (244 Variable Friction Magic Arm, Manfrotto, Cassola, Italy) was used for coarse movement of the OCT probe. The OCT probe was originally supplied with a rigid optical stand which presented multiple challenges during preliminary experiments. First, the stand could only be adjusted vertically, and it could be rotated around a vertical support. Moving the entire stand laterally was also possible but was difficult given the test setup. Since the surface of the skin being imaged was usually slightly tilted from being perpendicular to the probe's vertical

axis, pressure concentrations usually existed on one side of the skin contact surface. Since the goal was to create an even pressure distribution, more degrees of freedom were desired. The articulated arm attached to the frame of the study bed and ball joints enabled six degrees of freedom allowing for free adjustment of the probe. The arm was tightening using a single knob, which significantly increased efficiency of adjusting the probe placement. This device compared with the original placement stand are shown in Figure 3.10.

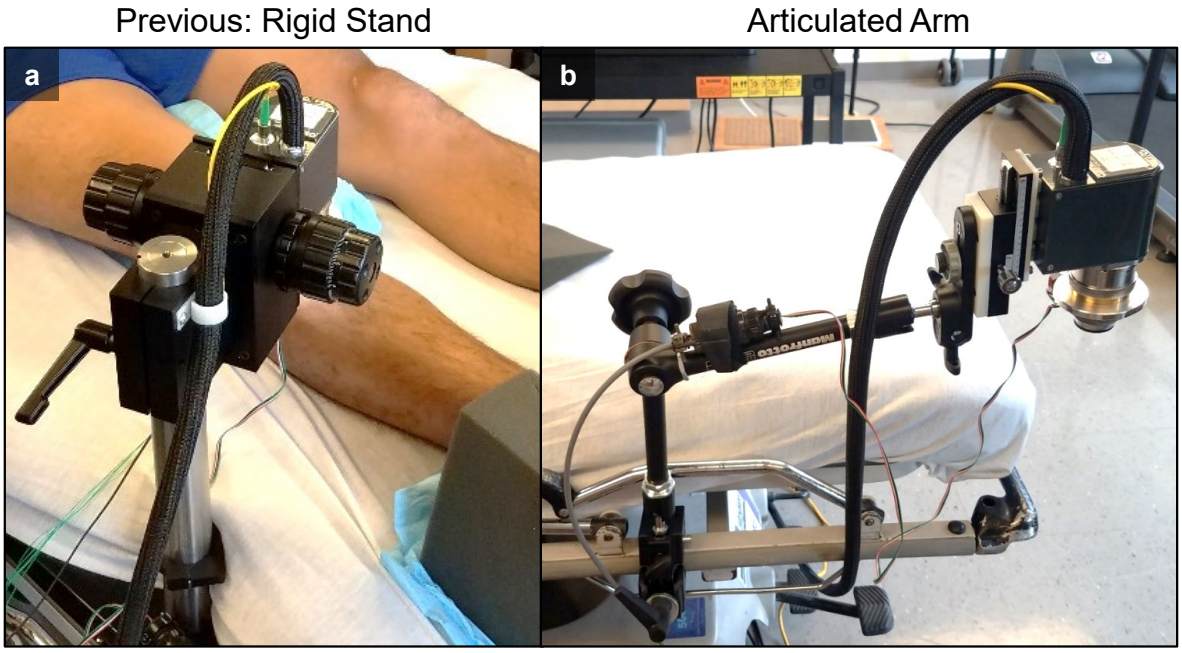

Figure 3.10. Articulated arm for OCT probe placement. (a) The previous stand was difficult to position and induced pressure concentrations on the skin. (b) The articulated arm provided more probe maneuverability.

Two rigid linear-motion stages were incorporated into the OCT probe setup to enable rapid fine tuning of OCT probe pressure and focal depth (Figure 3.11). One stage (ZWG90, Misumi USA, Inc., Schaumburg, IL, USA), was connected to the end of the articulated arm and interfaced with the OCT probe via a 3D-printed dovetail adapter. This stage was used to fine tune the z-axis position of the entire OCT probe. A second stage (M3906M, Parker Hannifin Corporation, Cleveland, OH, USA) was placed between the OCT probe and the skin contact surface, connected with custom 3D-printed adapters. Adjusting this stage changed the distance between the OCT probe and the skin surface. Thus, this stage enabled changes in the OCT image focus depth within the tissue, with some alteration in pressure as well. Using both stages together, pressure and focus adjustments could be de-coupled to allow for rapid adjustments of either or both.

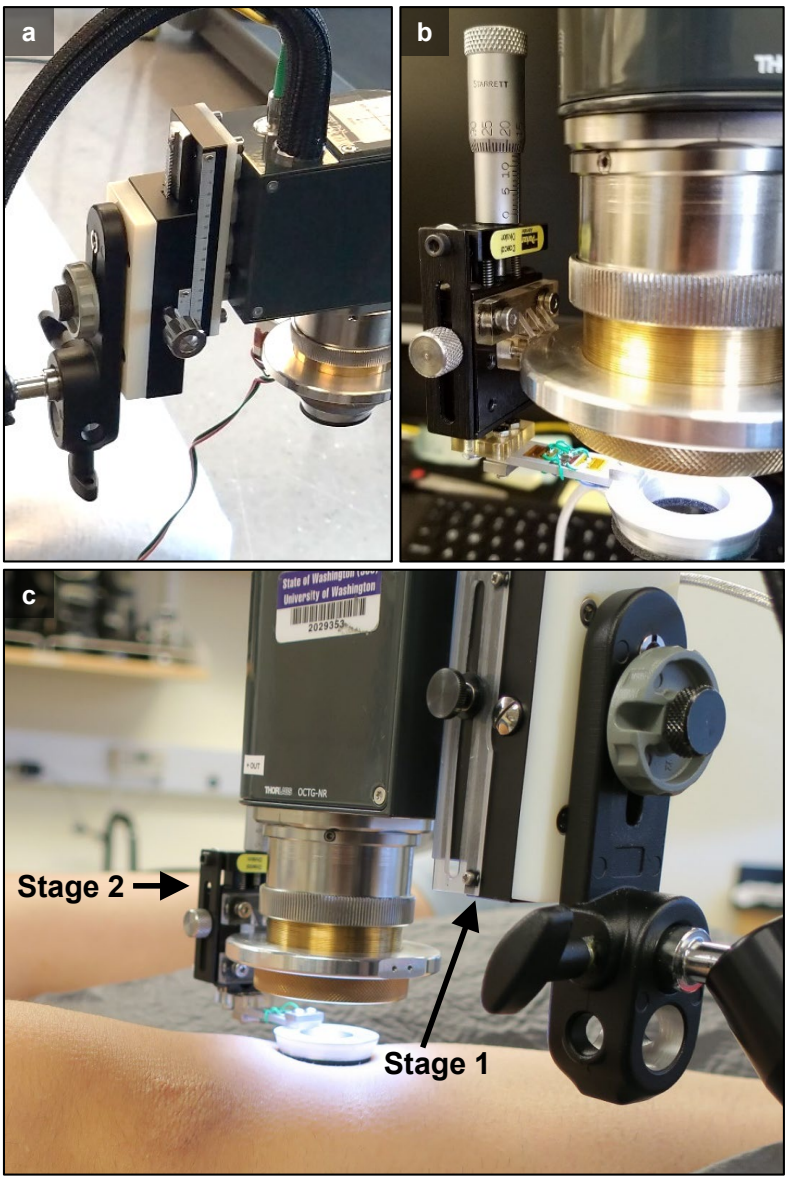

Figure 3.11. Linear stages used to adjust the fine tune OCT focus and pressure. (a) Stage 1 moved the probe vertically. (b) Stage 2 adjusted the skin contact probe away from the OCT probe. (c) The use of both stages together enabled adjustment of skin contact pressure and focal depth independently.

3.2.2 *Biaxial Load Applicator*

Rationale. A device called the Biaxial Load Applicator was developed to apply a prescribed cyclic stress to the skin's surface for use in the Reactive Hyperemia Test and Load Tolerance Test. The purpose of these tests was to assesses the functional response of the skin's microvasculature to mechanical stresses like those experienced within a transtibial prosthetic socket. It has been shown

that several key features of the microvascular response to mechanical stress are altered when the stress applied is altered, such as by varying the stress magnitude and duration [12]. As such, it was essential to develop a device that could apply repeatable stresses that were similar to transtibial residual limb-socket interface stresses.

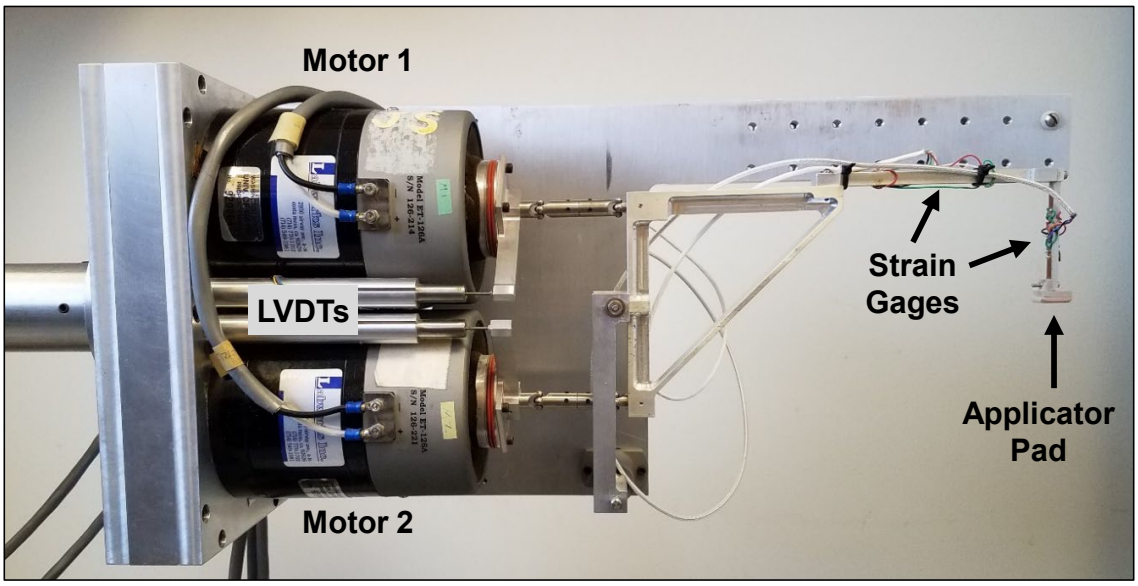

Figure 3.12. Biaxial Load Applicator. Motor movement was translated to normal and shear forces applied through the applicator pad. Applied forces and motor travel were continuously monitored using strain gages and LVDTs, respectively.

Device description. The Biaxial Load Applicator, as described previously in its original iteration by Sanders *et al.* [96], applied a prescribed cyclic compression and shear stress which were measured in real-time with on-board strain gauges (Figure 3.12). It achieved this using two shaker motors (ET-126A, Labworks Inc., Costa Mesa, CA, USA) with linkages and a rotation point designed to apply shear force when both motors moved in the same direction, and normal force when the top motor moved forward with respect to the bottom motor. Two LVDTs (linear variable differential transformers) were used to monitor motor armature displacement to ensure the motors operated within their recommended displacement range. The maximum force that could be achieved by the motors was 20 N in either the normal or shear direction. The skin contact surface, also referred to as the applicator pad, consisted of a firm prosthetic foam that was slightly rounded at the edges to reduce stress concentrations.

The device was used in past research efforts to apply cyclic shear and compressive stress to the skin of pigs [75] and humans [97], however, several updates to the system were required in order to bring it restore function and update it for the current study. These updates included a full replacement of the system controller and associated electronics, as well as the user interface. In the current study, the applicator pad was enlarged to 15.0 mm by 13.0 mm to ensure the entirety of the imaging region of the RH Test was located well within the stressed region. In both the RH and Load Tolerance Tests, forces were applied using a 1 Hz cyclic sinusoidal waveform. The target peak and trough stresses varied for each of the tests, as shown in Table 1. These values were chosen to simulate the stresses experienced by limb at its interface with the prosthetic socket in order to gain insight into how the skin may react to limb-socket interface stresses. While pressures of greater than 300 kPa have been measured at the limb socket interface of transtibial sockets and average pressure peaks during walking have been found around 100 kPa, slightly lower values were used in this test to extend the life of the system's motors and to decrease the chance of injuring participants, many of whom had never experienced these types of stresses on their limb [18,98,99].

Table 1. Biaxial Load Applicator stress targets

	Pressure (kPa)		**Shear Stress (kPa)**	
	Peak	**Trough**	**Peak**	**Trough**
Reactive Hyperemia Test	50.6	5.1	5.1	0.0
Load Tolerance Test	69.3	10.1	10.1	0.0

The system was controlled using a LabVIEW program (LabVIEW 2016, National Instruments, Austin, TX, USA) deployed onto a real-time controller unit with associated input and output modules (compactRIO-9030, National Instruments). The system included analog inputs for the strain gages which measured the applied loads and for the LVDTs which measured the motor displacements. The system outputs included two analog voltages, one used to control each motor. Prior to reaching the motors, each signal was first passed through a current source power amplifier (PA-119C, Labworks Inc.), which converted the voltage signal into an amplified current-controlled signal. The system architecture is depicted in Figure 3.13.

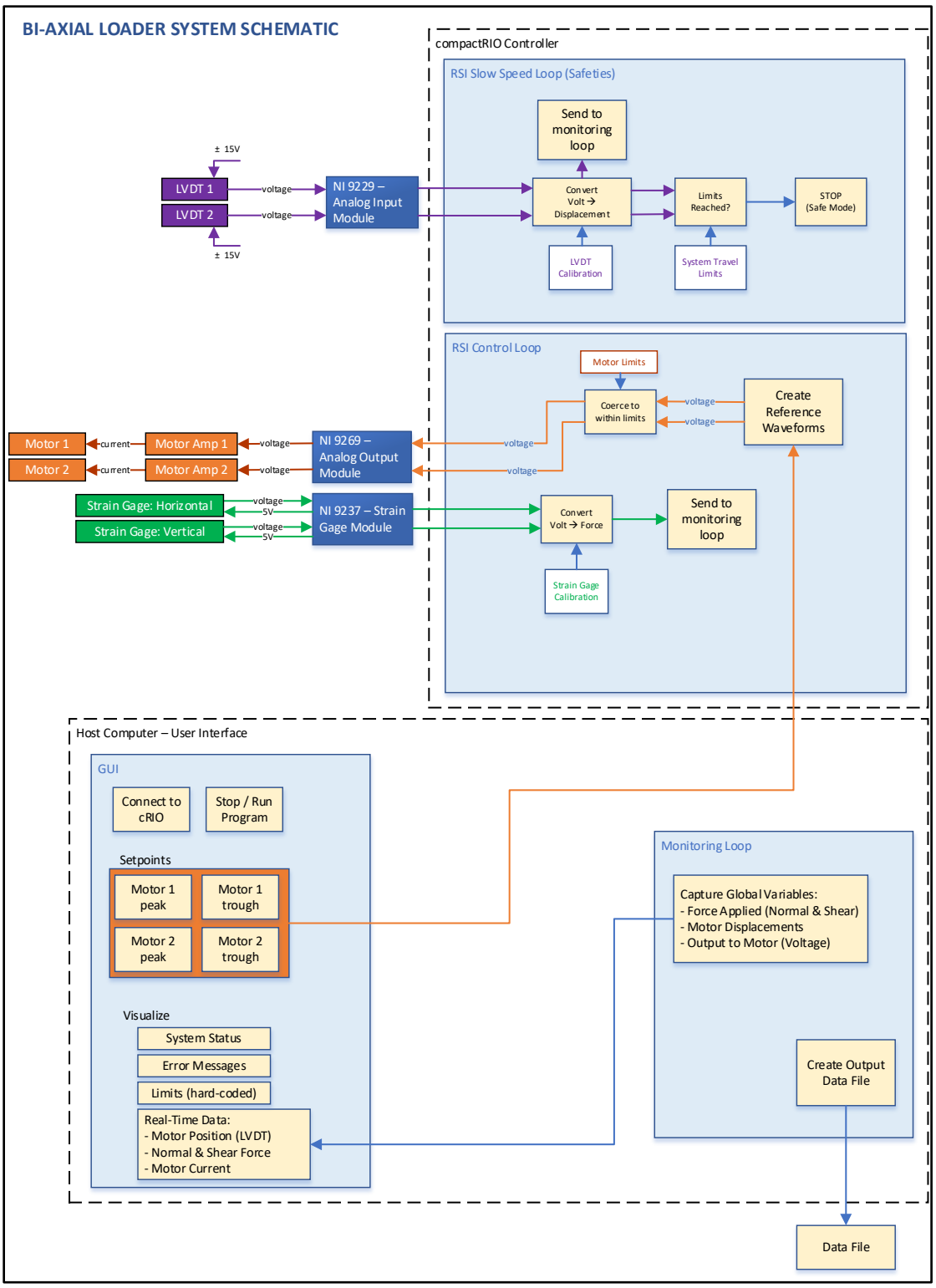

Figure 3.13. Biaxial Load Applicator control system architecture.

In the current study the system was operated manually using a LabVIEW user interface. Loading began with the operator situating the applicator pad of the Biaxial Load Applicator just above the study participant's skin at the region of interest (ROI). Care was taken to ensure the applicator pad surface was aligned to the surface of the skin so the load would be distributed evenly over the pad's surface, reducing pressure concentrations (see Figure 3.24). The loading protocol began by turning on the cyclic voltage output to the motor amplifiers and then gradually increasing the load over the course of several seconds. Throughout the loading protocol the system load application and motor displacements were monitored in real-time by the operator. Generally, once the load targets were reached, the system only required minor operator intervention, usually in response to small movements of the study participant. Automatic safety limits were also programmed into the system controller for the applied load, motor displacements, and output voltage to the motors. These limits provided an additional layer of protection to ensure the safety of the machine and of the study participants.

3.2.3 *Able-Bodied Socket*

Rationale. In the current dissertation a model was created to study lower limb skin adaptation using able-bodied study participants. To study skin adaptation most directly, skin must be studied from before it has adapted until after it has adapted. While the most clinically relevant study population would be individuals who have recently undergone amputation surgery and are beginning to use a prosthetic socket, that population also presents many confounding factors that may complicate the analysis of the collected OCT imaging-based data stemming from unpredictable levels of edema related to their surgery or blood flow alterations due to post-surgery healing. Additionally, executing such a study would be logistically more difficult to coordinate and since researchers would want to limit their impact on the clinical care the patient is receiving they would have less control over several aspects of the study, such as where socket stresses are concentrated or how the daily wear time progresses. As such, we chose to first use the developed test methods on a simplified model for skin adaptation to limb-socket interface stresses. An able-bodied adaptation model reduces many of the confounding factors that would be present in a post-amputation population and is logistically more accessible. The model used in the current study consisted of a modified prosthetic socket and a two-week wear program (described in Aim 2, 4.3.4). The sockets, called Able-Bodied Sockets, were designed and fabricated using standard

transtibial socket fabrication techniques with modifications so that the socket could be worn on a non-amputated limb. The goal was to create a socket that would induce similar interface stresses to those typically experienced by transtibial prosthesis users.

Prosthesis design. An Able-Bodied Socket was custom-made for every able-bodied participant in Aim 3. The design resembled off-loading dynamic AFO (Ankle-Foot Orthosis) devices used in rehabilitation practices to reduce load on the ankle and foot by slightly offloading the foot through the sides of the lower limb. The device contained three main sections: a socket, an AFO base, and an alignment assembly (Figure 3.14).

The AFO base (Zero G AFO Base, Certified Orthopedics, Inc., Fort Collins, CO, USA) is part of an off-loading dynamic AFO system available commercially. This base replaced the Aim 3 participant's shoe on their socket leg and contained a built-in padded foot contact surface and rubber sole with a built-in rocker shape to allow for a fluid gait. The base also contained built-in vertical support risers that were drilled through by the research team to bolt to the alignment assembly.

The alignment assembly connected the socket to the AFO base and was used to adjust the height and alignment of the socket with respect to the AFO base. The assembly was comprised of a common prosthetic pylon setup and custom-machined aluminum brackets above and below it. The pylon setup enabled adjustments to the height and alignment with six degrees of freedom. Two curved riser beams connected the vertical risers of the AFO base to the distal end of the prosthetic pylon components and provided a posterior height clearance of at least 24 cm to ensure step clearance for walking downstairs. One rectangular aluminum bracket connected the curved riser beams to the bottom of the pylon components and another aluminum bracket connected the top of the pylon components to the socket where it fastened into T-nuts that had been laminated into the posterior socket wall.

The socket design was modeled after a patellar-tendon bearing style transtibial prosthetic socket, with the distal end removed. The socket captured 60-70% of the tibial length. Two panels (one anterodistal and one posteroproximal) were cut out to allow each participant's foot to fit through the socket (Figure 3.15). The panels were tethered to the socket body using an adjustable prosthetic socket system (RevoFit, Click Medical, Steamboat Springs, CO, USA), and could be loosened and tightened by adjusting a dial laminated into the socket. A socket was molded to fit each participant's test limb while wearing a 3 mm thick prosthetic liner. The design of each socket

was directed by a research prosthetist and varied slightly from participant to participant, though many features were kept consistent. For all participants: a 4-6 mm patellar tendon bar was added; a posterior shelf was added to increase clearance for the sensitive hamstrings tendons; and posterior and distal trimline flares were added to reduce potential stress concentrations at these transitions. Some participants' sockets were also circumferentially reduced globally by 1%.

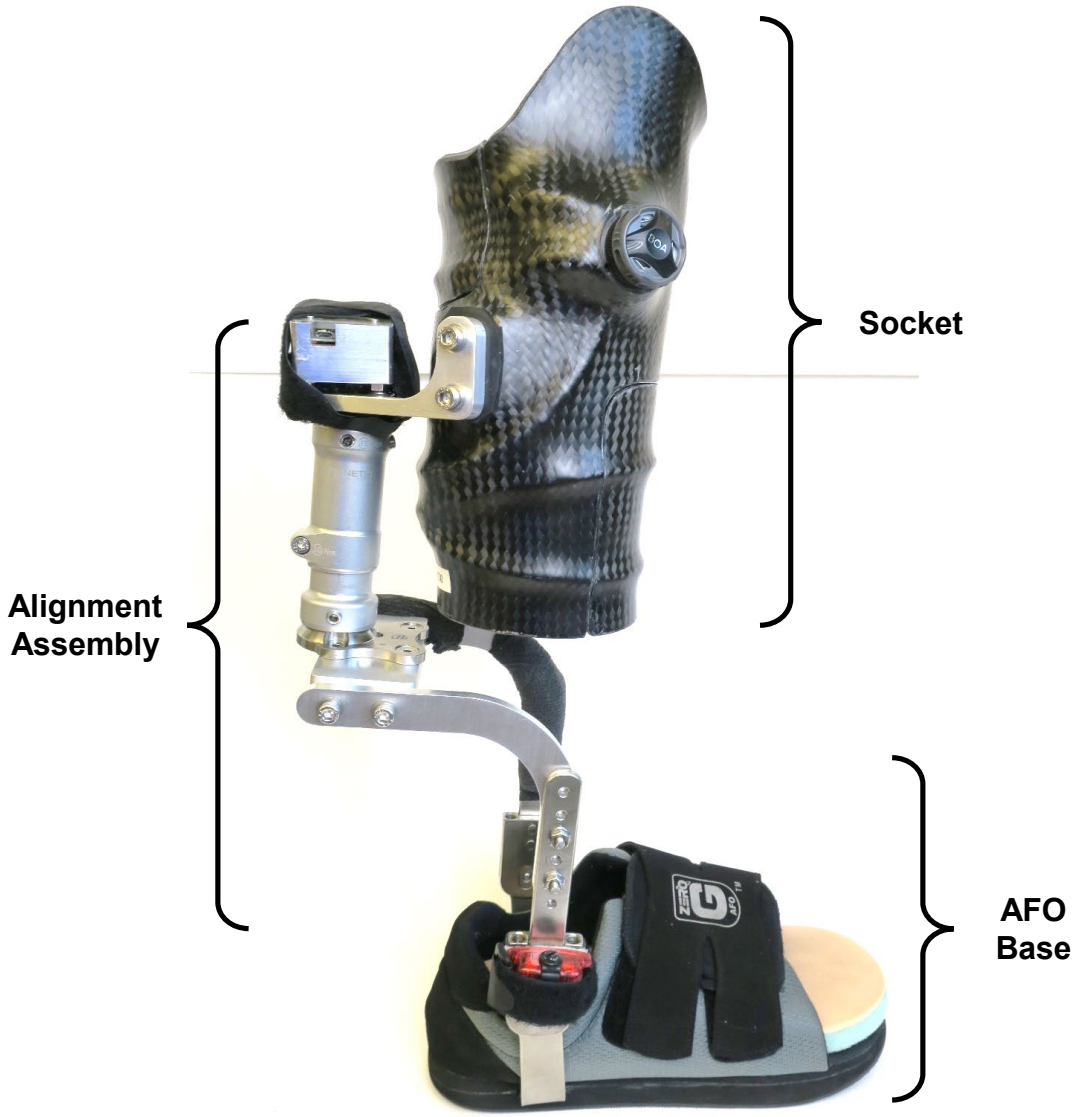

Figure 3.14. Able-Bodied Socket sections.

Finally, two prosthetic foam pads were adhered to the socket interior, one on either side (medial and lateral) of the tibial crest (Figure 3.16). The pads ensured load was removed from the sensitive tibial crest and increased in areas of known load bearing ability, including the ROI used in OCT imaging which was located within the medial pad. Some participants also had a pad added to the posterior tethered panel if the socket was deemed too loose at the time of fitting.

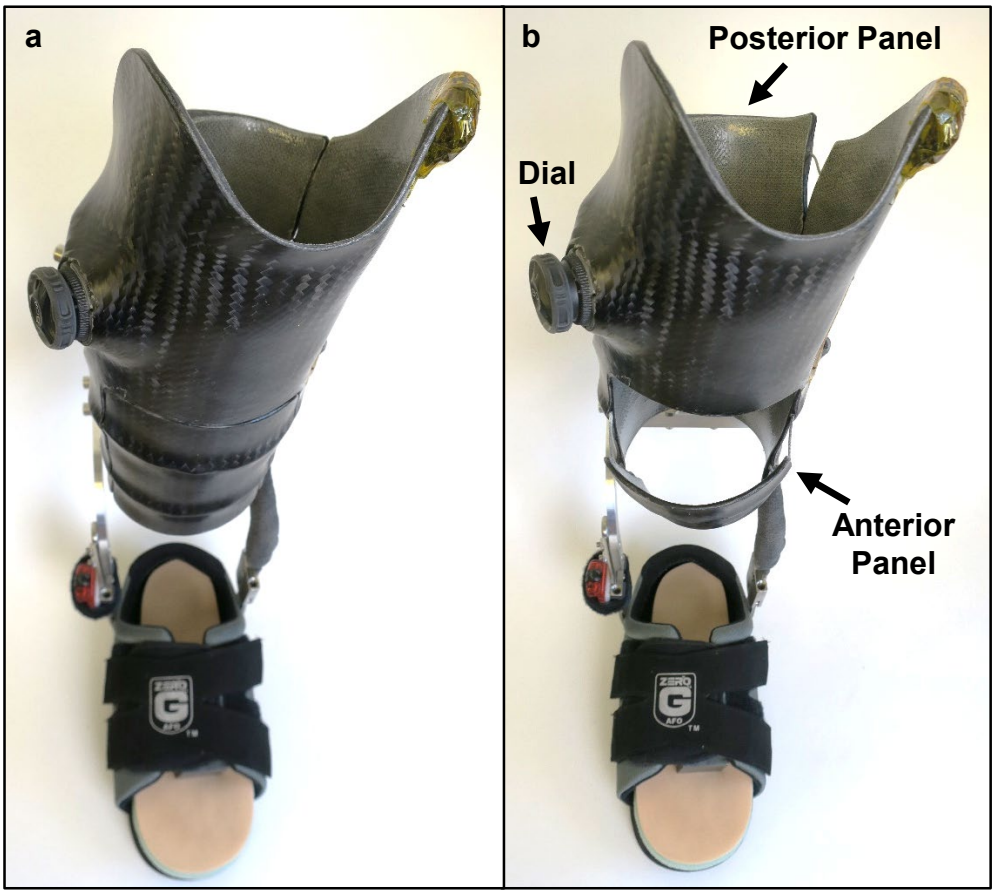

Figure 3.15. Able-Bodied Socket panels. (a) Socket with panels closed and dial locked. (b) Dial released and tethered panels opened for donning and doffing.

Socket fabrication. The socket was constructed using methods similar to standard transtibial socket manufacturing. Since participants wore a prosthetic liner during the study the limb shape was captured while wearing a prosthetic liner. The liners used for all participants were a model commonly worn by transtibial prosthesis users (Extreme Cushion BK Gel Liner, ALPS, St. Petersburg, FL, USA) with a liner thickness of 3 mm. The liner circumference was sized to each study participant by the research prosthetist and the distal ends were removed. Participants wore

the liner on their test limb while the study prosthetist casted their limb to capture the shape. Once dried, the inside surface of the cast was digitized using a mechanical coordinate measurement device (FaroArm Platinum, FARO Technologies, Lake Mary, FL, USA). The resultant three-dimensional point cloud was converted into a surface mesh which was converted into a three-dimensional CAD model using an engineering design program (Geomagic, Design X, 3D Systems, Rock Hill, SC, USA).

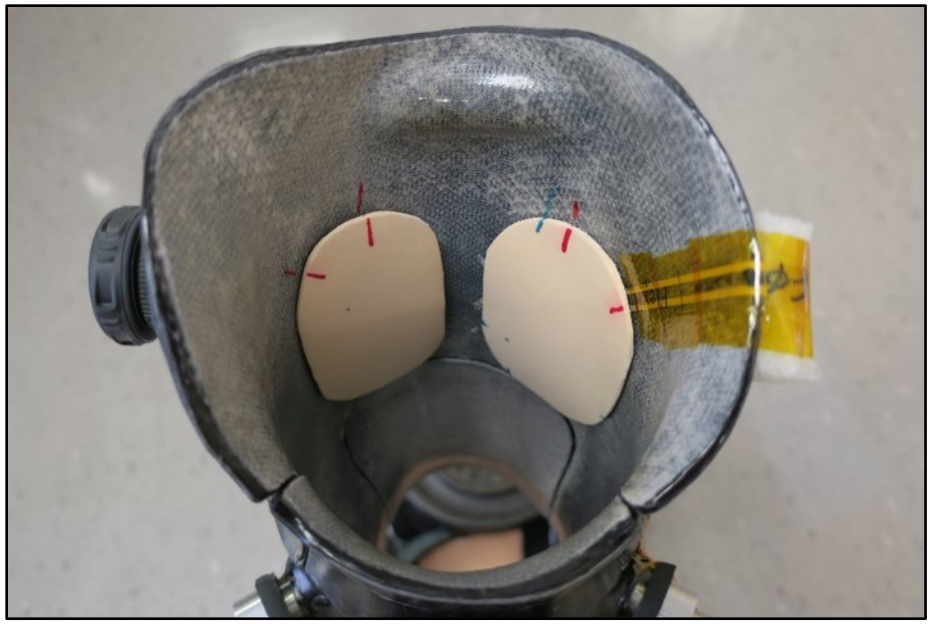

Figure 3.16. Able-Bodied Socket top view. Prosthetic foam pads on either side of the tibial crest were used to reduce stress on the tibial crest and increase stress on the medial and lateral side of the tibia.

Modifications to the CAD model were made using prosthetic CAD/CAM software (OMEGA, WillowWood, Mt. Sterling, OH, USA). This model was used to carve a foam positive of the limb with a three-axis CNC servo carving machine (C7 Carver, Provel, Cle Elum, WA, USA). Socket materials (carbon fiber and nylon-fiberglass composite) were then shaped around the foam positive and solidified through a series of three laminations. The ROI that would be used for future OCT imaging was also captured during the socket fabrication process and transferred so that the location could be visualized inside the finished socket. Fabrication steps are shown in Figure 3.17.

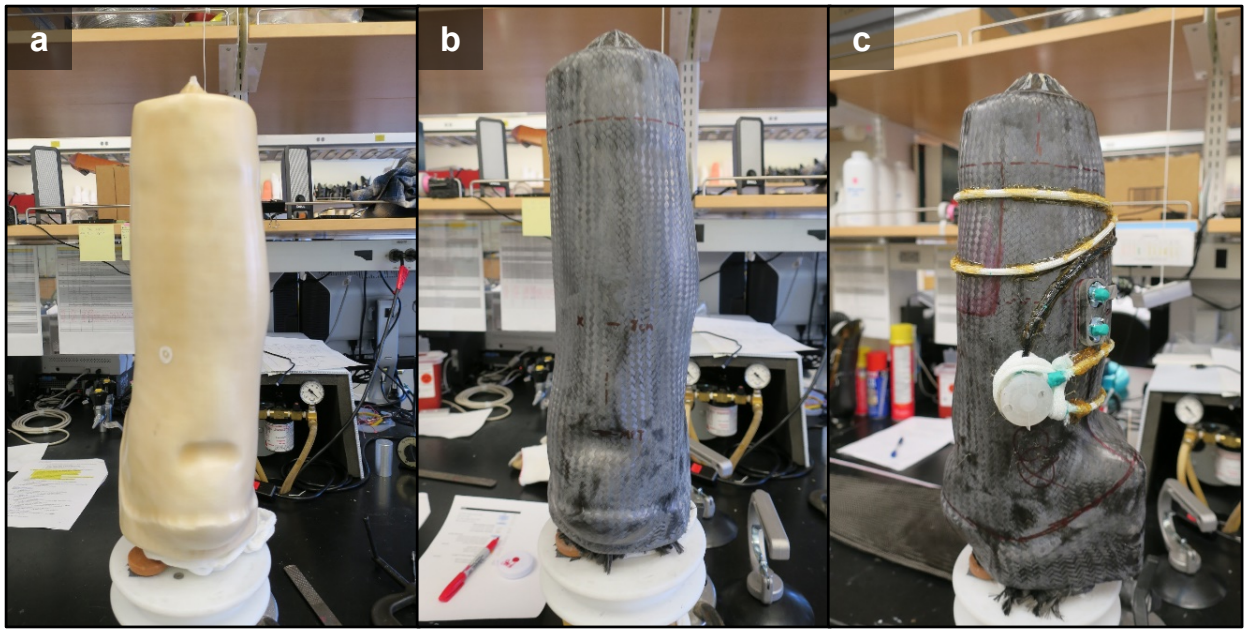

Figure 3.17. Able-Bodied Sockets were fabricated using three laminations. (a) 1: two layers of nylon-fiberglass formed the internal shape and provided a translucent material so the ROI could be seen inside the socket. (b) 2: two layers of carbon fiber provided a rigid base for socket componentry to be placed on. (c) 3: socket components were placed and two layers each of carbon fiber and nylon-fiberglass were laminated over them (shown prior to adding fiber layers).

Sensors. Sensors were used to monitor the participants' use of their sockets. Together, the sensors provided information related to the time the socket was worn, what general activities participants performed while wearing the socket, and gave an estimate of the pressure acting in the ROI.

Accelerometers. Two accelerometers were used to monitor activity during daily wear of the Able-Bodied Socket (Figure 3.18). The commercially available three-axis accelerometers (Actilife Actigraph GT3X+, Pensacola, FL, USA) recorded data continuously at 40 Hz to an onboard data acquisition unit. One accelerometer was adhered to the external surface of the participant's liner at the distal thigh, proximal to the socket trimline. A second accelerometer was placed at the ankle. Data from the accelerometers and don-doff information from the dial sensor and ROI force sensor (below) were input into an automatic activity classification algorithm previously developed in our lab (Figure 3.19) [100]. These data were used to better understand types of activities participants participated in while wearing the sockets. This information was collected to (1) verify the

participant had worn the socket for the approximate durations which they reported and (2) to provide additional information that could potentially explain differences in OCT measurements between participants.

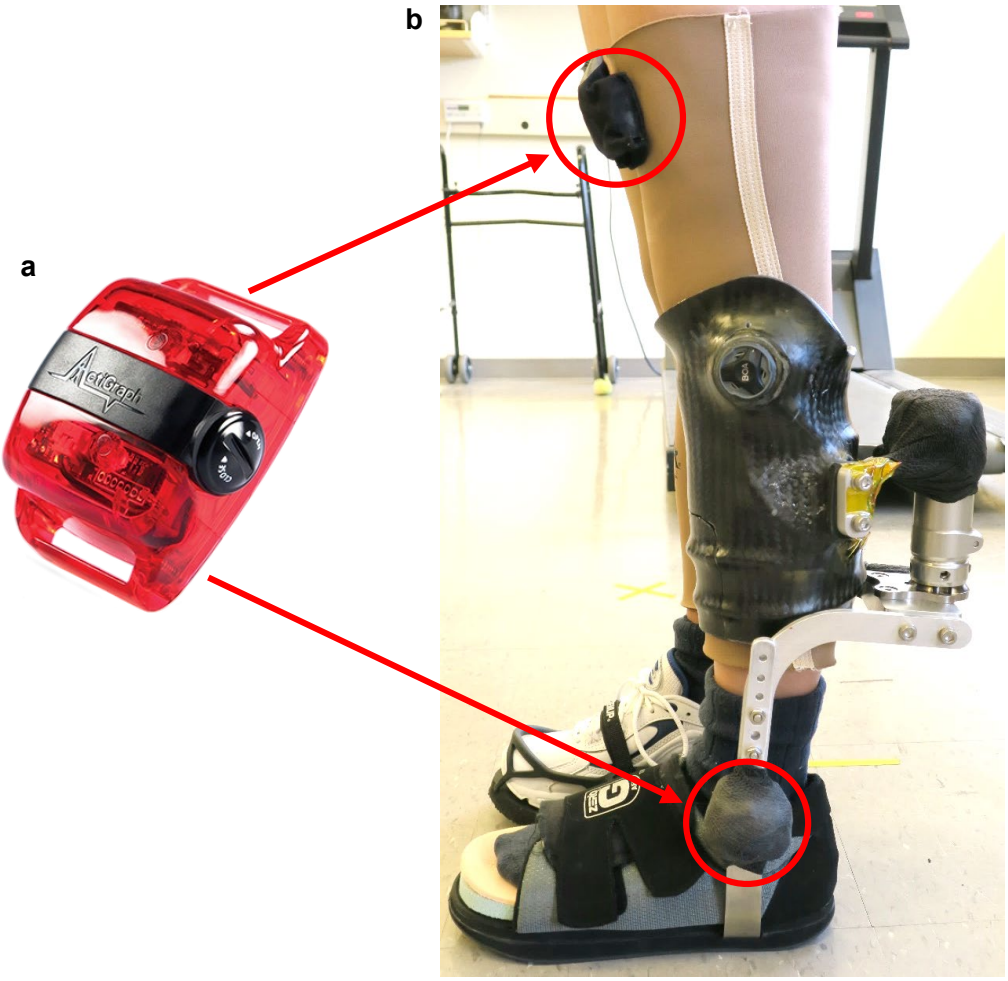

Figure 3.18. Accelerometers for activity classification. (a) Close-up of the accelerometer used in this study. (b) One accelerometer was placed at the thigh and one was placed at the ankle.

Figure 3.19. Sample activity classification data. Sitting (red), standing (yellow), walking (green), and doffed (blue) periods are shown for versus time and summarized for each day.

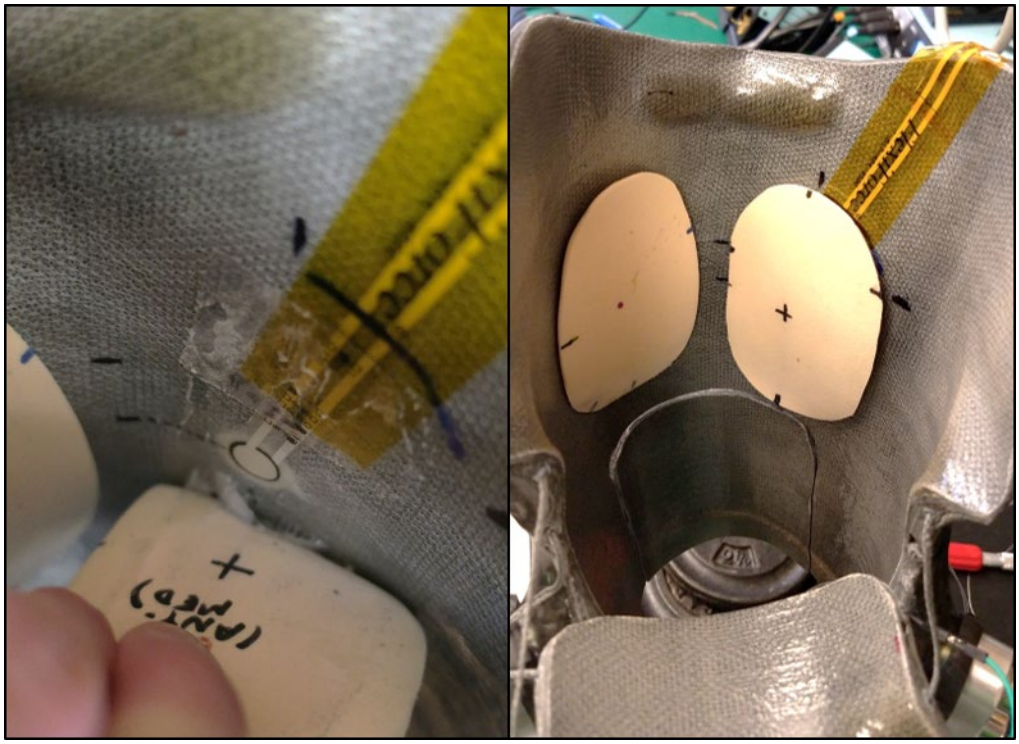

Figure 3.20. Force Sensing Resistor (FSR). Placed at the ROI to monitor trends in pressure between the limb and socket wall.

Force Sensing Resistors. A common force sensing resistor (FSR) model used in prosthetics research (Flexiforce A201, Tekscan, Inc., South Boston, MA, USA) was used here to monitor interface pressure between the limb and the socket wall. FSRs are piezoresistive sensors, whose resistance changes in response to changes in force applied to the sensing area. One FSR was adhered to each socket using two-sided adhesive tape (SpeedTape, FastCap, Ferndale, WA, USA) at the ROI that corresponded to the site of OCT imaging (Figure 3.20).

A Flexiforce sensor was chosen over other FSR options after extensive testing which suggested the Flexiforce sensor would perform better when used to measure limb-socket interface pressures in prosthetics [101]. Although the limitations of FSR accuracy for prosthetics interface measurements was well documented in the aforementioned study, the advantages of these sensors are that they are inexpensive, relatively easy to use, and low-profile enough so that they did not affect socket fit. It was shown that errors may be as large as ±44% for some activities when the FSRs are calibrated on the benchtop versus being installed in the socket [101]. As such, in the current study the sensors were not meant

to obtain reliable pressure measurements; rather, these data were used (1) as verification that contact was being made between the limb and socket at the ROI to further improve the accuracy of the activity classification algorithm and (2) as rough pressure estimates that could be compared between individuals to determine if individuals with significantly more pressure at the ROI experienced larger changes in OCT measurements.

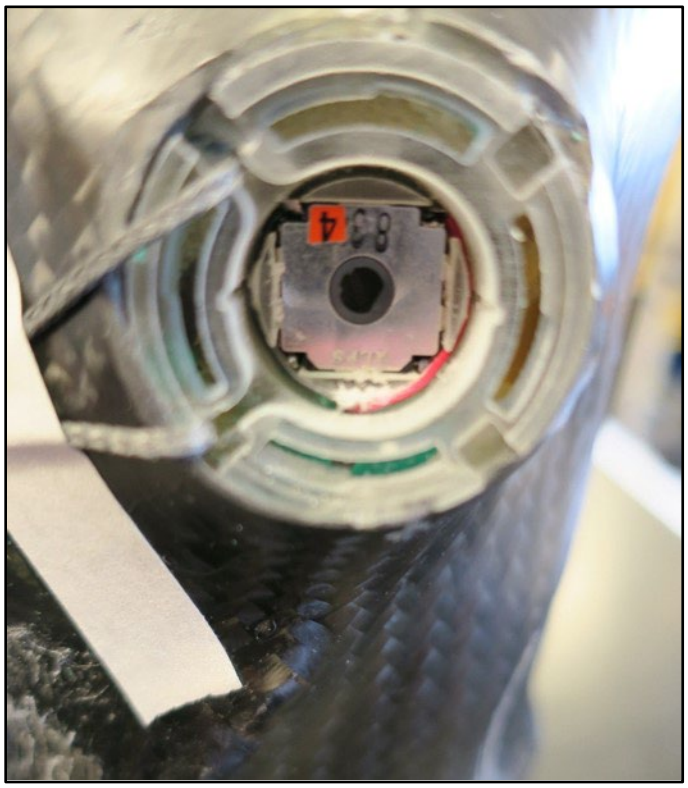

Figure 3.21. Dial sensor. Pictured here within the custom 3D-printed housing with the dial and coupler removed to expose the sensor.

Dial Sensor. A potentiometer-based sensor was used to track the rotary motion of the panel cable dial to monitor when study participants adjusted the socket panels (Figure 3.21). A custom housing was designed to contain the sensor and was laminated into the socket wall. A coupler was fabricated to connect the base of the dial to a rotary sensor which output a two-phase signal that tracked the rotational position of the dial. A tube was fabricated into the socket walls to serve as a conduit for the sensors' wires. The wires connected into the data acquisition device, described below, which collected dial position data. While this iteration of the sensor was unable to maintain the absolute position of the

dial throughout the course of the study, the sensor data was analyzed to determine when the participant had interacted with the socket to loosen or tighten it.

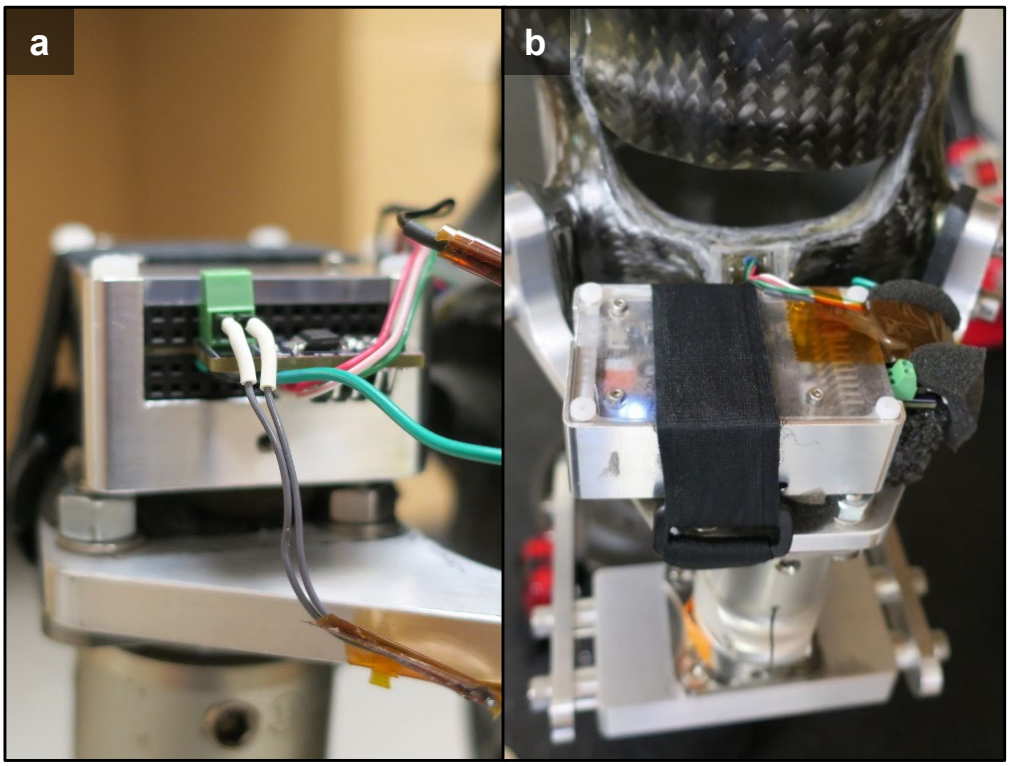

Figure 3.22. Data Acquisition Device (DAQ). (a) Close-up of the device's inputs and outputs showing the FSR shield designed for this study. (b) DAQ installation on top of the alignment assembly.

Data Acquisition Device (DAQ). A DAQ was used to record data from the FSR and dial sensor (Figure 3.22). Data were continuously stored to a microSD card at 32 Hz. The device was powered by an onboard lithium-polymer battery, requiring the unit to be plugged in by study participants at a minimum of once every two nights. The device used a 16-channel analog-to-digital converter (AD7173-8, Analog Devices, Norwood, MA, USA) and a 32-bit ARM Cortex-M0+ microcontroller (LPC11U67, NXP Semiconductors, Eindhoven, Netherlands). The entire unit was placed within a custom-designed aluminum enclosure (71.0 mm x 46.5 mm x 30.0 mm). The total mass was 114.4 g. For the current study, a custom electronics shield was designed and fabricated to enable data collection using the FSR. This circuit was needed to ensure the voltage supplying the FSR remained

below 2 V, since Flexiforce FSRs are known to suffer excitation voltage-dependent signal degradation at voltages above 2 V. These electronics are further described in Appendix B.

3.3 Test Method Development

Three tests will be developed for future aims:

3.3.1 *Reactive Hyperemia Test*

Rationale. Microvascular function was assessed by inducing and measuring a reactive hyperemia (RH) response to a repetitive stress. RH is a commonly studied biological response used to assess the function of blood vessels [39]. In the current research, the RH response was measured using repeated time-series OCTA images followed by quantifying the VAD (vessel area density) in each image. The RH response was induced using the BLA, which applied cyclic compressive and shear stress similar to the stresses imposed on transtibial residual limbs at the limb-socket interface.

Test preparation. At the start of all test sessions, the ROIs on the lower limbs to be imaged were selected and the areas were marked using a surgical marker. In the case of Aim 2 these marks were often preexisting temporary tattoo ink, placed at prior test sessions. These fiducial markers outlined the edges of the ROI and were spaced far enough to ensure the ink was outside of the imaging field-of-view and thus did not alter the OCT laser penetration. The RH Test began with an initial baseline OCT image, captured following an acclimation period of at least 15 minutes in the imaging position (supine, legs immobilized using a positioning pad and slightly elevated). The imaging window was selected by placing the center of the OCT image at the center of the fiducial markers. OCT imaging details used for this test are described below.

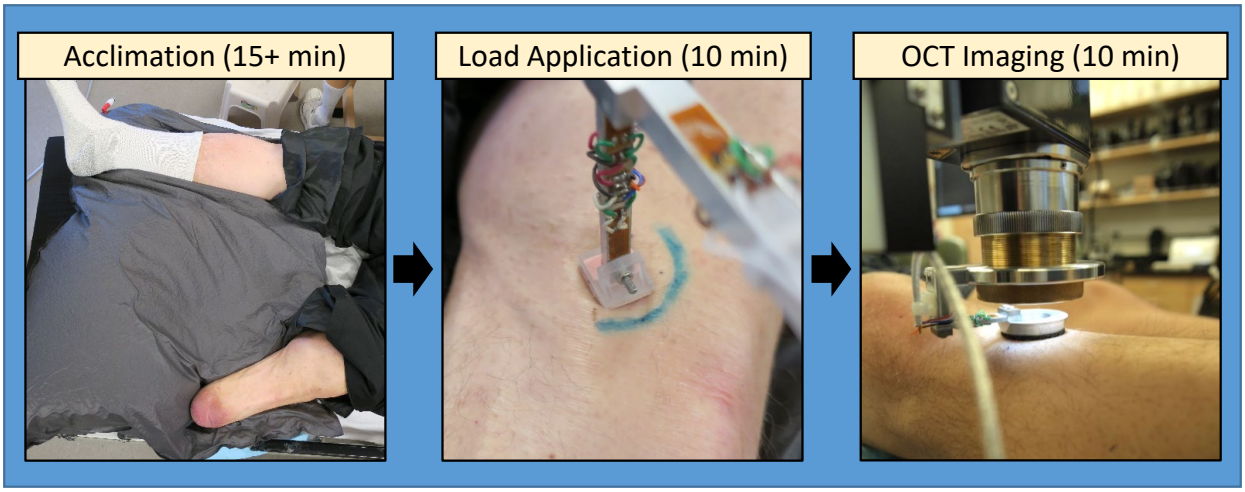

Figure 3.23. Reactive Hyperemia Test flow. The RH Test began with a supine acclimation period of at least 15 minutes. Load was then applied for 10 minutes using the Biaxial Load Applicator followed by OCT image collection for 10 minutes.

Load application. A stress stimulus was then applied using the Biaxial Load Applicator, followed by measurement of the response through repeat OCT images (Figure 3.23). Stress was applied in a sinusoidal cyclic waveform which cycled from approximately 50.6 kPa to 5.1 kPa pressure and 5.1 kPa to 0 kPa shear stress (Figure 3.24). These values represent common stresses seen during ambulation measured in individuals with transtibial limb loss [98]. Preliminary studies demonstrated that a 10-minute stress application period using this stress was sufficient to achieve a reliable RH response in able-bodied participants and transtibial prosthesis users (unpublished).

OCT image collection. For this test the OCT images had a 2.0 x 2.0 mm field-of-view, 200 x 200 pixel resolution, and five B-scan repeats for vessel imaging. These parameters were chosen to balance field-of-view, resolution, and speed of imaging. Care was taken by the operator to ensure each image was captured with the focal depth set to just below the DEJ and that the pressure applied by the OCT probe was always below 4.5 kPa to ensure blood flow was not perturbed by the probe itself. Pressure and focal depth were adjusted using the two vertical stages attached to the OCT probe.

Following the stress application, the Biaxial Load Applicator was moved away, and the OCT imaging probe was quickly placed back onto the skin, over the stressed region. As with the baseline image, the imaging window was centered once again by placing the center of the field-

of-view at the center of the fiducial markers. The vertical displacement stages were then adjusted to set the depth of focus and OCT probe pressure as described above. Post-loading imaging then began, with images captured every 10-15 seconds for a total of 10 minutes. Periodically the OCT system was switched into live B-scan mode so the imaging depth of focus could be verified. Changes were then made as needed to ensure the focal depth and pressure was maintained as the compressed skin recovered or in response to participant movement. This was done at least once every minute or any time a change was suspected, such as following any participant movements which could be visualized as changes in the real-time plot of OCT probe pressure.

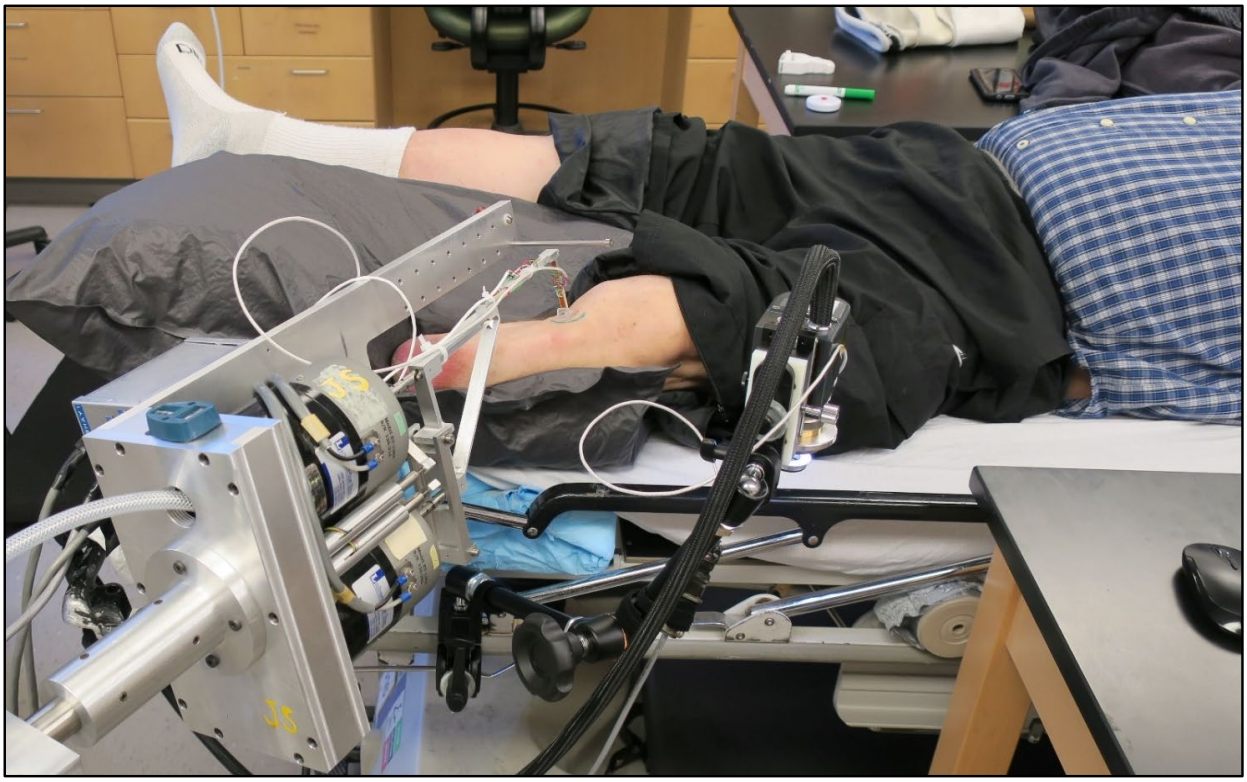

Figure 3.24. Load application during the RH Test. Participants laid supine on a hospital bed. As shown here, the Biaxial Load Applicator was often rotated so that the load applicator pad matched the angle of the skin's surface, thus reducing pressure concentrations on the edges of the pad.

OCT images captured during the RH Test were processed to create two-dimensional *en face* vessel images using the methods described in Section 3.2.1. The VAD (vessel area density) of each image was then calculated for each image. This measurement was an indication of amount of blood flowing through the tissue at the time the image was captured. While image processing

thresholds were varied slightly between tests to account for varying tissue illumination, resultant pixel intensities, or noisy image sets, all the images within a single RH Test were processed using the same parameters. Since the functional response of the microvasculature was of interest in this test, the VAD was plotted versus time. To account for variability between measurements the VAD curve was smoothed using a 3-point running average. An example of this is shown in Figure 3.25.

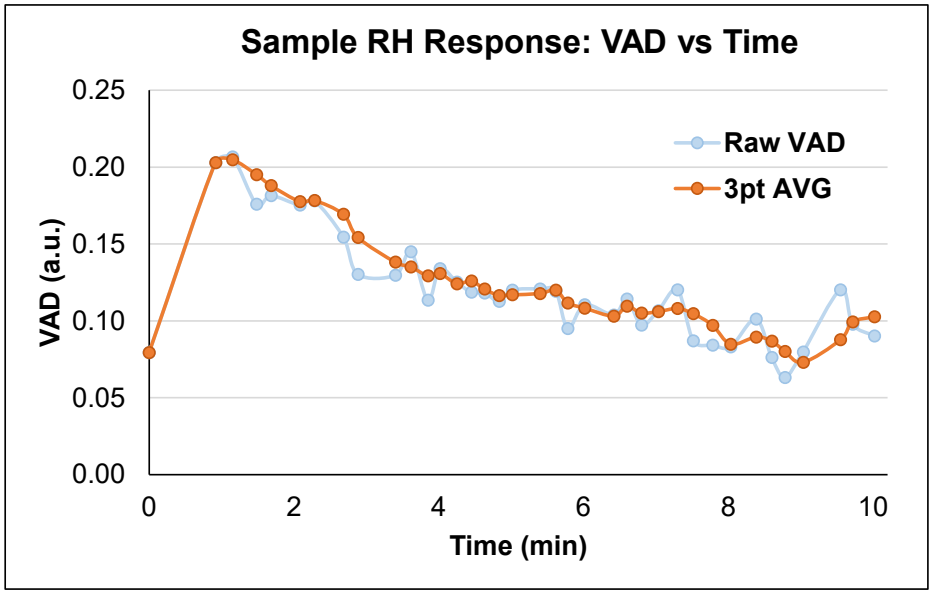

Figure 3.25. Sample RH curve showing raw and smoothed curve. VAD response curves were smoothed using a 3-point running average.

RH Test measurement quantification. The key features used to assess the response were extracted from the smoothed curve. These included "**peak VAD**," "**time-to-peak**" VAD, and "**recovery time**" (Figure 3.26). The calculation details and physiological significance of these features is described in Section 2.2.4. Briefly, the peak VAD was determined as the maximum VAD reached during the response, which indicated the magnitude of the blood flow increase in the RH response. The time-to-peak was then determined as the time it took to reach the peak VAD. To understand how well the tissue resolved its response to the imposed stress, the recovery time was determined. The recovery time was defined as the point at which the VAD returned 75% of the way back to the baseline VAD value from the peak VAD value, as determined by the following equation:

$$VAD_{baseline} + \left[\left(VAD_{peak} - VAD_{baseline}\right) * (1 - 0.75)\right] \quad (3.1)$$

A 100% return to baseline was not used because it was rare that the VAD fully recovered to the original baseline value within the time allowed for this test, despite visible redness resolving.

The 75% recovery was usually achieved. In the case that the 75% recovery value was reached but subsequently rose above this value, a later recovery time value was chosen where the VAD did not rise above the 75% recovery value for the remainder of the test.

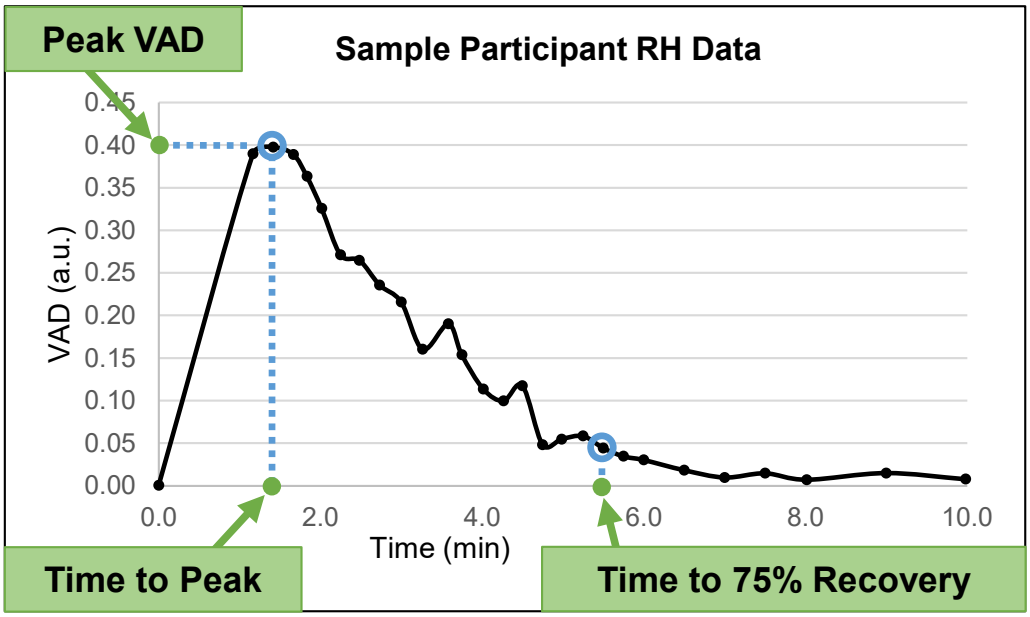

Figure 3.26. Sample RH curve with key features identified. These features include: **peak VAD**, analogous to peak blood flow; **time-to-peak**, the speed of the response; and **recovery time**, an indicator of how quickly the tissue returns to a near-normal state, defined as a 75% VAD recovery to baseline.

3.3.2 *Maximum Dilation Test*

Rationale. The Maximum Dilation Test was used to visualize and quantify cutaneous microvascular structure. The microvasculature of the skin is highly active and is actively modulated by several different mechanisms simultaneously. In order to measure vessel structures and enable reliable comparisons between limbs (Aim 2 and 3) and over the course of a multiple day adaptation protocol (Aim 2), a repeatable state had to be induced. This is commonly achieved in cutaneous microvascular studies by inducing a state of maximum vessel dilation through a local skin heating protocol [102]. In the current work, we applied heat locally using an electric heater and captured OCT images once a state of maximum dilation was reached. From the obtained OCT images, vessel structure was assessed qualitatively and quantitatively using the metrics VAD (vessel area density), vessel count, and vessel diameters.

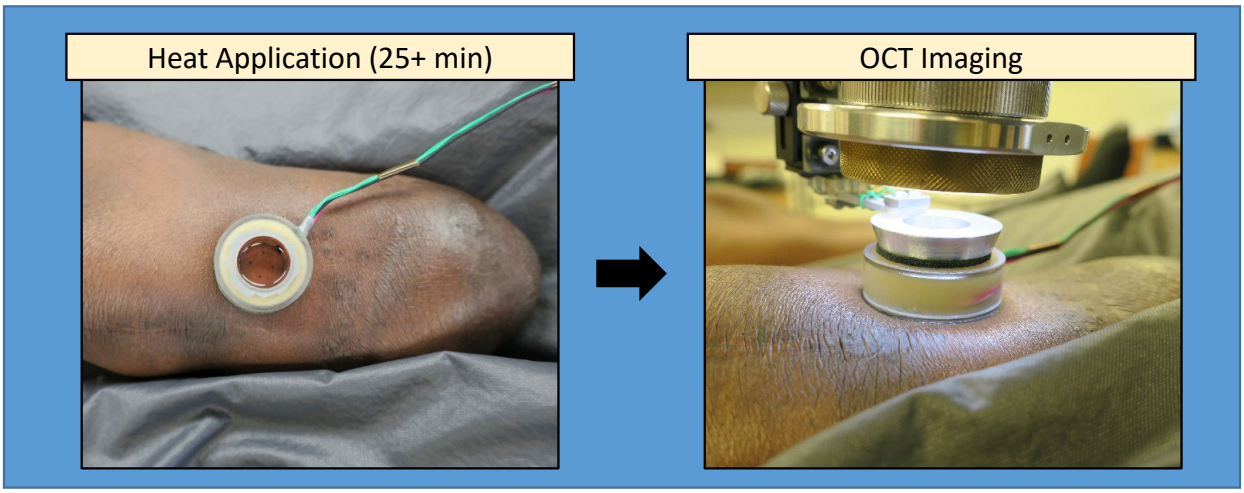

Figure 3.27. Maximum Dilation Test flow. A heater probe filled with mineral oil warmed the skin to 42-44 °C for at least 25 minutes to induce maximum vessel dilation. OCT images of the skin were then taken through the oil.

Methods. A skin heating probe was developed to induced maximum dilation in the skin ROI. OCT images were then captured of the heated skin (Figure 3.27). Our heating device was modelled after a commercially available skin heating device commonly used in cutaneous microvascular studies (moorVMS-HEAT and VHP3 probe, Moor Instruments, Axminster, UK). While OCT imaging had never previously been used in this manner before, the commercially available heater probe is commonly used with Laser Doppler Flowmetry and Laser Doppler Perfusion Imaging, which also use infrared light to penetrate and measure the skin.

Heater probe. The heating probe used in this study was shaped as a disc with a circular chamber at the center, creating an opening through which the skin could be imaged (Figure 3.28). The chamber was filled with a medium which was heated by a copper ring wrapped externally with a high resistance nichrome wire. The heater footprint (20.5 mm ID, 38.0 OD) was optimized to present a large enough surface of skin for the desired OCT field-of-view while maintaining a small enough outer footprint to fit on the flat medioproximal aspect of most tibias. The height (13.0 mm) was chosen to maximize the copper heating surface while still allowing the OCT probe with its pressure measurement attachment to get close enough to the skin so the focus could still reliably reach the desired depth. The heater probe enclosure was designed in-house and fabricated out of thermostable polymers using a 3D-printer.

The heater probe contained two surface-mount thermistors which were used to monitor operating temperatures. One thermistor was potted in an electrically insulating potting compound (Hysol ES2500, Henkel, Düsseldorf, Germany) and inserted into a small hole drilled in the side of the copper ring. This thermistor was used to monitor the temperature of the chamber medium. The second thermistor was installed in direct contact with the copper ring on the non-medium side of the ring in the device internals. Thus, this thermistor monitored the temperature of the copper ring and served as a back-up safety. The electronic schematics for the heater and thermistors are shown in Appendix A. Once wired, the internals of the probe enclosure were potted in silicone and polyurethane adhesive and sealed with polyurethane adhesive. These steps ensured that the heater would not be infiltrated by the chamber medium and potentially damage the device or risk harming the study participant.

The heater was controlled using a PID controller developed in a custom LabVIEW application which ran on the same controller device used for the Biaxial Load Applicator. The control system process variable was the temperature measurement from the medium-measuring thermistor. The PID controller output modulated the duty cycle of the 5 V USB power supplied to the heater coil in order to heat the probe and maintain temperature at the set point. The PID controller was able to control the heater to within 0.1°C of the set point. Safety limits were also programmed to shut off power to the heater if the temperature measured by either of the two thermistors became too high.

Accurate medium temperature measurement of the probe thermistor was verified by comparing a range of medium temperatures with measurements taken using a commercially purchased thermocouple device and commercially purchased thermistor device. Through multiple preliminary tests it was found that by setting the medium temperature at the thermistor to 51.5°C, the desired skin surface temperature of 42-44°C could be achieved.

Mineral oil was chosen as the heating medium to be placed in the chamber, though water, glycerol, and ultrasound gel were also trialed. Compared to all options tested, mineral oil provided the clearest vessel images. Water resulted in significant attenuation of the OCT signal and thus a noisy vessel image with poor imaging depth. Glycerol performed almost as well as mineral oil, however glycerol resulted in a slightly more attenuated OCT signal compared to mineral oil, as evidenced by a visibly apparent reduction in imaging depth. Ultrasound gel was trialed in an effort to further reduce motion artifacts that occurred when movements of the skin caused the medium

surface to ripple. While ultrasound gel's higher viscosity did significantly reduce the motion artifacts, we were unable to prevent the formation of bubbles, which severely disrupted the images. The gel also caused a slightly more attenuated OCT signal compared to the mineral oil. The chamber was filled with 2.0-3.0 ml of mineral oil for each test.

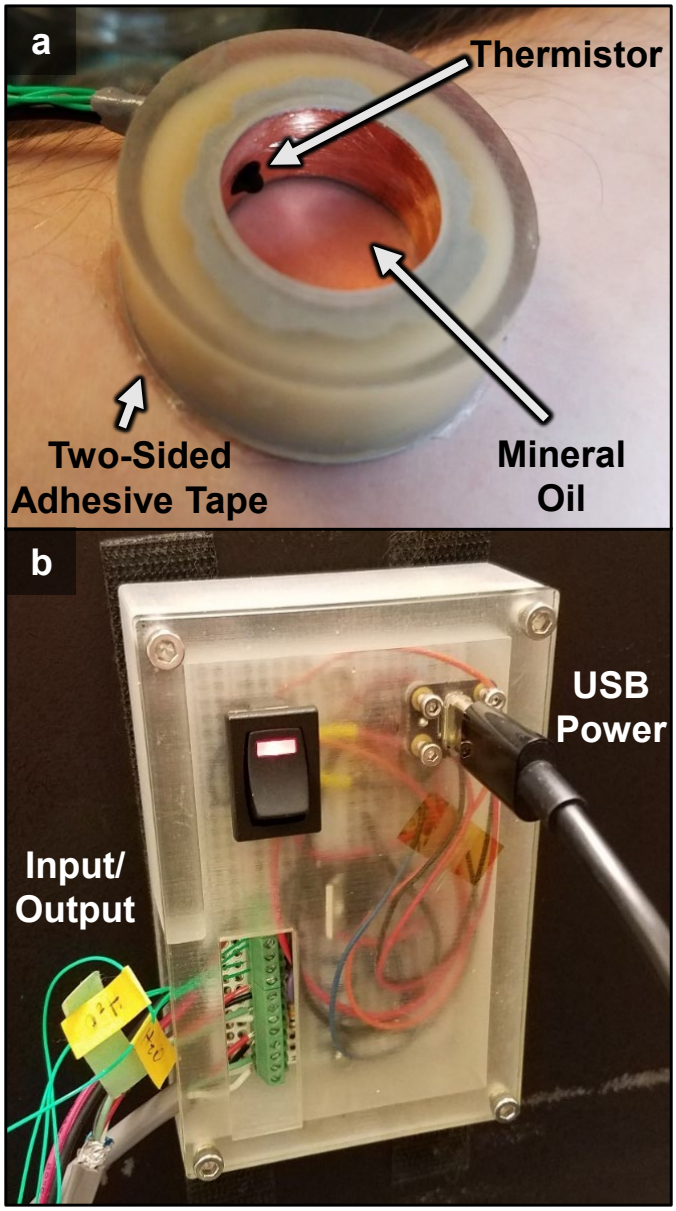

Figure 3.28. Skin heating system. (a) Heater probe, shown adhered to skin. (b) Heater electronics enclosure.

The heater probe was adhered to the skin using a double-sided adhesive (1522 double-coated medical tape, 3M, Minneapolis, MN, USA). While several other double-sided adhesive tapes were trialed, this tape provided the lightest adhesion among the options that did not allow the oil to leak. The tape was cut to the shape of the heater footprint using hollow punch tools.

Heating protocol. Skin was heated to 42-44°C, which is a commonly used temperature for maximum cutaneous vasodilation [102]. Past studies have suggested 20-30 minutes are required to achieve a stable maximum dilation [39]. In the current study we heated the limb for 25 minutes and then began collecting images.

OCT images. For this test two to three full field-of-view OCT images were captured once the skin had been heated for 25 minutes or longer. Each full OCT image was split into four sections in order to limit motion artifacts. In preliminary trials OCT images of 6 x 6 mm (600 x 600 pixels) and larger showed significant motion artifacts. The motion artifacts appeared periodic and were likely caused by small movements of the skin surface that were induced by the blood pulse. As described in Section 3.2.1, this artifact resulted when the five repeat B-scans taken at a single cross-section were moved with respect to one another. Thus, to reduce this motion, the time of each B-scan was reduced significantly by reducing the B-scan size to 2.0 mm, 250 pixels. The y-direction (C-scan) remained large and was chosen to be 7.4 mm, 740 pixels. An overlap of 0.2 mm between image sections was found to be sufficient. Thus, the final images after stitching were approximately 7.4 x 7.4 mm with 925 x 740 pixel resolution. The x-direction was oversampled to increase the image quality. A comparison of full versus split images is shown in Figure 3.29.

Image capture took approximately 17 seconds per segment and an additional 20 seconds to store each segment. During imaging, the OCT operator monitored the OCT probe pressure measurement signal and a video of the OCT probe alignment on the skin to verify no noticeable movements occurred. If movement occurred that was suspected to potentially induce a large motion artifact or shift the field-of-view, the segment or the full field-of-view image was redone.

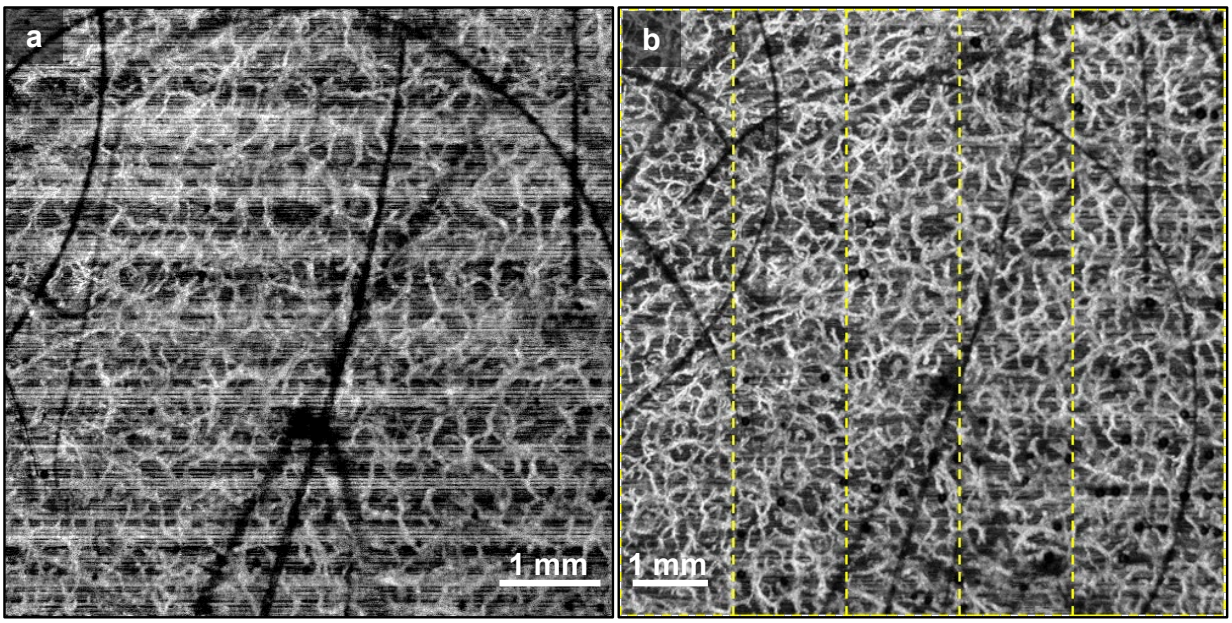

Figure 3.29. Maximum Dilation Test split field-of-view imaging. (a) Single *en face* OCTA image, 6.0 x 6.0 mm, 600 x 600 pix. (b) Split field-of-view image of the same region of skin. Four separate images (2.0 x 8.0 mm, 250 x 800 pix), indicated by the yellow dotted lines, were stitched into a full field-of-view image.

Images were processed as described in Section 3.2.1. Individual segments were stitched together to produce a full field-of-view image using a grid image stitching plugin in an image processing program (FIJI, ImageJ [103–105]). In addition to the full-depth image, two depth-segmented images were created for each test result: one approximated the more superficial papillary dermis and the other approximated the deeper reticular dermis. Since images had already been segmented to remove everything superficial to the DEJ, and since the imaging depth could not reach beyond the reticular dermis, each OCTA volume simply needed to be separated into two volumes. This was approximated to be at a single depth below the DEJ, chosen visually by scrolling through individual two-dimensional depth (x-y) slices and choosing a transition point just above where the first larger vessels appear. The separation usually occurred at a depth of 0.14-0.25 mm below the DEJ, which is consistent with values used by others [106,107]. An example is shown in Figure 3.30. It should be noted that due to a shadow effect often seen in OCT images, the reticular dermis images often contained some of the larger vessels from the papillary dermis. These depth sections were then transformed into *en face* images and quantified as described in Section 3.2.1.

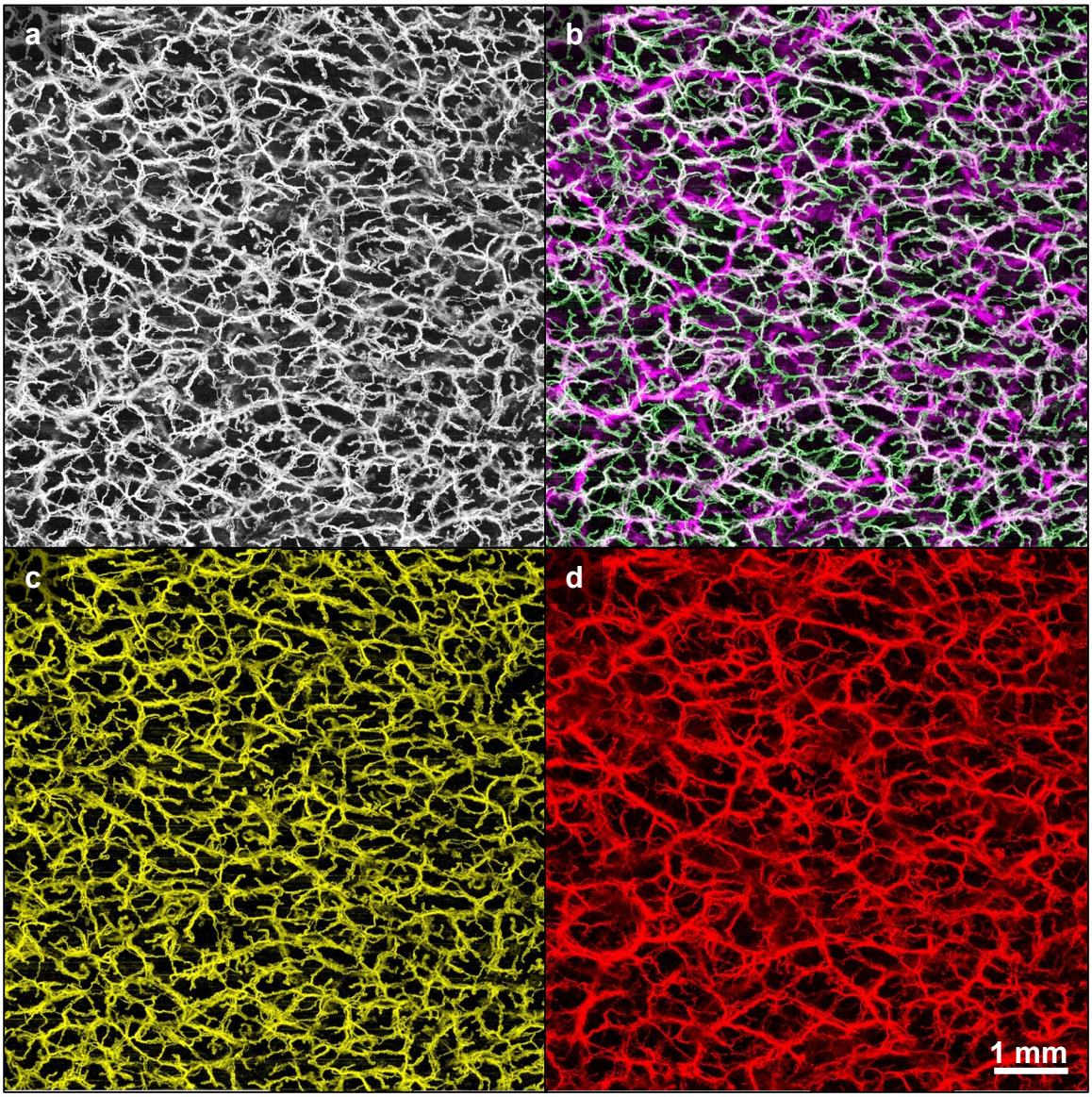

Figure 3.30. Maximum Dilation Test image with depth separation. (a) Stitched *en face* OCTA image. (b) Depth-separated image showing papillary dermis vessels (green), larger reticular dermis vessels (purple), and vessels shared by both layers due to shadow effects (white). (c) Papillary dermis. (d) Reticular dermis.

3.3.3 *Load Tolerance Test*

Rationale. In Aim 3, in order to determine if the able-bodied skin adaptation protocol had in fact made skin more load tolerant by current clinical assessment, a test was performed before and after the protocol to evaluate skin load tolerance. This test used methods similar to the current clinical means of determining skin load tolerance in order to determine if the Able-Bodied Socket wear

protocol had induced skin to become more load tolerant by current clinical measures. The test consisted of a mechanical load stimulus followed by a tolerance evaluation that was performed by a blinded clinical expert.

No objective measures for skin load tolerance currently exist. The method currently used in clinical practice to determine if skin is tolerating a load is to subject skin to socket interface stresses by having a patient walk in their prosthesis and then have them doff the socket while the clinician monitors the duration and type of skin redness. Skin that that exhibits blanchable erythema that resolves in less than 10-20 minutes is said to be tolerant to the load. Skin that exhibits blanchable erythema that does not resolve in less than 10-20 minutes or skin that exhibits non-blanchable erythema for any amount of time is said to be not tolerant to the load. Some sources cite this threshold as 10 minutes [25], others cite up to 20 minutes [55]. The Load Tolerance Test used in this study uses this method. The test protocol is summarized in Figure 3.31.

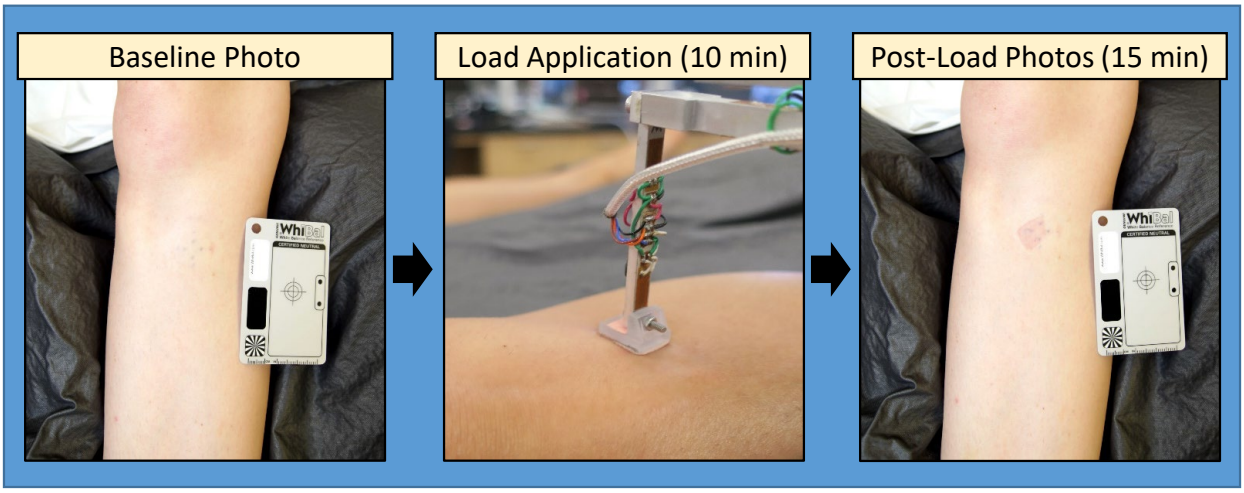

Figure 3.31. Load Tolerance Test protocol. Baseline photographs were taken, load was applied for 10 minutes, and post-load photos were taken for 15 minutes. A white-black balance card and flat lighting were used to for color repeatability.

Load stimulus. The Biaxial Load Applicator was used to apply the load for this test to ensure the stimulus that was applied to the skin was repeatable at each test. A repeatable load was essential so that tolerance to the same load was being assessed every time. Stress was applied for 10 minutes sinusoidally at 1 Hz from 10.1-69.3 kPa compression and 0.0-10.1 kPa shear stress. These values were chosen based on preliminary tests which suggested skin that had not undergone an adaptation loading protocol would maintain redness for greater than 10 minutes but no longer than 1 hour.

Tolerance evaluation. As described above, the current clinical load tolerance evaluation is to monitor skin redness following an applied load. If redness lasts for less than 10-20 minutes, the skin is said to be tolerant to the load, and if not, the tissue is said to be not tolerate to the load. In this study, the 10-minute threshold was used.

Redness was evaluated from photographs that were taken using a repeatable lighting setup followed by a color-correction method. These methods ensured the unstressed skin color remained approximately the same throughout the course of each test and between tests performed on a participant before and after wearing the Able-Bodied Socket for two weeks. A camera was placed 20.0 cm directly above the ROI and set to manual mode, using the same settings for every image. A photography soft box with a light diffuser was placed directly behind the camera to illuminate the skin with flat lighting, which has been shown to achieve photos with the most accurate skin color [108]. A white/black balance card (WhiBal G7 White Balance Pocket Card, PictureFlow LLC, Melbourne, FL, USA) was placed in the image next to the ROI. The setup is shown in Figure 3.32. Using this setup, a photograph was taken prior to the load stimulus to capture baseline redness and once per minute for 15 minutes following the load stimulus removal. Following the test session, the white and black balance within each photograph was set to the respective swatches of the white/black balance card in an image processing program (GIMP 2.8.22, www.gimp.org).

The color-corrected photographs within each test were randomized and presented to a physician specializing in rehabilitation of lower limb prosthetic users. Baseline images were not randomized and provided a sample photograph of skin that did not present any load stimulus related redness. Each post-load photograph was compared to the baseline image and the clinician graded the skin in the ROI as “red” or “not red.” Using these grades, the researcher was able to determine the time at which redness had resolved, according to clinical assessment.

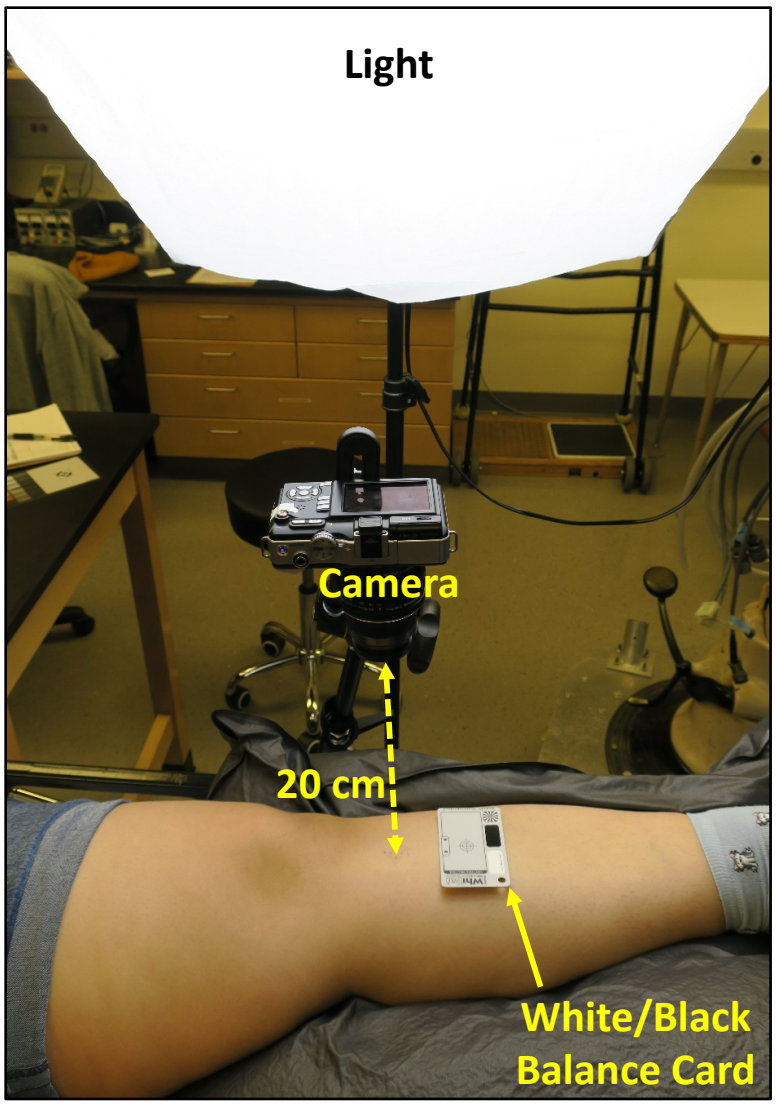

Figure 3.32. Load Tolerance Test setup.

Chapter 4. AIM 2: INVESTIGATE SKIN ADAPTATION THAT IS INDUCED IN ABLE-BODIED PARTICIPANTS

4.1 ABSTRACT

Background: A majority of lower limb prosthesis users are negatively impacted by skin breakdown induced by mechanical stresses at the interface between the residual limb and prosthetic socket. While it is known that skin can adapt to these stresses to become more resistant to breakdown, little is understood about skin adaptation and few methods exist to noninvasively investigate it. Optical Coherence Tomography (OCT) is a noninvasive imaging technique with a depth and resolution balance that is well-suited for investigating skin adaptation. The use of an able-bodied model for studying skin adaptation is desirable so that adaptation can be studied in a controlled manner as it occurs.

Objective: This study aimed to investigate biomarkers for skin adaptation to lower limb prosthesis stresses using noninvasive OCT imaging techniques in able-bodied participants whose skin was mechanically stressed by a modified below-knee prosthetic socket for two weeks.

Study Design: Repeated measures observational study of healthy study participants without a lower limb amputation (N=8).

Methods: Modified prosthetic sockets were molded specifically to match each participant's lower limb. Participants wore the socket for two weeks following a schedule of increasing daily wear times that resembled a prosthetic training program used to introduce a prosthetic socket for the first time after an amputation. The OCT-based microvascular tests developed in Aim 1 were used to capture cutaneous microvascular structure and function at three time points: (1) prior to limb loading, (2) after one week of socket wear time, and (3) after the completion of the two-week wear program. Skin measurements at a highly-loaded region within the socket—the test region of interest (ROI)—were compared longitudinally between these time points and were also compared to measurements taken at a location-matched control ROI on the unloaded contralateral limb.

Results: Participants wore the sockets without complications for the entire two-week period. Measurements of cutaneous vascular function demonstrated that a measurable reactive hyperemia response was reliably induced in the study participants, however no statistically significant differences in peak VAD, time-to-peak, or recovery time were found between the test limb and

control limb or between the three time points. Measurements of vessel structure demonstrated good repeatability of the imaging location throughout the course of the study. No statistically significant differences were found in measurements of vessel density, vessel count, and mean vessel diameter between time points or test versus control ROI. A small increase in epidermal thickness was demonstrated at the test ROI after wearing the socket for two weeks, however this difference was not statistically significant.

Conclusions: This study introduced new noninvasive techniques to investigate skin adaptation to mechanical stress, which could also be used to study skin health more broadly. The results highlighted the utility of these tests as well as current limitations of the methods. If the key limitations are addressed, these methods have the potential to provide insight into the function and structure of the cutaneous microvasculature that previously could not be attained.

4.2 RATIONALE

The purpose of this aim was to investigate physiological changes that occur in lower limb skin in response to dynamic shear and compressive stresses that may enable skin to become more load tolerant. This study focused on investigating adaptation within the cutaneous microvasculature due to the important role these vessels have in maintaining tissue viability and the recent development of noninvasive imaging techniques available to investigate it. The interface stress applied by the socket and the loading schedule were designed to mimic the prosthetic training process that is used to introduce the first prosthesis during rehabilitation from a transtibial amputation. An able-bodied model is useful because it enables the study of skin that is adapting to mechanical stresses for the first time without the presence of confounding variables that will be present in the study individuals who have recently had an amputation, such as activity limitations due to muscle atrophy or suture site sensitivity. We hypothesized that adaptations to the microvasculature may occur which would enhance the skin's ability to supply blood to the tissue, in particular following an occlusive stress.

4.3 METHODS

4.3.1 *Participants*

Study participants were chosen who were healthy individuals without a lower limb amputation (i.e. "able-bodied" participants). Individuals between the between the ages of 18-55 years were

recruited to limit confounding factors that are known to occur in skin with older age [109]. Participants were excluded if they had diabetes or dysvascular disorders, or if they were smokers, since changes in skin microvasculature have been demonstrated in these populations [109]. Participants were also excluded if they had any known incidences of skin breakdown at the regions of interest (ROIs) to be tested. Inclusion and exclusion criteria were assessed through self-reporting by the participant and a skin evaluation of the ROIs prior to beginning study activities. Participant demographics were collected using a self-reported survey. The survey included questions related to sunburn and suntan tendencies, which were used to estimate the Fitzpatrick Skin Phototype (FSPT) of each participant, as previously described [110,111]. FSPT ranges from I to VI and has been used in dermatology to predict the risk of skin cancer and provide sun-protection guidance, among other uses [112,113]. While skin type has not systematically been studied in relation to skin load tolerance or adaptation, clinical care often considers lighter, fairer skin to be generally more fragile than darker skin [114,115]. All study procedures were approved by a University of Washington Institutional Review Board and informed consent was obtained before any test procedures were initiated.

4.3.2 *Regions of Interest (ROIs)*

For each participant, a test ROI was selected on the test limb that would be the site of investigation used in all imaging sessions. The target location for the ROI was the medioproximal aspect of the tibia. This location was selected since it was an area where high interface stresses were expected within the Able-Bodied Socket and it was easily accessed by study instruments. A location-matched ROI on the contralateral limb served as a control during imaging sessions. A prosthetic liner was worn on both limbs when the socket was donned to control for potential changes induced in the skin due to mechanically interacting with the liner or heating of the skin by the liner. To ensure similar vessels were imaged during each session, the ROIs were marked throughout the study using semi-permanent temporary tattoo ink (Freehand Ink, InkBox, Toronto, ON, Canada). Marks were made around the ROI but not in the imaging region to ensure the ink did not obstruct penetration of the OCT light into the skin.

4.3.3 *Able-Bodied Sockets*

Able-Bodied Sockets were fabricated to fit the limb shape of each study participant. The socket was designed to apply mechanical stresses to the skin surface that would resemble the limb-socket interface stresses in a transtibial prosthetic socket. The Able-Bodied Socket design and features are described in detail in Section 3.2.3. Briefly, the device consisted of a base, an alignment assembly, and a socket. The base (Zero G AFO Base, Certified Orthopedics, Inc., Fort Collins, CO, USA) was part of a commercially available off-loading dynamic AFO brace system. Vertical aluminum supports were built into the base and were bolted to brackets on the sides of the alignment assembly. The alignment assembly consisted of a commercial prosthetic pylon assembly and custom-made brackets that connected the socket to the base and enabled adjustments of socket alignment and height with respect to the base. The bracing was designed to allow safe step clearance when walking downstairs. The socket was modeled after a patellar tendon bearing (PTB) style transtibial prosthetic socket. The socket captured 60-70% of the tibia length and contained two tethered panels (one anterodistal, one posteroproximal) that could be opened and closed to allow the foot to pass through the socket. The panels were locked, unlocked, and tightened using a dial that was laminated into the socket (RevoFit, Click Medical, Steamboat Springs, CO, USA).

The design of each socket was directed by a research prosthetist. In order to create the socket, the participant's limb shape was captured by first molding the limb in a plaster cast while wearing prosthetic liner they were to wear during the study. The inner surface of the cast was then captured as a three-dimensional CAD model using a mechanical coordinate measurement device (FaroArm Platinum, FARO Technologies, Lake Mary, FL, USA) and engineering design software (Geomagic, Design X, 3D Systems, Rock Hill, SC, USA). Minor modifications were made to reduce stress concentrations in sensitive areas and increase stress in load-bearing regions using prosthetic CAD/CAM software (OMEGA, WillowWood, Mt. Sterling, OH, USA). The CAD model was used to carve a foam positive of the socket interior with a three-axis CNC servo carving machine (C7 Carver, Provel, Cle Elum, WA, USA). Standard prosthetic socket fabrication methods were used to laminate the socket shape around the foam positive with multiple layers of carbon fiber and nylon-fiberglass composite. A marker was transferred from the ROI on the skin to the socket cast at the start of the limb shape capture process and was transferred throughout the fabrication so that the ROI could be marked on the inside of the finalized prosthetic socket and force sensor could be placed at the location.

Sensors were incorporated into each prosthesis to monitor the participants' use of the prosthesis, their activity level while wearing the socket, and the approximate pressures at the test limb ROI. Two accelerometers (Actilife Actigraph GT3X+, Pensacola, FL, USA) continuously collected movement data at 40 Hz, one placed on the prosthetic liner at the thigh and a second placed at the ankle of the device. Together, using an activity classification algorithm previously developed by our lab, these sensors provided measurement for how often the socket was being worn and the types of activities that were performed while wearing it, namely sitting, standing, or walking [100]. A force sensing resistor (FSR) (Flexiforce A201, Tekscan, Inc., South Boston, MA, USA) was used to monitor the interface pressure between the limb and the socket wall at the ROI. While accurate pressure measurements were not expected from the FSR due to well-documented limitations of their use in prosthetics [101], the sensor was used to verify contact between the limb and socket at the ROI while the socket was worn and to provide an estimate of pressures that could roughly be compared between individuals. A dial sensor was used to monitor when participants interacted with the panel cable dial. The sensor was installed into the base of the dial housing and monitored the rotary position of the panel cable dial. The dial sensor signal was analyzed to determine when the participant had interacted with the socket to loosen or tighten it, thereby providing a better understanding of how each participant used the socket and to verify the don-doff information gathered from the accelerometers. A data acquisition device (DAQ) was installed on the posterior aspect of the device and collected data at 32 Hz from both the FSR and dial sensor. Participants were requested to plug the DAQ in every night after completing their socket wear time for the day, though the DAQ could last for 2-3 days on a single charge.

The shape of each participant's limb was captured by the study prosthetist during the first study session (Figure 4.1). Participants returned once their socket was complete—usually 1-3 weeks later—to be fit in the socket and to initiate the daily socket wear protocol. During the fitting session the study prosthetist adjusted the prosthesis until a comfortable and safe socket fit was achieved. The target socket fit was one which slightly off-loaded the foot through the sides of the tibia and the calf without sensations of pain or signs of blood occlusion to the foot. Care was taken to ensure gait was fluid while wearing the socket and that both limbs were of equal length. For some participants, a shoe lift was added beneath the participant's shoe on their contralateral foot to equalize the limb length. Other adjustments included changing the alignment of the foot, changing the alignment of the socket, changing the socket height, or reshaping tibial foam pads.

Stress at the test ROI was confirmed by verifying skin redness at the ROI after briefly walking in the socket. For some participants, in order to increase the limb-socket interface stresses, an additional foam pad was installed on the posterior panel or the participant wore a prosthetic sock layer. The participant was trained on donning and doffing of the prosthetic liners and the socket. They were also taught how to perform a limb evaluation, which they were asked to complete at least twice per day while wearing the socket to ensure their limb was tolerating the socket loads safely. The fitting session concluded with a controlled-activity protocol that was used to further confirm a good socket fit and to provide ground truth activities for the socket sensor data. The protocol consisted of three cycles of sitting, standing, and walking, with each activity lasting 60-120 seconds.

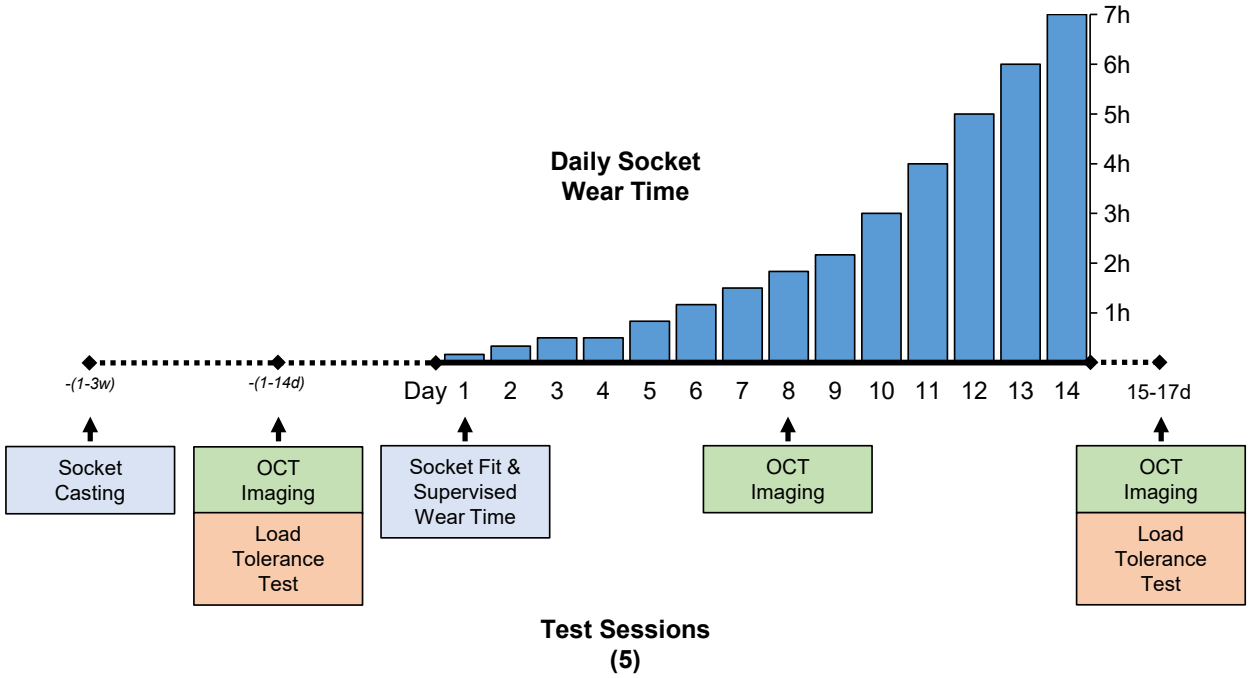

Figure 4.1. Aim 2 protocol summary. The target daily Able-Bodied Socket wear schedule is shown and each of the five study sessions are indicated below the timeline. The socket casting session and baseline imaging session occurred 1-3 weeks and 1-14 days, respectively, prior to first wearing the socket.

4.3.4 *Adaptation Protocol*

The Able-Bodied Socket was worn daily for two weeks in order to stress the lower limb skin of study participants. The wear protocol closely followed guidelines common to prosthetic training programs that are prescribed when individuals who have undergone a lower limb amputation begin adapting to their first prosthesis. Participants were asked to wear the socket for approximately 10 minutes on the first day and gradually increase the wear time as their limb and their comfort allowed. Participants were asked to split the wear time each day into a minimum of two segments with a break of at least 15 minutes in between. During this break and following completion of the daily wear time, participants were requested to perform a limb evaluation to ensure the limb was tolerating the socket loads appropriately. This included verifying any skin redness resolved within 10 minutes and there were no indications of tissue damage such as abrasions, blistering, or bruising. Participants were advised to notify the study team if they had any findings during a limb evaluation or if they experienced any other discomfort. A sample timeline was provided to participants, though if any discomfort or skin findings occurred the timeline was to be adjusted. The sample timeline, shown in Figure 4.1, began with 10 minutes on day one and increased to 90 minutes by day seven, and finally seven hours by day 14. Details on this protocol can be found in Appendix C.

4.3.5 *Imaging Sessions*

Imaging of the limb ROIs occurred three times throughout the study: (1) after the ROIs were selected and before the first time the socket was worn, (2) after approximately seven days wearing the socket, and (3) one to two days following the completion of the daily socket wear protocol (Figure 4.1). The one-week imaging session occurred prior to wearing the socket that day, and the final imaging session occurred at least 24 hours following the last time the socket was worn to reduce the risk that any skin irritation would still be present. Participants were requested to refrain from caffeine or alcohol use at least four hours prior to the test session to minimize the potential effect of the substances on microvascular responsiveness. All imaging sessions occurred at approximately the same time every day for each participant to limit the potential of diurnal vascular changes differences.

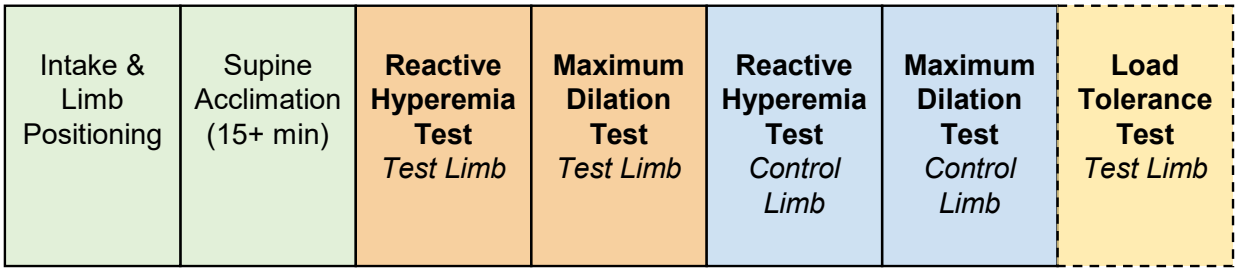

Figure 4.2. Aim 2 imaging session summary. Procedure order is shown from left to right. The Load Tolerance Test occurred only during the week 0 and week 2 imaging sessions.

At the start of each imaging session, the participant laid supine on the participant bed and the skin at the ROI on each limb was cleaned using an alcohol prep pad. Semi-permanent tattoo ink marked the boundaries of each ROI, however if the marks appeared faint at the start of the session, they were re-marked using a surgical marker and the tattoo ink was reapplied at the end of the session. The participant was situated into a comfortable position with their legs externally rotated with the ROI on each limb facing vertically to optimize access of the study instruments. The limbs were stabilized in this position using a formable positioning cushion (Vac-Lok Cushion, CIVCO Radiotherapy, Orange City, IA, USA) which allowed them to remain stabilized and relaxed throughout the duration of the session. The window blinds were closed and room lighting was turned on to reduce the potential influence of variable lighting conditions on OCT images or Load Tolerance Test photographs. Once positioned, the participant remained stationary for at least 15 minutes prior to any image collection in order to allow their cutaneous vasculature to acclimate to the room temperature and the position. If participants rose from the bed to use the restroom or to stretch during the session, they were re-acclimated for at least 15 minutes in the supine position prior to any subsequent imaging. Fifteen minutes was chosen since it is a commonly used acclimation period in cutaneous microvascular research [39], and it was reasonably short given the length of study sessions. The room temperature was maintained between 21-23°C. The test session protocol is summarized in Figure 4.2.

Each OCT imaging test was then performed at the test ROI, beginning with the Reactive Hyperemia (RH) Test, followed by the Maximum Dilation Test (described in detail in Sections 3.3.1 and 3.3.2, respectively). This test order was chosen to ensure baseline imaging for the RH Test always occurred on undisturbed skin and to ensure the RH response would not be altered by a previous heating protocol. The influence of the RH Test on the Maximum Dilation Test was not

a concern because 30-45 minutes always passed between the end of the RH Test load application and the first images in the Maximum Dilation Test. In this Aim, two full field-of-view Maximum Dilation images were captured. Following the Maximum Dilation Test at the test ROI, the study instruments were moved to the control ROI and both tests were performed, once again beginning with the RH Test followed by the Maximum Dilation Test. A Load Tolerance Test—described in Section 3.3.3—was performed at the test ROI at the end of the pre-socket and post-socket imaging sessions. This test used a similar, but slightly higher magnitude, load application as the RH Test and captured photographs which were later analyzed by a blinded clinical expert for the presence of redness. The duration of redness following a load is a common method used clinically in prosthetics to determine how well the tissue tolerates an imposed load. The test was performed here to determine if the skin had improved its load tolerance capability, based on the clinical measure, from before undergoing the Able-Bodied Socket adaptation protocol to after the protocol.

4.3.6 *Data Analysis*

OCT images were processed using the methods described in Section 3.2.1 and summarized in Figure 3.1 and Figure 3.2. Briefly, following motion-correction of OCT B-scans, OCT Angiography (OCTA) images were created using a High-Sensitivity Speckle Variance method (Section 2.5.3). The dermal-epidermal junction (DEJ) was automatically detected and a 150-pixel thick volume (approximately 0.84 mm) was segmented out, beginning 10 pixels above the DEJ. This volume was converted to a two-dimensional *en face* image using a maximum intensity projection. Maximum Dilation Test *en face* images were stitched together to create full field-of-view images, and the papillary dermis and reticular dermis were separated for further analysis. For both the RH and Maximum Dilation Tests, *en face* images were binarized to calculate the **vessel area density (VAD)** of the image. VAD was reported arbitrary units (a.u.) since it is not a direct measure of blood flow but rather provides a snapshot of the extent of tissue perfusion. Maximum Dilation Test *en face* images were further analyzed by skeletonizing them and calculating the **vessel count** (i.e. skeleton density) and the **mean vessel diameter**.

For each RH Test, VAD trends were smoothed using a three-point moving average and the resulting trend was plotted versus time, with the baseline image set to the 0 s time point. Key RH features were determined from the VAD plot, which included "**peak VAD**," "**time-to-peak**", and "**recovery time.**" These features are further described in Section 3.3.1 and outlined in Figure 3.7.

Since a full recovery of VAD back to baseline was uncommon given the time constraints of study sessions, the "recovery time" was defined as the time it took for the VAD to recover 75% of the way back to the baseline VAD from the peak VAD.

Epidermal thickness was also calculated at each ROI using the Maximum Dilation Test images. This was achieved by finding the mean difference between the automatically identified DEJ and skin surface. The mean epidermal thickness was calculated in every Maximum Dilation Test image and a final epidermal thickness value was calculated at each ROI by taking the mean of the epidermal thickness measurements from two full field-of-view images taken at that ROI.

For each participant, changes that occurred throughout the course of the study were assessed by comparing measurements obtained during the baseline (week 0) imaging session with those taken at the week 1 and week 2 imaging sessions. This was done at each ROI separately. The differences found were then compared between the test ROI and control ROI to determine if any changes that were identified in the skin had potentially been induced by Able-Bodied Socket interface stresses (the test ROI) versus those that may have occurred due to other sources of variability or due to wearing the liner only (the control ROI).

For RH Test and epidermal thickness measurements, the effect of wearing the Able-Bodied Socket versus the liner only was tested using a two-way repeated measures analysis of variance (ANOVA). For the Maximum Dilation Test, *en face* images from the ROI prior to socket loading (week 0) were physically registered to the images taken at week 1 and week 2 to ensure the same region of vessels was being compared. Significant overlap existed between all three time points for most of the data collected; however, rather than registering all three *en face* images together, in order to maximize the area of overlap, two separate comparisons were made: one comparing week 0 to week 1 and one comparing week 0 to week 2. Only vessels within the shared registered region were used to calculate the vessel structure parameters for each of the two registered images. A two-way repeated measures ANOVA was then run for each Maximum Dilation Test measurement (VAD, vessel count, and mean vessel diameter) to test the effect of wearing the Able-Bodied Socket versus wearing the liner only over time. For all comparisons from all tests, statistical significance was indicated by $p<0.05$. Statistical analyses were performed using SPSS statistical software (SPSS 26.0, IBM Corp., Armonk, NY, USA).

Load Tolerance Test photographs were color-corrected using the white-black balance card that was placed near the ROI in all photographs. The photographs within each test were

randomized before being evaluated by a clinical expert for the presence of redness. The baseline photograph, which was taken before the load application, was known to the clinical expert and was used as the non-red baseline to which other photographs were compared. The "recovery time" was defined as the time at which skin redness was no longer present, per the clinical expert's grades. Participants who demonstrated redness which lasted for longer than 10 minutes during the week 0 test and redness which lasted for 10 minutes or less during the week 2 test were considered to have increased load tolerance at their test ROI. All individuals who attained increased load tolerance per this test were then grouped and their OCT measurements were assessed to see if specific trends existed within the group.

Activity data were analyzed for each participant's two-week socket wear period and used to verify the amount of time each participant wore the socket each day and to determine the overall activity level of the participant while wearing the socket. Prior to analyzing socket sensor data, the accelerometer signals were time-synced with the FSR and dial sensor signals collected with the DAQ. Activity data were grouped into four activities: sitting, standing, walking, and socket-doffed based on an accelerometer algorithm previously published [100]. The activity algorithm required a don-versus-doff input to ensure periods of socket movement when it was not worn did not get included in wear data. This was determined manually by visually inspecting data from all of the sensors. These points were usually selected based on the dial data, which indicated when socket panels were being closed and opened, for donning and doffing, respectively. For cases when dial data did not provide a clear indication of don-versus-doff status, the FSR trend was used to determine when the limb was placed into the socket. Only activities that occurred within the socket-donned windows were retained for further analysis. For each participant, the total time the socket was worn and the total time spent in each activity type were calculated. FSR pressure measurements during walking activity were analyzed by calculating the mean of the pressure peaks during walking. Peaks were found using a peak detection algorithm in MATLAB. OCT measurements were then revisited to determine if individuals who (1) spent more time wearing the socket, (2) spent more time in high-intensity activities, or (3) had significantly higher FSR pressure measurements, demonstrated different results from the other participants.

4.4 RESULTS

4.4.1 *Participants*

Table 2. Aim 2 study participant characteristics.

Characteristic	Frequency
Age (yrs)	
< 25	6
25-50	1
>50	1
Gender	
Male	3
Female	5
Ethnicity	
Not Hispanic/Latino	2
Hispanic/Latino	6
Race	
White	5
Asian	1
Multiple*	1
Did not respond	1
Fitzpatrick Skin Type	
II	1
III	1
III-IV**	2
IV	3
IV-V**	1
Regular Caffeine Drinker	
Yes	2
No	6

* Participant responded yes to White, Black, and Asian
** Participants' skin phototype question responses spanned two different skin types

A total of 8 healthy, able-bodied individuals (5 females, 3 males) participated in the study. Participant ages ranged from 19 to 51 years with a mean age ± SD of 24.4 ± 11.1 years. The characteristics of these participants are described in Table 2. None of the participants had known diabetes or dysvascular disorders, used vasodilators, or were smokers. Fitzpatrick skin phototypes (FSPT) ranged from II to IV. Participants all reported having no past or current injuries to the skin in the area where the ROI would be chosen on each limb (anteroproximal lower limb, medial of

the tibial crest), as confirmed visually by the research prosthetist. Limb photographs including the ROI location are shown in Figure 4.3.

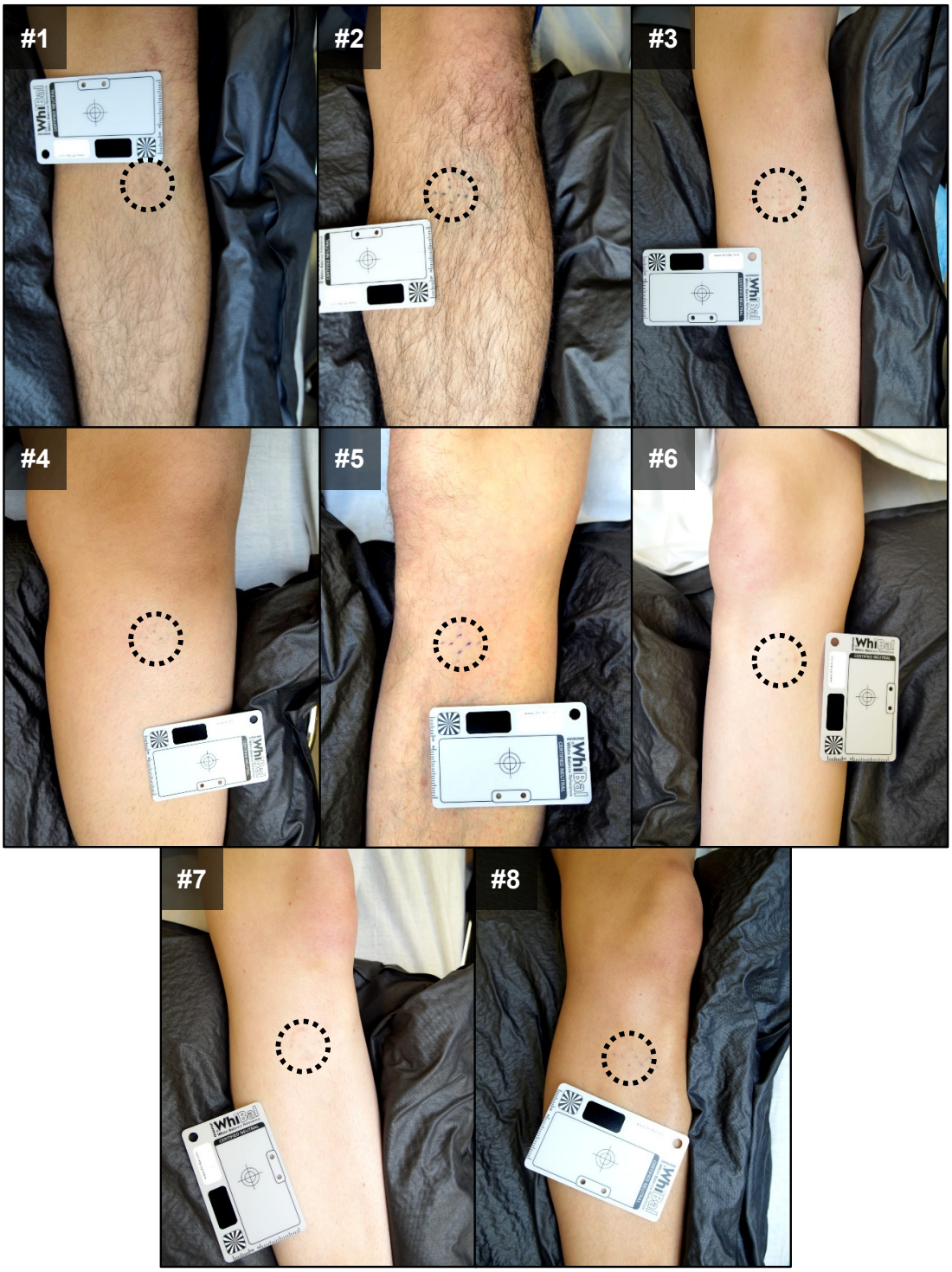

Figure 4.3. Aim 2 participant test limbs. ROIs indicated (dotted circle). Number in each panel is the participant identification number used in this document. Images here are baseline photographs from the Load Tolerance Test.

4.4.2 *Able-Bodied Sockets and Activity Monitoring*

For all participants, an ROI was selected for imaging the test limb skin that was located 6.0-9.0 cm distal of the mid-patellar tendon and 1.5-2.5 cm medial of the tibial crest. The ROI location was transferred from the initial limb cast through to the final socket and for all participants the ROI remained within the region of increased loading by the foam pad installed on the inside surface of the socket on the medial side of the tibia. Interface stress was confirmed at the skin test ROI for each participant during the fitting session by the presence of skin redness following a brief walk in the socket, as assessed by the study prosthetist. A good socket fit and fluid gait were achieved for all study participants during the fitting session without the need for a follow-up fitting session.

Data were collected continuously using the study sensors on all participants. Activities were classified based on the thigh and ankle accelerometers using dial sensor data to determine the periods when the socket was worn. As shown in Figure 4.5, the don-doff input from the dial was necessary for the activity classification algorithm since without it the algorithm would have falsely classified movements of the socket and liner when the socket was not worn. In a few instances when dial data were not clear—for example, with 2 participants who were able to don and doff their socket without releasing the panels—the FSR data were used to verify when the limb had been placed into the socket. The activity classification algorithm indicated that 5 of 8 participants wore the socket for greater than the total target wear times. Notable differences were found between total wear times of participants as well as the amount of time spent performing high activity (walking). The accumulated wear times for each participant, separated by sit and stand versus walking activities, is shown in Figure 4.6. Participants 3 and 8 each wore their socket for over 35.0 h, followed by participants 7, 6, and 5, respectively. Participant 8 was more active while wearing the socket, accumulating 11.6 h of walking time, compared to the next two participants who spent 5.9 h and 5.0 h walking (Participants 7 and 5, respectively).

FSR measurements indicated that notable differences were present between participants regarding how much pressure was imposed at the test limb ROI while wearing the socket. Mean peak pressures during walking are shown in Figure 4.7 along with the range of possible pressure values each measurement represents considering up to ± 44% error is known to be present in FSR measurements at the limb-socket interface. Mean peak pressures during walking ranged from 52.4 kPa for Participant 1 to 3.2 kPa for Participant 4. Following data collection for Participant 2 it was noticed that a minor error in the fabrication process resulted in an indent in the socket wall beneath

the FSR sensing area, which led to much lower pressure readings than were likely present at the interface. Participant 1 had the highest peak pressures, more than twice as much as Participant 8 and 2 who demonstrated the next highest mean peak pressures with 12.0 kPa and 11.7 kPa.

Three participants were chosen who demonstrated activity and interface pressure data which suggested they likely experienced more accumulated stress at their test ROI compared to other participants throughout the two-week wear period. Participant 8 was chosen due to having the second highest mean peak pressure measurement at the ROI with more wear time and significantly more walking time than all other participants. Participant 1 was chosen for having a mean peak ROI pressure measurement that was significantly higher than all other participants and demonstrating the fourth most time spent walking. Participant 3 was chosen for demonstrating the third highest peak ROI pressures with the second highest total wear time. This group was used for secondary analysis of data collected during the imaging sessions to determine if certain changes occurred more frequently or at higher magnitudes for these individuals.

Figure 4.4. Aim 2 participants wearing their Able-Bodied Sockets. The number in each panel is the participant identification number used in this document.

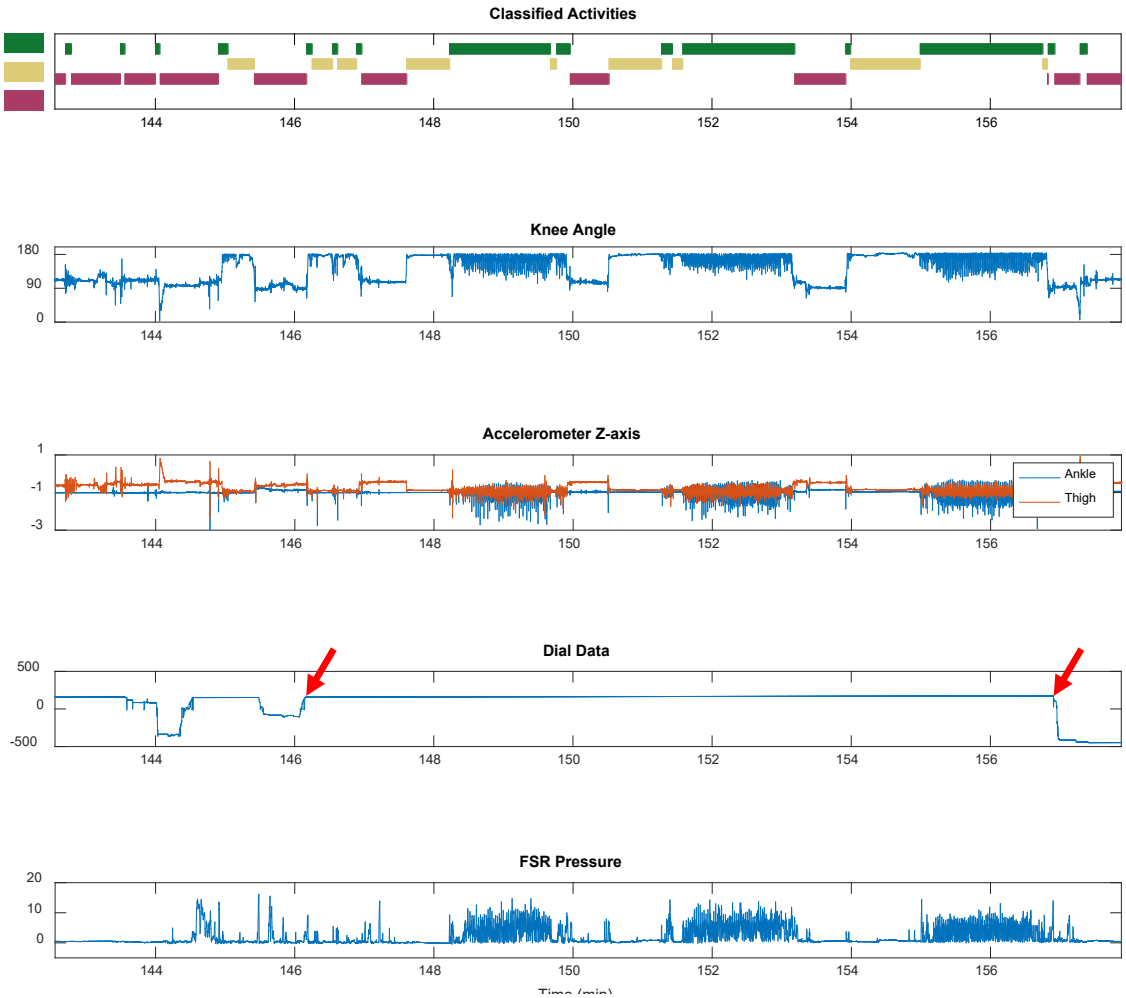

Figure 4.5. Sample Able-Bodied Socket sensor data. Shown for Participant 1 during wear day 1, depicting sensor data for in-lab wear time with known 3-cycle (sit-stand-walk) protocol. Activity classification shown in top panel. Dial interactions (red arrows) were used to determine when the socket was donned and doffed, and only the classified activities that occurred while donned were retained for analysis.

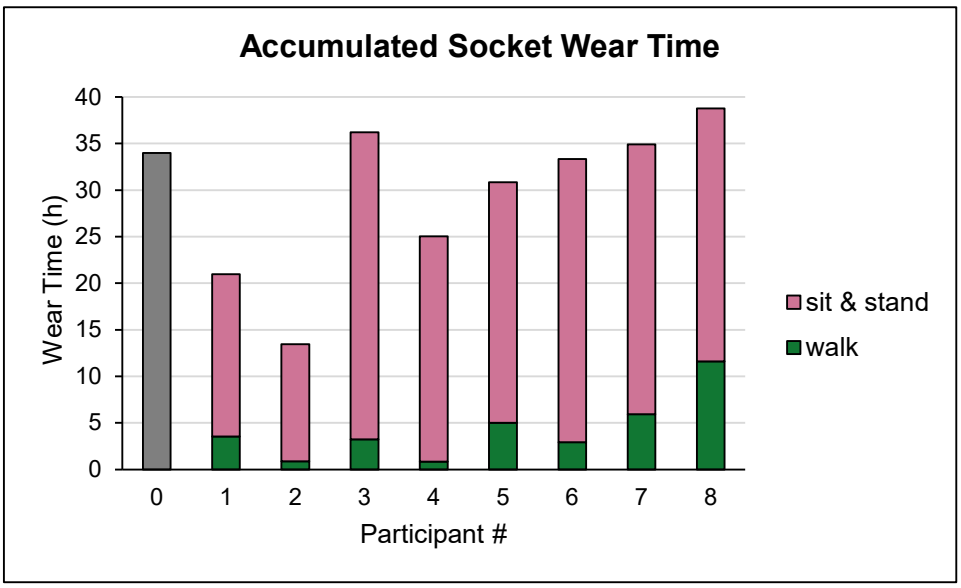

Figure 4.6. Accumulated socket wear times by activity for each participant.

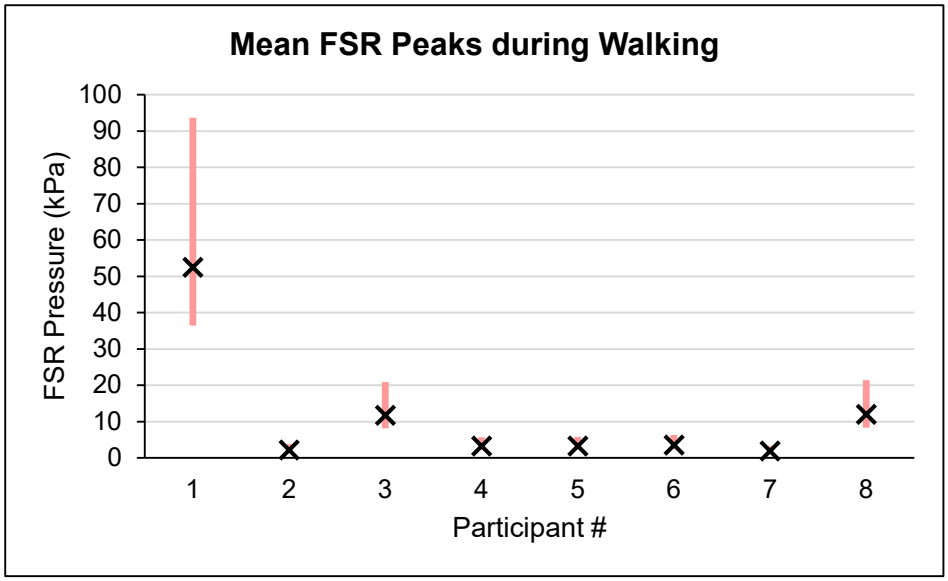

Figure 4.7. Pressure measured at ROI for each participant. Shown are the mean peak pressures measured during walking throughout the two-week wear period (black "**X**"). The vertical bar indicates the range of values that could be possible for each, given the error inherent in using FSRs for prosthetic interface measurements. Participant 2's measurement is likely lower than actual due to an indent on the socket wall where the FSR was adhered.

4.4.3 *Load Tolerance Test*

The results of the Load Tolerance Test are summarized in Table 3. Based on the assumptions used to design the Load Tolerance Test, 2 participants indicated an increased load tolerance at the test ROI. For 2 other participants, the week 0 photographs could not be reasonably assessed due to the continued presence of skin redness from the Maximum Dilation Test heater earlier in the session. However, since both of their week 2 tests had redness beyond 10 minutes, it would not have been possible for them to demonstrate increased load tolerance regardless of their week 0 results. The remaining 4 participants did not have redness that lasted longer than 10 minutes during the week 0 test, and therefore their limbs were already considered "tolerant" to the load stimulus used in the test. As such, in addition to the binary 10-minute redness determination, the redness time was also compared between participants' sessions (Table 4), which showed that 4 of the 8 participants demonstrated a decrease in skin redness time in week 2 compared to week 0. For these 4 individuals, the mean ± SD of this time decrease was 5.7 ± 3.7 min. These results were used to further interpret the results of the RH Test and Maximum Dilation Test, as described in the Discussion below.

Table 3. Load Tolerance Test results.

Participant #	**Week 0**	**Week 2**	**Increased Tolerance?**
1	< 10 min	< 10 min	No
2	< 10 min	< 10 min	No
3	< 10 min	< 10 min	No
4	< 10 min	< 10 min	No
5	**> 10 min**	< 10 min	**Yes**
6	n/a*	**> 10 min**	No
7	n/a*	**> 10 min**	No
8	**> 10 min**	< 10 min	**Yes**

*Skin Redness could not be assessed due to residual skin redness from Maximum Dilation Test heater earlier in test session.

Table 4. Load Tolerance Test results, by time.

Participant #	Week 0	Week 2	Decreased Time?
1	**5.0 min**	**4.0 min**	**Yes**
2	2.0 min	12.0 min	No
3	7.2 min	9.0 min	No
4	**9.1 min**	**4.0 min**	**Yes**
5	**12.0 min**	5.0 min	**Yes**
6	n/a**	**≥15.0 min**	No
7	n/a**	**≥15.0 min**	No
8	**≥15.0 min**	5.3 min	**Yes**

*Skin Redness could not be assessed due to residual skin redness from Maximum Dilation Test heater earlier in test session.

4.4.4 *Reactive Hyperemia Test*

Following the 10-minute load application of the RH Test, 40 of the 48 tests produced a standard RH response, with a rapid increase in VAD followed by a gradual decline back toward the baseline VAD. For the 8 tests in which an RH response was not measured, the VAD remained relatively stable and at a low magnitude throughout the test measurements. Six of these 8 tests came from the control ROI of Participant 1 and Participant 4. The other 2 came from the week 0 test at each of Participant 2's ROIs. Of the 40 tests where an RH response was measured, the peak of the response appeared to be captured in 12 tests. In the other tests, the first measurement taken after the load removal was the peak VAD of the measured response; therefore, it was not clear whether the peak occurred at this point or before this point. For these tests it was thus unknown whether the physiological time-to-peak was smaller than the value measured and if the peak VAD was larger than the value measured. Despite this missing information, relationships between the weeks could still be found in many cases when one of the three weeks had a captured peak. For example, although the peak was not captured in the week 1 or week 2 RH test for Participant 6's test ROI, since the peak was captured in week 0 and the peak occurred approximately 30 seconds later than in week 1 or week 2, we can determine that the peak was faster in week 1 and 2 versus week 0.

The RH peak VAD, RH time-to-peak, and RH recovery time measurements for all participants are shown in Figure 4.10, Figure 4.11, and Figure 4.12, respectively. As demonstrated in these figures, various trends were exhibited in this test. These trends are summarized in Figure

4.9 for the relationships that could be determined given the missing peak information. Excluding tests where a RH response was not measured, the difference between the week 2 versus week 0 measurements, given as mean ± SD for all tests, the peak VAD changed by 0.01 ± 0.08 a.u. and -0.03 ± 0.06 a.u (test ROI and control ROI, respectively); the time-to-peak increased by 0.11 ± 0.31 min and 0.08 ± 0.65 min (test ROI and control ROI, respectively); and the recovery time changed by 1.53 ± 2.65 min and -2.42 ± 2.51 min (test ROI and control ROI, respectively). The high amount of variability in responses was further confirmed by the large standard deviations for the measurements.

A two-way repeated measures ANOVA was used to statistically determine the effect of stressing the limb with the Able-Bodied Socket over time on the RH peak VAD, RH time-to-peak, and RH recovery time. Analysis of the studentized residuals showed normality in the data, as determined by the Shapiro-Wilk normality test, and the lack of outliers, as verified by the lack of studentized residuals greater than ± 3 standard deviations. Mauchly's test for sphericity indicated that the time-to-peak and recovery time data could be assessed without further corrections (p>0.05), however sphericity was violated for peak VAD and a Greenhouse-Geisser correction was applied to these data. No statistically significant relationships existed (p>0.05) for any of the RH measurements for neither the test ROI nor control ROI when comparing between week 0, week 1, and week 2.

Grouping the individuals who demonstrated increased load tolerance in the Load Tolerance Test (Participants 1, 4, 5, and 8) showed that all 3 of the individuals in the RH Test who demonstrated a slower time-to-peak in week 2 belonged to this group. The fourth individual in the group did not produce RH Test results that could be compared due to missing RH peaks. For all other test measurements, no additional patterns were highlighted by the group of individuals who demonstrated a load tolerance increase. The three individuals whose activity and pressure data suggested their test ROIs were stressed more than the other participants' ROIs (Participants 1, 3, and 8) also demonstrated a slower time-to-peak at the test ROI by week 2. These two participants were also part of the load tolerance group. Participant 3's week 2 versus week 0 time-to-peak could not be calculated due to an RH peak not being captured.

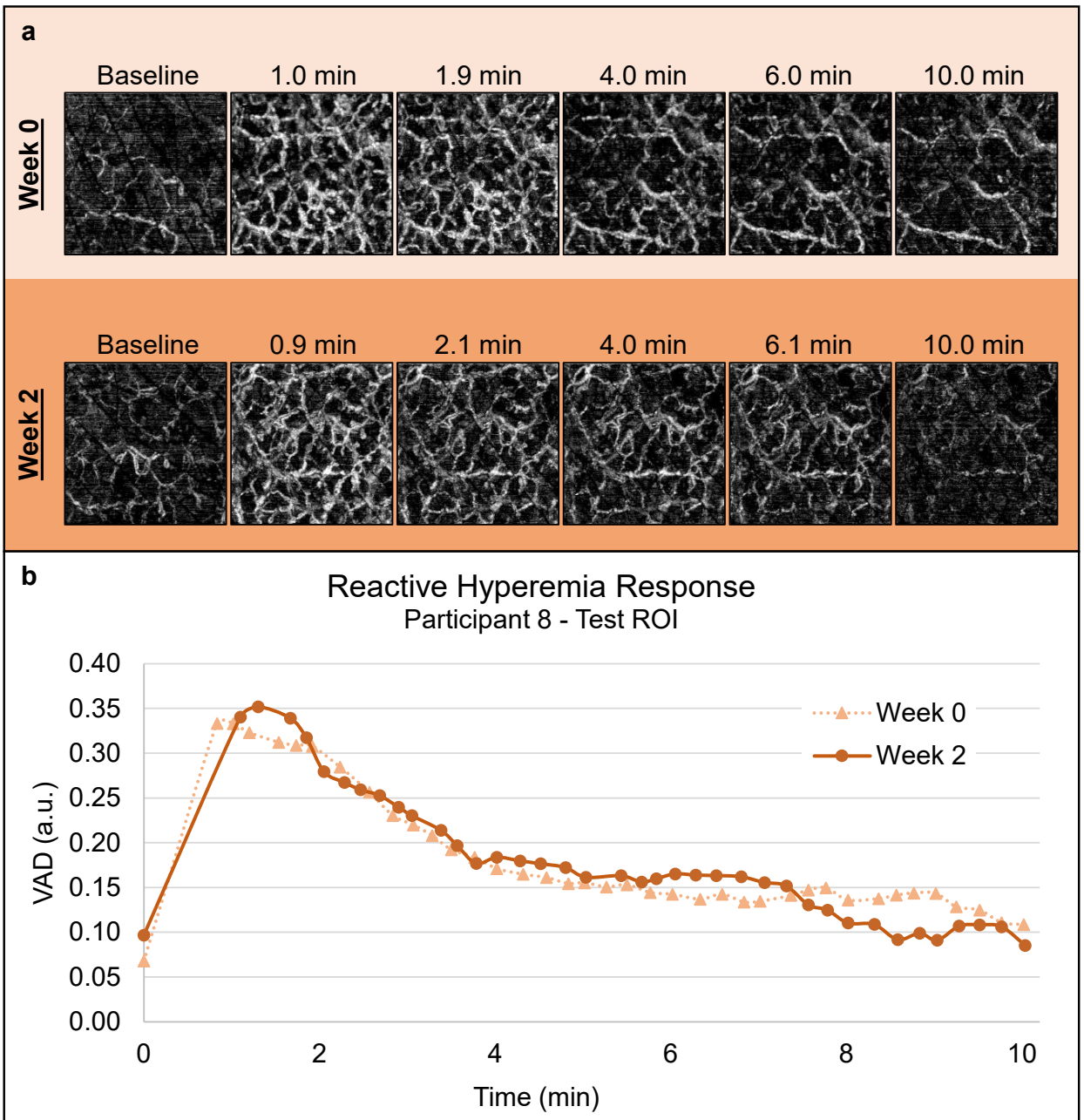

c	Peak VAD	Time-to-Peak	Recovery Time
Week 0	≥ 0.33 a.u.	≤ 0.8 min	9.2 min
Week 2	0.35 a.u.	1.3 min	6.9 min

Figure 4.8. Representative RH Test results. Results from Participant 8's test ROI at week 0 and 2. (a) Select *en face* images of the RH response (2 x 2 mm each). (b) VAD vs. time plots. (c) Quantified vascular response characteristics. The peak appears to have been captured in the week 2 response, but not week 0.

Week 2 vs Week 0

Test Limb

Participant	Peak VAD			Time-to-Peak			Recovery Time		
	w2 larger	*w2 smaller*	*similar*	*w2 faster*	*w2 slower*	*similar*	*w2 faster*	*w2 slower*	*similar*
1			X		X			X	
2	*no RH*			*no RH*			*no RH*		
3	X			*missed peak*				X	
4		X			X		X		
5			X	*missed peak*				X	
6	X			X					X
7			X	*missed peak*				X	
8			X		X		X		

Control Limb

Participant	Peak VAD			Time-to-Peak			Recovery Time		
	w2 larger	*w2 smaller*	*similar*	*w2 faster*	*w2 slower*	*similar*	*w2 faster*	*w2 slower*	*similar*
1	*no RH*			*no RH*			*no RH*		
2	*no RH*			*no RH*			*no RH*		
3		X				X	X		
4	*no RH*			*no RH*			*no RH*		
5		X		*missed peak*			X		
6		X		*missed peak*			X		
7			X	*missed peak*					X
8			X	X					X

Week 1 vs Week 0

Test Limb

Participant	Peak VAD			Time-to-Peak			Recovery Time		
	w1 larger	*w1 smaller*	*similar*	*w1 faster*	*w1 slower*	*similar*	*w1 faster*	*w1 slower*	*similar*
1	X			*missed peak*				X	
2	*no RH*			*no RH*			*no RH*		
3		X		*missed peak*				X	
4		X		*missed peak*			X		
5		X		*missed peak*				X	
6	X			X				X	
7			X	X			X		
8			X			X	X		

Control Limb

Participant	Peak VAD			Time-to-Peak			Recovery Time		
	w1 larger	*w1 smaller*	*similar*	*w1 faster*	*w1 slower*	*similar*	*w1 faster*	*w1 slower*	*similar*
1	*no RH*			*no RH*			*no RH*		
2	*no RH*			*no RH*			*no RH*		
3		X		*missed peak*					X
4	*no RH*			*no RH*			*no RH*		
5		X		*missed peak*					X
6	X			*missed peak*			X		
7			X		X		X		
8			X	X					X

Figure 4.9. Summary of trends seen in RH Test. Comparisons of RH measurements from week 1 and 2 with week 0 for each ROI on each participant. Differences within ± 15% of the week 0 value were considered "similar." Gray boxes indicate tests which did not produce an RH response or tests where RH peaks were not captured in a manner that made the comparison impossible.

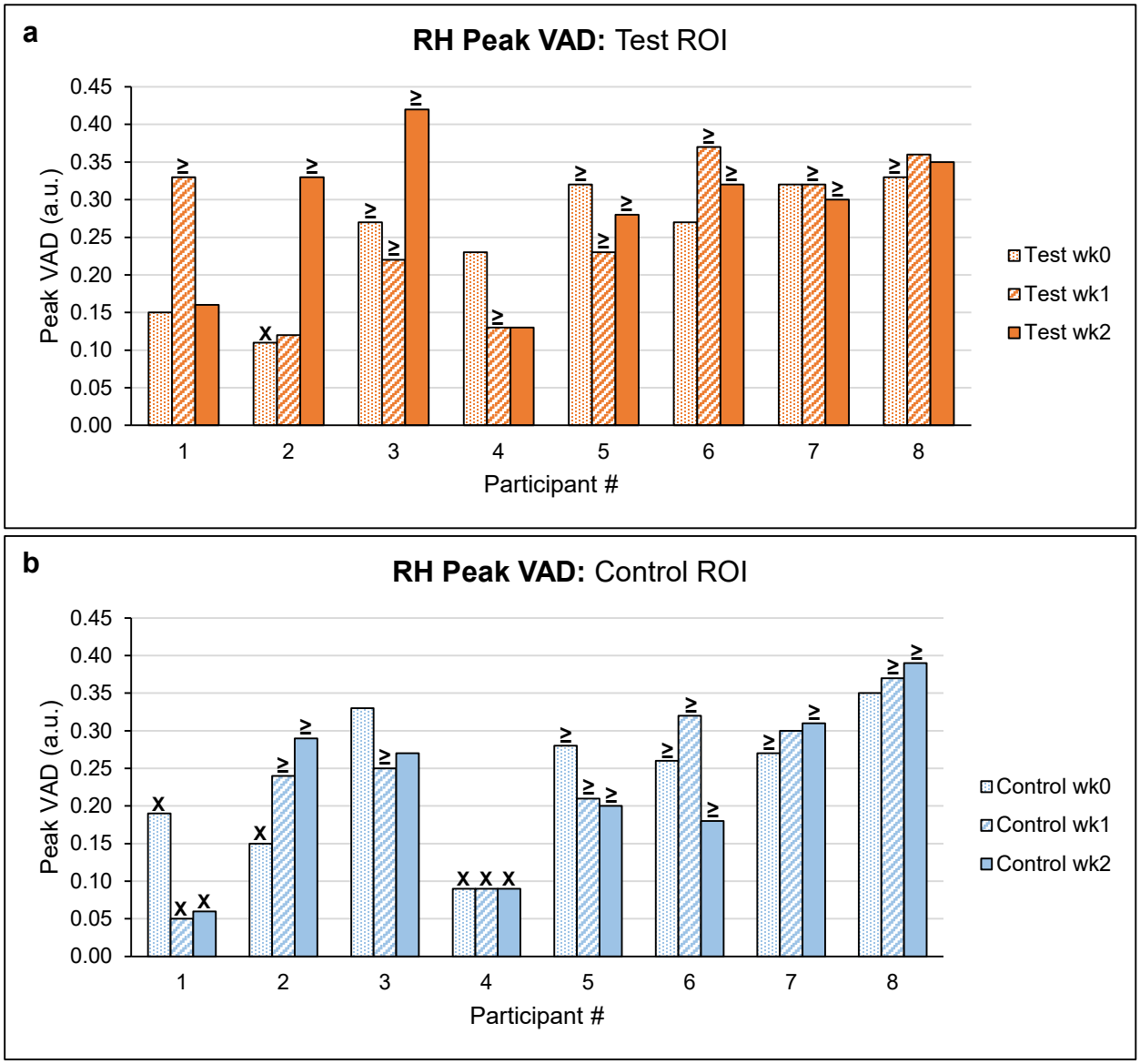

Figure 4.10. RH peak VAD measurements. An "**X**" indicates that an RH response did not occur. A "**≥**" indicates that the peak was the first point captured, therefore the physiological peak VAD was greater than or equal to the measured value.

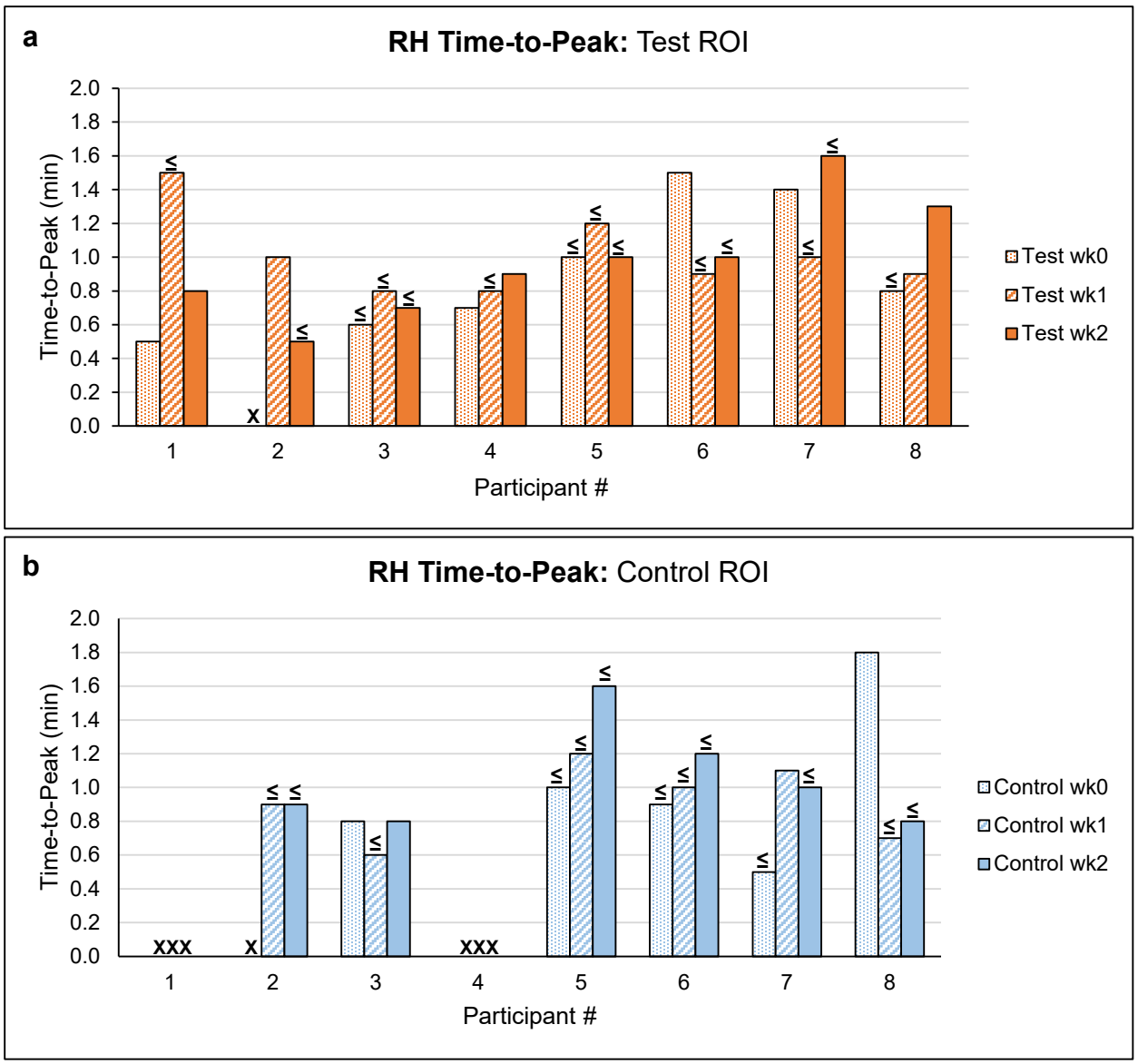

Figure 4.11. RH time-to-peak measurements. An "**X**" indicates that an RH response did not occur. A "**≤**" indicates that the peak was the first point captured, therefore the physiological peak was less than or equal to the measured value.

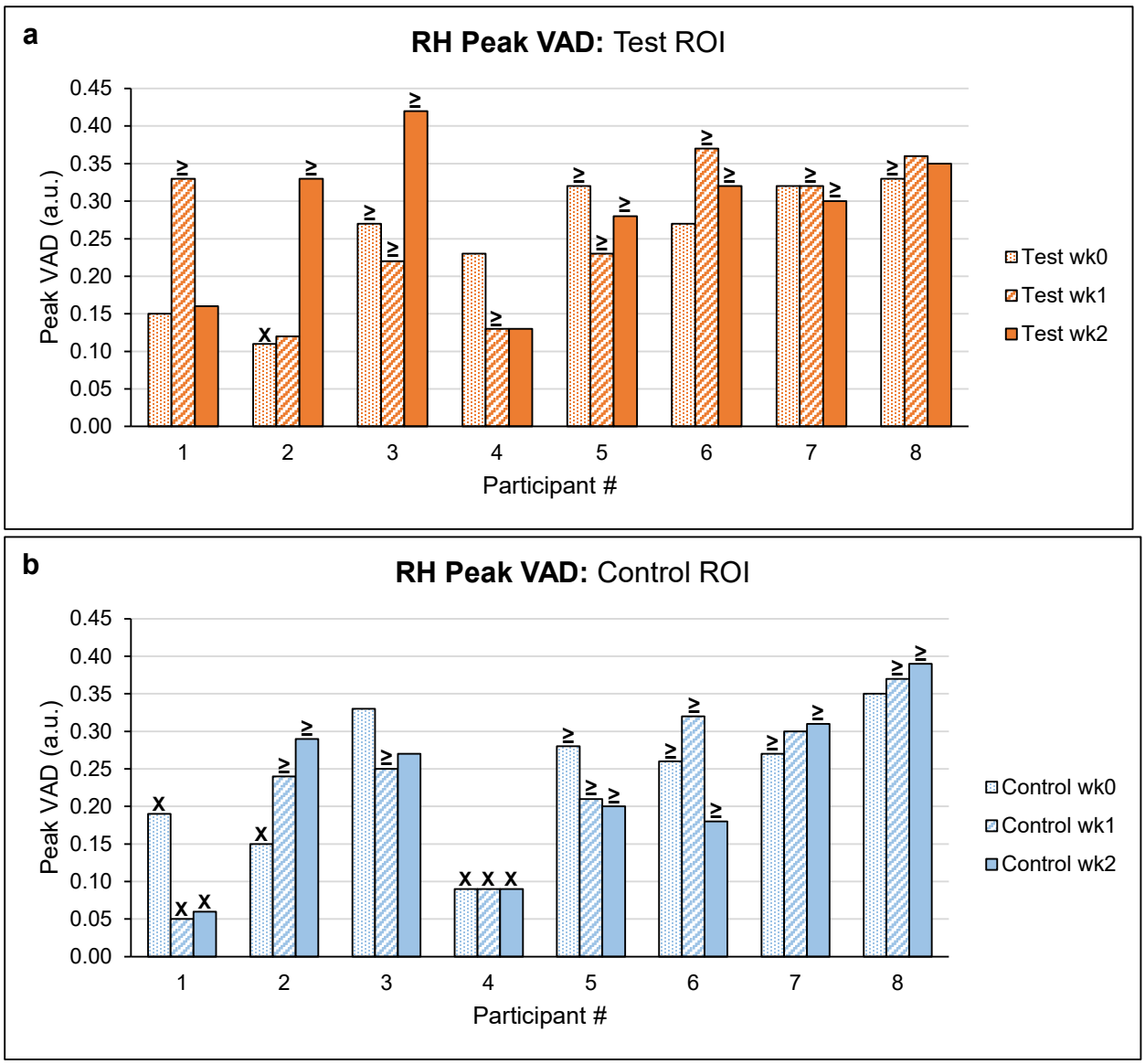

Figure 4.12. RH recovery time measurements. An "**X**" indicates that an RH response did not occur. A "**≥**" indicates that the peak was the first point captured, therefore the physiological peak was greater than or equal to the measured value.

4.4.5 *Maximum Dilation Test*

Structural vessel images were captured at each participant ROI after a 25-minute localized skin heating protocol was used to induce maximum dilation. Most images were relatively free of imaging artifacts such as motion-induced noise and hair, and the structural vessel parameters (VAD, vessel count, and mean vessel diameter) could be measured without issues. Since Participant 1's imaging sessions took place prior to implementing several noise-reducing techniques in the Maximum Dilation Test, measurements could not be quantified from Participant 1's images due to the poor vessel signal-to-noise ratio. Thus, only results from participants 2 through 8 were included in this analysis. Registration of full field-of-view images taken at each ROI between imaging sessions resulted in overlapping ROI regions of 758,761 ± 65,078 pixels (mean ± SD), equivalent to a square imaging area with a side length of 7.0 ± 0.3 mm. The minimum equivalent side length achieved was 6.3 mm.

A representative registered image set with vessel structure quantification is shown in Figure 4.14. Some differences in the measurements were identified between time points, as summarized in Figure 4.15; however, these differences appeared small compared to the variability of the measurements, as evidenced by the large standard deviation in these differences. The mean differences between weeks and their standard deviations are shown in Figure 4.13. Individual participant measurements for the papillary dermis from the week 0 to week 2 comparison are shown in Figure 4.16.

A two-way repeated measures ANOVA was used to statistically determine the effect of stressing the limb with the Able-Bodied Socket over time on the vessel structure measurements VAD, vessel count, and mean vessel diameter. The data appeared normally distributed, as demonstrated by the Shapiro-Wilk normality test of the studentized residuals and the lack of outliers, as verified by the lack of studentized residuals greater than ± 3 standard deviations. No statistically significant relationships existed (p>0.05) for any of the vessel structure measurements for either layer (papillary or reticular) or either comparison (week 0-to-1 and week 0-to-2).

Qualitative assessment of registered vessels showed similar vessel structures over time, as demonstrated in Figure 4.14. Additionally, all participants possessed similar vessel structures compared to each other. Sample images for each participant are shown in Appendix E.

Grouping the individuals who demonstrated increased load tolerance in the Load Tolerance Test did not highlight any patterns in the Maximum Dilation Test measurements. One of the four

individuals (Participant 1) was not included in the Maximum Dilation Test analysis due to excessive noise in the images making them unquantifiable. The other three participants demonstrated measurement trends that did not appear to coincide with each other and separating this group from the others did not highlight any patterns in those individuals that remained. The three individuals whose activity and pressure data suggested their test ROIs were stressed more than for other participants (Participants 1, 3, and 8) did not display any notable trends. Again, Participant 1 was not included in the test results due to poor image quality.

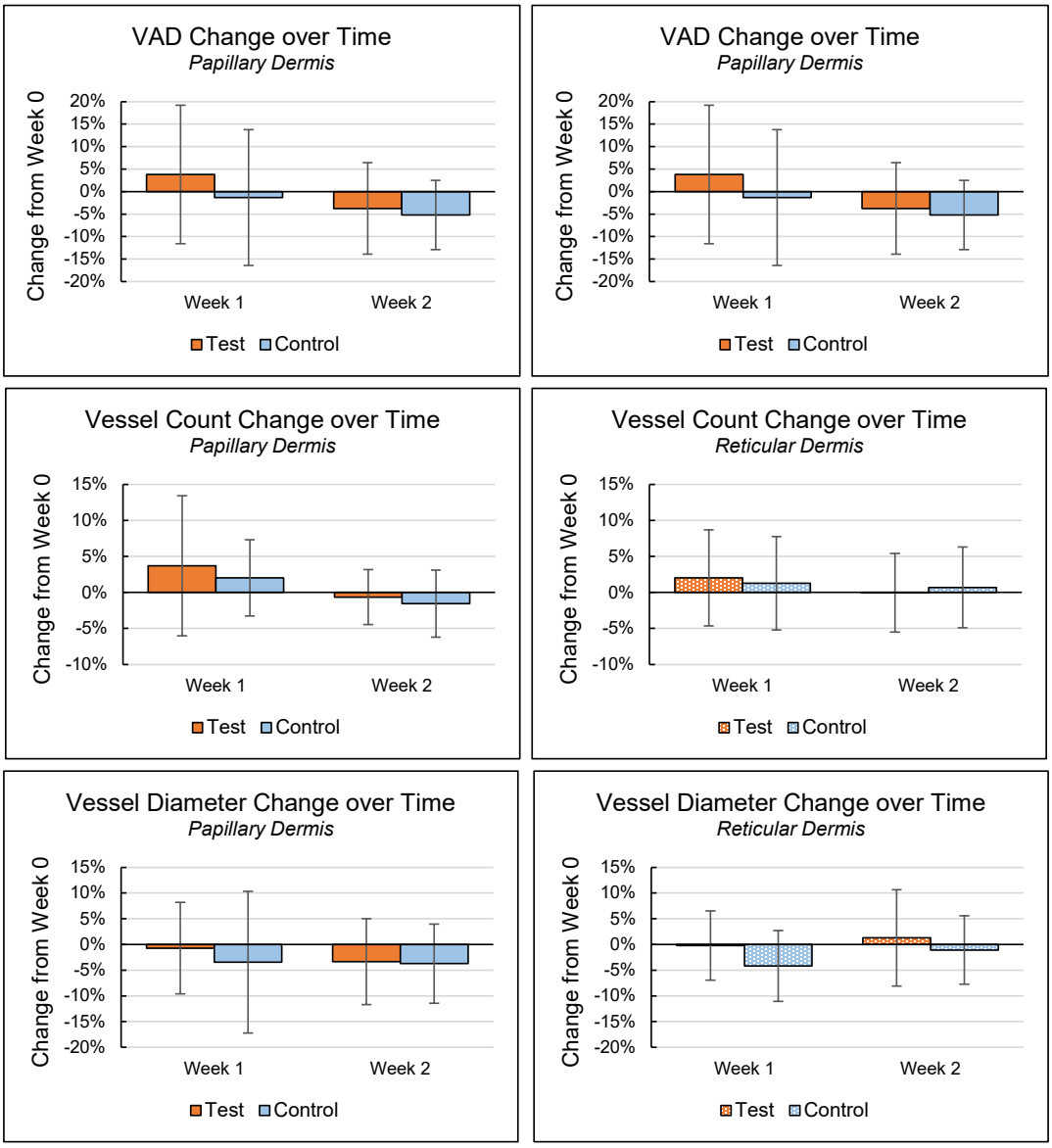

Figure 4.13. Maximum Dilation Test measurement mean differences between weeks. Data are from participants 2-8. Error bars are one standard deviation.

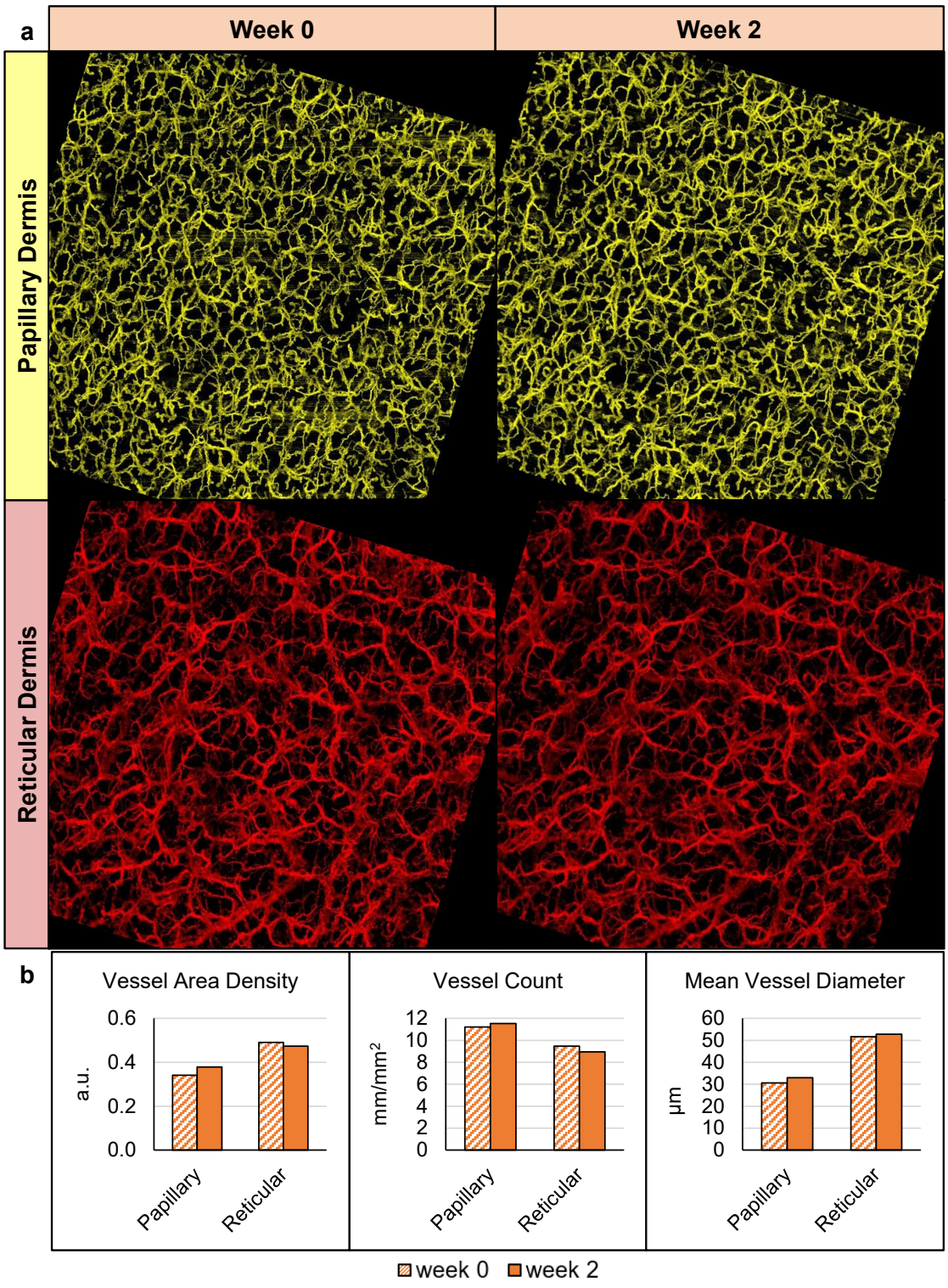

Figure 4.14. Representative Maximum Dilation Test data. Data from Participant 8's test ROI. (a) *En face* images separated by week and depth after vessel registration and removal of non-shared pixels. (b) Vessel measurements quantified from the images.

Week 2 vs Week 0 - Papillary Layer

Test Limb

Participant	VAD			Vessel Count			Mean Vessel Diameter		
	w2 larger	*w2 smaller*	*similar*	*w2 larger*	*w2 smaller*	*similar*	*w2 larger*	*w2 smaller*	*similar*
2		X				X		X	
3		X				X		X	
4		X			X			X	
5		X				X		X	
6			X			X			X
7	X					X	X		
8	X					X	X		

Control Limb

Participant	VAD			Vessel Count			Mean Vessel Diameter		
	w2 larger	*w2 smaller*	*similar*	*w2 larger*	*w2 smaller*	*similar*	*w2 larger*	*w2 smaller*	*similar*
2		X				X		X	
3		X			X				X
4		X				X		X	
5			X		X				X
6			X			X			X
7	X			X					X
8		X			X				X

Week 2 vs Week 0 - Reticular Layer

Test Limb

Participant	VAD			Vessel Count			Mean Vessel Diameter		
	w2 larger	*w2 smaller*	*similar*	*w2 larger*	*w2 smaller*	*similar*	*w2 larger*	*w2 smaller*	*similar*
2		X			X			X	
3	X					X			X
4			X			X			X
5	X			X					X
6	X					X	X		
7	X					X	X		
8			X		X				X

Control Limb

Participant	VAD			Vessel Count			Mean Vessel Diameter		
	w2 larger	*w2 smaller*	*similar*	*w2 larger*	*w2 smaller*	*similar*	*w2 larger*	*w2 smaller*	*similar*
2		X		X				X	
3	X					X	X		
4	X			X					X
5		X			X				X
6			X			X	X		
7			X			X			X
8			X			X			X

Figure 4.15. Maximum Dilation Test summary of trends between week 2 and week 0. Comparisons of measurements from week 2 to week 0 for each ROI on each participant. A threshold of ±5% was used here as the threshold to determine if measurements were larger, smaller, or similar. Week 1 to week 0 comparisons are shown in Appendix E.

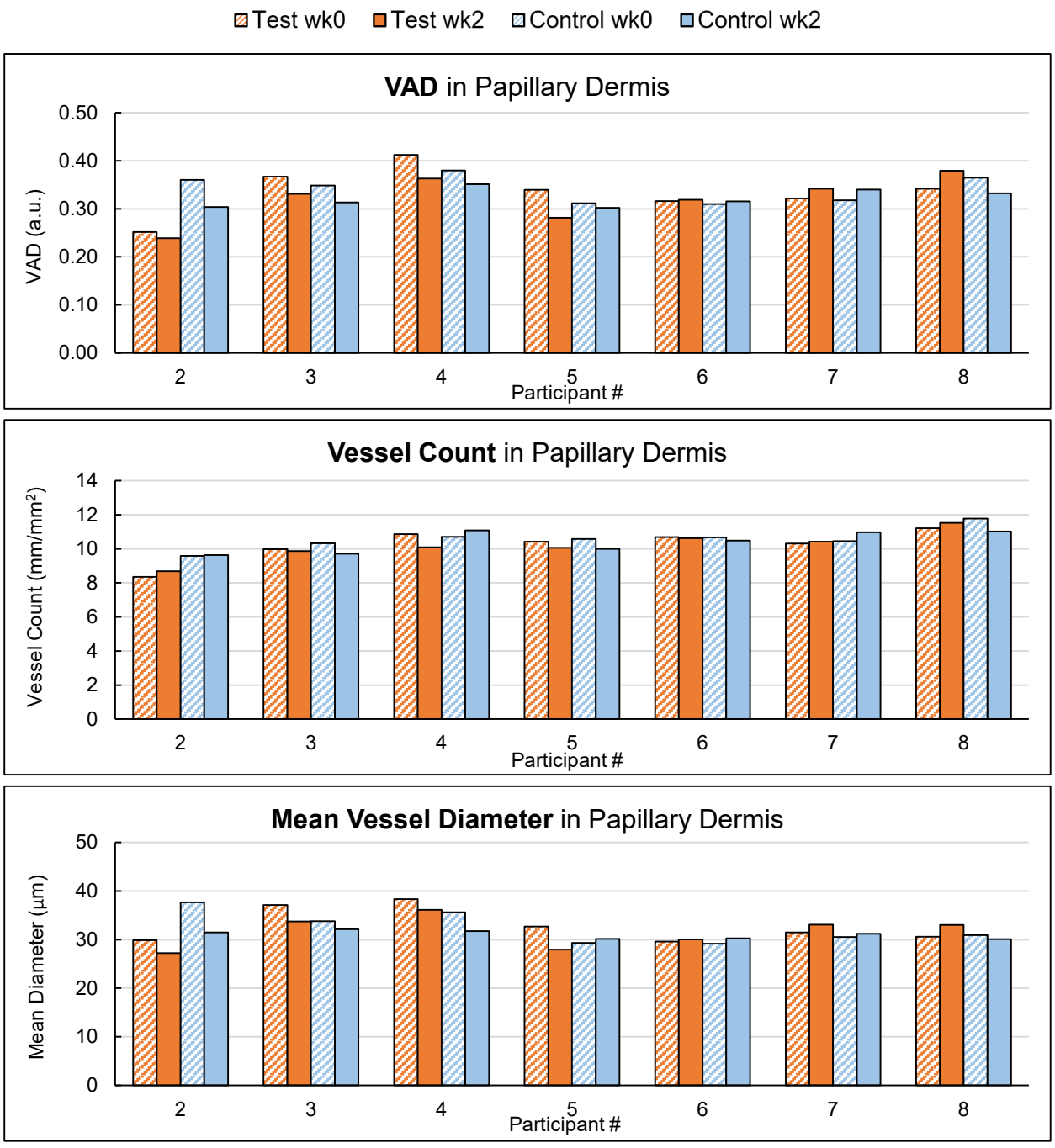

Figure 4.16. Maximum Dilation Test measurements by participant for 0 and week 2. The test ROI and control ROI are shown for vessels in the papillary dermis. Participant 1 was excluded due to changes still being made to the test methods.

4.4.6 *Epidermal Thickness*

Epidermal thickness was measured from the Maximum Dilation Test images for all study participants. Measurements taken from before the Able-Bodied Socket was worn (week 0) and after it was worn (week 2) are shown in Figure 4.18. A small increase in epidermal thickness was demonstrated from week 0 to week 1 and again to week 2, as shown in Figure 4.17. These differences were statistically tested using a two-way repeated measures ANOVA. The data did not contain outliers and was normally distributed, as assessed by boxplot and Shapiro-Wilk test (p>0.05), respectively. A statistically significant two-way interaction was found (p=0.034), however upon further investigation of the simple main effects, no statistically significant relationships existed.

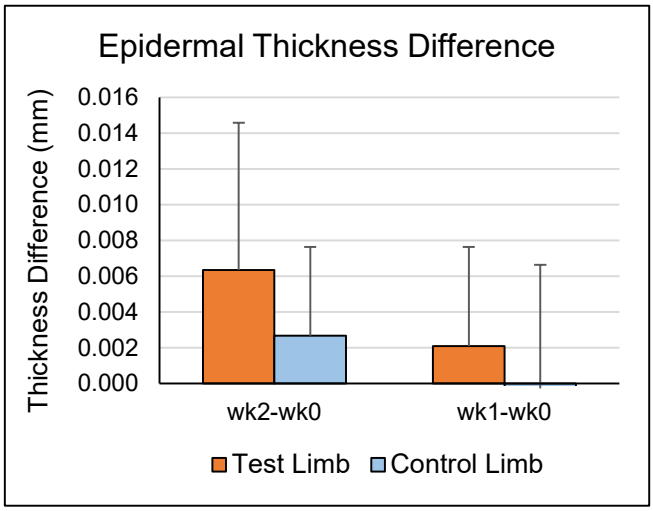

Figure 4.17. Epidermal thickness difference from week 0 to weeks 1 and 2. Shown are the means for each participant. Error bars are one standard deviation.

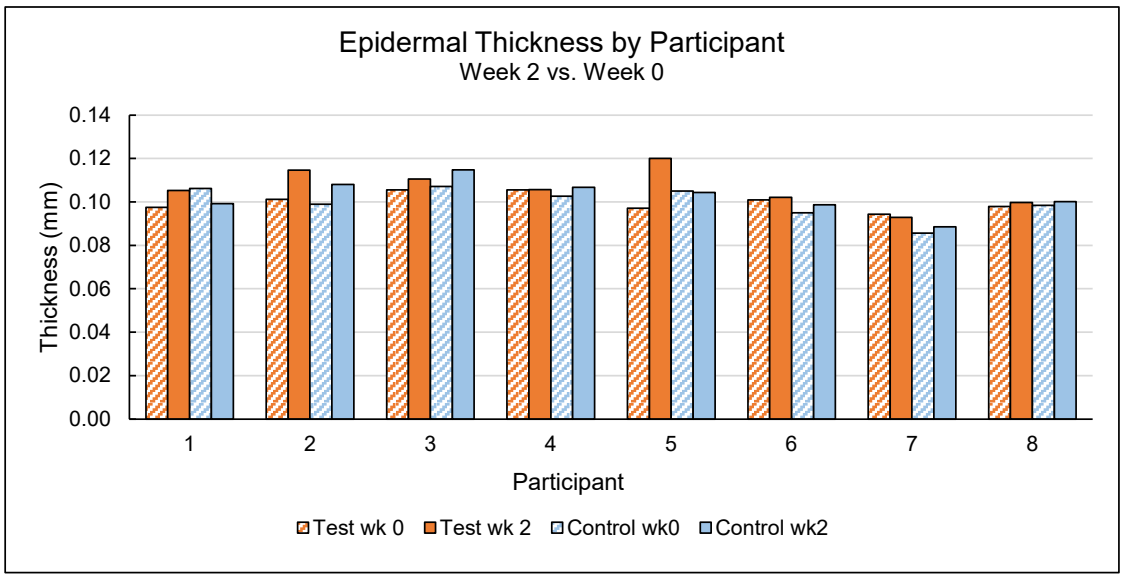

Figure 4.18. Epidermal thickness for all study participants, week 0 and week 2.

4.5 DISCUSSION

In the current study, we demonstrated the use of new noninvasive techniques for the investigation of skin adaptation using an able-bodied model for adaptation to a below-knee prosthetic socket. This study highlighted the utility of OCTA for investigating skin health by providing rich data sets measuring microvascular function and structure. The study also emphasized several of the advantages that OCTA has over other noninvasive techniques currently available for the assessment of the cutaneous microvasculature. For one, no current method can provide images of vessels down to 1.0 mm in the skin, thereby enabling the assessment of vessel morphologies *in vivo*. Additionally, because of this advantage, OCTA measurements possess a repeatability of imaging area and imaging depth that cannot be accomplished by other imaging methods. In the current study these capabilities were exercised to ensure the same depths of vessels were used for every measurement and, in the Maximum Dilation Test, to ensure the same vessels were being analyzed several weeks apart. Also, since vessel images were used to obtain vessel measurements it was possible to identify when measurements errors occurred, thus offering an additional step of data verifiability which is usually not possible with other measurement techniques.

The current study also identified several challenges currently present with the OCTA-based measurements. These challenges are discussed in detail in Section 4.5.5. Briefly, the key limitation present in the functional vascular assessment (RH Test) was that imaging did not begin quickly

enough following the load stimulus removal and the RH peak was not captured in several tests. This limited the ability to measure key functional parameters and thus limited the ability of the current study to compare measurements taken at each ROI during separate test days. It was also apparent that some variability in image quality was present which may have limited the reliability of vessel measurements. For one, some variability in tissue illumination and imaging focus depth was clear in both tests which led to some variability in vessel signal-to-noise ratio and vessel diameters, respectively. Similarly, vessel quantification in the current study relied on a user-selected threshold to determine what intensity magnitude would be used to identify which pixels were considered vessels. As such, these measurements were likely subjected to inaccuracies and potential biases inherent in using a subjective method such as this. Section 4.5.5 also includes suggested strategies for overcoming these challenges in future studies.

In terms of the able-bodied model for adaptation, all participants were able to wear the Able-Bodied Socket for the approximate daily wear times outlined in the sample timeline without any complaints of pain or discomfort and without any indications of skin not tolerating the loading. However, based on the results of the OCT-based measurements, no statistically significant changes were found in the region of skin that was subjected to limb-socket interface stresses in the study. This either suggests that skin adaptation did not take place at the test ROI—potentially due to the ROI not receiving enough stress—or that the measurements taken were not involved in the skin adaptation process. While a main goal of this study was to maintain participant safety and to limit the risk of a skin injury, the fact that no instances of minor skin damage were even found indicated that perhaps the approach used here was too conservative. This was further supported by the FSR data which indicated that interface pressures imposed at the test ROI were far below those experienced by the residual limb in a transtibial socket. Even taking into account potential errors up to ± 44% for using FSRs to measure limb-socket interface pressures [101], many participants demonstrated peak interface pressure measurements that were still at least 47.6% less than those typically seen in lower limb prostheses. It is likely the participants' limbs could have withstood higher interface stresses (i.e. more offloading of the foot) or a more aggressive daily wear regimen that ramped up more quickly in the first week. This is discussed further in the Limitations section below.

4.5.1 *Microvascular Function*

In the Reactive Hyperemia (RH) Test, a standard RH response appeared to be induced in most tests, as evidenced by a measured increase in blood perfusion (VAD) that was well above the baseline perfusion and then a gradual decrease back towards the baseline. In 8 total tests a RH response was not measured. Six of these 8 tests came from two ROIs—the control limbs of Participants 1 and 4—which did not produce a measured RH response in all 3 tests taken at the site. The other two non-RH responses came from Participant 2, one from each limb. In all of these cases, no notable and sustained increase in perfusion was measured by the VAD trend during the test. One possible explanation for this lack of an RH response is that a response did occur but had already resolved by the time the imaging began. Alternatively, it is possible that an RH response did not occur in the papillary plexus or was too small to be noticed by the imaging methods used. Either way, the fact that this behavior was consistently seen in these participants supports the repeatability of the RH Test methods.

Of the 40 tests which produced a measured RH response in the current study, only 12 of them appeared to have had the peak captured. For the other tests, the peak VAD measurement occurred in the first image that was captured following the stress removal. The fact that in many tests the peak was not captured limited the insights that could otherwise have been gained from this study. For these tests it is unknown if a higher peak VAD or a faster time-to-peak would have been measured if imaging would have occurred sooner. Failing to capture the peak also slightly impacted the recovery time measurement since it was calculated as a recovery 75% of the way back to the baseline VAD from the peak VAD. Therefore, if a higher peak VAD would have been measured, the recovery time would have been reduced. Still, it is expected that the recovery time measurement would have only been minimally impacted, unless a significantly larger peak VAD occurred. Despite the lack of RH peak capture, insights could still sometimes be gained from data sets when the peak was found in one of the three time points (week 0, 1, or 2).

A variety of trends were seen in the RH measurements when compared over the course of the study. As summarized in Figure 4.9, for each ROI and each parameter, some participants demonstrated increases with time, while others demonstrated decreases, and others had similar measurements. Four participants demonstrated a slower recovery time in the test ROI both at week 1 and at week 2, compared to week 0. Three of these participants displayed the trend in both weeks (Participant 1, 3, and 5), whereas Participant 6 and 7 had a slower recovery time only in week 1

and week 2, respectively. A delayed RH recovery time usually indicates poor tolerance to an imposed stress, which forms the basis for using skin redness duration as a clinical evaluation of load tolerance. A delayed RH recovery may also be indicative of tissue damage [54]. It is possible this trend was seen in the current study due to irritation of the skin still present form the final day wearing the socket. It is also possible the skin had not fully adapted to the socket stresses and that more time spent at the current daily load time was needed to adapt the skin. Future studies should use a longer recovery period between the final day wearing the socket and the final imaging session and should also consider extending the number of days the socket is worn.

Both of the individuals who demonstrated an increased load tolerance at the test ROI in the Load Tolerance Test also showed a decreased time-to-peak in the RH Test. Usually a delayed RH time-to-peak is indicative of vascular dysfunction [53] or tissue damage [54]. As explained above, this result may have occurred due to residual irritation in the skin from the final day wearing the socket. Alternatively, it could be that this is representative of a functional adaptation, perhaps to limit ischemia-reperfusion injury, although this explanation is not well-supported by existing research.

OCT images collected in the RH Test did not use a refractive-index matching medium or glass on the skin surface, despite these methods being commonplace for OCT imaging of the skin. Refractive-index matching mediums, such as mineral oil, and smooth IR-transparent materials, such as glass or plastic, are commonly used to enhance the transmission of the OCT laser into the tissue, leading to improved signal-to-noise ratio and penetration depth. In the current study, RH Test images were taken of bare skin to minimize the amount of time between the stress stimulus removal and the start of imaging to increase the chance of capturing the peak of the RH response. Additionally, preliminary tests using glass and mineral oil sometimes resulted in images with severe hyper-reflection artifacts that occurred when the glass or oil surface was oriented perpendicularly to the OCT laser. In these cases, the data sets were not useful because an accurate image of the vessels could not be obtained when hyper-reflection was present. In the current study, the exclusion of oil and glass did result in reduced vessel signal-to-noise ratio and a limited penetration depth, however no data sets were lost due to hyper-reflection. Additionally, a smooth RH curve was obtained for a vast majority of tests. Taken together, these results support the collection of OCTA images on bare skin for the purposes of measuring an RH response. Future iterations of the test could attempt to reintroduce oil and glass to improve image quality, however

engineering measures would need to be put in place to enable rapid placement of these materials and to ensure the glass remains tilted at a minimum of 10° from the OCT laser.

While the repeatability of RH feature measurement in response to a cyclic combined compression and shear stimulus has not been assessed, excellent repeatability of the RH response to forearm occlusion has been demonstrated. Using Laser Doppler Flowmetry (LDF) to measure blood flow, Yvonne-Tee *et al.* measured forearm RH following a 3-minute cuff occlusion of the brachial artery with LDF [116]. On two separate days, two repeat measurements were taken with at least one hour between and them, for a total of four measurements. The researchers found excellent repeatability (defined as an intraclass correlation coefficient greater than 0.75) for the peak RH perfusion and time-to-peak measurements. Recovery time was not assessed. It is likely that the RH Test measurements obtained in the current study had slightly less repeatability than LDF, largely due to the layer of vessels that each signal most represents. LDF measurements are heavily dictated by larger vessels in the subpapillary plexus whereas OCTA measurements are focused on smaller vessels in the papillary plexus which are highly active and whose flow is influenced by a variety of factors. Furthermore, it was not expected that a repeatable RH response would be measured in the current study since changes were anticipated to be occurring in the skin at both of the ROIs. Even the control ROI skin was subjected to repeated heating and tension due to wearing the prosthetic liner. That said, some participants did demonstrate similar RH measurements over the course of the study. Participant 7 and 8 demonstrated similar peak VAD measurements during all 3 tests (week 0, 1, and 2) performed at each of their ROIs. Participant 8 also demonstrated a similar recovery time at the control ROI across all three imaging sessions. Recovery time measurements were also similar between week 0 and week 1 for Participants 3 and 5. Despite the variations measured in responses, it was encouraging that a smooth, measurable RH response was captured in a majority of tests, and that most of the non-RH responses occurred across all tests run at their respective ROIs. These results suggest repeatability of the measurement techniques; though further investigation would be needed to verify this. Further improvements enabling the reliable capture of the RH peak would further enhance the usefulness of this test and the potential insights that could be gained from it.

4.5.2 *Microvascular Structure*

The values obtained for mean vessel diameter in the papillary dermis were consistent with vessel diameters commonly found in the cutaneous microvasculature. Mean diameters ranged from 27.2 μm to 37.7 μm in this superficial vessel layer, which was within the range expected of arterioles and venules in the papillary plexus, which range from 8-35 μm [35]. Vessels measured in deeper, reticular dermis segment in the current study ranged from 47.1-58.2 μm. It is expected that these vessels were still part of the papillary plexus of the microvasculature since the penetration depth of the OCT laser was unlikely to have reached the subpapillary layer in the lower one-third of the dermis. As such, these vessel diameters are slightly larger than expected. It is possible that some subpapillary vessels extended up into the OCT imaging range, as these vessels range from 34-50 μm in diameter. More likely, however, is that the diameters measured in the reticular dermis were inflated due to overlapping of multiple vessels and vessels running next to each other that were not resolved as two vessels. As such, the vessel diameter calculation made in the current study was a rough estimate of the diameters present in the tissue.

Based on the appearance of vessel loops in the papillary plexus, it is believed that at least some of the capillaries present in the tissue were present in the OCTA images. While capillaries generally range from 4-12 μm, making most capillary loops smaller than the 20 μm lateral resolution limit of the OCT system used, OCTA can often capture smaller vessels, however the diameter of these vessels will only appear as small as the resolution limit.

OCT-measured vessel density has previously demonstrated excellent repeatability as a measure of tissue perfusion. Men *et al.* tested the repeatability of the VAD measurement in the skin of healthy volunteers in the wrist, forearm, shoulder, and upper arm. Separating the papillary and reticular dermal layers and comparing measurements over three images taken 5 minutes apart, the researchers found VAD to be a repeatable measurement producing coefficients of variation ranging from 2.0-2.4 and intraclass correlation coefficients ranging from 0.854-0.943 [117]. No studies have systematically tested the repeatability of OCTA vessel count and vessel diameter measurements. However, since these parameters are determined from the same images as the vessel density measurement it is expected that the repeatability would be similar for all of the measurements with only slight differences due to the algorithms used for quantification. It is known that the quantification methods used in the current study were subject to some limitations, namely the use of a subjective user-defined threshold for determining which pixels were part of a

vessel and the potential for differences in OCT focal depth leading to differences in vessel diameters. These limitations, as well as suggestions for overcoming them in the future, are discussed further in Section 4.5.5.

The skin marking method used proved to be a repeatable means of imaging the same regions of skin throughout the course of the 2-4 weeks between the baseline imaging session and the final imaging session. Registration of *en face* vessel images taken in the same ROIs throughout the study demonstrated a mean overlapping region equivalent to a square region with sides of 7.0 mm (SD ± 0.3 mm). In most cases the loss of overlap occurred due to rotation of one image with respect to the other. In the current study, additional measures were not taken to ensure the same OCT probe rotation above the ROI was used. In the future, using additional marks to ensure rotation is repeatable could yield even better overlap in the imaging field-of-view. The ability of OCTA to register vessels so that only measurements from the same regions are analyzed over the course of several weeks highlights one of the key advantages of OCT over other skin measurement techniques. Other methods commonly used in skin microvascular studies such as Laser Doppler Flow and Laser Speckle Contrast Imaging can only, at best, try to maintain a repeatable imaging location using fiducial markers on the skin surface. As demonstrated by our skin marking method here, relying on skin surface marks alone can still lead to shifts in the field-of-view up to 38% (the resultant overlapping field-of-view divided by the full image field-of-view of the worst overlap between two images at the same ROI). Here, we were able to remove areas from analysis that did not overlap. Considering the heterogeneity of the cutaneous microvasculature even small shifts in the imaging field-of-view could notably impact results.

Vessel morphologies appeared similar between registered images at each ROI over the course of the study. In many images the appearance of some of the small vessels was inconsistent. This occurred heterogeneously across all time points, for example some vessels would be present in week 0 but not week 2, and vice versa. These differences were likely due to the size of these small vessels being near the resolution limit of the imaging system. Thus, a small change in OCT depth focus, tissue illumination, or red blood cell velocity may have been enough to dictate whether the vessel was measured or not. Despite our efforts to induce a repeatable vascular state small differences may have also existed because the cutaneous microvasculature is highly active and a true repeatable state is likely not possible. Prior microvascular studies which have used heating to induce maximum dilation have used methods that were unable to distinguish differences

as minute as individual capillaries and arterioles. This further highlights an advantage of OCTA over existing flux-based techniques to measure the microvasculature. In the future, more inclusive and thus more accurate images of vessel structure could be obtained with OCTA by taking multiple full field-of-view images and combining all of the vessels identified into one.

The utility of OCTA for measuring the cutaneous microvasculature in response to a local heating protocol was recently demonstrated for the first time by Smith *et al.*[118]. The researchers used a commercially available skin heating probe (PF450, Perimed AB, Stockholm, Sweden) to warm the skin on the ventral forearm of study participants and imaged the skin with OCTA. While the study did well to introduce the concept of using OCTA with local heating and to demonstrate the value of this type of vascular assessment for exercise physiology research, we believe that the methods developed in this dissertation offer several improvements over these methods that may help to advance the methods even further. For one, the researchers did not appear to use a heating medium and instead used the heating probe only to directly heat the skin surrounding the OCTA imaging area. The lack of a heating medium likely resulted in greater variability within the OCTA imaging region. The lack of a heating medium may have also been the reason why a temperature of only approximately 34°C was used, rather than the 42-44°C required for a stable state of maximum dilation. It is possible the researchers chose to not to use a medium in order to limit motion artifacts that become more prevalent when a liquid heating medium is used. By using mineral oil as the heating medium along with several motion artifact-reducing techniques, the current study achieved a reproducible state of maximum dilation with minimal motion artifacts which enabled the comparisons of vessel structure in images recorded up to three weeks apart. Another critical aspect of the vessel structure comparisons in this thesis was that vessels were registered to each other and any non-registered regions were removed from the analyses. Smith *et al.* analyzed vessels in the entire 5 x 5 mm imaging region, which appeared to result in fields-of-view which were slightly translated with respect to each other when comparing images taken at the same location in two separate test sessions. While the researchers showed good repeatability of quantified values at skin sites between two test sessions, these results would be more accurate if a similar vessel registration method were used to ensure the same vessel regions are compared in each session.

4.5.3 *Epidermal Thickness*

Epidermal thickness measurements taken on able-bodied participants in the current study compared closely to values commonly reported in literature. Measurements ranged from 0.086 mm to 0.120 mm, while commonly accepted epidermal thickness of most body sites, excluding the palms of the hands and soles of the feet, is 0.06-0.10 mm [29]. This suggests that the methods used here may have slightly over-estimated the epidermal thickness. Using OCT to measure epidermal thickness has been well-documented. Gambichler *et al.* demonstrated that OCT-measured epidermal thickness compared closely with measurements made from using routine histological measurements. In patients with psoriasis and actinic keratosis, using a system with a slightly finer depth resolution than the system used in the current study (3.0 μm vs. 5.6 μm), they found the upper and lower 95% limits of agreement between measurements to be 4.7 μm and -20.3 μm respectively [119]. Additionally, automatic skin layer detection for measuring epidermal thickness in OCT images has been shown to be a reliable method of obtaining the measurement. A study by Josse *et al.* which used a similar automatic epidermal thickness calculation demonstrated measurements that differed by less than 5 μm compared to expert-measured epidermal thicknesses on the same OCT images [120].

Epidermal thickness measurements taken of skin that was not stressed by the Able-Bodied Socket (all control ROI measurements and week 0 test ROI measurements) compared closely to measurements taken at a similar anatomical location on individuals with lower limb loss in the Aim 3 study. The means in the current study were 0.101 mm and 0.100 mm for the control ROI (all weeks) and the week 0 test ROI, respectively, compared to 0.100 mm in the Aim 3 study. The 0.006 mm increase seen in the mean of the test ROI by week 2 in the current study is one-third as large as the 0.017 mm difference between the residual limb and contralateral limb ROI in the Aim 3 study.

Though no statistically significant differences were identified in the epidermal thickness over time at the test ROI and control ROI, there was an overall mean increase in thickness at the test ROI from week 0 to week 1, and again from week 1 to week 2. A marginal increase was seen in the control ROI as well, though the magnitude was about one-third of the change measured at the test ROI. Comparing participants who showed improved skin load tolerance via the Load Tolerance Test versus those who did not, no patterns in epidermal thickness results were noted. Of the four participants who showed decreased redness time, one possessed the largest thickness

increase from week 0 to week 2 (0.020 mm), however the others showed minimal to increase (0.008 mm, 0.005 mm, 0.000 mm, and 0.002 mm), differences which are near the 5.59 μm depth resolution limit of the system. It is possible the increases seen here represent some form of skin adaptation to the interface stresses of the Able-Bodied Socket and/or prosthetic liner on each limb.

4.5.4 *Load Tolerance Test*

Following the redness evaluation of Load Tolerance Test photographs by a blinded clinical expert, it was found that two participants had skin redness that lasted longer than 10 minutes in the week 0 test and less than 10 minutes in the week 2 test. This indicated that, using the current clinical measure of skin redness duration, these two participants had increased the tolerance of their skin to the load stimulus used during the test. Since this load stimulus was designed to mimic the interface stresses that the participants' test legs had been subjected to in the Able-Bodied Socket, this may be an indication that the skin of these individuals had adapted into a more load tolerant state as a result of wearing the socket for two weeks. Interestingly, one of these participants (Participant 8) spent more time wearing the socket and significantly more walking time than all other participants, and demonstrated the second highest ROI interface pressures. The other, Participant 5, ranked near the median of all participants in these categories. For the rest of the participants, an increase was not found in load tolerance from before wearing the socket to after the two-week wear period.

While this test method shows promise for monitoring changes in skin load tolerance, the results here were subjected to several confounding factors. For one, while preliminary tests suggested that the stress stimulus used in this study would produce redness that lasted for longer than 10 minutes in some individuals, redness lasted less than 10 minutes during the week 0 test session for 4 of the 8 participants. As such, rather than using 10 minutes as a binary indicator of "tolerance" we graded the responses by the time it took for the redness to resolve. While doing so indicated that 4 participants decreased the tolerance time, the others did not. Of the remaining four participants, one participant showed an increase in redness duration of 10.0 minutes; however, the redness assessment was difficult to perform on this individual due to the presence of excessive hair at the ROI, suggesting that hair at the ROI should be trimmed in the future. Another participant showed a redness duration increase of 1.8 min by week 2, with no obvious confounding factors present. This may indicate the limits of the repeatability of the Load Tolerance Test, or the result

may have been due to minor skin damage that had not yet resolved following the last day of wearing the socket. Pressure-induced skin damage has been shown to cause increased vascular recovery time following an imposed occlusive stress [54]. The remaining two participants who did not show a decrease in redness duration by week 2 produced this result because their week 0 test could not be evaluated due to excessive redness still present from the Maximum Dilation Test heater at the test ROI. The presence of this redness made it impossible to accurately determine redness due to Load Tolerance Test stress stimulus. However, for these two participants, they could not have shown an increase in tolerance given the study methods since in their week 2 test the skin was still red up until the end of the 15-minute photo collection period. Interestingly, though the same methods were used during the week 2 and week 0 tests, these two participants did not experience sustained redness from the Maximum Dilation Test during the week 2 test. Though further investigation would be needed, it is possible this was due to adaptation of the skin, either due to mechanical stresses of the Able-Bodied Socket, repetitive heating from wearing the liner, or due to the Maximum Dilation Test heater itself.

Each participant responded differently to the applied stress of the Load Tolerance Test prior to first wearing the socket, some with redness lasting as short as 2.0 min and others who had redness last beyond the full 15-minute recovery period. It is likely that the load stimulus used may need to be adjusted to suit the individual if redness greater than 10 minutes during the week 0 test is to be achieved. As described in the following paragraph, the results of the current study suggest that it may be helpful to use the Fitzpatrick skin type as a starting point for distinguishing who gets a higher or lower load.

Though it was not a main focus of the current study, a correlation was observed between participant Fitzpatrick Skin Phototype (FSPT) and skin redness recovery time during the Load Tolerance Test (Figure 4.19). A Spearman's rank-order correlation was run to assess the relationship between FSPT and redness recovery time following the prescribed mechanical stress of the Load Tolerance Test. After preliminary visual assessment of a scatterplot demonstrated the relationship to be monotonic, there was a statistically significant, strong negative correlation between FSPT and redness recovery time, $r_s(6)=-0.778$, $p=0.023$. To our knowledge this relationship between FSPT and measured skin reactivity to a mechanical load has not been investigated previously. However, FSPT has been suggested for use as a contributing factor in the risk assessment for hospital-acquired pressure ulcers, though its predictive value has not been

thoroughly validated [121]. One possible explanation for the correlation seen in the current study may be that differences in skin complexion associated with each skin type which could alter the ability of a redness evaluator to notice the differences in color. This difficulty to assess skin discoloration and early skin damage in individuals with darker skin tones has been reported. A recent review by Gunowa *et al.* on pressure injuries in individuals with darker skin tones highlighted that individuals with darker skin tones are less likely to develop low-stage pressure injuries but more likely to develop high-stage pressure injuries, which the authors suggest may be due to the ineffectiveness of current colorimetric-based assessments used to diagnose early skin damage [115]. As such, it may be that a more direct measurement of cutaneous microvascular reactivity to an imposed mechanical stress would be a better predictor of skin breakdown risk, for example using a method similar to the RH Test used in the current study. Although the correlation between skin type and redness duration found here is an interesting finding, since our study was not specifically designed to test the relationships between FSPT and skin recovery from a mechanical load, further testing would be needed to confirm these findings.

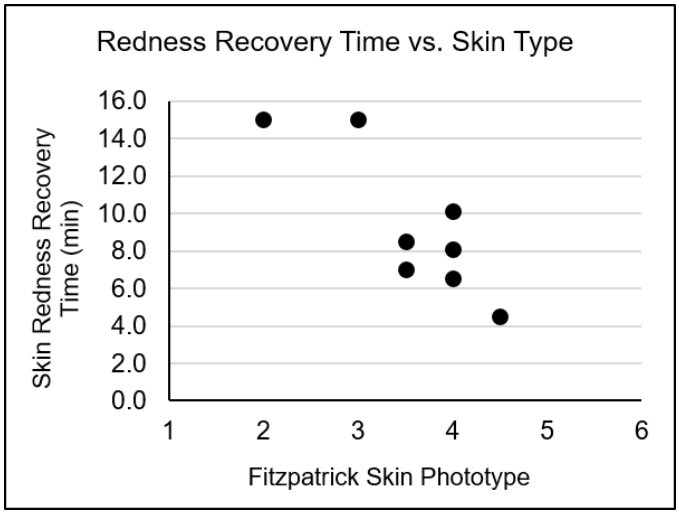

Figure 4.19. Load Tolerance Test redness recovery time versus Fitzpatrick Skin Phototype. Each data point represents one participant and includes the mean of their Load Tolerance Test skin redness recovery measurements and their self-reported FSPT. A statistically significant, strong negative correlation was found between the two variables in the current study.

4.5.5 *Limitations*

Though the current study set out to identify markers of skin adaptation to mechanical stress, no statistically significant changes were identified in skin that had been mechanically stressed over time versus a liner-only control. In fact, OCTA images taken at maximum dilation suggested that very few structural changes had occurred at all over the course of the two-week socket wear period. While this may represent a real physiological result, and it may be that the parameters measured are in fact not involved in skin adaptation, an alternative explanation is that adaptation was not induced by the able-bodied model that was used. A key limitation with the current study was that we could not easily control the stress that was delivered to the test ROI and it was thus likely lower than required to induce adaptation to the level that could be identified with the study methods. Additionally, two weeks of gradually increasing socket wear time may not have been enough of a stimulus to induce adaptation.

In regions of high interface stress within a transtibial prosthetic socket, the limb has been shown to experience pressure in the range of 100-250 kPa peak pressure during walking [18,98,99]. In the current study, the FSR-measured walking peak pressure at the ROI in the Able-Bodied Socket ranged from 3.3-53.4 kPa. The participants with the three highest peak pressures had mean peak measurements of 53.4 kPa, 22.0 kPa, and 16.0 kPa, respectively. Considering the potential for FSR measurement errors up to ±44% [101], the highest these values could have reached were 95.3 kPa, 39.5 kPa, and 28.6 kPa. This suggests that the pressure delivered to the ROIs were much lower than the interface pressures typically experienced by a transtibial residual limb. Though stress was increased at the ROI by using firm foam pads on either side of the tibial crest, it was difficult to increase stress beyond a certain point due to the shape of the limb and the fact that blood supply to the foot needed to be safely maintained. Additionally, the lack of a measurement for interface shear stress limited our ability to determine how well the Able-Bodied Socket stresses mirrored those of a transtibial prosthetic socket. Shear stress plays a major role in occlusion of cutaneous blood flow when both pressure and shear are imposed [64], and shear can be present at large magnitudes in a prosthetic socket [18,122]. Thus it is likely to be an important factor in skin adaptation for transtibial prosthetic users. In the future, it would be beneficial to measure both pressure and shear applied at the ROI. Better methods for measuring pressure would also be beneficial. It would be especially beneficial in future studies to use a more accurate means of pressure and shear measurement at the ROI that can be visualized in real-time during the socket

fitting session so that changes may be made in a more targeted manner to get closer to the desired stress targets. One possible solution may be to install a strain gage-based tri-axial force sensor at the ROI either through the side of the socket wall or incorporated into a 3D-printed socket insert, which is a strategy that has been demonstrated with low-profile sensors previously [123].

Despite the desire to increase stress to the ROI, the Able-Bodied Socket model was limited in its ability to increase stresses beyond a certain point. We aimed to offload the foot by suspending the limb in the socket, however full offloading could not be achieved without creating a circumferential stress point which occluded blood flow to the foot. Occlusion could be identified quickly as the presence of a strong pulsing sensation in the limb and was avoided. As such, limbs were only partially offloaded. Still, for all participants, stress at the ROI was confirmed during the socket fitting session by noting the presence of redness following a bout of walking in the socket. However, the ROI did not always appear to be the region of highest stress on the limb. While the ROI was selected by the study prosthetist as a region that was anticipated to be in a region of high stress, it was not possible to predict the extent of the loading at this site compared to other nearby sites. Furthermore, it was difficult to precisely control the stress concentration location on the foam pad while still maintaining a prosthetic design similar to a traditional below-knee socket design. For example, Participant 8's test ROI region did appear red after wearing the socket, however a region approximately 1.2 cm distal of the ROI and 0.4 cm closer to the tibial crest demonstrated intense redness that lasted longer after doffing. Moving pad locations and adjusting socket alignment did not cause redness to increase at the ROI. A possible solution to this issue in the future would be to select the ROI after the socket is first worn and regions of highest load are identified. Since the limb experiences a significant amount of stress during the fitting session from repeatedly donning and doffing the socket and performing various activities to assess the fit a period of 1-2 weeks would likely be necessary prior to the first OCT imaging session to allow the tissue to fully recover from the stress. Similarly, the chance of inducing adaptation at the ROI could be further improved by extending the wear time. In the current protocol participants only reached 90 minutes of wear time by the end of week 1 and 7 hours by the final day. Stressing the limb for 1-2 more weeks at higher wear times would significantly increase the accumulated stress imposed on the limb. However, these proposed strategies would likely limit participant recruitment and could lead to a higher drop-out rate considering the protocol used was already fairly long and time-intensive. A better solution may be to increase the wear time more rapidly, especially during

the first week. The target wear schedule used in the current study was based off of a typical wear schedule that might be used by an individual who is adapting to their prosthetic socket for the first time following an amputation surgery. Participants in this study progressed through the target wear times without any issues and without any reports of discomfort. It is likely that a more aggressive wear schedule could have been used.

Stress imposed on the limb could also be increased by modifying the manner in which the load is applied to enable increased stress magnitudes and to ensure that the stress application is more consistent among participants. This could be accomplished by creating sockets with a panel, or panels, in the side of the socket that can be mechanically controlled. Sockets using this design have recently gained popularity for lower limb prosthetic users. Electromechanically controlled versions of the system have also been used in prosthetics research [124]. A system such as this, which is automatically controlled based on the load that is being applied by the panel could result in a more controllable able-bodied model for adaptation and significantly increase the likelihood that adaptation is induced.

Another key limitation was that the RH peak was not reliably captured in the RH Test, which resulted in several gaps in the data collected in that test. As such, it was thus not possible to compare all of the desired parameters over time. This lack of RH peak capture was caused by the time delay between the load stimulus removal and the first post-load image lasting longer than it took for most participant ROIs to reach the peak of the RH response. While some insights could still be gained from this test due to the peaks which were captured, if this test is to be used in the future it should be improved so that the RH peak is more reliably captured. The transition from load removal to imaging was limited by the time it took to remove the loading device, center the OCT imaging location on the skin and in the software, and adjust the OCT pressure and focus into the target ranges. It is likely this process could be hastened by 10-15 seconds by including additional personnel to complete these tasks, however doing so may introduce additional possible failure points into the test. A more reliable approach would be to automate part of the transition process. For example, a motorized system attached to the OCT probe could be designed that could rapidly and automatically set the desired OCT pressure and focus. In addition, software improvements could be made to the OCT imaging controller that would automatically center the field-of-view between fiducial markers on the skin. A more comprehensive solution may be to

redesign the stress application probe to incorporate the OCT probe so that only a minor changeover is needed when switching from the load application step to the imaging step.

Some limitations were also present in the OCT imaging methods used. One of these was the reliance on a user-defined threshold for determining how vessel images were binarized. The threshold was chosen for each set of *en face* images to balance the inclusion of all pixels that visibly appeared to be a part of a vessel with the exclusion of background noise and motion artifacts. Despite efforts to make this process consistent, inherent biases and inconsistencies were likely present. To increase the reliability of future measurements less subjective methods should be developed. Biases could be reduced from imaging results if a blinded researcher was used to choose the threshold. Another alternative would be to develop an automatic thresholding algorithm, such as those that have been used by others when quantifying OCT data [94,125]. Additionally, OCTA is known to commonly possess shadow artifacts, whereby vessels in the more superficial regions of the tissue are extended into the tissue below them. While this does not directly affect *en face* images of the superficial vessels, or of the entire skin vessels, when the lower vascular region is separate out these shadows are often present even though they do not represent vessels physiologically present in that depth of tissue. In the current study, this can be seen in the reticular dermis sections of vessels. In the future, vessel de-shadowing techniques used by others [126] could be adapted for use with the Maximum Dilation Test images. This would enable more direct and accurate analysis of the reticular dermis vessels.

4.6 CONCLUSION

In the current study, new noninvasive techniques were introduced for the investigation of skin adaptation to mechanical stresses. These OCT-imaging based techniques were tested on eight able-bodied participants whose skin was mechanically stressed by a modified below-knee prosthetic socket. Participants wore the sockets for two weeks using a protocol of gradual increases in daily wear times up to 7 hours per day. Measurements of cutaneous vascular function were taken using the developed Reactive Hyperemia (RH) Test and demonstrated that a measurable RH response was reliably induced in the study participants. Measurements of vessel structure using the developed Maximum Dilation Test demonstrated good repeatability of the imaging location throughout the course of the study, which included the ability to verify the same vessels were being compared at each time point. Measurements of vessel density, vessel count, and mean vessel

diameter were fairly consistent over time at each ROI and did not produce any statistically significant relationships between time points or test versus control ROI. A small increase in epidermal thickness was demonstrated at the test ROI after wearing the socket for two weeks, however this difference was not statistically significant. No significant differences in any of the OCT measurements were found, even when grouping participants by activity and interface pressure level or looking at only those individuals who demonstrated increased load tolerance at the ROI in the Load Tolerance Test. We believe this is because the skin at the region of interest was not stressed enough by the current Able-Bodied Socket design to induce measureable skin adaptation.

In addition to highlighting advantages of the developed methods, the current study identified some limitations that should be addressed if they are to be used to continue investigating skin adaptation. For one, in order to reliably obtain all of the desired measurements from the RH Test, imaging must occur more quickly following the stress stimulus removal. This could be accomplished through automating some of the activities required during this transition or by incorporating the OCT probe into the stress application device. Additionally, to increase the chance that adaptation is physiologically induced in the able-bodied participants, changes should be made to either increase the stress magnitudes imposed at the test limb ROI or increase the total amount of time the socket is worn. This could be accomplished by extending the socket wear time, or perhaps increasing the time more quickly, or by incorporating a controlled electromechanical stress application system into the socket. An alternative solution would be to forego further improvements to the able-bodied skin adaptation model and instead use participants who have recently undergone a transtibial amputation surgery and monitor their skin as it adapts to their first prosthetic socket.

Overall, this study highlighted the potential of using OCT-based imaging methods for the investigation of skin adaptation. With the implementation of the suggested improvements, skin adaptation and skin health as a whole as it relates to lower limb prosthetic users can be investigated noninvasively at a level of detail that was previously not possible. By improving the understanding of skin adaptation to prosthetic socket-limb interface stresses, tools could be created for clinicians to better assess the skin health of their patients or to monitor skin adaption during rehabilitation from an amputation surgery. Furthermore, it is possible that noninvasive methods such as these could open up new avenues of research leading to the development of rehabilitation or therapeutic

methods for adapting skin into a stronger state. These improvements could greatly reduce the likelihood of skin breakdown for wearers of prosthetic sockets and significantly improve their quality of life.

Chapter 5. AIM 3: INVESTIGATE SKIN ADAPTATION IN PARTICIPANTS WITH TRANSTIBIAL LIMB LOSS

5.1 ABSTRACT

Background: Mechanically-induced skin breakdown is a significant problem that impacts a majority of lower limb prosthesis users. It is known that skin can adapt to the mechanical stresses of prosthesis use thereby reducing the risk of breakdown, yet little is understood about the biology behind skin adaptation and few methods exist to noninvasively investigate the phenomenon. Optical Coherence Tomography (OCT) is a noninvasive imaging technique with a depth and resolution that makes it well-suited for investigating skin adaptation.

Objective: This study was a proof-of-concept for the use of novel, noninvasive OCT imaging techniques to investigate skin adaptation in individuals with transtibial limb loss.

Study Design: Case study (N=3) of individuals with unilateral transtibial limb loss.

Methods: Two OCT imaging-based tests were used to evaluate features of the skin that may be involved in adaptation to mechanical stresses. A Reactive Hyperemia Test was used to evaluate skin microvascular function by applying a cyclic compression and shear stress and then using OCT to measure the vascular response induced by the stress. A Maximum Dilation Test was used to evaluate skin microvascular structure by applying local skin heating to dilate the cutaneous vasculature. Epidermal thickness was also quantified from the images collected. Tests were run in a region of the residual limb believed to be highly stressed within the prosthetic socket and on a location-matched site on the contralateral limb. Results were compared between the two testing locations and between study participants.

Results: Differences in functional and structural characteristics of the microvasculature were found between the residual limb and contralateral limb of study participants and between the residual limbs of all study participants. Reactive Hyperemia Test data demonstrated a larger magnitude vascular response and a faster time-to-peak vascular response in the residual limb of two of the three participants compared to their contralateral limb. Maximum Dilation Test data demonstrated a larger vessel density in two of the three participants' residual limb compared to the contralateral limb. This difference was due to both a higher vessel count and a larger mean

vessel diameter. Epidermal thickness was also larger in the residual limb versus contralateral limb for all participants. This was the only statistically significant difference found ($p<0.05$).

Conclusions: This study demonstrated the utility of two novel OCT imaging techniques for investigating skin adaptation in users of lower limb prosthesis. While some potential insights into mechanically-induced skin adaptation were identified, further research is needed to confirm these findings and better understand the populations to whom they may apply.

5.2 RATIONALE

The cutaneous microvasculature represents an important target in the study of skin adaptation because of its critical role in maintaining tissue health. The microvasculature supplies tissue with oxygen and nutrients which are essential to maintaining cell viability. When the skin is stressed and blood vessels are fully or partially occluded, oxygen transport into the tissue is reduced, which leads to a key mechanism of skin breakdown [61]. As described in Section 2.3, if the tissue is hypoxic for long enough, usually several minutes, cells will enter an anaerobic state and produce lactic acid and other harmful byproducts that will damage surrounding cells if they are allowed to accumulate. To prevent breakdown, oxygen and nutrients must be restored so that cells can return to a normal metabolic state and the accumulated anaerobic byproducts can be removed from the tissue. While skin adaptation is not well understood in users of prosthetic devices, we hypothesized that adaptations to the microvasculature may occur which would enhance the skin's ability to supply blood to the tissue, in particular following an occlusive stress.

The purpose of Aim 3 was to determine if potential signs of skin adaptation were present in the skin of transtibial prosthesis users. Using the Optical Coherence Tomography (OCT) methods for analyzing cutaneous vascular structure and function that were developed in Aim 1, we studied chronically-stressed regions of skin and compared these measurements to location-matched sites on the contralateral limb—referred to here as the regions of interest (ROIs). Individuals without skin breakdown issues at the ROI were chosen to increase the likelihood that any differences identified would be indicative of skin that had adapted into a more load tolerant state, thus increasing the likelihood that any differences seen could be interpreted as potential markers of adaptation worthy of further investigation.

5.3 METHODS

5.3.1 *Participants*

Study participants were chosen who had a transtibial amputation on one limb and a fully intact contralateral limb. Inclusion criteria required that participants were 18 years of age or older, were at least 9 months' post amputation surgery, regularly visited a prosthetist, and wore their prosthesis at least 7 hours per week. Participants were excluded if they had a history of skin breakdown at the ROI or if they had signs of skin breakdown at the ROI or elsewhere on the limb at the time of study enrollment. Each participant visited the lab for one visit in which all study procedures were completed. All study procedures were approved by a University of Washington Institutional Review Board and informed consent was obtained before any test procedures were initiated.

5.3.2 *Session Protocol Summary*

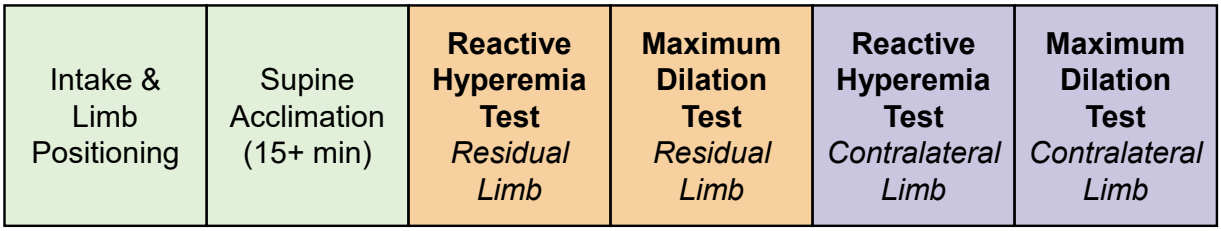

Figure 5.1. Imaging session protocol summary. Test order shown left to right.

Participants were requested to refrain from caffeine or alcohol use at least four hours prior to the test session to minimize the potential effects of the substances on the microvasculature. Test sessions began with participants doffing their socket and completing a brief intake to gather information related to the participant's health status and prosthesis. The research prosthetist then performed a skin evaluation to verify no regions of breakdown were present. The blinds on the windows were closed and the room were closed and room lighting was turned on to reduce the potential influence of variable lighting conditions on OCT images. The test session protocol is summarized in Figure 5.1. The room temperature was maintained between 21-23°C.

Participants then laid supine on the participant bed. A residual limb skin ROI was selected by the research prosthetist on the medial aspect of the tibia that was believed to be in an area of high load within the socket. This decision was based on the shape of the limb and socket and the presence of residual redness after doffing the socket which indicated the skin at the ROI had been

stressed by the socket. The ROI was marked with a surgical marker, taking care to mark only outside of the imaging field-of-view boundaries so that ink did not obstruct the OCT laser. The ROI location was replicated on the contralateral limb using the measurements taken from the mid-patellar tendon and tibial crest, and this location was also marked. Prior to marking the limb, the skin was prepped using an alcohol skin prep pad to remove any substances that could alter OCT images. The participant was maneuvered into a comfortable position with their limbs naturally externally rotated and stabilized by a formable patient positioning cushion (Vac-Lok Cushion, CIVCO Radiotherapy, Orange City, IA, USA). The position ensured the ROI on each leg was oriented facing vertically, which was required for the study instruments to function properly. By removing air from the positioning cushion, the pad shape was solidified and the participant was able to lay with the limbs fully relaxed. Participants remained in the supine position for at least 15 minutes prior to any image collection in order to allow their cutaneous vasculature to acclimate to the room temperature and the position.

Each OCT test was then performed on the residual limb, beginning with the Reactive Hyperemia (RH) Test, followed by the Maximum Dilation Test. These test methods are described in detail in Sections 3.3.1 and 3.3.2, respectively. This test order was chosen so that a baseline image of undisturbed skin could be obtained at the start of the RH Test and to ensure the RH response would not be altered by the prior heating protocol. The influence of the RH Test on the Maximum Dilation Test was believed to be minimal considering 30-45 minutes passed between the load application of the RH Test and the first images of the Maximum Dilation Test. In this aim, three full field-of-view Maximum Dilation images (7.4 x 7.4 mm) were captured.

Following the Maximum Dilation Test on the residual limb, study instruments were moved to the contralateral limb side and both tests were performed on the contralateral ROI, once again beginning with the RH Test followed by the Maximum Dilation Test.

5.3.3 *Data Analysis*

OCT images were post-processed using the methods described in Section 3.2.1 and outlined in Figure 3.1 and Figure 3.2. Briefly, B-scan repetitions were registered to one another to reduce motion artifacts and three-dimensional OCT Angiography (OCTA) images were created using High-Sensitivity Speckle Variance (Section 2.5.3). Images were then weighted by dividing each OCTA pixel intensity by the intensity of the corresponding pixel in the structural OCT image,

which further reduced noise and normalized the intensity of vessels in low-intensity regions to those in higher intensity regions. The dermal-epidermal junction (DEJ) was automatically detected and only the vessel-containing depths were retained, which equated to 150 pixels of depth (0.84 mm) beginning 10 pixels above the DEJ. The images were then converted to two-dimensional *en face* images using a maximum intensity projection. Maximum Dilation Test images were then stitched together to create full field-of-view images and the papillary dermis and reticular dermis were separated for further analysis steps. For both the RH and Maximum Dilation Tests, *en face* images were binarized and used to calculate **vessel area density (VAD)**. Since VAD is an indirect measure of blood flow, VAD was reported arbitrary units (a.u.). For Maximum Dilation Test data, *en face* images were also skeletonized and used to calculate the **vessel count** (i.e. skeleton density). **Mean vessel diameter** was calculated for each image by dividing VAD by vessel count.

For each RH Test, a three-point moving average of VAD was calculated to smooth the data and this was plotted versus time, with the baseline image set to the zero second time point. From this plot "**peak VAD**," "**time-to-peak**," and "**recovery time**" were determined, as described in Section 3.3.1 and outlined in Figure 3.7. The recovery time was defined as the time it took for the VAD to recover 75% of the way back to the baseline VAD from the peak VAD since a full recovery to baseline was uncommon within the test duration.

Epidermal thickness was also calculated for each section of skin using the Maximum Dilation Test images. This was accomplished by subtracting the mean pixel depth of the skin surface from the mean DEJ pixel depth, both of which were automatically identified during post-processing. The mean epidermal thickness was calculated in every Maximum Dilation image and the mean of the thickness found in each of the three full field-of-view images was used for the comparisons described below.

On a participant-by-participant basis, all measurements described above were compared between the ROI on the residual limb versus the ROI on the contralateral limb. Additionally, for Maximum Dilation Test measurements, the mean difference between measurements on the residual limb and contralateral limb were compared and the differences were statistically tested using paired-samples *t*-tests. Significance was indicated by $p<0.05$ for all comparisons. Statistical analyses were performed using SPSS statistical software (SPSS 26.0, IBM Corp., Armonk, NY, USA). The effect size and future study sample size calculations were performed using power

analysis software (G*Power [127]). Maximum Dilation images were also qualitatively assessed noting features such as vessel shape and orientation.

5.4 RESULTS

5.4.1 *Participants*

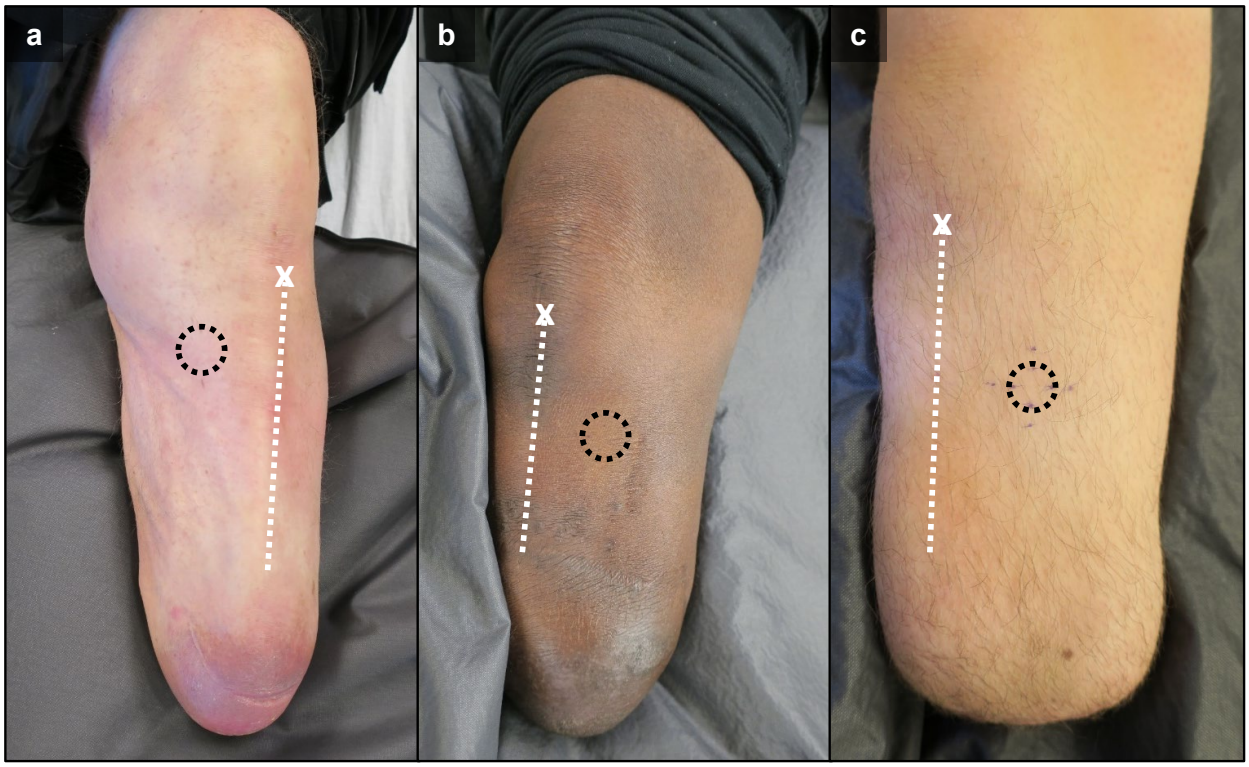

Figure 5.2. Aim 3 participant residual limbs with ROI locations noted. (a) Participant 1, (b) Participant 2, (c) Participant 3. Shown are: ROI locations where imaging occurred (black dotted circle), tibial crest (white dotted line), and mid-patellar tendon (white "x").

A total of three individuals with a unilateral below-knee amputation participated in the study. The characteristics of each participant are described in Table 5. Participant 1 was a 58-year-old male with type II diabetes who lost his limb over 14 years ago due to dysvascular causes. Participant 2 was a 44-year-old male with high blood pressure who lost his limb over 6 years ago due to trauma causes. He regularly smoked cigarettes for several years but had stopped smoking over 1.5 years prior to the study. Participant 3 was a 25-year-old female with no known comorbidities who lost her limb over 8 years ago due to trauma causes. All participants wore their prosthesis for 14 hours

or more per day and did not have a history of skin breakdown near the ROI. For all participants the ROI selected for imaging was located 4.0-5.5 cm distal of the mid-patellar tendon and between 2.5-3.0 cm medial of the tibial crest. As assessed by the study prosthetist, this location was believed to be in an area of high load within the prosthetic socket and did not exhibit signs of skin breakdown. Limb photographs including the ROI location are shown in Figure 5.2.

Table 5. Aim 3 study participant characteristics.

Characteristic	Participant 1	Participant 2	Participant 3
Demographics			
Gender	Male	Male	Female
Age	58 yr	44 yr	25 yr
Ethnicity	Not Hispanic/Latino	Not Hispanic/Latino	Not Hispanic/Latino
Race	White	African-American	White
Height	193 cm	175 cm	168 cm
Weight (with prosthesis)	130 kg	93 kg	57 kg
Health Information			
Diabetes	Type II	No	No
Hypertension	No	Yes	No
Smoker	No	No (> 1.5 yr)	No
Caffeine drinker	No	Yes	Yes
Vasodilator use	No	Yes	No
Residual Limb/ Prosthesis			
Residual limb side	Left	Right	Right
Years since amputation	> 14 yr	> 6 yr	> 8 yr
Cause of amputation	Dysvascular	Trauma	Trauma
Socket type	PTB	PTB	TSB*
Suspension style	Lock & Pin	Lock & Pin	Elevated Vacuum*
Hours/day worn	18	16-18	14
MFCL K-level	K-3	K-3	K-3
Skin health	Breakdown rare	Breakdown rare	Breakdown rare

PTB: Patellar Tendon Bearing
TSB: Total Surface Bearing
MFCL: Medicare Functional Classification Level [128]
* Participant 3 had previously used a PTB socket with lock & pin suspension but changed to a new elevated vacuum prosthesis 1 month prior to the study.

5.4.2 *Reactive Hyperemia Test*

Participant 1. Following the 10-minute load application of the RH Test, Participant 1 displayed a RH response in both limbs (Figure 5.3a). Visually, the residual limb *en face* images displayed a much more extensive vascular response than on the contralateral limb, with more vessel

recruitment throughout. This was supported by the quantified VAD data (Figure 5.3b-c). The peak VAD for the residual limb and contralateral limb were 0.71 a.u. and 0.21 a.u., respectively; however, the peak VAD value in the residual limb occurred in the first post-load image, so it is likely the real physiological peak of the RH response was not captured. The contralateral limb peak occurred in the second post-load image, and after further inspection of the images this appeared to be due to an increased vessel intensity rather than being caused by an imaging artifact. Since the peak of the response was likely not captured in the residual limb, the time-to-peak was interpreted as ≤0.9 min, whereas the contralateral time-to-peak was 1.2 min. The recovery towards baseline was faster in the contralateral limb, with a recovery time of 7.1 min and 5.8 min in the residual limb and contralateral limb, respectively. A full recovery to baseline was not reached in either limb, as confirmed in the *en face* images. Images from the residual limb contained more pulse-induced motion artifacts than the contralateral side, which may have slightly increased the VAD quantification; however, as the *en face* images confirm, it is clear that the vascular response in the residual limb was much more extensive than in the contralateral limb, and the noise appears consistent throughout the images, so the shape of the RH curve appeared reasonable.

Participant 2. The RH Test images for Participant 2 exhibited a distinct RH response in both limbs (Figure 5.4a). The *en face* images that were captured appeared similar between the two limbs in terms of the magnitude of the response. This was supported by the quantified VAD values, which reached a peak VAD of ≥0.28 a.u. and 0.28 a.u. in the residual and contralateral limbs, respectively (Figure 5.4b-c). As with Participant 1, the first residual limb post-load image collected was the quantified peak VAD, thus it is not clear if this accurately represented the physiological RH peak or if the peak had already occurred prior to capturing this image. The contralateral limb peak appeared to have been captured, as confirmed by a larger vessel density in the second post-load image versus the first. The time-to-peak was ≤0.9 a.u. and 1.3 min for the residual and contralateral limb, respectively. Both limbs exhibited some background noise and motion artifacts, however this noise appeared fairly consistent throughout, thus the RH curves seemed to accurately depict the overall perfusion trend. The recovery time appeared slightly faster in the residual limb compared to the contralateral limb, despite similar recovery times (2.0 min versus 2.1 min, respectively).

Participant 3. Data from the RH Test for Participant 3 demonstrated a clear RH response in the contralateral limb but a complete absence of a RH response in the residual limb (Figure 5.5a). The residual limb VAD decreased slightly below the baseline following the load application (Figure 5.5b). The contralateral limb peak VAD occurred during the first post-load image, similar to the residual limb for participants 1 and 2. As such, the peak VAD was ≥0.34 a.u. and the time-to-peak was ≤1.0 min. The recovery time was 3.7 min (Figure 5.5c).

All participants. Comparisons of data collected on all participants are shown in Figure 5.6 and are discussed at greater lengths in the Discussion section below.

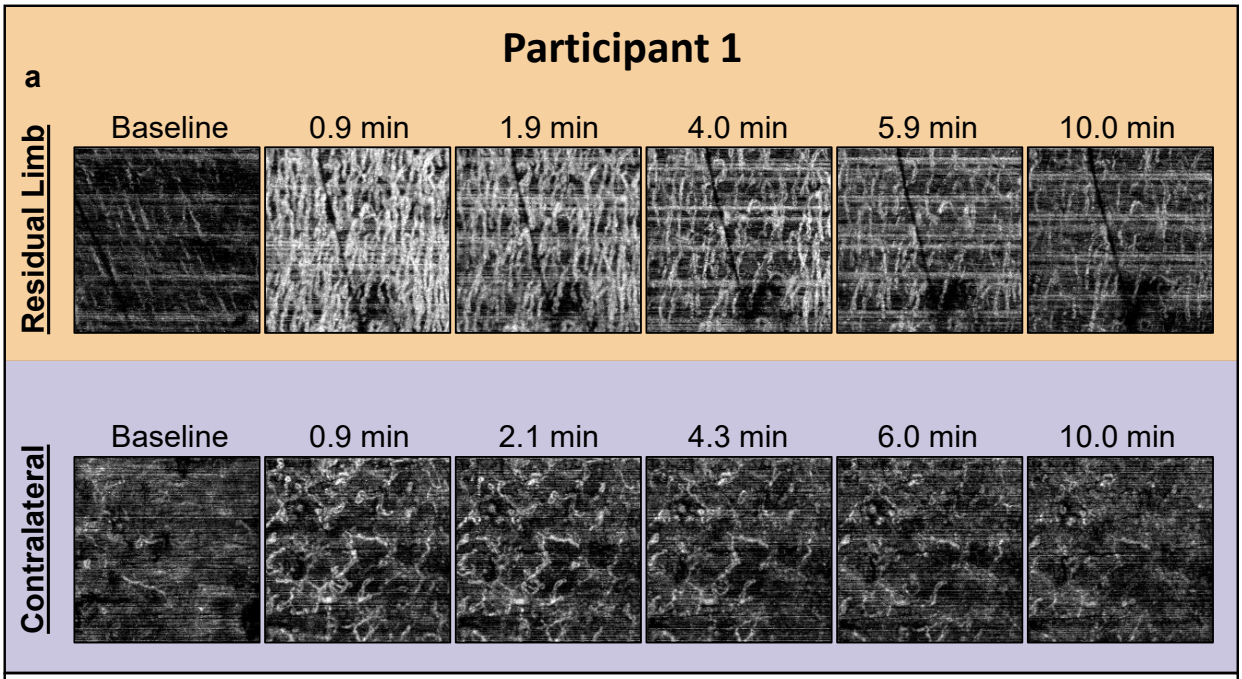

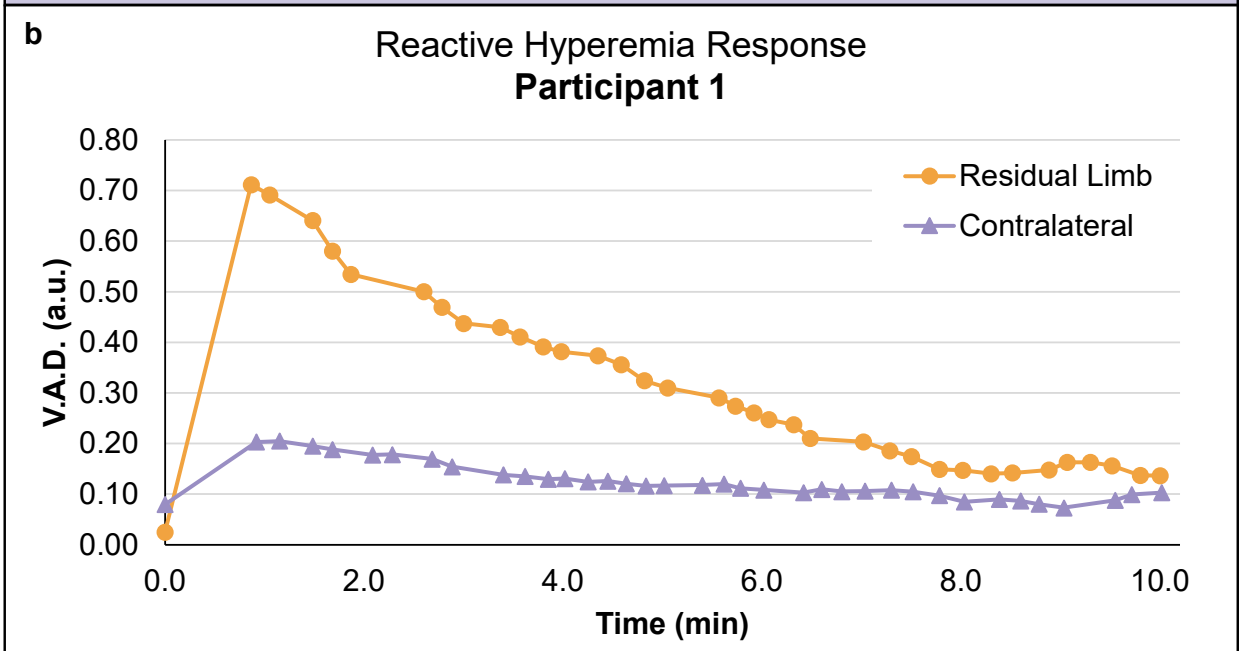

c	Peak VAD	Time-to-Peak	Recovery Time
Residual Limb	≥ 0.71 a.u.	≤ 0.9 min	7.1 min
Contralateral	0.21 a.u.	1.2 min	5.8 min

Figure 5.3. RH Test results for Participant 1. (a) Select *en face* images from the RH Tests on each limb. Images are 2 x 2 mm. Horizontal white lines are motion artifacts. (b) Plot of VAD vs. time from both limbs. (c) Quantified vascular response characteristics.

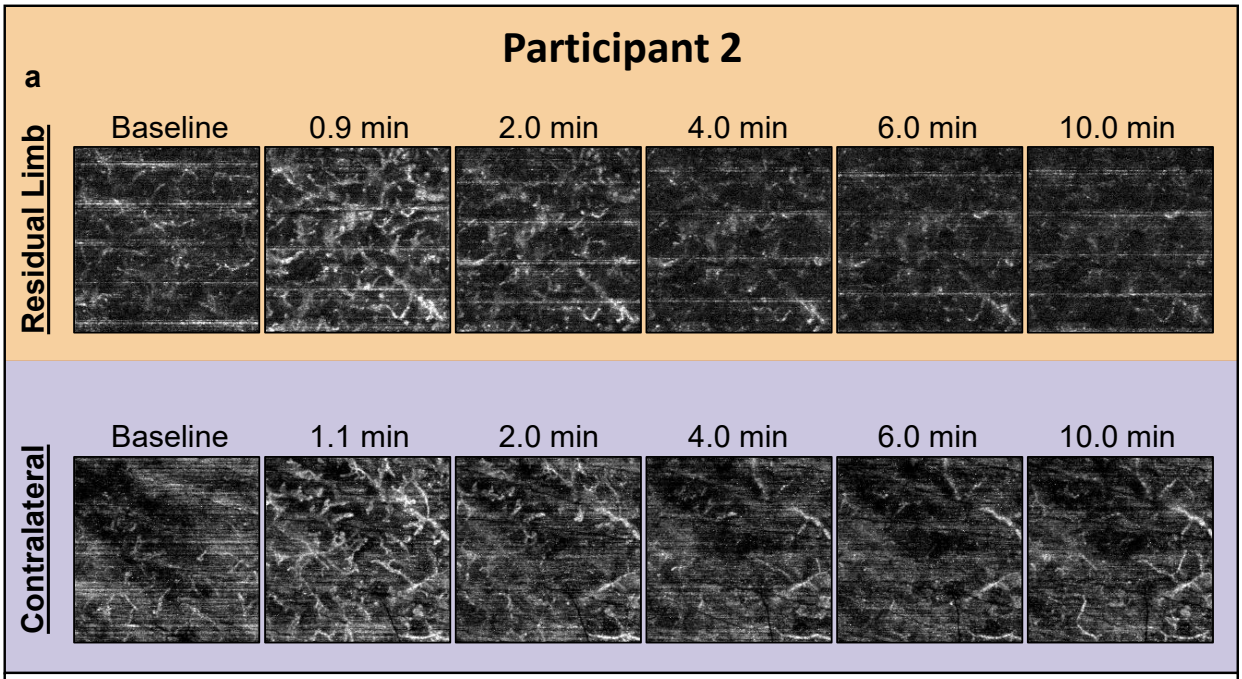

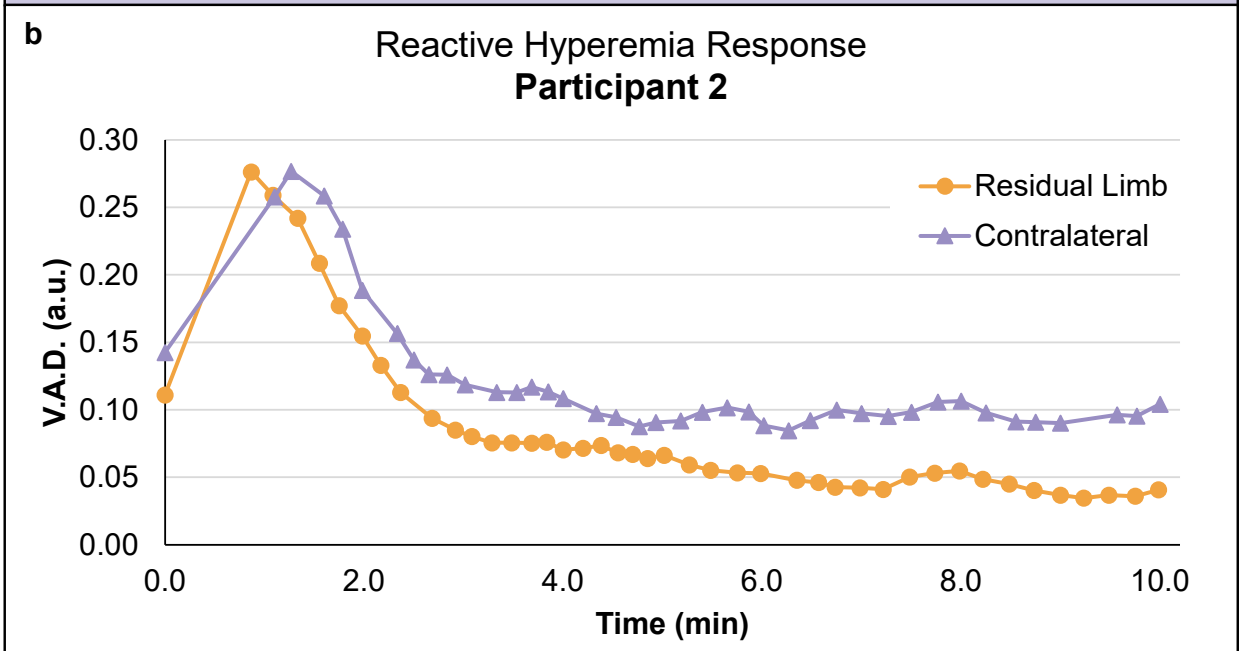

c	Peak VAD	Time-to-Peak	Recovery Time
Residual Limb	≥ 0.28 a.u.	≤ 0.9 min	2.0 min
Contralateral	0.28 a.u.	1.3 min	2.1 min

Figure 5.4. RH Test results for Participant 2. (a) Select *en face* images from the RH Tests on each limb. Images are 2 x 2 mm. (b) Plot of VAD vs. time from both limbs. (c) Quantified vascular response characteristics.

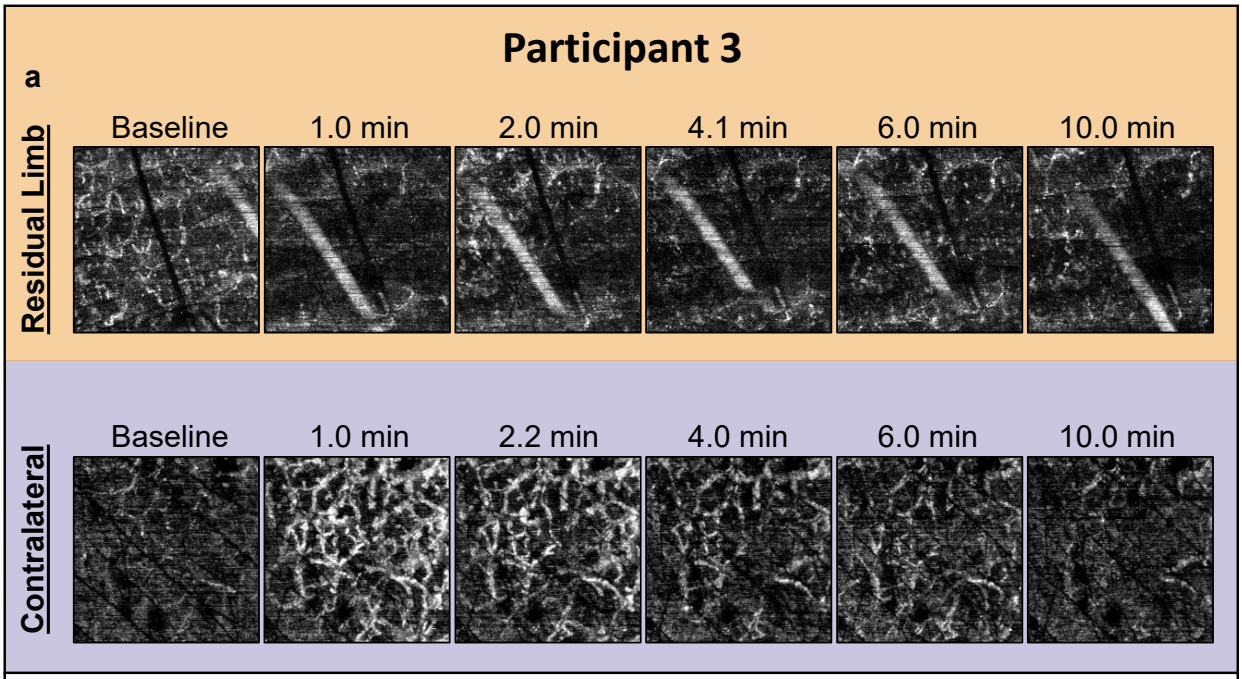

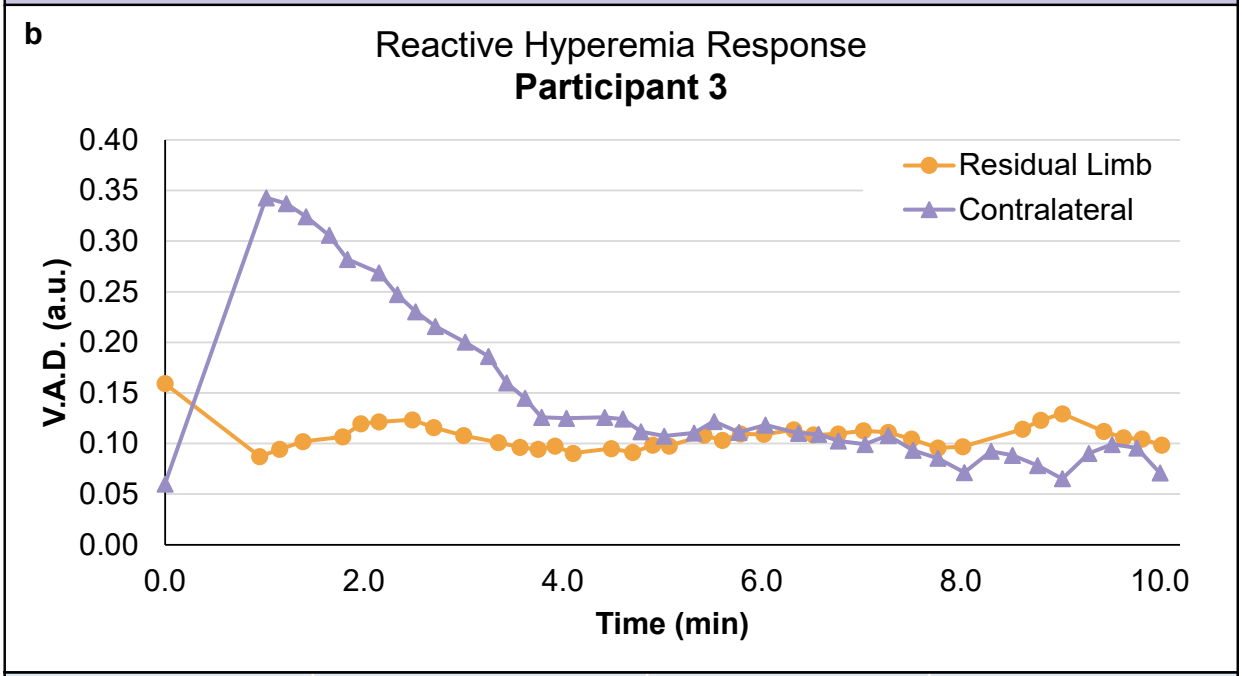

c	Peak VAD	Time-to-Peak	Recovery Time
Residual Limb	n/a – RH response not captured		
Contralateral	≥ 0.38 a.u.	≤ 1.0 min	3.7 min

Figure 5.5. RH Test results for Participant 3. (a) Select *en face* images from the RH Tests on each limb. Images are 2 x 2 mm. (b) Plot of VAD vs. time from both limbs. (c) Quantified vascular response characteristics.

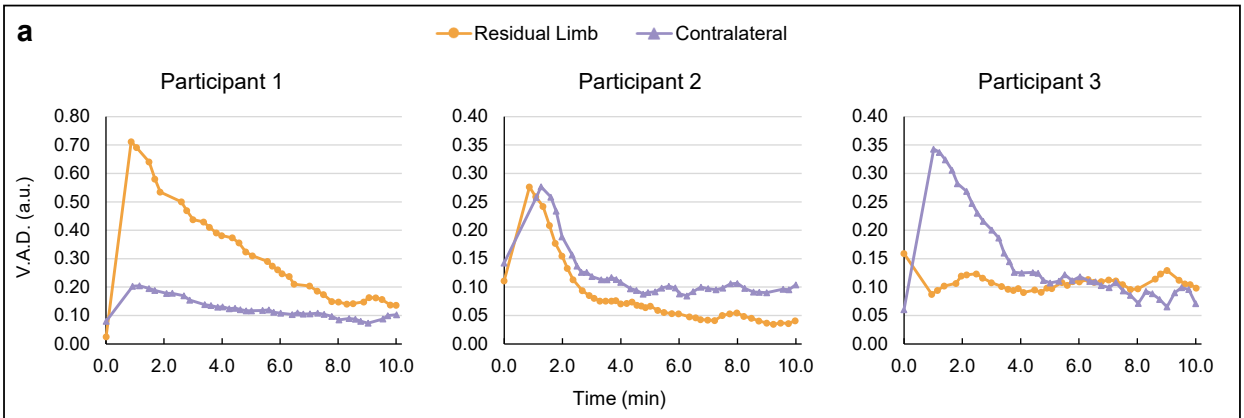

b

	Peak VAD (a.u.)			Time-to-Peak (min)			Recovery Time (min)		
Participant #	**1**	**2**	**3**	**1**	**2**	**3**	**1**	**2**	**3**
Residual Limb	≥ 0.71	≥ 0.28	n/a	≤ 0.9	≤ 0.9	n/a	7.1	2.0	n/a
Contralateral	0.21	0.28	≥ 0.38	1.2	1.3	≤ 1.0	5.8	2.1	3.7

Figure 5.6. RH Test data for all participants. (a) VAD response shown in arbitrary units (a.u.). (b) Quantified vascular response characteristics.

5.4.3 *Maximum Dilation Test*

Participant 1. The Maximum Dilation Test images for Participant 1 demonstrated notably different vascular morphologies between the residual limb and contralateral limb which held for both the papillary and reticular dermis layers (Figure 5.7). The residual limb contained a dense vascular network with vessels that appeared aligned in the same approximate direction. After aligning the image field-of-view with anatomical locations on the limb, it appeared the alignment of the vessels was at approximately a 45° angle between the medial and proximal directions (Figure 5.8). The denser network was confirmed by a larger VAD measurements in the papillary dermis (0.38 versus 0.27 a.u., residual versus contralateral limb) and in the reticular dermis (0.58 versus 0.38 a.u., residual versus contralateral limb). The vessel count was also greater in the residual limb compared to the contralateral: 11.90 versus 9.10 mm/mm^2 (residual versus contralateral limb) in the papillary dermis, and 9.93 versus 7.94 mm/mm^2 (residual versus contralateral limb) in the reticular dermis. The mean vessel diameter was also slightly larger for the residual versus contralateral limb, with 31.77 versus 29.65 µm in the papillary dermis and 59.26 versus 47.42 µm in the papillary dermis.

Participant 2. Similar to Participant 1, the Maximum Dilation Test images for Participant 2 also showed a denser vascular network in both layers of the reticular limb versus the contralateral limb

(Figure 5.9). This was confirmed by VAD measurements in the papillary dermis (0.28 versus 0.20 a.u., residual versus contralateral limb) and in the reticular dermis (0.48 versus 0.35 a.u., residual versus contralateral limb). The vessel count measurement suggested this increase was largely driven by a greater number of vessels in the residual versus contralateral limb (10.19 versus 8.02 mm/mm^2 in the papillary dermis and 8.39 versus 6.57 mm/mm^2 in the reticular dermis). The mean vessel diameter was marginally larger in the residual limb versus contralateral limb (27.35 versus 25.16 μm in the papillary dermis and 56.91 versus 52.81 μm in the papillary dermis).

Participant 3. The Maximum Dilation Test images for Participant 3 demonstrated a notably different vessel morphology in both layers of the residual limb compared to the contralateral limb (Figure 5.10). Vessels in both layers of the residual limb appeared organized in shorter, less continuous segments than in the contralateral limb. These short vessel segments in the residual limb also appeared slightly aligned in the same direction, though this distinction was less obvious than for Participant 1. Contrary to the other participants' quantified vessel characteristics, Participant 3 demonstrated larger values in the contralateral limb compared to the residual limb for all measurements. Though this difference was minimal in the papillary dermis it was more substantial in the reticular layer. The VAD in the papillary dermis was 0.27 versus 0.30 a.u. (residual versus contralateral limb), and in the reticular dermis it was 0.34 versus 0.52 a.u. (residual versus contralateral limb). This difference appeared to be driven by both a larger vessel count and mean vessel diameter. The vessel count in the papillary dermis was 9.88 versus 10.19 mm/mm^2 (residual versus contralateral limb), and in the reticular dermis it was 7.62 versus 9.68 mm/mm^2 (residual versus contralateral limb). The mean vessel diameter in the papillary dermis was 27.51 versus 29.99 μm (residual versus contralateral limb), and in the reticular dermis it was 43.96 versus 54.08 μm (residual versus contralateral limb).

All participants. From data collected on these three participants, none of the residual limb versus contralateral limb differences were shown to be statistically significant ($p>0.05$). Comparisons of data collected on all participants are shown in Figure 5.11 and Figure 5.12, and they are discussed at greater lengths in the Discussion section that follows.

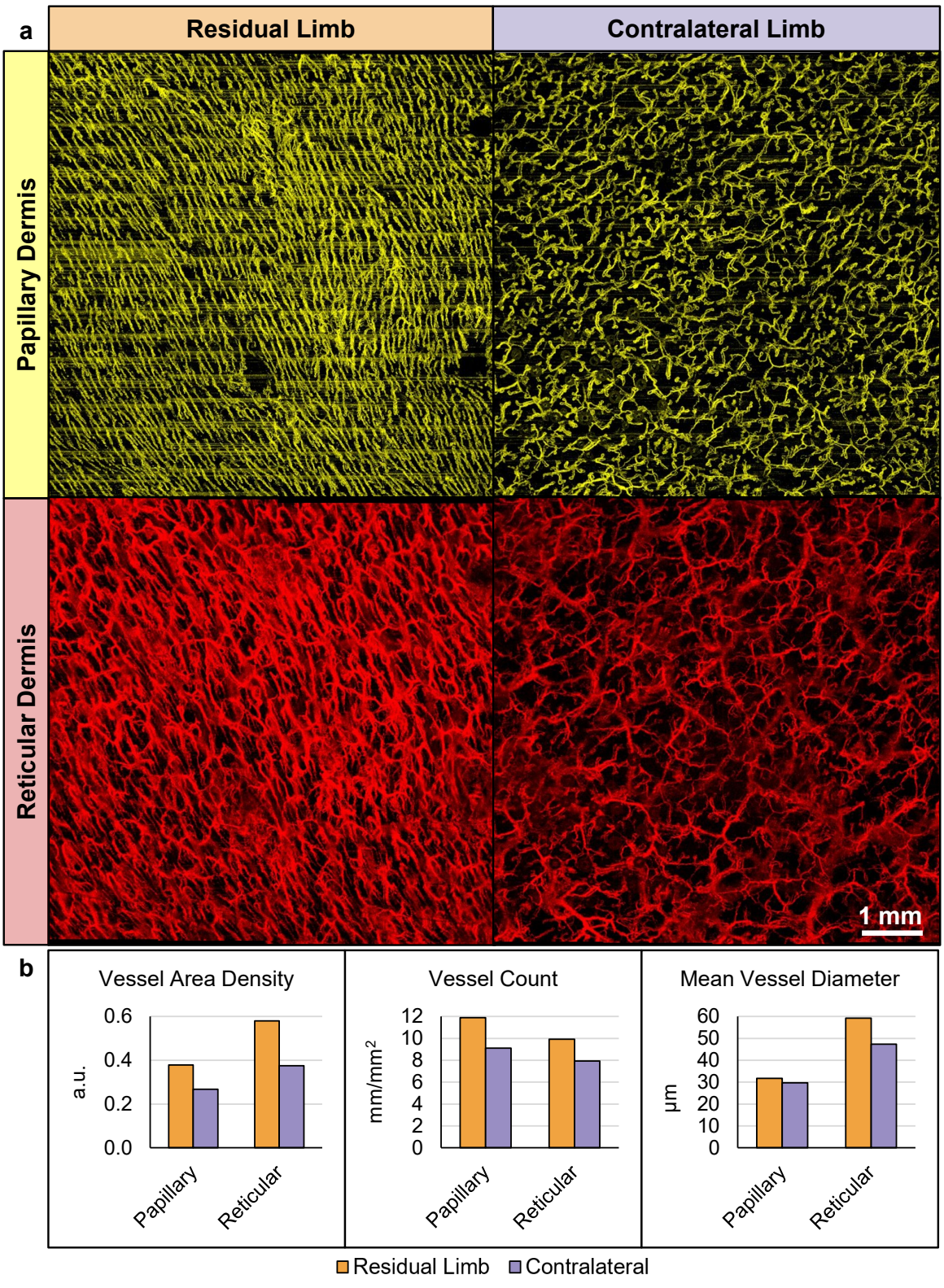

Figure 5.7. Maximum Dilation Test results for Participant 1. (a) *En face* images separated by limb and by depth. The horizontal lines in the papillary images are motion artifacts. (b) Vessel measurements quantified from the images above.

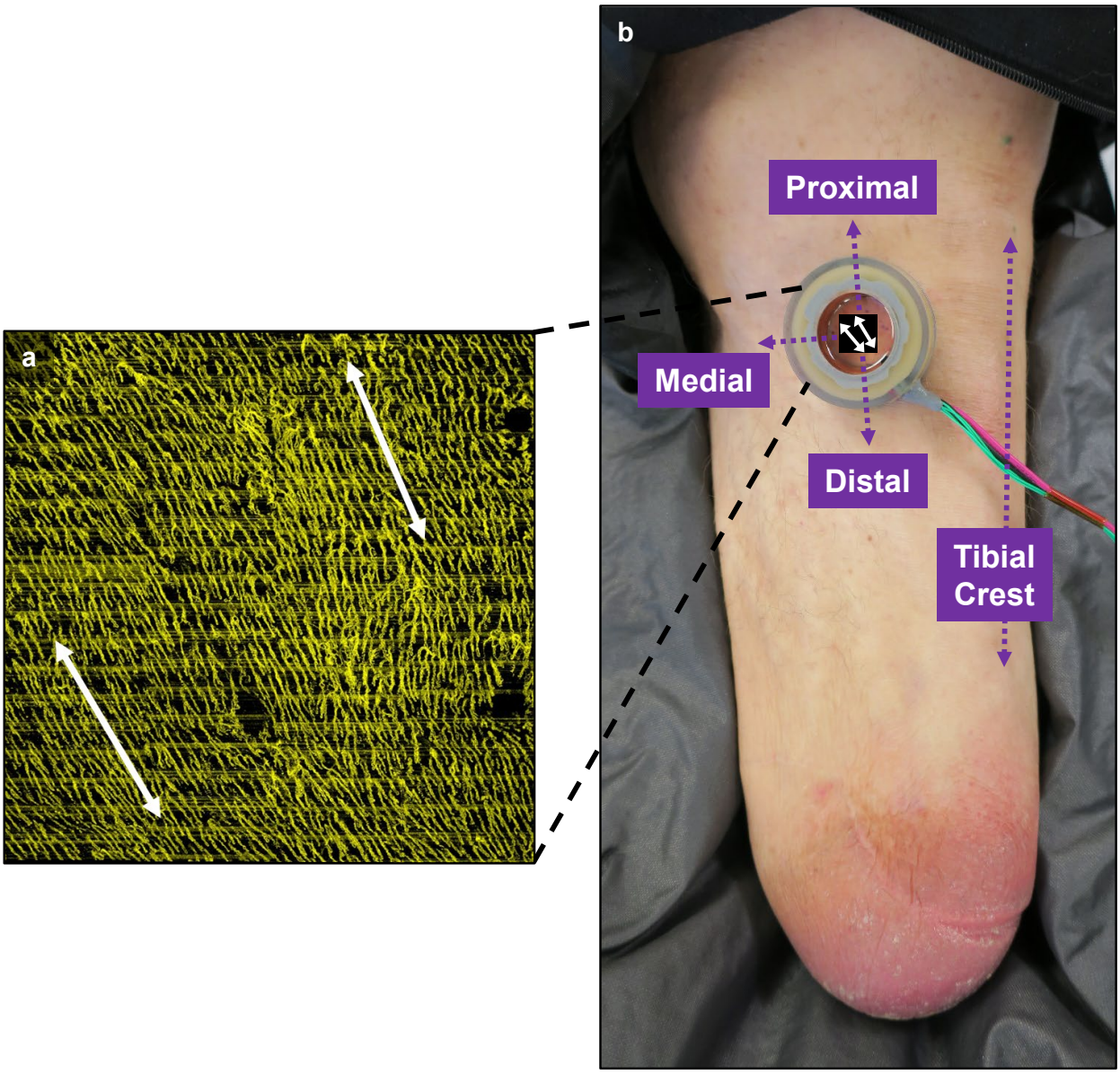

Figure 5.8. Participant 1 vessel alignment. (a) Maximum Dilation Test *en face* image shown with approximate vessel alignment indicated (white arrows). (b) Participant 1's residual limb with vessel alignment superimposed over ROI (white lines) in relation to anatomical directions and landmarks (purple dotted lines).

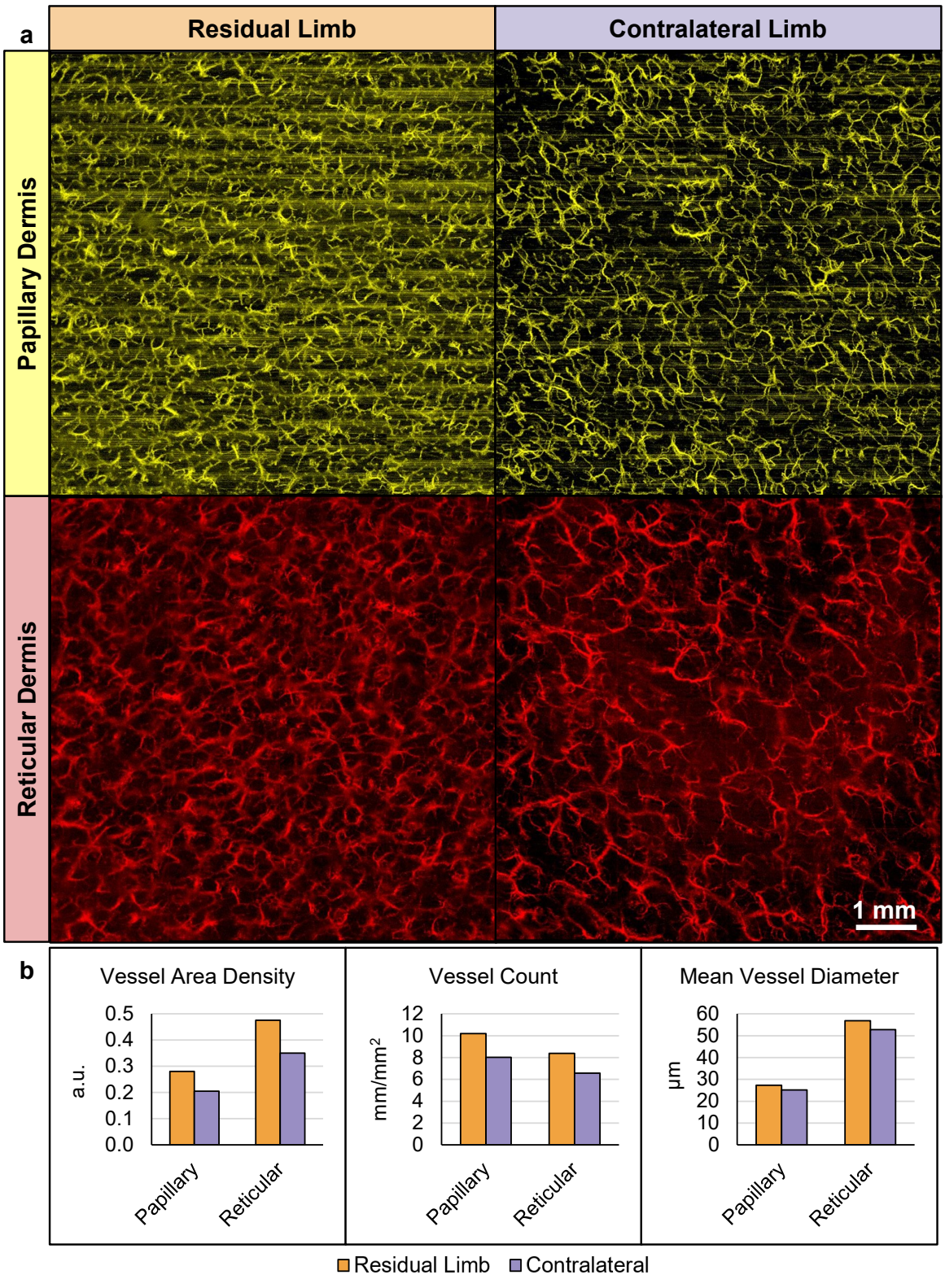

Figure 5.9. Maximum Dilation Test results for Participant 2. (a) *En face* images separated by limb and by depth. The horizontal lines in the papillary images are motion artifacts. (b) Vessel measurements quantified from the images above.

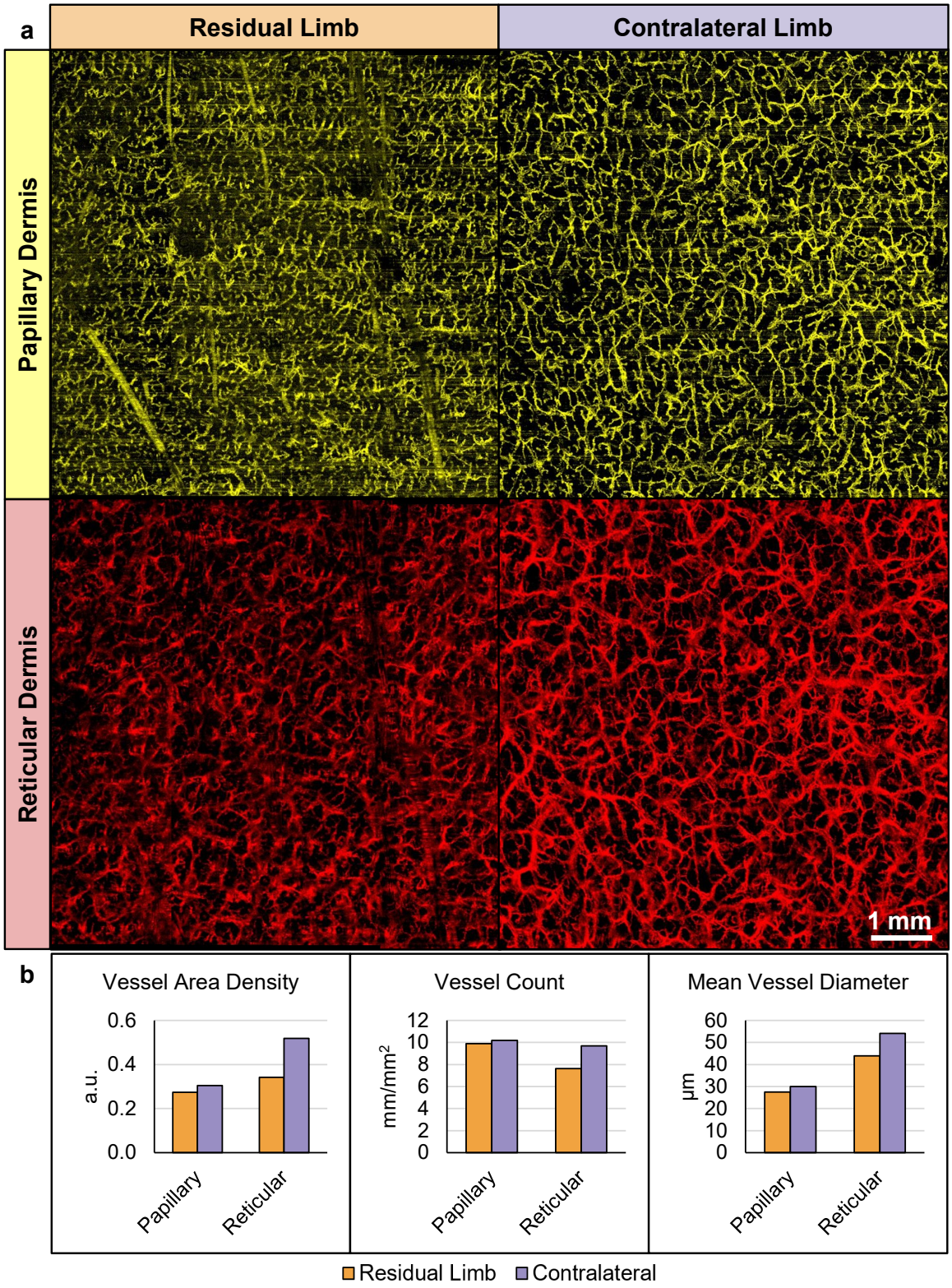

Figure 5.10. Maximum Dilation Test results for Participant 3. (a) *En face* images separated by limb and by depth. (b) Vessel measurements quantified from the images. Regions containing hair artifacts were removed from quantification.

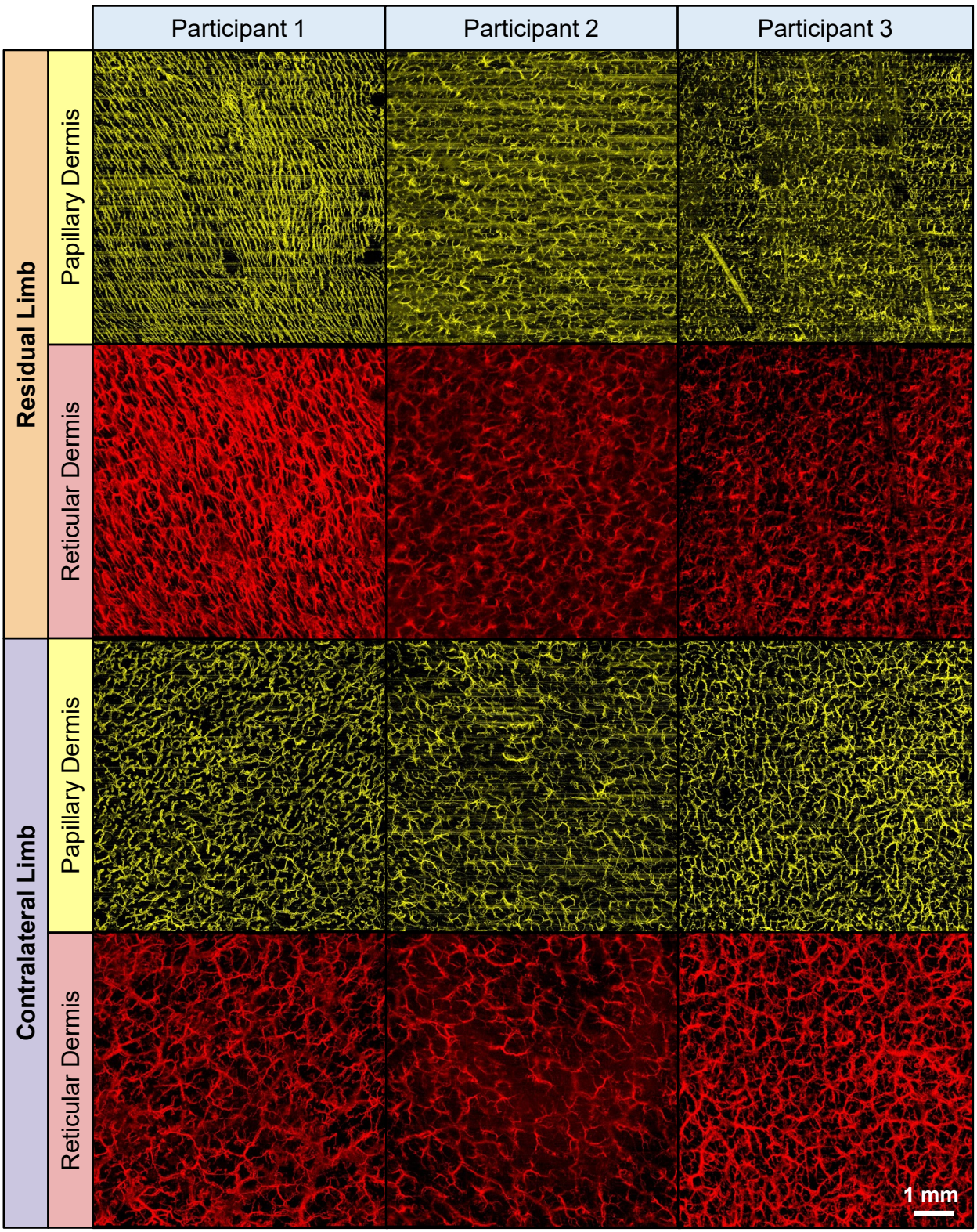

Figure 5.11. Maximum Dilation Test images, all participants.

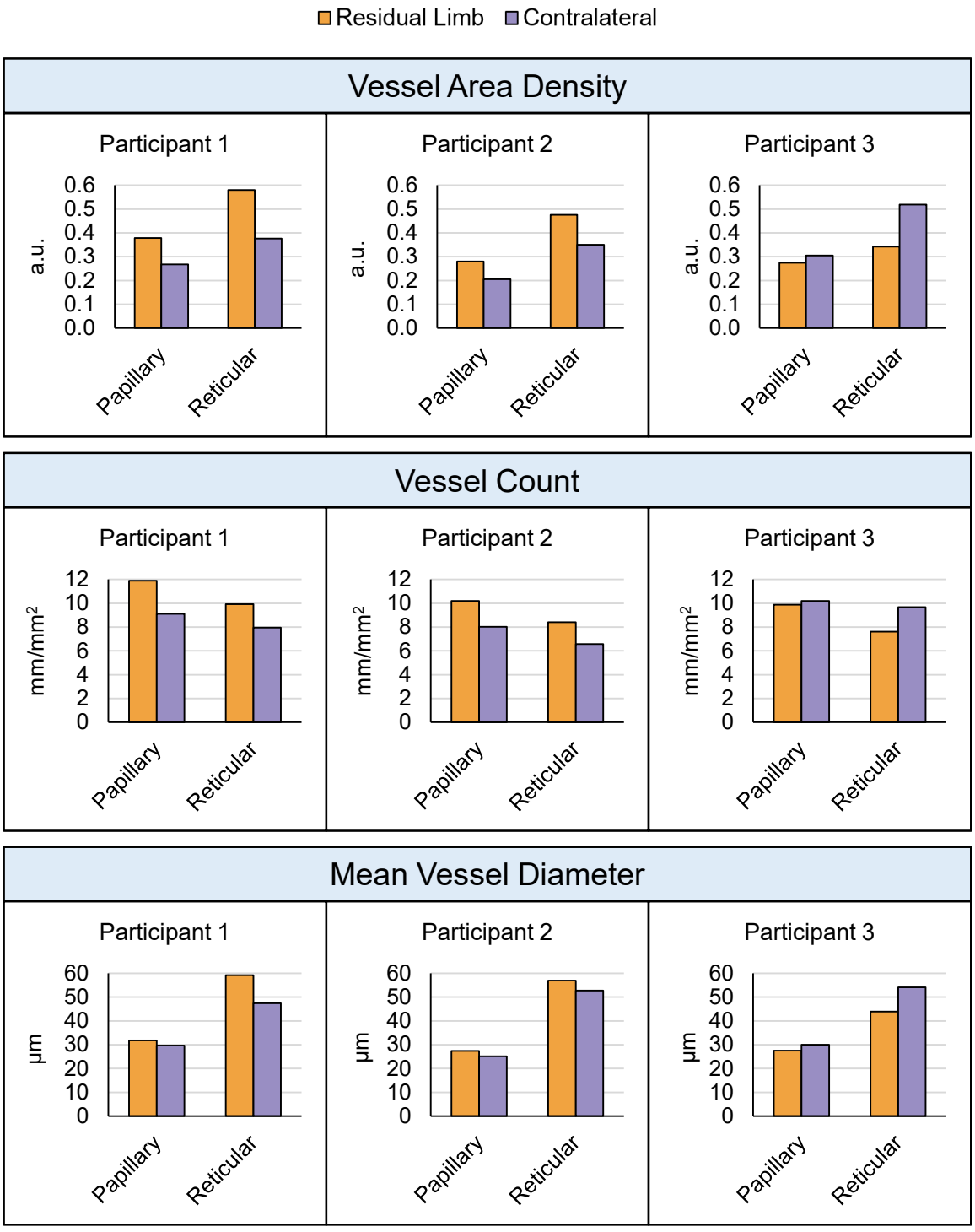

Figure 5.12. Maximum Dilation Test measurements, all participants.

5.4.4 *Epidermal Thickness*

All participants demonstrated a thicker epidermal layer in the residual limb versus contralateral limb (Figure 5.13). Combining data for all three participants demonstrated a mean thickness of 0.117 ± 0.003 mm (mean ± SD) in the residual limb versus 0.100 ± 0.005 mm in the contralateral limb, a statistically significant mean difference of 0.017 mm (p=0.026, Cohen's d effect size=3.5).

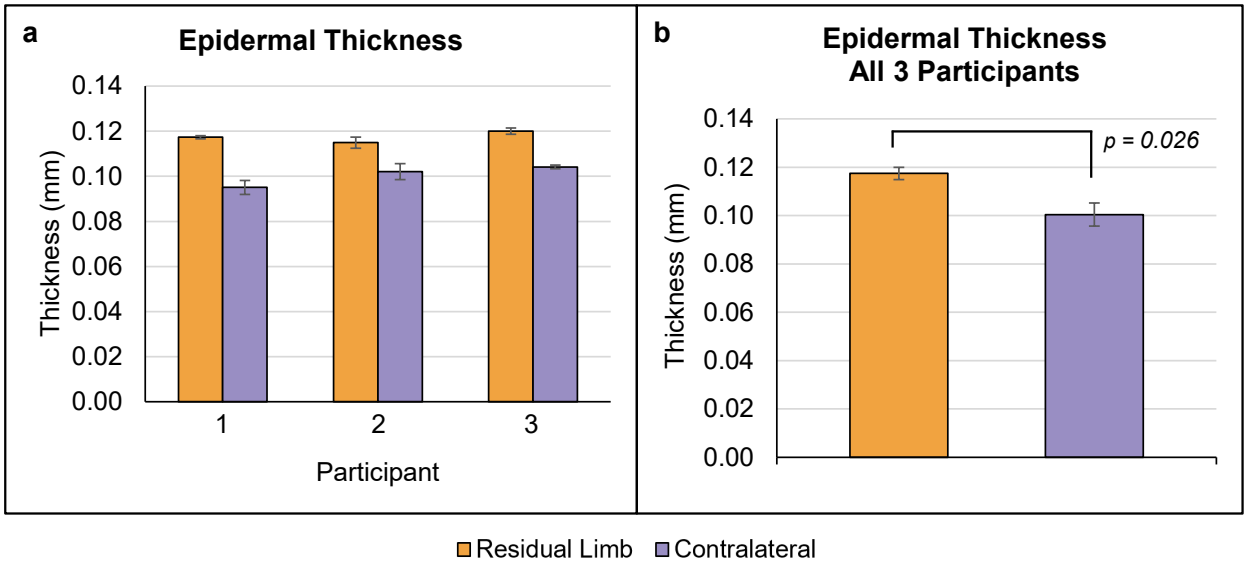

Figure 5.13. Epidermal thickness measurement. (a) Data for each participant, shown as the mean of the thickness calculated in each of three full field-of-view images captured during each test. Error bars are ± SD. (b) Mean measurements for all participants combined. Error bars ± SD of the three measurements.

5.5 Discussion

5.5.1 *Microvascular Function*

Residual limb vs. contralateral limb. In five of the six RH Tests executed in the current study a standard RH response was produced: a rapid increase in tissue perfusion, followed by a more gradual return toward the baseline level. The one ROI tested which did not produce RH was Participant 3's residual limb, which displayed a slight decrease in perfusion from the baseline following the load removal. This result was unexpected since this participant was the youngest and the only participant without comorbidities. While this response could have been caused by a load application that was not centered on the imaging ROI, it is unlikely since care was taken to ensure

the load application pad was centered and an indent was confirmed prior to OCT probe placement. Based on the presence of skin redness that was confirmed visually following the load removal during this test, it is believed that the peak and the recovery occurred prior to the first post-load image. Improvements to the test methods, described below, could provide a more definitive result in the future.

For Participants 1 and 2, their residual limb vasculature reached the peak of the RH response more quickly than in their contralateral limb (Figure 5.6). It is likely the residual limb peak RH was reached for these participants even earlier than the first post-load image at 0.9 min; however, since the contralateral peak VAD occurred after the first post-load image a measurable time-to-peak difference existed between their residual and contralateral limbs. If this difference was the result of adaptation to repetitive stresses from wearing a prosthetic socket, this change could have resulted from functional adaptations, structural adaptations, or a combination of the two. Functional adaptations refer to enhancements to the biomechanical and biochemical cascade of events that take place to induce vessel dilation and cause more blood to enter the vascular bed; whereas structural adaptations refer to vascular remodeling that takes place to allow for more rapid and/or more extensive perfusion into the tissue. While definitively making this distinction was not within the scope of the current study, the latter explanation was supported by results from the Maximum Dilation Test which demonstrated that each of the participants had denser vascular networks in their residual limb compared to the contralateral limb (Figure 5.11). There is support in the literature that similar vascular remodeling occurs in response to mechanical and ischemic stresses, and this is described further in Section 2.4. Support also exists for the possibility of functional adaptations, largely in the field of exercise physiology. Functional vascular adaptations can result in vessels that may be dilated more rapidly and closer to their maximum diameter despite the same stresses acting on the tissue as were before. Researchers have found these adaptations following training programs that were used to elicit repetitive bouts of hyperemia in skin including exercise, arm heating, whole body heating, and repeated pressure cuff-induced occlusion [78,129]. The studies also found support that multiple stimuli contribute to the initiation of this functional adaptation, namely the mechanical stress that endothelial and smooth muscle cells experience from repetitive bursts of reperfusion. One key mechanism that has been elucidated is that endothelial cells adapt by upregulating genes for NO and NO-precursor production, therefore more vasodilators become available for future RH responses [130,131]. These adaptations can occur

rapidly, which enhances their benefit during the early stages of skin adaptation. As demonstrated by Tinken *et al*. after two weeks of an exercise training program—30 minutes of cycling and running three times per week—conduit vessel dilation to an occlusive stress was shown to increase while only a small increase was seen in maximum vessel diameter [132].

In terms of peak vascular response, Participant 1 demonstrated a much higher peak VAD, even though the physiological RH peak likely occurred prior to the first post-load image and may have reached an even higher VAD magnitude. Participant 2's peak VAD was similar in each of his limbs, though it is possible the physiological peak in the residual limb would have produced a higher VAD magnitude since the quantified peak occurred in the first post-load image and the steep slope of the curve suggested that some recovery had already occurred. In the future, a faster transition from load removal to imaging will allow this to be tested. Similar to the faster time-to-peak described in the paragraph above, if a higher peak VAD was representative of adaptation that had taken place, this could be made possible through functional adaptations, structural adaptations, or a combination of the two. As explained in the prior paragraph, support exists for both mechanisms.

Differences between participants. Both of Participant 1's limbs exhibited a delayed recovery that lasted much longer than other participants' responses. It is possible that this behavior resulted from vascular dysfunction secondary to his diabetic condition. A common effect of diabetes is that chronically increased blood sugar causes non-enzymatic glycosylation of many molecules and proteins, which leads to further complications. In the skin, the enzymes that digest collagen protein are often hindered as a result of this non-enzymatic glycosylation, which reduces collagen turnover and can result in a stiffer, thicker dermal layer. Microangiopathies are also common in diabetic vasculature and can include decreased responsiveness to sympathetic innervation, reduced ability to respond to thermal and hypoxic stress, and pathological vessel wall permeability [133]. This decrease in autoregulation is likely to have contributed to the delayed recovery time in both of Participant 1's limbs and potentially also explains the slightly stunted and delayed peak response in the contralateral limb. Interestingly, this ability to reach a high peak response seems to have been recovered in the residual limb, though this appears to be at least partially due to the much denser vascular network in this ROI versus the contralateral limb ROI. Though more research is needed, such a finding would provide important insights into how individuals with different health conditions adapt differently from one another.

Despite a comorbidity of hypertension, Participant 2 demonstrated a time-to-peak that appeared on par with Participant 3 (no known comorbidities) and a peak VAD that was slightly lower. While hypertension has been shown to reduce peripheral blood flow in both the resting state and at maximum dilation [134] vasodilator use is known to recover vascular function. Sprigle *et al.* demonstrated a faster RH time-to-peak when vasodilators were used. The researchers also found a longer duration RH recovery time when using vasodilators [44]. While Participant 2 did not demonstrate a delayed RH recovery compared to the other participants here, it is possible his recovery would have been faster without vasodilator use. While hypertension is one possible explanation for the slightly lower peak RH compared to Participant 3, another potential explanation may be damage induced from years of smoking. Celermajer *et al.* found that former smokers had significantly reduced RH peaks compared to non-smokers [135].

The effects of participants' ages may also have factored into the differing responses seen in the RH Test. Aging has been shown to decrease the RH response, both in terms of time-to-peak and magnitude of peak blood flow. It is believed this is largely the result of accumulated endothelial cell damage which leads to a reduction in vasodilator release [109]. It is possible this was an additional factor which lead to the lower peak VAD demonstrated in Participant 2 versus 3 and may have exacerbated diabetes-related endothelial cell damage in Participant 1's contralateral limb, leading to its delayed, low magnitude response.

5.5.2 *Microvascular Structure*

Residual limb vs. contralateral limb. Vessel morphologies differed significantly between each participant's residual limb and contralateral limb, as confirmed qualitatively and quantitatively (Figure 5.11 and Figure 5.12). Participant 1 and 2 displayed a significantly larger vessel density in the residual limb compared to the contralateral limb, which was largely driven by an increase in vessel count, with some mean vessel diameter increase as well. Participant 2 and 3 appeared to have vessels that were in shorter segments and less continuous in the residual limb compared to their contralateral ROIs. Participant 1, and to a lesser degree Participant 3, showed a higher degree of vessel alignment in the residual limb versus the contralateral. It is unlikely that the differences between the residual and contralateral limb vessel structure existed in these study participants prior to them wearing a prosthetic device. This is particularly true for Participants 2 and 3 who lost their limbs to trauma.

Though further investigation is needed, the stark differences found in the current aim between vascular structure in the residual limb and the contralateral limb may have been induced by several years of mechanical stresses at the limb-socket interface. An alternative explanation is that the differences were induced by the altered limb vasculature following amputation surgery; however, this seems unlikely since the vascular regions tested were located far from the distal end, where these injury and surgical changes occurred. It is also possible that vascular remodeling occurred due to other local stimuli, such as repetitive heating of the limb skin from the limb being placed inside a liner and socket for several hours each day. This said, support exists in the literature for vascular remodeling, through the addition of new vessels, in response to stimuli that are similar to those present in the case of residual limb skin interacting with a prosthetic socket. Angiogenesis, the primary process by which new vessels are created, has been well-studied [10]. A primary trigger for angiogenesis is tissue hypoxia [7], a stimulus which is chronically present in most highly loaded skin regions of the residual limb within the socket, considering that cutaneous vessels can be occluded by as little as 11.6 kPa applied externally [95], far less than that experienced in highly loaded regions of the prosthetic socket. Angiogenesis in skin in response to a slightly different stress type—tension—has been shown to produce new vessels following only two days of a one-hour stress protocol. This was demonstrated in the mouse dorsum by Chin *et al.* [136]. The researchers determined that tissue stress had induced ischemia which initiated angiogenesis, as evidenced by upregulated hypoxia-stimulated angiogenic factors in the tissue (VEGF and HIF-1α). Similarly, Erba *et al.* found an increase in cutaneous microvascular vessel density in the dorsum of mice following a four-hour tension application [137]. The researchers found visual and biochemical evidence that angiogenesis had led to the formation of new capillaries, again proposing that hypoxia induced by the stress had triggered the adaptation.

In the current study, the larger mean vessel diameter in residual limbs compared to contralateral limbs also has some basis in known vascular remodeling mechanisms that can be present in mechanically stressed skin. The main pathway by which vessels increase in diameter is known as arteriogenesis [138]. The stimulus for arteriogenesis is believed to be increasing shear stress on vessel walls, which occurs through repeated bouts of considerably increased blood flow, such as during RH [139]. Arteriogenesis as a mechanism of adaptation has been demonstrated in exercise physiology research as well as skin adaptation via tissue expansion. Tinken *et al*. demonstrated increases in brachial and popliteal conduit artery diameters by the fourth week of an

exercise training program that consisted of 30 minutes of running and cycling three times per week [132]. Using a rat ear model to study tissue expansion, Pietramaggiori *et al*. demonstrated vessel diameter increases of 30% after only eight hours of cyclic tension. Continuous static tension increased vessel diameters by 60% on day two and by 100% on day four [73].

The high degree of vessel alignment in both dermal layers of Participant 1's residual limb may have been induced by chronic shear stress acting through the skin. The vessels were oriented at approximately 45° between the medial and proximal limb directions. This matches closely with the likely direction of shear force chronically imposed on the limb within this particpant's socket. While the direction of shear force was not measured in this participant's socket, it has been demonstrated previously in similarly designed sockets that shear commonly acts approximately at 45° in the medial-proximal direction (Figure 5.14), similar to what was found in the current study [2]. Erba *et al.* found a similar increased vascular alignment and increased vessel density in the cutaneous microvasculature of the dorsum of mice after 7 days of a 4-hour daily tension [137]. Though their study did not test for the cause of this alignment, the researchers hypothesized that aligned vessels in stressed tissue may be preferred to more tortuous pathways because they may enable more efficient transport of blood into the stressed area.

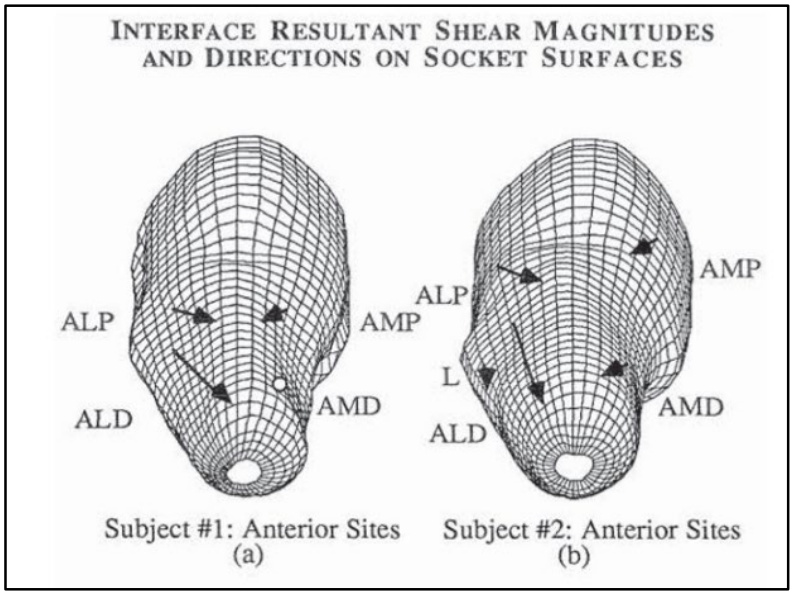

Figure 5.14. Common limb-socket interface shear directions. From [2]. The ROI tested in the current aim is located near the AMP (anteromedial proximal) site. Limbs shown above are right limbs, whereas Participant 1's is left.

Differences between participants. Qualitative and quantitative evaluation of Maximum Dilation Test images also revealed several differences in vessel structure between individuals. This was especially true of residual limbs but also true of contralateral limbs. For one, Participant 1's residual limb VAD and vessel count were greater than the same measurements taken at all other participant ROIs in the current study and much larger than the mean VAD and vessel counts measured in the Aim 2 study at a similar anatomical location on the limbs of healthy able-bodied participants. Compared to the mean of the test and control ROIs of able-bodied individuals, Participant 1's residual limb VAD was 14% and 32% larger and vessel count was 15% and 19% larger in the papillary and reticular layers, respectively. If the differences seen in the residual limbs versus contralateral limbs was induced by mechanical stresses, the differences seen between individuals highlights how differently the microvasculature can respond to mechanical stress from person to person. Understanding how these differences would have come about was not within the scope of this study, however a few possible explanations are presented here.

One possibility for differences between individuals is that differences existed in the stresses experienced within the tissue which provided different stimuli for remodeling. It is possible that differences existed in the limb-socket forces imposed on each of the limbs at the ROI. All three participants were active individuals who had worn a PTB style socket for several years, which is meant to impose high loads along the medial side of the tibia, where the ROI was located. However, the specific loads imposed on the limb are dictated largely by the socket fit, and differences in fit could have led to large differences between the three participants. The mass of each individual also likely contributed to determining the loads that the sides of the limb were subjected to. The participants in this study varied widely in their weight from 130 kg (Participant 1) to 57 kg (Participant 3). Stresses within the tissue could have also varied considerably based on the mechanical properties of the tissue itself or the underlying tissue. While tissue mechanical properties were not assessed in the current study, some insight may be gleaned from the visual appearance of the limbs and from palpation of the tissue during imaging. Participant 1's limb was bonier than the others, with only a thin layer of soft tissue between the skin layers imaged and the tibia. Participant 3's limb had the most underlying soft tissue of the three which likely led to less internal stress in the skin due to having a thicker layer through which to distribute stresses. Participant 2's limb had more underlying soft tissue than Participant 1 but less than Participant 3, and his skin was more resistant to deformation than the others. These characteristics perhaps led

to less deformation of the dermis and thus less vessel occlusion when stresses were imposed. This is one possible explanation for why Participant 2's residual limb vasculature appeared the most like unstressed tissue compared to the other participants; it may not have received the stimuli to increase the vessel density quite to the magnitude of the other residual limbs tested.

Another possible cause of differing residual limb cutaneous vessel structure could have been the differing health states of the individuals. Participant 1's ROIs displayed several features indicative of the peripheral vasculature of diabetic individuals. In both limbs Participant 1's papillary dermis displayed a larger density of capillary loops than the other participants. Diabetes is known to stimulate angiogenesis in microvascular beds secondary to hypoxia resulting from damaged vessels. This combination of vessel damage and angiogenesis stimulation does not necessarily lead to increases in vessel density, but it does commonly lead to vessels that appear more tortuous, an early indicator of angiogenesis initiation. This is supported by the morphology of Participant 1's vessels in both limbs versus the more continuous and straighter vessel segments of the other participants. And while Participant 1's residual limb images were very dense with vessels, the contralateral limb images had a similar density to the other participants' images. It is also possible that the diabetic state of Participant 1's microvasculature altered how the vessels responded to the mechanical stresses of wearing a prosthetic socket, thus leading to the vessel network dense with aligned capillary loops running parallel to the skin's surface.

Participant 2 demonstrated a lower vessel density in both layers of the contralateral limb than the other two participants' contralateral limbs. One possible explanation is hypertension, which is known to induce vascular remodeling and can lead to decreased vessel count [140]. Chronic smoking can also damage the vasculature and lead to capillary loss [141]. Though it is possible the skin may have recovered from this influence considering Participant 2 had not smoked for >1.5 years prior to the study.

In agreement with known age-related effects on microvascular structure, the youngest participant (Participant 3) demonstrated the densest papillary vessel network of all the unstressed limbs. Cutaneous capillary density commonly decreases with age [142]. However, despite being the oldest participant, Participant 1 had by far the densest papillary network of all residual limbs, which again suggests that this vessel structure may be the result of altered skin adaptation.

5.5.3 *Epidermal Thickness*

Though the current study focused on adaptation to the cutaneous microvasculature, a measure of epidermal thickness was also readily available as a result of the methods used. The residual limb epidermis was found to be thicker than the contralateral side for all three participants. The 0.017 mm mean difference (16.9%) was found to be statistically significant. The measured thicknesses of 0.117 mm (mean of the residual limb) and 0.100 mm (mean of the contralateral limb) are close to the values expected based on commonly quoted skin thickness measurements. Epidermal thickness of most body sites is typically 0.06-0.10 mm, whereas the epidermis is closer to 0.60 mm for the palms of the hands and soles of the feet [29]. Additionally, the contralateral ROI mean of 0.100 mm matches closely with the 0.101 mm mean epidermal thickness measurement taken on the control limb of able-bodied participants in the Aim 2 study at an anatomical location that closely matched the ROI location used here. It is possible that the participants in this study have gained a thicker epidermis through skin adaptation to mechanical stress. Based on the appearance of the participants' limbs it is unlikely that this thicker epidermis was due to callusing of the skin. Callus formation is generally undesirable on the residual limb since the stiff callus mass can lead to increased stress concentrations in tissues below or at the edges of the callus and calluses are more prone to skin breaks than non-callused skin. Furthermore, callusing has been shown to increase the risk of pressure ulcers to the underlying tissue in load-bearing regions of skin [143]. While it is unknown whether this finding represents a beneficial adaptation or not, it deserves further investigation.

5.5.4 *Adaptation Versus Passive or Harmful Changes*

If the functional and structural differences that were detected between the residual limb and contralateral limb of these participants in fact represented changes that occurred in response to mechanical loading from wearing a prosthetic socket, the question that remains is if these changes represented physiological adaptation or a passive change. The term "adaptation" implies that tissue has transformed in a manner that imparts a beneficial physiological advantage to oppose a stress. Alternatively, tissue can transform in response to stresses in a way that is harmful to the tissue, increasing the risk future breakdown, or in a way that is passive, providing neither a positive nor a negative impact on the health of tissue.

Since the participants here did not regularly experience breakdown at the ROI even though their sockets were designed to impart large interface stresses at the ROI, it is believed that the physiological differences identified in their residual limbs here did not represent harmful changes. While we cannot distinguish between passive versus adaptive changes based on the information collected in the current study, we can offer some potential explanations for why the measured changes could represent adaptation.

Faster and larger magnitude RH response. Participant 1 and 2 exhibited indications that their residual limb skin may respond more quickly and with a greater magnitude of blood flow compared to the contralateral limb. As described in the Section 2.3, a key mechanism of skin breakdown involves mechanically-induced tissue ischemia, whereby oxygen and glucose cannot reach the tissue and altered cellular metabolism results in the build-up of harmful chemicals, such as lactic acid. In the case of stress imposed on a transtibial residual limb, the duration and magnitude of loading and unloading are often unpredictable, and periods of rest where tissue recovery can occur may be short. Thus, even incremental improvements in the efficiency of tissue reperfusion between loading may be beneficial in reducing the accumulation of the harmful byproducts and improve the tissue's ability to restore normal metabolic processes.

Alternatively, it is known that tissue can also be damaged during reperfusion following an occlusive event ("ischemia-reperfusion injury") and it is possible a higher magnitude RH response would exacerbate this injury. Ischemia-reperfusion injury is a cellular injury that occurs because reactive oxygen species precursors accumulate during ischemia and become activated into highly reactive oxygen species once oxygen is reintroduced. These substances react with cell membranes and damage cellular DNA [62]. The mechanisms of ischemia-reperfusion injury are still largely unknown, and it is unclear whether a RH response that is of higher magnitude or more rapid would exacerbate skin damage in the case of transtibial prosthesis users, but it is possible.

Increased vessel density: increased vessel count and/or vessel diameters. Maximum Dilation Test images of Participant 1 and 2 demonstrated that their residual limb skin contained a larger vessel density compared to the contralateral limb. This was due to both a larger vessel count and larger mean vessel diameter. A more extensive network of vessels through which blood can supply oxygen and nutrients to the tissue would likely make skin more resistant to breakdown for multiple reasons. For one, increased vascularity would likely enable the tissue to reperfuse more efficiently

following an occlusive event, as described in the previous section. In addition, increased vascularity could potentially reduce the harmful effects of tissue ischemia downstream of occluded vessels by providing more conduits through which blood could reach the surrounding tissues.

New vessels that are ultimately added could be in the form of capillaries or larger vessels and it is unclear which would be more beneficial in the case of lower limbs prosthesis users. In a review on therapeutic vascularization strategies, Phelps and Garcia suggests that the most beneficial strategy for tissue in general may be to induce the formation of both capillaries and larger vessels to balance the benefit of each [144]. Larger arteriole-level vessels would result in larger conduits that could supply more blood more rapidly, thereby more fully perfusing capillaries. Capillary formation would have the benefit of enhancing the exchange of oxygen, nutrients, and fluids with the tissue.

Increased epidermal thickness. If the epidermal thickness difference found in the current study was induced by limb-socket interface stresses, it is likely to have been caused by shear stress (no-slip), yet a thicker epidermis may also be caused by friction (slip). Current transtibial prosthetic systems for lower limbs are designed to reduce friction imposed on the skin. Commonly a gel liner is worn on the skin, usually of comprised of silicone or polyurethane). The gel material contacts the skin and, due to a high coefficient of friction, slip between the two surfaces is expected to be minimal. A fabric-backing is built into the outer surface of most liners which interacts with the socket interface, encouraging slip and thus reducing slip that may occur between the liner and skin.

Shear stresses imposed on the residual limb at its interface with the prosthetic socket have been extensively documented [18,99,122]. A thicker epidermis may be beneficial to absorb more of the energy caused by the imposed shear forces thereby limiting the shear that is able to act on the more fragile, vascularized tissues below. Deformation due to shear acting on the tissue may also be reduced in skin with a thicker, stiffer epidermis. This could be investigated further by measuring the mechanical properties of skin that is believed to have adapted via epidermal thickening.

5.5.5 *Sample Size Calculations for Future Study*

Data collected in the current study was used to perform an *a priori* prospective power analysis for continuing this work. This was performed for two separate differences that were noted between the residual limb and contralateral limb in the Maximum Dilation Test. The three participants of

this study demonstrated a higher magnitude VAD in the papillary dermis of the residual limb versus the contralateral limb with a mean difference (± SD) of 0.052 ± 0.074 a.u. (Cohen's *d* effect size=0.7). The participants also demonstrated a greater vessel count in the papillary dermis of the residual limb versus the contralateral limb with a mean (± SD) difference of 1.55 ± 1.64 mm/mm^2 (Cohen's *d* effect size=0.95). To show statistically significant mean differences of the same sizes, given a Type I error probability (α) of 5% and a power ($1 - \beta$) of 80%, sample sizes of 24 and 14 would be required for the VAD and vessel count measurements, respectively. Therefore, a future sample size of 24 would be large enough to measure both effects.

5.5.6 *Limitations*

While this study demonstrated the ability of novel noninvasive imaging techniques to identify differences in cutaneous microvascular function in lower limb prosthesis users, the small subject number limited the statistical power of the tests. Rather, this study served a proof-of-concept for the potential value of the developed test methods for investigating skin adaptation and skin health in individuals with lower limb loss. And, while the methods used here proved able to identify some interesting findings, including multiple potential biomarkers for skin adaptation, the study also highlighted some of the current limitations of the methods that future efforts would benefit from addressing.

In the RH Test, the delay that occurred between the load application removal and the first post-load image resulted in multiple tests where it was unknown whether the peak of the RH response had been captured. Since the first image collected for these tests was often also quantified as the peak VAD it is likely the peak occurred prior to the first post-load image. For Participants 1 and 2, however, the RH peak appeared to have been captured in the contralateral limb, making it a valuable finding that the residual limb had a peak VAD in the first post-load image. However, for Participant 3 it is unknown if the peak had already occurred or if the limb truly did not exhibit a RH response. Additionally, since it was unknown for these tests whether the peak was captured or not, the recovery time measurement was less reliable since it was based on a percentage of the difference between the peak VAD and baseline VAD. For example, if the peak RH was captured for Participant 2's residual limb and the peak VAD was much higher for the residual limb than what was actually measured here, this could have indicated that the recovery time was faster in the residual limb versus the contralateral limb, instead of being similar. The transition to the first post-

load image was limited by the time it took to remove the loading device, place the OCT probe, center the OCT field-of-view, then set the pressure and focus targets by modulating each of two vertical stages. It is likely this process could be hastened by 10-15 seconds by including additional personnel to complete these tasks, however that would require a significant degree of coordination, thus introducing additional possible failure points into the test. A more reliable approach would be to automate this process, or at least some of the key steps. This could be accomplished through incorporating the OCT probe into the load application device or through replacing the vertical stages with motors with a control system that quickly attains the target OCT probe pressure and imaging depth. Additionally, software improvements to the OCT imaging control could enable automatic centering of the field-of-view between fiducial markers on the skin.

While OCTA offers valuable insights into vascular structure and function unlike any other measurement technique, the imaging method also presents several challenges, not all of which were overcome for the current study. For one, vessel shadowing is a common artifact in OCTA, whereby vessels appear to have a much larger diameter in the depth direction than they do in reality. This usually does not affect *en face* images, since depth information is not presented; however, in the current study this shadowing effect did impact the reticular dermis Maximum Dilation Test. Shadow artifacts from vessels in the papillary dermis resulted in many of the mid-sized vessels being present and quantified in both the papillary and reticular images and made it difficult to evaluate the reticular vessels independently. This issue could be overcome in the future through developing post-processing techniques to de-shadow the image. One such method is described by Mahmud *et al.* [126].

Additionally, for the purposes of the current study, some of the vessel quantification algorithms were simplified, which should be taken into consideration when interpreting the results. In some cases, when vessels overlapped or ran too close next to each other, the vessel skeleton algorithm was unable to resolve them as separate vessels. This could be overcome in future test methods by utilizing additional vessel information to separate them, such as using depth information after de-shadowing or by using Doppler OCT methods which also provides information related to red blood cell velocity and direction. This could enable an even more accurate and richer data set. The vessel diameter calculation was also simplified as the mean diameter of the entire *en face* image, which limited the insight provided by these data. Future works could use methods such as one proposed by Liew *et al.* [145], which operates along each vessel

skeleton line and takes measurements of vessel diameters perpendicular to the line at regular intervals. This method would provide additional insight by producing a distribution of vessel diameters.

Another limitation of the current methods is that the thresholds chosen for the vessel area density binarization and the skeletonization steps were done visually, thus increasing the risk of including subjective biases into the quantifiable data. To increase the reliability of future measurements less subjective methods should be developed. One alternative would be to have key post-processing steps performed by a blinded researcher. Another alternative would be to use a set threshold method for all images. Since a set threshold value was shown to be ineffective for the current study due to inaccurate quantification of vessels and noise, a more complex method would be needed, such as an adaptive thresholding algorithm which has been used by others when quantifying OCT data for comparisons [94,125]. The method uses a moving window to set different thresholds throughout the image based on the mean intensity of pixels within the window [146]. Using a single threshold value across all images collected in a study may also be made possible if image intensities were automatically normalized first to eliminate the differences that often exist in image intensities between different participants and between images collected on the same participant. Lang *et al.* presents one such method that was used to normalize data sets prior to training machine learning algorithms [147].

One potential source of tissue illumination variability that was likely present in the current study was a difference in tissue illumination that may have occurred due to differences in epidermal thickness. The epidermis is a dense cellular structure which notably absorbs and reflects the OCT laser light. Since all three participants demonstrated a thicker epidermis in the residual limb versus the contralateral, it is likely the OCT laser did not illuminate the dermal tissue as intensely in the residual limbs. This may have resulted in slightly less intense vessel pixels in the residual limbs. Again, in the future this difference in tissue illumination could be adjusted for by normalizing image intensities prior to constructing *en face* images. Importantly, the difference in epidermal thickness did not affect the depth of vessels that were analyzed since the vessels were always extracted from a set depth beginning at the dermal-epidermal junction, which is situated at the base of the epidermis.

Image accuracy could also be improved by undertaking more complex noise removal techniques. One example is a method called Eigen-Decomposition, which is an adaptive filtering

technique used in MRI and Ultrasound imaging and has recently been adapted for use in OCT by Zhang *et al.* [148]. Motion artifacts could also be reduced further by employing more complex B-scan registration techniques or through registering multiple three-dimensional images together. The current data uses a simple translation correction through cross-correlation, but methods such as step-by-step rigid affine registration followed by cubic B-spline volume registration have been shown to be effective in reducing noise in OCT images [149].

This study chose to focus on a select few possible adaptations based on the measurements that could be made given the test methods used though it should be noted that support exists for additional mechanisms of adaptation that are worth considering for further investigation. For one, support exists that structural adaptations may occur within the extracellular matrix of skin that would strengthen dermal tissue. This could lead to decreased deformation to mechanical stress and potentially limit vessel occlusion. Using a porcine model and daily stress protocol designed to replicate stresses experienced by a transtibial residual limb, Sanders *et al.* previously demonstrated an increase in collagen fibril diameters in the stressed tissue [75]. In that study, measurements were taken of biopsied tissues, whereas noninvasive methods are needed to study this in a population of prosthesis users. While such methods are still sparse, polarization-sensitive OCT has shown promise. Polarization-sensitive OCT composes images of birefringent tissue components based on changes in polarization of the light as it travels through the sample. Since collagen is the primary birefringent molecule in skin it is possible to get images and measurements of collagen density and alignment. Polarization-sensitive OCT has been used to study skin burns in humans, including measuring collagen density in burn scars [150], collagen denaturation due to burns [151], and burn depth [152].

5.6 CONCLUSION

In the current study, novel OCT imaging-based test methods were used to investigate skin adaptation biology in individuals with transtibial limb loss. The methods measured the cutaneous vascular response to stress, the vessel structure, and the epidermal thickness in a highly stressed region of the residual limb and at a location-matched site on the intact contralateral limb. Vessel density, vessel count, vessel diameters, and epidermal thickness differed between the two limbs and may represent adaptations that have occurred to the mechanical stresses of prosthesis use. Additionally, in response to a cyclic mechanical stress, residual limb skin responded with a

reactive hyperemia response that reached the peak blood flow more quickly and at a higher magnitude than on the contralateral limb. These differences may represent functional adaptations of the cutaneous microvasculature. This study also highlighted vast differences in vascular function and structure between individuals, potentially due to differing comorbidities and/or age. The differences found between individuals' microvascular function and structure presents an interesting area of future investigation for the methods developed in this research. If individuals adapt differently based on differences in health states, limb mechanical properties, or limb-socket interactions, it may be possible to leverage these differences to glean insights into some of the underlying mechanisms of skin adaptation to mechanical stress.

The results of this study demonstrated the utility of OCT imaging as a noninvasive tool to better understand skin adaptation, and skin health as a whole, in individuals whose skin experiences chronic mechanical stress. Further research is needed to confirm the consistency of the reported residual limb versus contralateral limb differences across a larger subject population and to determine if they are indicative of changes that represent beneficial adaptations or if they are merely passive changes that have occurred secondary to other tissue remodeling. Improvements to the test methods such as enabling faster RH Test image capture following load removal or by combining OCT imaging with other structural and functional skin measurement techniques could provide an even richer data set that could be used in future studies to further enhance our understanding of skin adaptation to the mechanical stresses lower limb prosthetic socket use.

While the cost of the OCT system used in the current study would likely preclude its use in the clinic at present time, the cost of OCT systems is decreasing steadily, with a recently published point-of-care system costing just $8,000 USD [153]. Using these methods to further improve the understanding of skin adaptation in people with lower limb amputations could lead to improved skin adapting rehabilitation techniques and therapeutics or to tools that could be used by clinicians to better assess skin health and help to guide periods when skin adaptation is desired.

Chapter 6. CONCLUSION

6.1 RESEARCH SUMMARY

Skin breakdown is a problem that affects many users of lower limb prosthetic devices. Breakdown results from mechanical stresses that are imposed on the limb at its interface with the prosthetic socket. While skin has the ability to adapt to these stresses, thereby making it more resistant to breakdown, little is known about the biology behind skin adaptation and no methods exist to measure it in the clinic or research setting. Optical Coherence Tomography (OCT) is a noninvasive imaging technique with a depth and resolution balance that is well-suited for investigating skin adaptation. This thesis introduced new OCT-based methods for the investigation of skin adaptation in users of lower limb prostheses, highlighted advantages and limitations related to these methods, and identified potential biological markers for skin adaptation that are worth further investigation.

In Aim 1, novel methods were developed to measure key structural and functional features of the cutaneous microvasculature that may be involved in skin adaptation. A Reactive Hyperemia (RH) Test was developed to assess microvascular function in response to a controlled cyclic load stimulus. A Maximum Dilation Test was developed to assess vessel structure after a repeatable vascular state was induced using a skin heating device. A model for the study of mechanically-induced skin adaptation using able-bodied participants was also developed. A modified transtibial prosthesis was designed to stress the lower limb skin of the able-bodied participants using stresses similar those imposed on the residual limb of transtibial prosthesis users. The purpose of the device was to mechanically stress the skin in a manner that would induce adaptation similar to adaptation that occurs the skin of an individual adapting to their first prosthetic device following amputation surgery. As a part of this model, a Load Tolerance Test was developed to determine if the skin of able-bodied participants had adapted into a more load tolerant state following two weeks of wearing the modified prosthetic socket. The test was based on the clinical assessment for load tolerance, in which skin redness duration is monitored following a short walking bout. Here, the test applied a cyclic compressive and shear stress followed by the collection of photographs which were later randomized and assessed for redness by a blinded clinical expert.

In Aim 2, the devices and test methods developed in Aim 1 were used to investigate skin adaptation to mechanical stress on eight able-bodied participants who wore a modified below-knee

prosthetic socket for two weeks. Study results demonstrated good repeatability of the OCT-based measurement methods with the exception of a couple measurement features. Most notably, in the RH Test, the gap in time that occurred between removal of the stress stimulus and the first image of the RH response was too long, resulting in several tests where the RH peak perfusion was not recorded. This delay must be reduced to enable reliable measurements in the future. Additionally, it appeared that skin adaptation had not been reliably induced, as evidenced by the lack of participants who demonstrated an increase in load tolerance in the Load Tolerance Test. This was further supported by the pressure estimates measured by force sensors in the sockets. Thus, in the future, the modified prosthetic device must be modified to impose larger magnitude stresses or the socket must be worn for more time to stress the limb further. No statistically significant differences were found in any of the OCT measurements taken at different time points throughout the study or between the test site and a location-matched control site on the contralateral limb.

Aim 3 was a proof-of-concept study for the use of the developed noninvasive OCT imaging techniques to investigate skin adaptation in three individuals with transtibial limb loss. Measurements of cutaneous vascular function and structure, and epidermal thickness, were taken at a highly stressed region of the residual limb and were compared to measurements taken at a location-matched site on the intact contralateral limb. Notable differences in functional and structural characteristics of the microvasculature were found between the residual limb and contralateral limb of study participants. Differences were also found among the participants and may have been due to the differing health and age-related characteristics of the individuals. The Reactive Hyperemia Test found a larger magnitude RH response and a faster RH time-to-peak in the residual limb of two of the three participants compared to their contralateral limb. The Maximum Dilation Test demonstrated a larger vessel density in two of the three participants' residual limbs compared to the contralateral limbs. This difference was due to both a higher vessel count and larger mean vessel diameter. Vessels appeared more aligned to each other in the residual limb versus the contralateral limb, and this was most notable in the participant with diabetes. A statistically significant difference in epidermal thickness was found between the residual limb and contralateral limb of all participants, with increased thickness on the residual limb. These findings represent potential biomarkers for skin adaptation that are worth further investigation.

If we can develop a better understanding of the biology of mechanically-induced skin adaptation and introduce noninvasive methods to track its progress, we can provide clinicians with

more objective tools for monitoring skin health and ultimately reduce the risk of skin breakdown in individuals with lower limb loss. Additionally, it may be possible to use these methods to develop new therapeutics or rehabilitation strategies to promote skin adaptation rather than breakdown. Furthermore, although this thesis focused on developing methods for the investigation of skin as it relates to adaptation to transtibial socket-limb interface stresses, these methods may have broader applications for researching skin health in other populations at risk for breakdown, such as bedridden individuals or people with diabetic foot ulcers.

6.2 FUTURE WORK

6.2.1 *Improvements to Measurement Methods*

Enable more reliable RH peak capture. While the developed OCT test methods identified several interesting findings related to skin vessel structure and function that are worth further investigation, it would be best to execute a few key improvements prior to continuing the research efforts. By addressing the most critical limitations, the data collected will provide a more complete and more reliable snapshot of the microvasculature.

In Aim 2 of this thesis, of the 40 RH Tests that produced a measured RH response, only 12 of the tests reliably captured the peak perfusion of the response. In the remaining tests, the first data point collected after the stress stimulus removal was the peak of the measured response. Since no time points with less perfusion were captured prior to this point it was not possible to determine if this point represented the physiological peak of the response or if it had occurred prior to this time point. Thus, for these tests, we did not obtain a trustworthy measurement of peak VAD or time-to-peak. The transition from load removal to imaging was limited by the time it took to remove the loading device, center the OCT imaging location physically on the skin and in the software, and adjust the OCT pressure and focus into the target ranges. This process usually took between 40-60 seconds. This time will need to be shortened considerably in order to reliably capture the RH peak during every test.

First, a decrease in 10-15 seconds could likely be achieved by adding personnel and coordinating the completion of these tasks. A potentially more reliable approach would be to automate part of this transition process. The imaging location could be automatically set by modifying the OCT control software. For example, the four dots that are used by the OCT operator

to visually center the imaging location could be used in an image analysis algorithm that would detect them as fiducial markers, calculate the center point between them, and automatically move the OCT imaging location to that point. This would require discontinuing use of the commercial software provided with the OCT device and instead using the developmental research kit also provided with the system. LabVIEW virtual instruments are contained in this research kit and may be the easiest place to start prototyping these changes.

Also, through leveraging this OCT research kit, it may be possible to reduce the transition considerably by automating the focus and pressure setting step. This step caused a majority of the delays and was also the most variable. In future iterations the two manual stages used by the OCT operator to change the focus depth and OCT probe pressure could be modified to be modulated by small motors as part of control system. The control system could be made to maintain a target force being measured by the OCT probe strain gages and maintain the focal depth within the skin. If the control system works well enough it may be possible to motorize only one of the stages, thus allowing one to be set manually. Determining focal depth could be done automatically in real-time using an algorithm similar to that used in this thesis to automatically detect the skin surface and dermal-epidermal junction. This improvement would have the added benefit of maintaining a consistent focus throughout the course of the study. This was not a notable issue in the current study because the focus was checked and adjusted every 60 seconds or less, but it is likely that small differences in focus did exist that could be eliminated using this method. While simply maintaining the skin surface or dermal-epidermal junction at a known depth would maintain focus consistency throughout a single data set, there is also an opportunity to develop a method to obtain a repeatable focal depth between data sets. The repeatability of the depth focus is a known issue in OCTA imaging of the skin that can lead to differences in vessel diameters and alter which vessels are captured in an image. The depth of focus for our current system occurred within a band of approximately 0.1 mm, however the depth-location of this band changed frequently as it is highly dependent on the optical properties of the medium and tissue through which the OCT laser travels. Furthermore, it was not always obvious where this focus location was in the tissue. Automating the identification of the focal depth location so that it could be set consistently within the tissue—ideally just below the dermal-epidermal junction where the smallest vessels reside—would be a novel contribution to OCTA imaging of the skin that would greatly improve consistency of measurements.

A more comprehensive solution to the RH Test imaging delay may be to redesign the stress application system to incorporate the OCT probe or to include an adapter that allows for rapid placement of the OCT probe following the load application. This would likely take a significant engineering effort to accomplish, given the mass of the OCT probe.

Image post-processing improvements. While the developed OCTA measurements offered interesting insights into vascular function and structure, several improvements could be made to the image processing methods that would notably enhance the quality of the images and the reliability of the measurements. Many of these remaining limitations have been addressed by other researchers using a variety of methods. It is likely that undertaking this effort would be a matter of choosing which of these methods would best suit the needs and then figuring out how to adapt the methods for use with the RH Test and Maximum Dilation Test images.

Perhaps the most important improvement needed would be to limit human input into the selection of key processing parameters in order to make the images more consistent and less vulnerable to biases. A key post-processing step in the current measurements relies on a user-selected intensity threshold which sets pixels with an intensity greater than this value to a "1" (vessel) and those below the value to a "0" (non-vessel). Thus, VAD measurements rely heavily on this step and the vessel count can also be affected by it. To increase the reliability of future measurements, less subjective methods should be developed. One alternative is to have these critical steps performed by a blinded researcher. This would decrease inherent biases, though likely not eliminate them. It would also not address the need for more consistent parameter selection across different images. A good option may be to create an adaptive thresholding algorithm, similar to those used by other researchers when quantifying OCT data to make comparisons across data sets [94,125]. The method uses a moving window to set different thresholds throughout the image based on the mean intensity of pixels within the window [146]. Similarly, it may be beneficial to normalize OCT pixel intensities prior to threshold selection since differences in tissue illumination are a common cause of differences between images. Lang *et al.* presents one such method that was used to normalize data sets prior to training machine learning algorithms [147].

Another issue present in the images collected in this thesis was vessel shadowing. Vessel shadowing is a common artifact in OCTA, whereby vessels appear to have a much larger diameter in the depth direction than they do in reality. This usually does not affect *en face* images, since they do not present contain information; however, in the current study this shadowing effect did

noticeably impact the reticular dermis images in the Maximum Dilation Test. Shadow artifacts from vessels in the papillary dermis led to some of these vessels appearing in both the papillary and reticular images when in reality these vessels should have only appeared in the papillary image. This made it difficult to evaluate the reticular vessels independently. De-shadowing algorithms have been developed by others, such as one by Mahmud *et al.* [126]. Similar methods could be adapted for use with the images taken using the OCTA methods developed in this thesis.

Image accuracy could also be improved by using more sophisticated noise removal techniques. In the current study cross-correlation of B-scans within each B-scan set was used to perform a translational motion correction to account for large bulk tissue movements that occurred due to the pulse. More complex methods of B-scan registration have been used by others which could significantly reduce motion artifacts. One method that has shown promise for correcting motion in OCTA images of skin is applying a rigid affine registration followed by cubic B-spline volume registration [149]. In addition to improving image motion correction methods, alternatives exist to the way in which vessels are identified that may provide a beneficial increase in the image signal-to-noise ratio. In place of the High-Intensity Speckle Variance processing method used in this thesis, it may be worth investigating the use of Eigen-Decomposition—an adaptive filtering technique used in MRI and Ultrasound imaging which has shown promise in OCT imaging [148].

Maximum Dilation Test images could also further be improved by combining information gathered from multiple full field-of-view images to form a more complete and accurate snapshot of the microvasculature. One issue that was identified was that if multiple maximum dilation images of the same skin site were compared there were often several small vessels that would appear in one image but not the other, and vice versa. If an algorithm were developed to combine multiple repeat maximum dilation images, this could ensure that all vessels that can be captured by the imaging method would be accounted for. This method could also be extended to remove unwanted regions of an image, such as those disturbed by imaging artifacts. In these cases, the unwanted regions could be removed and replaced by clean versions of the sections from another image. A strategy to accomplish this was recently described by Wei *et al.* [149].

6.2.2 *Improve Able-Bodied Skin Adaptation Model and Continue Aim 2 Study*

Another potential future direction of this work is to continue the Aim 2 study on able-bodied participants to continue investigating skin adaptation to limb-socket interface stresses. Before

continuing this work, in addition to making some of the improvements to the OCT test methods as mentioned above, it would be beneficial to make a few improvements to the Able-Bodied Socket design and the wear protocol. These are described below. While performing a skin adaptation study on individuals who are undergoing adaptation to their first below-knee prosthetic socket would allow a more direct study of the population of interest, an able-bodied model has benefit of eliminating many confounding variables and logistical challenges associated with studying individuals who have recently undergone amputation surgery.

Increase stress imposed at the imaging region of interest. In the Aim 2 study, no statistically significant changes were found in the region of skin that was subjected to limb-socket interface stresses. While it is possible that adaptation did occur and the measurements taken were in fact not involved in the adaptation, it is also possible that the skin was not subjected to enough mechanical stress to induce the level of adaptation. The latter explanation was further supported by pressure measurements collected by a force sensing resistor (FSR) at the region of interest (ROI) throughout the two-week socket wear period. FSR data indicated that interface pressures imposed at the test ROI were far below those experienced by the residual limb in a transtibial socket. Even considering a worst-case 44% error—the error that can occur when using FSRs to measure limb-socket interface pressures [101]—many participants demonstrated peak interface pressure measurements that would have still been at least 50% less than those typically seen in lower limb prostheses. It is likely the participants' limbs could have withstood higher interface stresses (i.e. more offloading of the foot), however the Able-Bodied Socket model used here was limited in its ability to increase stresses beyond a certain point. We aimed to offload the foot by suspending the limb in the socket, however, full offloading could not be achieved without creating a choke point which occluded blood flow to the foot. Occlusion could be identified quickly as the presence of a strong pulsing sensation in the limb, and it was avoided. As such, limbs were only partially offloaded. While it was possible for some participants to safely achieve regions of high interface stress, as evidenced by significant skin redness lasting several minutes, it was also not easy to dictate the focus of that stress, even by moving the location of the pads on the socket wall. Since the current study design required that the ROI be selected prior to fabricating the participant's socket, these regions of seemingly higher stress did not always occur at the ROI.

One possible solution to address the location of stress concentrations in relation to the ROI would be to select the ROI after the socket is first worn and locations of high stress on the limb

are identified. While the ROI was selected in the Aim 2 study by the study prosthetist as a region that was anticipated to be in a region of high stress, it was not possible to predict the extent of the loading at this site compared to other nearby sites. By waiting until the socket is worn, regions of highest loading can be verified, either visually or by measuring interface stresses. If this were done, the study would need to be extended by 1-2 weeks to allow the limb to recover between the fitting session and the first imaging session since the skin will likely become irritated and potentially begin to adapt while wearing the socket during the fitting session.

Similarly, the chance of inducing adaptation at the ROI could be further improved with the existing Able-Bodied Socket design by increasing the total amount of stress imposed on the limb throughout the adaptation protocol. One method for doing this would be to extend the wear protocol by 1-2 weeks, continuing with more days of 6-8 hours of wear time. In the current protocol participants only reached 90 minutes of wear time by the end of week 1 and were up to 7 hours by the final day. Stressing the limb for 1-2 more weeks at these higher wear times would significantly increase the accumulated stress imposed on the limb. However, these proposed strategies would likely limit participant recruitment and could lead to a higher drop-out rate considering the current protocol already lasts for several weeks and is time-intensive. Another method that could be trialed would be to increase the wear time more rapidly, especially during the first week. The wear schedule used in the Aim 2 study was developed to replicate a wear schedule that would commonly be seen in practice for an individual who is adapting to their first prosthetic socket following an amputation surgery. Participants in this study progressed through the target wear times without any issues and without any reports of discomfort. It is likely that a more aggressive wear schedule could have been used.

Stress imposed on the limb could also be increased by modifying the manner in which the load is applied. If done properly, this method could also enable a more repeatable stress application that could nearly eliminate differences in interface stress magnitude and activity level which was a confounding factor present in the current study. One way this could be accomplished is by creating socket with a panel, or panels, cut out of the socket wall that could be mechanically controlled to tighten and loosen onto the limb. Sockets using this design have recently gained popularity for lower limb prosthetic users. Additionally, electromechanically controlled versions of the system have been proposed and tested by researchers [124]. A system that is automatically controlled based on the load that is applied by a panel would result in a more controllable able-

bodied model for adaptation. Furthermore, this would likely enable higher magnitude loading at the ROI because the panel could apply force acting in the direction of the limb rather than relying on suspension of the limb to redirect vertical ground reaction forces into the sides of the limb. Applying stresses in a cyclic manner, even when participants are seated, could further reduce the risk of occluding blood flow with increasing loads, since any large vessels that may become impinged would only be occluded for a short amount of time.

Improve stress measurements at the imaging region of interest. The able-bodied model for skin adaptation could also benefit from improving the accuracy of the interface stress measurement at the ROI in the Able-Bodied Socket. FSRs were used in the Aim 2 study to estimate the limb-socket interface pressure at the ROI. While this sensor type is cost effective, easy to use, and provided a general estimate of stresses that could be compared between individuals, it was known that the measurements would be subject to large errors. Errors in FSR measurements when used in a similar manner have been shown to be as large as ± 44% [101]. More accurate measurements of interface pressures at the ROI are desired so that more definitive comparisons can be made between the pressures experienced by different participants and so that researchers can better understand how well the applied stress compares to stresses in a typical below-knee prosthetic socket.

One way to improve the accuracy of pressure measurements would be to perform an in-socket calibration of each FSR. FSRs were calibrated in the Aim 2 study in a manner that attempted to replicate the socket environment on the benchtop, however several differences were known to exist, namely curvature of the socket and of the actuator (the limb). For improved accuracy, FSRs should be calibrated in the exact conformation in which they will be used. Pressure bladders have been used by some researchers to accomplish this, however they do not take shear stresses into consideration which are known to contribute to FSR error [101]. Additionally, FSRs are known to experience measurement drift and hysteresis, thus the measurement at a given point in time has some dependence on past activities. More complex calibrations that take into account this history dependence could lead to further improvements in accuracy. Alternatively, using a more accurate sensor type, such as strain-gage based sensors, may be a more effective way to obtain accurate measurements of the interface stresses.

Shear stress present at the ROI is also of interest due to the role it plays in skin breakdown, and its likely role in adaptation, however it could not be measured using the Able-Bodied Socket design used here. Shear stress plays a major role in occlusion of cutaneous blood flow when both

pressure and shear are imposed [64], and shear can be present at large magnitudes in a prosthetic socket [18,122]. Thus, shear is likely an important factor in skin adaptation for transtibial prosthetic users. In the future, it would be beneficial to measure both pressure and shear applied at the ROI. It would be especially beneficial in future studies to use a more accurate means of pressure and shear measurement at the ROI that can be visualized in real-time during the socket fitting session so that changes may be made in a more targeted manner to get closer to the desired stress targets. One possible solution may be to install a strain gage-based tri-axial force sensor at the ROI either through the side of the socket wall or incorporated into a 3D-printed socket insert, which is a strategy that has been demonstrated with low-profile sensors previously [123].

Sample size estimate. The sample size for a future able-bodied skin adaptation study was estimated based on data collected in this thesis work. Since the results of the Aim 2 study were highly variable and it is believed that this variability was largely due to limitations in the testing methods that will largely be addressed prior to continuing the study, the data collected in Aim 2 were not used to perform a sample size calculation. Instead, data were used from the Aim 3 study which compared measurements on the residual limb skin versus contralateral limb skin of prosthesis users. In the Maximum Dilation Test of that study the three participants demonstrated a higher magnitude VAD and vessel count, both in the papillary dermis, with mean differences (± SD) of 0.052 ± 0.074 a.u. (Cohen's *d* effect size=0.7) and 1.55 ± 1.64 mm/mm^2 (Cohen's *d* effect size=0.95), respectively. Since it is expected that the differences measured after 2-3 weeks of socket wear time will not be as drastic as those measured in the skin of individuals who have worn a socket for several years, a mean difference one-half the magnitude of those measured in the Aim 3 study was used in this calculation. Additionally, it is expected that the variability in the data among the three participants in the Aim 3 study was greater than it would be in an able-bodied study due to the varying health states of the Aim 3 participants. Thus, a standard deviation one-half that of the Aim 3 standard deviation was used. Using these assumptions, to show statistically significant differences given a Type I error probability (α) of 5% and a power ($1 - \beta$) of 80%, sample sizes of 18 and 11 would be required for the VAD and vessel count measurements, respectively. Therefore, a future sample size of 18 would be large enough to measure both effects based on these estimates.

6.2.3 *Study Skin Adaptation During First Prosthetic Training*

An alternative to improving the able-bodied model for skin adaptation would be to use the developed OCT measurement methods to investigate skin adaptation as it is first occurring in the target population: individuals with lower limb loss. By taking measurements throughout the prosthetic training period of an amputation rehabilitation program, adaptation to limb-socket interface stresses could be investigated as it is happening. One challenge associated with choosing this model over the able-bodied model is that it would be logistically more difficult to find willing study participants and to schedule test sessions. However, if partnering with a clinic that oversees amputation rehabilitation programs, it may be possible to recruit from their patient pool, to store study equipment in the clinic, and to schedule imaging sessions to coincide with frequent clinic visits. It is also unknown how many confounding factors will be present that cannot be controlled for and what their impact would be on the study measurements. For example, a significant amount of edema will likely be present in the tissue, even in regions of skin that are not near the suture site. Edema would likely alter the optical properties of the tissue and possibly alter blood flow in the region. It is possible that choosing a skin site that is far enough away from the surgery site would minimize this factor. Additionally, researchers will likely need to choose an ROI prior to the participant wearing the socket for the first time and they probably will not be able to alter the socket stresses for the sake of the study. If an ROI is chosen that is not highly loaded in the socket, then skin adaptation may occur slowly or not at all. However, it is likely that highly loaded regions on a residual limb in a standard prosthetic socket will be more easily predicted than in a much less understood able-bodied modified socket. As such, inclusion criteria for this initial study should include only those individuals likely to wear socket types where the load profiles are well understood, such as a patellar tendon bearing socket. If the logistical challenges can be overcome and if confounding factors turn out to not significantly impact study results, this model could provide much more meaningful insights into skin adaptation than an able-bodied model can.

6.2.4 *Characterize the Repeatability and Accuracy of the Developed OCTA Measurements.*

If the OCTA test methods used in the current study are to be used in future efforts, it would be beneficial to undertake an effort to more fully characterize the repeatability and accuracy of the measurements. This would enhance the ability of researchers to make more definitive conclusions based on the data collected. For example, in the current study the exact limitations of the capillary

diameter size that could be captured was unknown. It was also unknown the extent to which this limitation was based on the diameter of the vessels versus the velocity of red blood cells travelling within them.

In order to test the repeatability and accuracy of a measurement, the ground truth measurements of the system being assessed should be reasonably well known. Therefore, *in vivo* human testing would likely not provide a reliable assessment of the OCTA methods since the vasculature being measured is highly active and is variable moment-to-moment. As such, if an *in vivo* human model were used, any variability seen would be a combination of variability in the measurement methods and in the system, and it would be impossible to separate the two. One possible option would be to use an animal model followed by histology or corrosion casting of vessels and electron microscopy; however, this system would still present many challenges. For one, the ground truth measurements would still be largely unknown since it is likely vessels would deform slightly due to the tissue-fixing process. Still, this method could be useful to assess the Maximum Dilation Test by determining which vessels are and are not captured by the method.

Since OCTA captures images and quantifies perfusion in individual vessels, the best model may be a benchtop system that can control diameters and flow in individual vessels, such as an engineered tissue phantom. Benchtop tissue flow phantoms have been developed by others for the purpose of characterizing their OCTA methods [82,92,154,155]. These have ranged from simple single vessel-like conduits embedded into a single material to more complex multi-layered structures. These systems would be a good starting point for the system that would be used to assess the developed OCTA methods, though the systems would need to be adapted to specifically answer the questions important to the developed methods for investigating skin adaptation.

It would be especially important to understand the diameter and flow required in a capillary for it to be distinguished by the developed OCTA methods. It would also be important to understand the accuracy of the current system for measuring diameters, especially for capillaries that are below the resolution limits of our system. It would also be helpful to understand how accuracy varies with depth. Similarly, it would be interesting to vary the optical qualities of the bulk tissue material to match that of different skin types to better understand how imaging depth and accuracy may be different when measurements are taken in individuals with different skin types. For the purposes of skin adaptation studies, it would also be helpful if a benchtop model could be induced to move in manners that are present during imaging of human skin since this will

likely impact the accuracy of measurements that are taken. An approximate 1 Hz vertical displacement of 0.1-0.2 mm could mimic pulse-induced movement of the skin seen in the current studies, but it may also be of interest to mimic smaller magnitude motions that occur such as those due to respiration. By developing a better understanding of the accuracy and repeatability of the OCTA methods used, measurements collected could be interpreted more clearly and more definitive conclusions could be determined from the experiments.

6.2.5 *Continue Residual Limb vs. Contralateral Limb Investigation*

It may be of interest to continue the work of the Aim 3 study by using the developed OCTA methods to investigate differences in the skin of individuals who use a below-knee prosthesis. The Aim 3 study identified a few stark differences in skin between residual limbs and contralateral limbs of prosthesis users, and between the prosthesis users. Among these differences were greater vessel densities and more vessel alignment in the residual limb compared to the contralateral limb. A larger RH peak VAD and RH time-to-peak were also measured in the residual limb versus contralateral limb, as was a thicker epidermis. Since only three participants were tested and they differed significantly in health characteristics, testing on a larger study population could allow more definitive conclusions to be made. Based on the sample size calculation described in the Discussion of the Aim 3 study, 24 participants would be required to demonstrate vessel density and vessel count differences that were measured between the residual limb and contralateral limb in the Maximum Dilation Test.

Ideally, a study that continues the work of Aim 3 should be designed so that the results will not simply highlight differences between the limbs, but rather provide insights into skin adaptation and skin health. One method that may promote this is to compare two populations: one who experiences frequent skin breakdown and one who does not. An interesting first step would be to investigate skin where breakdown frequently occurs to determine if there are qualities present that can be easily identified in these sites compared to other sites. It is expected that the tissue will possess significant differences due to the breakdown and healing process, and this may prove to be a good initial indicator of skin that is prone to breakdown. It may also be interesting to then compare sites where breakdown has occurred, but no longer occurs, to sites where breakdown is still common. This may help to determine which differences may be due to breakdown and healing versus those that are indicative of greater breakdown risk. In order to focus more on factors related

to skin adaptation it may also be worthwhile to study regions of skin that are less highly loaded within the socket and have not experienced breakdown. Comparing measurements at these sites to similarly loaded sites on the limbs of prosthesis users without skin breakdown problems could give insights into load tolerant versus non-load tolerant skin or potential identify early risk factors for breakdown.

It would also be beneficial to study individuals who have worn a prosthesis regularly but are about to undergo a significant change to their prosthetic socket that will result in altered limb-socket interface stresses. While the effect size of any changes that occur may not be as large as those in the skin of individuals who are adapting to their very first prosthetic socket, the model proposed here would not be subject to the same logistical challenges and confounding factors as the post-surgery.

6.2.6 *Additional Measurement Techniques Worth Considering*

Additional measurement techniques may be beneficial to include in future studies of skin adaptation to supplement the OCT methods developed in this thesis. Comprehensive reviews on several options these techniques have been written by Deegan and Wang [156], Cracowski and Roustit [157], and Allen and Howell [87].

Additional OCT-based measurements. One method worth considering would be to use the current system with a **closed-end OCT probe** to study reactive hyperemia while a pressure is applied at the imaging ROI. Doing this may provide a more realistic measurement of how the microvasculature is able to response while the socket is worn, since periods of intense loading are likely to be followed by lower magnitude stresses of standing or sitting, rather than full offloading of the tissue. Full off-loading would likely only occur if the socket is fully or partially doffed, which for many individuals only happens a few times each day. This test could be executed using a similar protocol to the RH Test developed in this thesis except using an OCT probe that is closed at the end rather than open. The closed end would contain a lens transparent to the OCT laser, such as glass or PMMA. For this test it would be important to maintain a consistent pressure application throughout the entire duration of the RH response. It would also be important to move the probe into place and apply pressure quickly so that the time the skin is unloaded is minimized. This test would also provide beneficial information to other researchers using OCTA to measure skin microvasculature. Many researchers use OCTA on skin with a transparent closed-end probe

without measuring the pressure applied. It would be helpful to determine what the effect of this pressure has on the underlying microvasculature.

Since collagen remodeling has been implicated in previous skin adaptation studies, it would also be beneficial to investigate changes in the extracellular matrix of the skin in future adaptation studies. Using a porcine model and daily stress protocol designed to replicate stresses experienced by a transtibial residual limb, Sanders *et al.* found an increase in collagen fibril diameters in healthy stressed tissue [75]. While noninvasive methods to measure collagen fibril diameters do not exist, **polarization-sensitive OCT** has shown promise in measuring different aspects of the extracellular matrix that could provide additional insight into skin adaptation. Polarization-sensitive OCT composes images of birefringent tissue components based on changes in polarization of the light as it travels through the sample. Since collagen is the primary birefringent molecule in skin it is possible to get images and measurements of collagen density and alignment. Polarization-sensitive OCT has been used to study burns in human skin, including measuring collagen density in burn scars [150], collagen denaturation due to burns [151], and burn depth [152]. While the cost of a polarization-sensitive OCT system may preclude its use by many researchers, some OCT system manufacturers offer it as a module that can be used with existing OCT systems.

Additional measurements techniques. While OCT imaging can provide novel insights into cutaneous microvascular structure and function, it suffers certain limitations such as limited field-of-view and relatively slow capture time of larger field-of-view images. Additionally, while the papillary plexus of the cutaneous microvasculature was the target of study in this current research effort it would be beneficial to gain insights related to skin adaptation from multiple different depth levels in the tissue and other non-vascular characteristics of the tissue.

Laser Doppler Flowmetry (LDF) has been used for many years by researchers to measure cutaneous microvascular perfusion. Like OCT, this method emits infrared laser light into the skin and measures light that is reflected back to the device. Unlike OCT, LDF provides a single measurement of blood "flux" in a volume of tissue that is approximately beneath the probe. This flux value is calculated based on the Doppler shift of the incident light as it is scattered by moving particles in the blood, namely red blood cells. By using different wavelengths of light, multiple depths of tissue can be measured. The key benefits of LDF as they relate to the work in this thesis are that LDF is relatively inexpensive and it can provide very rapid time-series measurements at a single location of skin. Due to the small size of these probes, it may be possible to incorporate an

LDF probe near the OCT probe contact surface to measure LDF alongside OCTA. It would be beneficial to perform the RH Test developed in this thesis while simultaneously measuring with LDF and OCTA. This could ensure full capture of the RH response and could provide a comparison for the OCTA measurements of this test with a well-accepted measurement technique to more thoroughly validate the OCTA RH Test. A direct one-to-one correlation would not be expected between OCTA and LDF measurements in this test because it is not possible to know the exact volume of skin from which LDF is measuring perfusion [88], whereas this is possible with OCTA. Smith *et al.* recently demonstrated the use of LDF adjacent to OCTA for measuring cutaneous blood flow in the forearm for use in exercise physiology research [118]. While these researchers were comparing the repeatability of each measurement technique and thus only took measurements of heated skin, a similar setup may be used for measuring a functional response such as reactive hyperemia.

Laser Doppler Perfusion Imaging (LDPI) is a non-contact, full field-of-view imaging form of LDF. The method is essentially a scanning version of LDF and provides an image where each pixel corresponds to the perfusion "flux" in the region of tissue below that pixel location. Similar to LDF, the depth information of this measurement is variable and unknown, but it usually includes flow in the tissue down to a depth of 1.0-1.5 mm. LDPI images can be captured around 1-5 Hz. LDPI could be beneficial for the study of skin adaptation by leveraging its benefits of being non-contact and having a large field-of-view. One possible application of LDPI would be to use it in the RH Test in conjunction with OCTA, to provide a faster measurement of tissue perfusion. Since the method is non-contact it could be placed directly above the imaging site while the RH Test load application is occurring and could begin capturing images immediately after the load is removed. Due to LDPI's slightly deeper penetration depth, however, it is often largely influence by flow of the larger, thermoregulatory vessels deeper in the dermis. While this would make it difficult to compare these findings directly with those of the OCTA system, by using both systems concurrently, information would be gathered from two different depths in the tissue. However, if it is desired to maintain approximately the same depth of information, **Laser Speckle Contrast Imaging (LSCI)** may be a better fit to use alongside OCTA. Similar to LDPI, LSCI also provides an image where each pixel represents a "flux" measurement of perfusion in tissue below that pixel location. LSCI composes images by illuminating tissue with a coherent light source and capturing an image of the reflected light with a digital camera. When photons in the incident light

interact with moving particles, namely red blood cells, this creates a speckle pattern in the captured photographs. From this image, a perfusion flux measurement is obtained at each pixel location. The light generally penetrates to around 0.3 mm, and thus is thought to capture mainly information from the superficial, nutritive papillary plexus of vessels. LSCI can capture images up to 100 Hz. While LSCI systems are fairly expensive, low-cost versions have been proposed which could potentially be built in-house [158].

LSCI and LDPI are also important methods to keep in mind if markers for adaptation are eventually identified using OCTA since these methods can assess large regions of tissue at once and are currently easier to use than OCTA. A known limitation of OCTA is that only a small region of skin can be assessed at a time. While this is reasonable for research applications that require the level of detail OCTA provides, it may be possible to simplify the findings of OCTA-based studies and adapt these measurement techniques to LSCI or LDPI to make them more clinically applicable. For example, if OCTA highlights markers of adaptation such as increased vessel density during Maximum Dilation or faster RH time-to-peak, it may be possible to adapt the tests so that larger areas of skin could be assessed at once. If this point is reached, **infrared imaging** would also be worth considering due to its low cost and ease of use. However, infrared imaging only measures the surface temperature of skin, which is largely influenced by cutaneous blood flow but is also affected by many other factors.

As mentioned above, support exists that components of the extracellular matrix in skin may remodel as part of the skin adaptation process. While it may not be feasible to directly measure these changes noninvasively, insight into extracellular matrix adaptations could be gained by taking **biomechanical measurements** of skin in an adaptation study. Suction-based skin measurement devices, such as the Cutometer Skin Elasticity Meter (Cutometer SEM575, Courage and Khazaka, Cologne, Germany), have been used in skin research to take noninvasive, *in vivo* biomechanical measurements of skin. The devices work by contacting the skin with a probe that applies a negative pressure and measures the deflection of the skin in real-time. Indirect measurements of various mechanical properties can be attained from various parameters indicated by the deflection-versus-time curve produced by a suction test. By varying the diameter of the probe aperture, different layers of skin can be targeted. For example, a 4 mm diameter aperture has been recommended for targeting the dermal layer. It may be more applicable to use a method that measures skin deformation to an imposed positive pressure or pressure-and-shear, rather than

to suction, since these are the stresses that residual limb skin adapts to resist in a prosthetic socket. To the author's knowledge such a device is not widely available and would likely need to be developed in-house.

6.2.7 *Closing Remarks*

Overall, this dissertation introduced new noninvasive methods for investigating skin adaptation to mechanical stress. The Future Work section above outlined several ways in which these methods could be improved to further enhance the reliability and richness of data that these methods provide. We also described several future lines of research that could extend the work of this dissertation into more applicable subject populations and larger participant numbers. By executing some of these future works, we hope to gain new insights into the biology of skin adaptation in prosthetics. If successful, this could lead to new tools and rehabilitation techniques that can be used by clinicians to better monitor the skin health of their patients and to promote skin adaptation rather than breakdown.

REFERENCES

[1] Meulenbelt HE, Geertzen JH, Jonkman MF, Dijkstra PU. Determinants of Skin Problems of the Stump in Lower-Limb Amputees. Arch Phys Med Rehabil 2009;90:74–81. doi:10.1016/j.apmr.2008.07.015.

[2] Sanders JE, Daly CH, Burgess EM. Interface shear stresses during ambulation with a below-knee prosthetic limb. J Rehabil Res Dev 1992;29:1–8.

[3] Oomens CWJ, Bader DL, Loerakker S, Baaijens F. Pressure Induced Deep Tissue Injury Explained. Ann Biomed Eng 2014;43:297–305. doi:10.1007/s10439-014-1202-6.

[4] Peirce SM, Skalak TC, Rodeheaver GT. Ischemia-reperfusion injury in chronic pressure ulcer formation: A skin model in the rat. Wound Repair Regen 2000;8:68–76. doi:10.1046/j.1524-475X.2000.00068.x.

[5] Thorfinn J, Sjoberg F, Lidman D. Perfusion of buttock skin in healthy volunteers after long and short repetitive loading evaluated by laser Doppler perfusion imager. Scand J Plast Reconstr Surg Hand Surg 2007;41:297–302. doi:Doi 10.1080/02844310701633249.

[6] Mueller MJ, Maluf KS. Tissue adaptation to physical stress: a proposed "Physical Stress Theory" to guide physical therapist practice, education, and research. Phys Ther 2002;82:383–403.

[7] Singh S, Swerlick RA. Structure and function of the cutaneous vasculature. In: Freinkel RK, Woodley DT, editors. Biol. Ski., New York: The Parthenon Publishing Group; 2001, p. 177–89.

[8] Wang H, Shi L, Qin J, Yousefi S, Li Y, Wang RK. Multimodal optical imaging can reveal changes in microcirculation and tissue oxygenation during skin wound healing. Lasers Surg Med 2014;46:470–8. doi:10.1002/lsm.22254.

[9] Chen C-L, Wang RK. Optical coherence tomography based angiography. Biomed Opt Express 2017;8:1056–82. doi:10.1364/BOE.8.001056.

[10] Logsdon EA, Finley SD, Popel AS, MacGabhann F. A systems biology view of blood vessel growth and remodelling. J Cell Mol Med 2014;18:1491–508. doi:10.1111/jcmm.12164.

[11] Davis MJ, Hill MA, Kuo L. Reactive hyperemia. In: Tuma RF, Duran WN, Ley K, editors. Handb. Physiol. Microcirc., vol. 4. Second Edi, Amsterdam: Elsevier/Academic Press; 2008, p. 203–7.

[12] Mayrovitz HN, Macdonald J, Smith JR. Blood perfusion hyperaemia in response to graded loading of human heels assessed by laser-Doppler imaging. Clin Physiol 1999;19:351–9. doi:10.1046/j.1365-2281.1999.00184.x.

[13] Ziegler-Graham K, MacKenzie EJ, Ephraim PL, Travison TG, Brookmeyer R. Estimating the prevalence of limb loss in the United States: 2005 to 2050. Arch Phys Med Rehabil 2008;89:422–9. doi:10.1016/j.apmr.2007.11.005.

[14] Meulenbelt HEJ, Geertzen JHB, Jonkman MF, Dijkstra PU. Skin problems of the stump in lower limb amputees: 1. A clinical study. Acta Derm Venereol 2011;91:173–7. doi:10.2340/00015555-1040.

[15] Dudek NL, Marks MB, Marshall SC, Chardon JP. Dermatologic conditions associated with use of a lower-extremity prosthesis. Arch Phys Med Rehabil 2005;86:659–63. doi:10.1016/j.apmr.2004.09.003.

[16] Buikema KES, Meyerle JH. Amputation stump: Privileged harbor for infections, tumors,

and immune disorders. Clin Dermatol 2014;32:670–7. doi:10.1016/j.clindermatol.2014.04.015.
[17] Dudek NL, Marks MB, Marshall SC. Skin problems in an amputee clinic. Am J Phys Med Rehabil 2006;85:424–9. doi:10.1097/01.phm.0000214272.01147.5a.
[18] Sanders JE, Zachariah SG, Jacobsen AK, Fergason JR. Changes in interface pressures and shear stresses over time on trans-tibial amputee subjects ambulating with prosthetic limbs: comparison of diurnal and six-month differences. J Biomech 2005;38:1566–73. doi:10.1016/j.jbiomech.2004.08.008.
[19] Skinner H, PJ M. Amputations. Curr. Diagnosis Treat. Orthop. 5th editio, McGraw-Hill; 2014.
[20] Kapp SL, Fergason JR. Transtibial Amputation: Prosthetic Management. In: Smith DG, Michael JW, Bowker JH, editors. Atlas Amputations Limb Defic. 3rd ed., Rosemont, IL: American Academy of Orthopaedic Surgeons; 2004, p. 503–15.
[21] Jagoda A, Madden H, Hinson C. A friction blister prevention study in a population of marines. Mil Med 1981;146:42–4.
[22] Gambichler T, Moussa G, Sand M, Sand D, Altmeyer P, Hoffmann K. Applications of optical coherence tomography in dermatology. J Dermatol Sci 2005;40:85–94. doi:10.1016/j.jdermsci.2005.07.006.
[23] Sanders JE, Goldstein BS, Leotta DF. Skin response to mechanical stress : Adaptation rather than breakdown — A review of the literature. J Rehabil Res Dev 1995;32:214–26.
[24] Berke G. Standards of Care. J Prosthetics Orthot 2004;16:S1–12.
[25] Lusardi MM, Nielsen CC. Orthotics and Prosthetics in Rehabilitation. 2nd ed. St. Louis, MO: Saunders Elsevier; 2007.
[26] Sanders JE, Fatone S. Residual limb volume change: Systematic review of measurement and management. vol. 48. 2011. doi:10.1682/JRRD.2010.09.0189.
[27] Sanders JE, Cagle JC, Allyn KJ, Harrison DS, Ciol MA. How do walking, standing, and resting influence transtibial amputee residual limb fluid volume? J Rehabil Res Dev 2014;51:201–12.
[28] Sanders JE, Allyn KJ, Harrison DS, Myers TR, Ciol M a, Tsai EC. Preliminary investigation of residual-limb fluid volume changes within one day. J Rehabil Res Dev 2012;49:1467–78.
[29] Haake A, Scott GA, Holbrook KA. Structure and function of theskin: overview of the epidermis and dermis. In: Freinkel RK, Woodley DT, editors. Biol. Ski., New York: CRC Press; 2001, p. 19–46.
[30] Madison KC. Barrier function of the skin: “La Raison d’Être” of the epidermis. J Invest Dermatol 2003;121:231–41. doi:10.1046/j.1523-1747.2003.12359.x.
[31] Mathes SH, Ruffner H, Graf-Hausner U. The use of skin models in drug development. Adv Drug Deliv Rev 2014;69–70:81–102. doi:10.1016/j.addr.2013.12.006.
[32] Lodish H, Berk A, SL Z. Collagen: The Fibrous Proteins of the Matrix. Mol. Cell Biol. 4th editio, New York: Freeman, WH; 2000, p. Section 22.3.
[33] Ventre M, Mollica F, Netti P a. The effect of composition and microstructure on the viscoelastic properties of dermis. J Biomech 2009;42:430–5. doi:10.1016/j.jbiomech.2008.12.004.
[34] Ottenio M, Tran D, Ní Annaidh A, Gilchrist MD, Bruyère K. Strain rate and anisotropy effects on the tensile failure characteristics of human skin. J Mech Behav Biomed Mater 2015;41:241–50. doi:10.1016/j.jmbbm.2014.10.006.

[35] Braverman IM. The cutaneous microcirculation. J Investig Dermatology Symp Proc 2000;5:3–9. doi:10.1046/j.1087-0024.2000.00010.x.
[36] Walløe L. Arterio-venous anastomoses in the human skin and their role in temperature control. Temperature 2016;3:92–103. doi:10.1080/23328940.2015.1088502.
[37] Persons EL. STUDIES ON RED BLOOD CELL DIAMETER: III. The Relative Diameter of Immature (Reticulocytes) and Adult Red Blood Cells in Health and Anemia, Especially in Pernicious Anemia. J Clin Invest 1929;7:615–29.
[38] Skobe M, Detmar M. Structure, function, and molecular control of the skin lymphatic system. J Investig Dermatology Symp Proc 2000;5:14–9. doi:10.1046/j.1087-0024.2000.00001.x.
[39] Roustit M, Cracowski JL. Non-invasive Assessment of Skin Microvascular Function in Humans: An Insight Into Methods. Microcirculation 2012;19:47–64. doi:10.1111/j.1549-8719.2011.00129.x.
[40] Lewis T, Grant R. Observations upon Reactive Hyperaemia in Man. Heart 1926;12:73–120.
[41] Davis MJ, Hill MA, Kuo L. Local Regulation of Microvascular Perfusion. In: Tuma RF, Duran WN, Ley K, editors. Handb. Physiol. Microcirc. Second Edi, Amsterdam: Elsevier/Academic Press; 2008, p. 161–284.
[42] Bliss MR. Hyperaemia. J Tissue Viability 1998;8:4–13. doi:10.1016/S0965-206X(98)80028-4.
[43] Rees DD. Cardiovascular Actions of Nitric Oxide. In: Fang FC, editor. Nitric Oxide Infect., Hingham, MA, USA: Kluwer Academic Publishers; 1999, p. 151–74.
[44] Sprigle S, Linden M, Riordan B. Characterizing reactive hyperemia via tissue reflectance spectroscopy in response to an ischemic load across gender, age, skin pigmentation and diabetes. Med Eng Phys 2002;24:651–61. doi:10.1016/S1350-4533(02)00149-2.
[45] Brienza DM, Geyer MJ, Jan YK. A comparison of changes in rhythms of sacral skin blood flow in response to heating and indentation. Arch Phys Med Rehabil 2005;86:1245–51. doi:10.1016/j.apmr.2004.11.038.
[46] Wong BJ, Wilkins BW, Holowatz L a, Minson CT. Nitric oxide synthase inhibition does not alter the reactive hyperemic response in the cutaneous circulation. J Appl Physiol 2003;95:504–10. doi:10.1097/00005768-200305001-01958.
[47] Bader DL. The recovery characteristics of soft tissues following repeated loading. J Rehabil Res Dev 1990;27:141–50. doi:10.1682/JRRD.1990.04.0141.
[48] Koller A, Bagi Z. On the role of mechanosensitive mechanisms eliciting reactive hyperemia. Am J Physiol Heart Circ Physiol 2002;283:H2250–9. doi:10.1152/ajpheart.00545.2002.
[49] Holloway G, Daly C, Kennedy D, Chimoskey J. Effects of external pressure loading on human skin blood flow measured by 133Xe clearance. J Appl Physiol 1976;40:597–600. doi:10.1166/jnn.2012.6247.
[50] Holstien P, Nielsen PE, Baras JP. Blood flow cessation at external pressure in the skin of normal human limbs. Microvasc Res 1979;17:71–9. doi:10.1016/0026-2862(79)90008-6.
[51] McLellan K, Petrofsky JS, Zimmerman G, Lohman E, Prowse M, Schwab E, et al. The influence of environmental temperature on the response of the skin to local pressure: the impact of aging and diabetes. Diabetes Technol Ther 2009;11:791–8. doi:10.1089/dia.2009.0097.
[52] Sanders JE. Thermal response of skin to cyclic pressure and pressure with shear: a

technical note. J Rehabil Res Dev 2000;37:511–5.
[53] Meijer J, Germs P, Schneider H, Ribbe M. Susceptibility to decubitus ulcer formation. Phys Med Rehabil 1994;75:318–23.
[54] Herrman EC, Knapp CF, Donofrio JC, Salcido R. Skin perfusion responses to surface pressure-induced ischemia: implication for the developing pressure ulcer. J Rehabil Res Dev 1999;36:109–20.
[55] Department of Veterans Affairs, Department of Defense. VA/DoD Clinical Practice Guideline for Rehabilitation of Lower Limb Amputation. 2008.
[56] Meulenbelt H. Skin problems of the stump in lower limb amputees: 1. A clinical study. Acta Dermato- … 2011;91:173–7.
[57] Almassi F, Mousavi B. Skin disorders associated with bilateral lower extremity amputation. Pakistan J … 2009.
[58] Edsberg LE, Black JM, Goldberg M, McNichol L, Moore L, Sieggreen M. Revised National Pressure Ulcer Advisory Panel Pressure Injury Staging System. J Wound, Ostomy Cont Nurs 2016;43:585–97. doi:10.1097/WON.0000000000000281.
[59] Bouten C V, Oomens CW, Baaijens FP, Bader DL. The etiology of pressure ulcers: skin deep or muscle bound? Arch Phys Med Rehabil 2003;84:616–9. doi:10.1053/apmr.2003.50038.
[60] Gerhardt L-C, Schmidt J, Sanz-Herrera J a, Baaijens FPT, Ansari T, Peters GWM, et al. A novel method for visualising and quantifying through-plane skin layer deformations. J Mech Behav Biomed Mater 2012;14:199–207. doi:10.1016/j.jmbbm.2012.05.014.
[61] Stekelenburg A, Gawlitta D, Bader DL, Oomens CW. Deep tissue injury: how deep is our understanding? Arch Phys Med Rehabil 2008;89:1410–3. doi:10.1016/j.apmr.2008.01.012.
[62] Eltzschig HK, Collard CD. Vascular ischaemia and reperfusion injury. Br Med Bull 2004;70:71–86. doi:10.1093/bmb/ldh025.
[63] Goldstein B, Sanders J. Skin response to repetitive mechanical stress: a new experimental model in pig. Arch Phys Med Rehabil 1998;79:265–72.
[64] Bennett L, Kavner D, Lee B, Trainor F. Shear vs pressure as causative factors in skin blood flow occlusion. Arch Phys Med Rehabil 1979;60:309–14.
[65] Serra R, Ielapi N, Barbetta A, de Franciscis S. Skin tears and risk factors assessment: A systematic review on evidence-based medicine. Int Wound J 2017:1–5. doi:10.1111/iwj.12815.
[66] Brand PW. Mechanical Factors in Joint Stiffness and Tissue Growth. J Hand Ther 1995;8:91–6. doi:10.1016/S0894-1130(12)80305-X.
[67] Sasaki GH, Pang CY. Pathophysiology of skin flaps raised on expanded pig skin. Plast Reconstr Surg 1984;74:59–67. doi:10.1097/00006534-198407000-00009.
[68] Cherry GW, Austad E, Pasyk K, McClatchey K, Rohrich RJ. Increased Survival and Vascularity of Random-Pattern Skin Flaps Elevated in Controlled, Expanded Skin. Plast Reconstr Surg 1983;72:680–7.
[69] Pasyk KA, Argenta LC, Austad ED. Histopathology of human expanded tissue. Clin Plast Surg 1987;14:435–45.
[70] Jeong C, Chung HY, Lim HJ, Lee JW, Choi KY, Yang JD, et al. Applicability and Safety of in Vitro Skin Expansion Using a Skin Bioreactor : A Clinical Trial. Arch Plast Surg 2014;41:661–7.
[71] Zollner AM, Tepole AB, Kuhl E. On the biomechanics and mechanobiology of growing

skin. J Theor Biol 2012;297:166–75. doi:10.1016/j.biotechadv.2011.08.021.Secreted.
[72] Verhaegen PD, Schouten HJ, Tigchelaar-Gutter W, Van Marle J, Van Noorden CJ, Middelkoop E, et al. Adaptation of the dermal collagen structure of human skin and scar tissue in response to stretch: An experimental study. Wound Repair Regen 2012;20:658–66. doi:10.1111/j.1524-475X.2012.00827.x.
[73] Pietramaggiori G, Liu P, Scherer SS, Kaipainen A, Prsa MJ, Mayer H, et al. Tensile forces stimulate vascular remodeling and epidermal cell proliferation in living skin. Ann Surg 2007;246:896–902. doi:10.1097/SLA.0b013e3180caa47f.
[74] Chin MS, Ogawa R, Lancerotto L, Pietramaggiori G, Schomacker KT, Mathews JC, et al. In vivo acceleration of skin growth using a servo-controlled stretching device. Tissue Eng Part C Methods 2010;16:397–405. doi:10.1089/ten.tec.2009.0185.
[75] Sanders JE, Goldstein BS. Collagen fibril diameters increase and fibril densities decrease in skin subjected to repetitive compressive and shear stresses. J Biomech 2001;34:1581–7.
[76] Sanders JE, Mitchell SB, Wang YN, Wu K. An explant model for the investigation of skin adaptation to mechanical stress. IEEE Trans Biomed Eng 2002;49:1626–31. doi:10.1109/TBME.2002.805469.
[77] Green DJ, Carter HH, Fitzsimons MG, Cable NT, Thijssen DHJ, Naylor LH, et al. Obligatory role of hyperaemia and shear stress in microvascular adaptation to repeated heating in humans. J Physiol 2010;588:1571–7. doi:10.1113/jphysiol.2010.186965.
[78] Green DJ, Hopman MTE, Padilla J, Laughlin MH, Thijssen DHJ. Vascular Adaptation to Exercise in Humans: Role of Hemodynamic Stimuli. Physiol Rev 2017;97:495–528. doi:10.1152/physrev.00014.2016.
[79] Thorlabs. Swept Source OCT Systems: Vega series. User Manual. 2017:1–55.
[80] Gramatikov BI. Modern technologies for retinal scanning and imaging: An introduction for the biomedical engineer. Biomed Eng Online 2014;13:1–34. doi:10.1186/1475-925X-13-52.
[81] An L, Qin J, Wang RK. Ultrahigh sensitive optical microangiography for in vivo imaging of microcirculations within human skin tissue beds. Opt Express 2010;18:8220–8. doi:10.1364/OE.18.008220.
[82] Choi WJ, Reif R, Yousefi S, Wang RK. Improved microcirculation imaging of human skin *in vivo* using optical microangiography with a correlation mapping mask. J Biomed Opt 2014;19:036010. doi:10.1117/1.JBO.19.3.036010.
[83] Iftimia N, Ferguson RD, Mujat M, Patel AH, Zhang EZ, Fox W, et al. Combined reflectance confocal microscopy/optical coherence tomography imaging for skin burn assessment. Biomed Opt Express 2013;4:680–95. doi:10.1364/BOE.4.000680.
[84] Kaatz M, Sturm A, Elsner P, König K, Bückle R, Koehler MJ. Depth-resolved measurement of the dermal matrix composition by multiphoton laser tomography. Skin Res Technol 2010;16:131–6. doi:10.1111/j.1600-0846.2009.00423.x.
[85] Bazin R, Flament F, Colonna a, Le Harzic R, Bückle R, Piot B, et al. Clinical study on the effects of a cosmetic product on dermal extracellular matrix components using a high-resolution multiphoton tomograph. Skin Res Technol 2010;16:305–10. doi:10.1111/j.1600-0846.2010.00432.x.
[86] Cicchi R, Kapsokalyvas D, Pavone FS. Clinical nonlinear laser imaging of human skin: a review. Biomed Res Int 2014;2014:903589. doi:10.1155/2014/903589.
[87] Allen J, Howell K. Microvascular imaging: techniques and opportunities for clinical physiological measurements. Physiol Meas 2014;35:R91–141. doi:10.1088/0967-

3334/35/7/R91.
[88] Fredriksson I, Larsson M, Strömberg T. Measurement depth and volume in laser Doppler flowmetry. Microvasc Res 2009;78:4–13. doi:10.1016/j.mvr.2009.02.008.
[89] Thorlabs. OCS1300SS Swept Source OCT System - User Guide 2011.
[90] Wang H, Baran U, Li Y, Qin W, Wang W, Zeng H, et al. Does optical microangiography provide accurate imaging of capillary vessels?: validation using multiphoton microscopy. J Biomed Opt 2014;19:106011. doi:10.1117/1.JBO.19.10.106011.
[91] Choi WJ, Wang H, Wang RK. Optical coherence tomography microangiography for monitoring the response of vascular perfusion to external pressure on human skin tissue. J Biomed Opt 2014;19:56003. doi:10.1117/1.JBO.19.5.056003.
[92] Choi WJ, Qin W, Chen C-L, Wang J, Zhang Q, Yang X, et al. Characterizing relationship between optical microangiography signals and capillary flow using microfluidic channels. Biomed Opt Express 2016;7:2709. doi:10.1364/BOE.7.002709.
[93] Cobb MJ, Chen Y, Underwood R a, Usui ML, Olerud J, Li X. Noninvasive assessment of cutaneous wound healing using ultrahigh-resolution optical coherence tomography. J Biomed Opt 2006;11. doi:10.1117/1.2388152.
[94] Chu Z, Lin J, Gao C, Xin C, Zhang Q, Chen C-L, et al. Quantitative assessment of the retinal microvasculature using optical coherence tomography angiography. J Biomed Opt 2016;21:066008. doi:10.1117/1.JBO.21.6.066008.
[95] Goossens RH, Zegers R, Hoek van Dijke GA, Snijders CJ. Influence of shear on skin oxygen tension. Clin Physiol 1994;14:111–8. doi:10.1111/j.1475-097X.1994.tb00495.x.
[96] Sanders JE, Garbini JL, Leschen JM, Allen MS, Jorgensen JE. A bidirectional load applicator for the investigation of skin response to mechanical stress. IEEE Trans Biomed Eng 1997;44:290–6.
[97] Sanders J. Thermal response of skin to cyclic pressure and pressure with shear: a technical note. J Rehabil Res … 2000.
[98] Sanders JE, Daly CH, Burgess EM. Clinical measurement of normal and shear stresses on a trans-tibial stump: characteristics of wave-form shapes during walking. Prosthet Orthot Int 1993;17:38–48.
[99] Sanders JE, Jacobsen AK, Fergason JR. Effects of fluid insert volume changes on socket pressures and shear stresses: case studies from two trans-tibial amputee subjects. Prosthet Orthot Int 2006;30:257–69. doi:10.1080/03093640600810266.
[100] Gardner DW, Redd CB, Cagle JC, Hafner BJ, Sanders JE. Monitoring Prosthesis User Activity and Doffing Using an Activity Monitor and Proximity Sensors. J Prosthetics Orthot 2016;28:68–77. doi:10.1097/JPO.0000000000000093.
[101] Swanson E, Weathersby E, Cagle J, Sanders JE. Evaluation of Force Sensing Resistors for the Measurement of Interface Pressures in Lower Limb Prosthetics. J Biomech Eng 2019;141:101009-1-101009–13. doi:10.1115/1.4043561.
[102] Johnson JM, Kellogg DL. Mechanisms and Modulators of Temperature Regulation Local thermal control of the human cutaneous circulation. J Appl Physiol 2010;109:1229–38. doi:10.1152/japplphysiol.00407.2010.
[103] Schindelin J, Arganda-Carreras I, Frise E, Kaynig V, Longair M, Pietzsch T, et al. Fiji: an open-source platform for biological-image analysis. Nat Methods 2012;9:676–82. doi:10.1038/nmeth.2019.
[104] Preibisch S, Saalfeld S, Tomancak P. Globally optimal stitching of tiled 3D microscopic image acquisitions. Bioinformatics 2009;25:1463–5. doi:10.1093/bioinformatics/btp184.

[105] Rueden CT, Schindelin J, Hiner MC, DeZonia BE, Walter AE, Arena ET, et al. ImageJ2: ImageJ for the next generation of scientific image data. BMC Bioinformatics 2017;18:1–26. doi:10.1186/s12859-017-1934-z.
[106] Deegan AJ, Talebi-Liasi F, Song S, Li Y, Xu J, Men S, et al. Optical coherence tomography angiography of normal skin and inflammatory dermatologic conditions. Lasers Surg Med 2018:1–11. doi:10.1002/lsm.22788.
[107] Sapozhnikova V V, Kuranov R V, Cicenaite I, Esenaliev RO, Prough DS. Effect on blood glucose monitoring of skin pressure exerted by an optical coherence tomography probe. J Biomed Opt 2012;13:021112. doi:10.1117/1.2909671.
[108] Stack, Lawrence B, Storrow AB, Morris MA, Patton DR. Technique by body location. Views: Skin. In: Stack, Lawrence B, Storrow AB, Morris MA, Patton DR, editors. Handb. Med. Photogr., Philadelphia, PA: Hanley & Belfus, Inc; 2001, p. 374–80.
[109] Petrofsky JS. Resting blood flow in the skin: does it exist, and what is the influence of temperature, aging, and diabetes? J Diabetes Sci Technol 2012;6:674–85. doi:10.1177/193229681200600324.
[110] He SY, McCulloch CE, Boscardin WJ, Chren MM, Linos E, Arron ST. Self-reported pigmentary phenotypes and race are significant but incomplete predictors of Fitzpatrick skin phototype in an ethnically diverse population. J Am Acad Dermatol 2014;71:731–7. doi:10.1016/j.jaad.2014.05.023.
[111] Fitzpatrick TB. The Validity and Practicality of Sun reactive skin types I and IV. Arch Dermatol 1988;124:869–71.
[112] Stern RS, Momtaz K. Skin Typing for Assessment of Skin Cancer Risk and Acute Response to UV-B and Oral Methoxsalen Photochemotherapy. Arch Dermatol 1984;120:869. doi:10.1001/archderm.1984.01650430055010.
[113] Gogia R, Binstock M, Hirose R, Boscardin WJ, Chren MM, Arron ST. Fitzpatrick skin phototype is an independent predictor of squamous cell carcinoma risk after solid organ transplantation. J Am Acad Dermatol 2013;68:585–91. doi:10.1016/j.jaad.2012.09.030.
[114] Wesley NO, Maibach HI. Racial (Ethnic) Differences in Skin Properties: The Objective Data. Am J Clin Dermatol 2003;4:843–60. doi:10.2165/00128071-200304120-00004.
[115] Gunowa NO, Hutchinson M, Brooke J, Jackson D. Pressure injuries in people with darker skin tones: A literature review. J Clin Nurs 2018;27:3266–75. doi:10.1111/jocn.14062.
[116] Yvonne-Tee GB, Rasool AHG, Halim AS, Rahman ARA. Reproducibility of different laser Doppler fluximetry parameters of postocclusive reactive hyperemia in human forearm skin. J Pharmacol Toxicol Methods 2005;52:286–92. doi:10.1016/j.vascn.2004.11.003.
[117] Men SJ, Chen C-L, Wei W, Lai T-Y, Song SZ, Wang RK. Repeatability of vessel density measurement in human skin by OCT-based microangiography. Ski Res Technol 2017:1–6. doi:10.1111/srt.12379.
[118] Smith KJ, Argarini R, Carter HH, Quirk BC, Haynes A, Naylor LH, et al. Novel Noninvasive Assessment of Microvascular Structure and Function in Humans. Med Sci Sports Exerc 2019;51:1558–65. doi:10.1249/MSS.0000000000001898.
[119] Gambichler T, Valavanis K, Plura I, Georgas D, Kampilafkos P, Stücker M. In vivo determination of epidermal thickness using high-definition optical coherence tomography. Br J Dermatol 2014;170:737–9. doi:10.1111/bjd.12668.
[120] Josse G, George J, Black D. Automatic measurement of epidermal thickness from optical coherence tomography images using a new algorithm. Ski Res Technol 2011;17:314–9.

doi:10.1111/j.1600-0846.2011.00499.x.
[121] Lindgren M, Unosson M, Krantz A-M, Ek A-C. A risk assessment scale for the prediction of pressure sore development : reliability and validity. J Adv Nurs 2002;38:190–9.
[122] Sanders JE, Bell DM, Okumura RM, Dralle AJ. Effects of alignment changes on stance phase pressures and shear stresses on transtibial amputees: Measurements from 13 transducer sites. IEEE Trans Rehabil Eng 1998;6:21–31. doi:10.1109/86.662617.
[123] Swanson EC, McLean JB, Allyn KJ, Redd CB, Sanders JE. Instrumented socket inserts for sensing interaction at the limb-socket interface. Med Eng Phys 2018;51:111–8. doi:10.1016/j.medengphy.2017.11.006.
[124] Sanders JE, Garbini JL, McLean JB, Hinrichs P, Predmore TJ, Brzostowski JT, et al. A motor-driven adjustable prosthetic socket operated using a mobile phone app: A technical note. Med Eng Phys 2019;68:94–100. doi:10.1016/j.medengphy.2019.04.003.
[125] Men S, Wong JM, Welch EJ, Xu J, Song S, Deegan AJ, et al. OCT-based angiography of human dermal microvascular reactions to local stimuli: Implications for increasing capillary blood collection volumes. Lasers Surg Med 2018:1–9. doi:10.1002/lsm.22944.
[126] Mahmud MS, Cadotte DW, Vuong B, Sun C, Luk TWH, Mariampillai A, et al. Review of speckle and phase variance optical coherence tomography to visualize microvascular networks. J Biomed Opt 2013;18:50901. doi:10.1117/1.JBO.18.5.050901.
[127] Faul F, Erdfelder E, Lang A-G, Buchner A. G*Power 3: A flexible statistical power analysis program for the social, behavioral, and biomedical sciences. Behav Res Methods 2007;39:175–91. doi:10.1088/1755-1315/148/1/012022.
[128] Gailey RS, Roach KE, Applegate EB, Cho B, Cunniffe B, Licht S, et al. The Amputee Mobility Predictor : An Instrument to Assess Determinants of the Lower-Limb Amputee ' s Ability to Ambulate 2002;83. doi:10.1053/apmr.2002.32309.
[129] Jones H, Hopkins N, Bailey TG, Green DJ, Cable NT, Thijssen DHJ. Seven-Day Remote Ischemic Preconditioning Improves Local and Systemic Endothelial Function and Microcirculation in Healthy Humans. Am J Hypertens 2014;27:918–25. doi:10.1093/ajh/hpu004.
[130] Delp MD, McAllister RM, Laughlin MH. Exercise training alters endothelium-dependent vasoreactivity of rat abdominal aorta. J Appl Physiol 1993;75:1354–63.
[131] Chen HI, Li HT. Physical Conditioning Can Modulate Endothelium-Dependent Vasorelaxation in Rabbits. Arter Thromb 1993;13:852–6.
[132] Tinken TM, Thijssen DHJ, Black MA, Cable NT, Green DJ. Time course of change in vasodilator function and capacity in response to exercise training in humans. J Physiol 2008;586:5003–12. doi:10.1113/jphysiol.2008.158014.
[133] Kalus A, Chien A, Olerud J. Diabetes Mellitus and Other Endocrine Diseases. In: Goldsmith L, Katz S, Gilchrest B, Paller A, LeffelL D, Wolff K, editors. Fitzpatrick's Dermatology Gen. Med. 8th ed., New York, NY: McGraw-Hill; 2012, p. 1840–65.
[134] Carberry PA, Shepherd AM, Johnson JM. Resting and maximal forearm skin blood flows are reduced in hypertension. Hypertension 1992;20:349–55.
[135] Celermajer DS, Sorensen KE, Georgakopoulos D, Bull C, Thomas O, Robinson J, et al. Cigarette smoking is associated with dose-related and potentially reversible impairment of endothelium-dependent dilation in healthy young adults. Circulation 1993;88:2149–55. doi:10.1161/01.CIR.88.5.2149.
[136] Lancerotto L, Orgill DP. Mechanoregulation of Angiogenesis in Wound Healing. Adv Wound Care 2014;3:626–34. doi:10.1089/wound.2013.0491.

[137] Erba P, Miele LF, Adini A, Ackermann M, Lamarche JM, Orgill BD, et al. A Morphometrical Study of Mechanotransductively Induced Dermal Neovascularization. Plast Reconstr Surg 2011;128:288e-299e. doi:10.1016/j.jsbmb.2011.07.002.Identification.
[138] Carmeliet P. Mechanisms of angiogenesis and arteriogenesis. Nat Med 2000;6:389–95. doi:10.1038/74651.
[139] Prior BM, Yang HT, Terjung RL. What makes vessels grow with exercise training? J Appl Physiol 2004;97:1119–28. doi:10.1152/japplphysiol.00035.2004.
[140] Levy BI, Schiffrin EL, Mourad JJ, Agostini D, Vicaut E, Safar ME, et al. Impaired tissue perfusion a pathology common to hypertension, obesity, and diabetes mellitus. Circulation 2008;118:968–76. doi:10.1161/CIRCULATIONAHA.107.763730.
[141] Lehr HA. Microcirculatory dysfunction induced by cigarette smoking. Microcirculation 2000;7:367–84. doi:10.1111/j.1549-8719.2000.tb00135.x.
[142] Holowatz L a, Kenney WL. Peripheral mechanisms of thermoregulatory control of skin blood flow in aged humans. J Appl Physiol 2010;109:1538–44. doi:10.1152/japplphysiol.00338.2010.
[143] Murray HJ, Young MJ, Hollis S, Boulton AJ. The Association Between Callus Formation, High Pressures and Neuropathy in Diabetic Foot Ulceration. Diabet Med 1996;13:979–82. doi:10.1002.
[144] Phelps EA, Garcia AJ. Update on therapeutic vascularization strategies. Regen Med 2009;4:65–80. doi:10.2217/17460751.4.1.65.
[145] Liew YM, McLaughlin R a, Gong P, Wood FM, Sampson DD. In vivo assessment of human burn scars through automated quantification of vascularity using optical coherence tomography. J Biomed Opt 2013;18:061213. doi:10.1117/1.JBO.18.6.061213.
[146] Reif R, Qin J, An L, Zhi Z, Dziennis S, Wang R. Quantifying optical microangiography images obtained from a spectral domain optical coherence tomography system. Int J Biomed Imaging 2012;2012. doi:10.1155/2012/509783.
[147] Lang A, Carass A, Hauser M, Sotirchos ES, Calabresi PA, Ying HS, et al. Retinal layer segmentation of macular OCT images using boundary classification. Biomed Opt Express 2013;4:1133. doi:10.1364/BOE.4.001133.
[148] Zhang Q, Wang J, Wang RK. Highly efficient eigen decomposition based statistical optical microangiography. Quant Imaging Med Surg 2016;6:557–63. doi:10.21037/qims.2016.10.03.
[149] Wei DW, Deegan AJ, Wang RK. Automatic motion correction for *in vivo* human skin optical coherence tomography angiography through combined rigid and nonrigid registration. J Biomed Opt 2017;22:066013. doi:10.1117/1.JBO.22.6.066013.
[150] Jaspers MEH, Feroldi F, Vlig M, de Boer JF, van Zuijlen PPM. In vivo polarization-sensitive optical coherence tomography of human burn scars: birefringence quantification and correspondence with histologically determined collagen density. J Biomed Opt 2017;22:1. doi:10.1117/1.JBO.22.12.121712.
[151] Pierce MC, Sheridan RL, Hyle Park B, Cense B, De Boer JF. Collagen denaturation can be quantified in burned human skin using polarization-sensitive optical coherence tomography. Burns 2004;30:511–7. doi:10.1016/j.burns.2004.02.004.
[152] Srinivas SM, de Boer JF, Park H, Keikhanzadeh K, Huang HL, Zhang J, et al. Determination of burn depth by polarization-sensitive optical coherence tomography. J Biomed Opt 2004;9:207–12.
[153] Dsouza R, Won J, Monroy GL, Spillman DRJ, Boppart SA. Economical and compact

briefcase spectral-domain optical coherence tomography system for primary care and point-of-case applications. J Biomed Opt 2018;23:1–11. doi:10.1117/1.
[154] Bykov A V., Popov AP, Priezzhev A V., Myllyla R. Multilayer tissue phantoms with embedded capillary system for OCT and DOCT imaging. Opt Coherence Tomogr Coherence Tech V 2011;8091:80911R. doi:10.1117/12.889923.
[155] Chen C, Ahmed M, Häfner T, Klämpfl F, Stelzle F, Schmidt M. Fabrication of a turbid optofluidic phantom device with tunable μ a and μ' s to simulate cutaneous vascular perfusion. Sci Rep 2016;6:1–12. doi:10.1038/srep30567.
[156] Deegan AJ, Wang RK. Microvascular imaging of the skin. Phys Med Biol 2019;64. doi:10.1088/1361-6560/ab03f1.
[157] Cracowski J-L, Roustit M. Current Methods to Assess Human Cutaneous Blood Flow: An Updated Focus on Laser-Based-Techniques. Microcirculation 2016;23:337–44. doi:10.1111/micc.12257.
[158] Richards LM, Kazmi SMS, Davis JL, Olin KE, Dunn AK. Low-cost laser speckle contrast imaging of blood flow using a webcam. Biomed Opt Express 2013;4:2269–83. doi:10.1364/BOE.4.002269.

APPENDIX A. HEATER FOR MAXIMUM DILATION TEST: ELECTRONICS SCHEMATIC

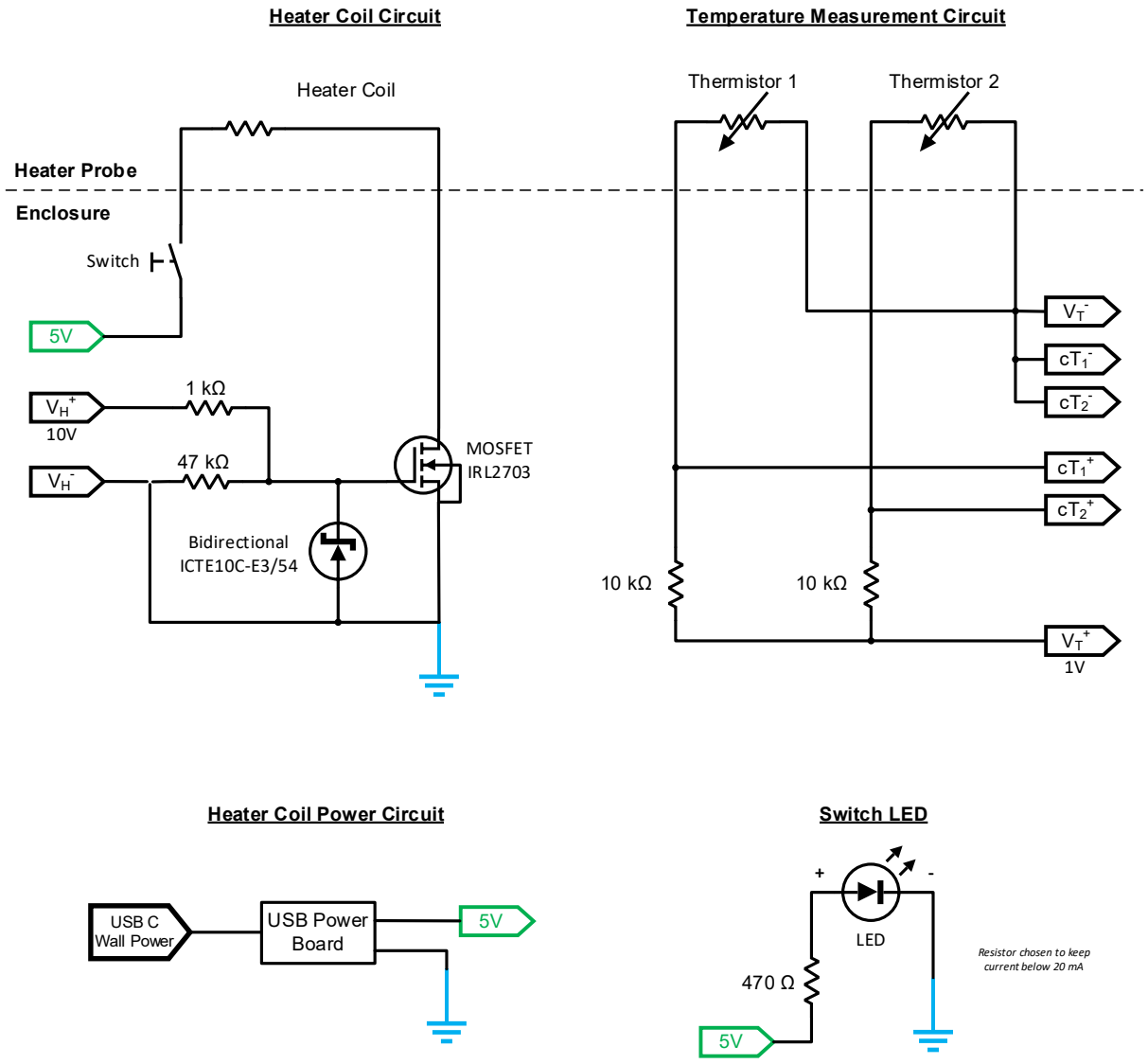

Figure A.1. Heater probe electronics schematic. V_H is the heater coil voltage supply. V_T is the excitation voltage for the thermistors, and cT_1/cT_2 are the voltage measurement outputs of the thermistors.

APPENDIX B. FSR SHIELD FOR USE WITH PORTABLE LAB DAQ: ELECTRONICS SCHEMATIC

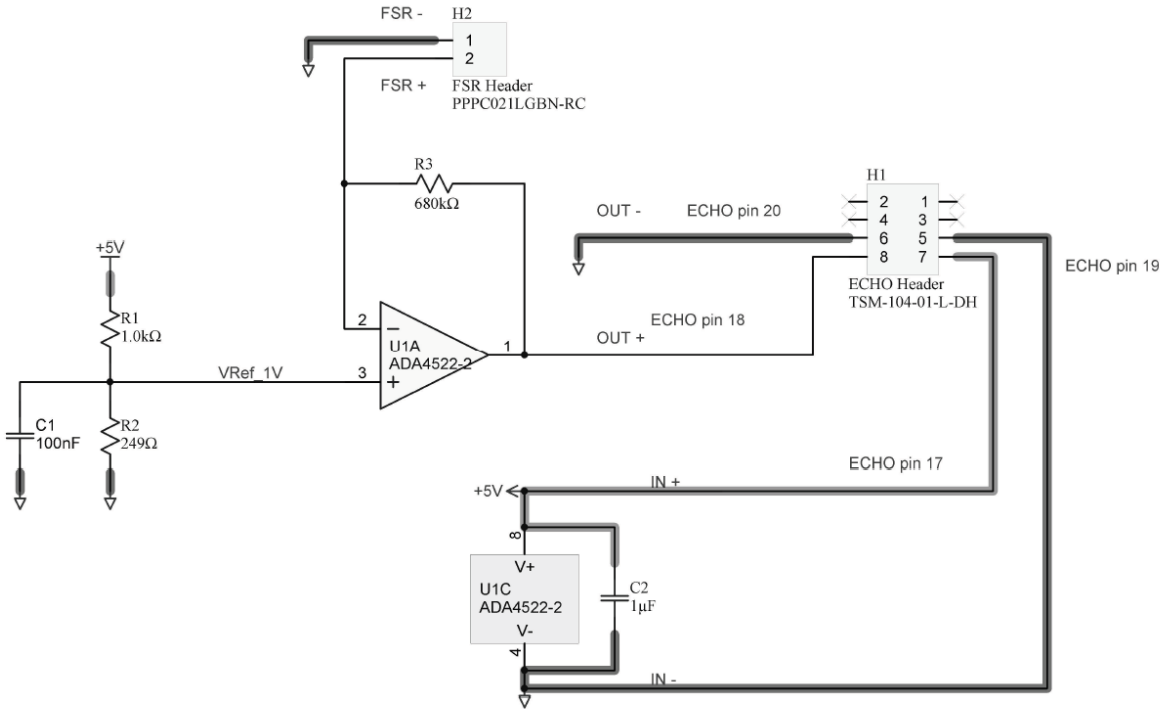

Figure B.1. FSR DAQ shield electronics schematic. The DAQ is referred to here as the "ECHO" device.

APPENDIX C. ABLE-BODIED ADAPTATION PROTOCOL

Initial In-Lab Assessment (supervised: lab)

- Prosthetist will verify a good fit and ensure load is being applied in the region to be measured with OCT
- Day 1: perform 3 cycles of sitting, standing, and walking for 60-90 s for each activity, rest 15 min & evaluate limb
- Send home with device and begin unsupervised program

Daily Loading Program (unsupervised: home/work)

- **Following all wear periods, evaluate limb tolerance.** If any of the following are found, contact the study team: areas of redness that do not go away within 10 min, pain, blistering, or abrasions. The study team will then modify the program to either decrease use or temporarily suspend use.
- Day 2: wear for 10 min then rest 15 min & evaluate limb, repeat once
- Next 2 days: wear for 15 min then rest 15 min & evaluate limb, repeat once
- Increase 15-20 min per day as limb is tolerating load; maintain 2 wear segments with a rest and limb evaluation of at least 15 min rest between segments.
- Once 2 h total (2 x 1 h) is well-tolerated, increase by 1 h per day, as tolerated
- When to stop: begin with a 2-week training period and evaluate from there. If skin tolerance assessment does not indicate more load tolerance, continue the program 1 more week. Repeat.
- Activity limitations: running

Sample Timeline

Supervised

- Day 1: 10 min walking

Unsupervised

- Day 2: 20 min wear (2 x 10 min)
- Day 3: 30 min wear (2 x 15 min)
- Day 4: 30 min wear (2 x 15 min)
- Day 5: 50 min wear (2 x 25 min)
- Day 6: 70 min wear (2 x 35 min)
- Day 7: 90 min wear (2 x 45 min)
- Day 8: 110 min wear (2 x 55 min)
- Day 9: 130 min wear (2 x 65 min) *(2x1 h threshold met)*
- Day 10: 180 min wear (2 x 90 min)
- Day 11: 240 min wear (2 x 120 min)
- Day 12: 300 min wear (2 x 150 min)
- Day 13: 360 min wear (2 x 180 min)
- Day 14: 420 min wear (2 x 210 min)

APPENDIX D. OCT PRESSURE MEASUREMENT BENCHTOP CHARACTERIZATION

D.1. DRIFT TEST

Method summary

- Warm up strain gage for at least 30 min
- Tap end adapter to release any built-up charge
- Hang 400g weight for 15 min
- Perform calibration before & after using hanging weights (0-600 g)
- Determine sensor drift, when loaded
- Repeat 3 times

Result

- Drift was 6.2 mV (SD ±0.9 mV) over 15 min load
  - Force equivalent: 0.03 N (SD ±0.005 N)
- P-P Noise was 15.8 mV (SD ±1.4 mV)
  - Force equivalent: 0.08 N (SD ±0.008 N)
- Calibration before & after were similar. At most, points differed by 0.01 V

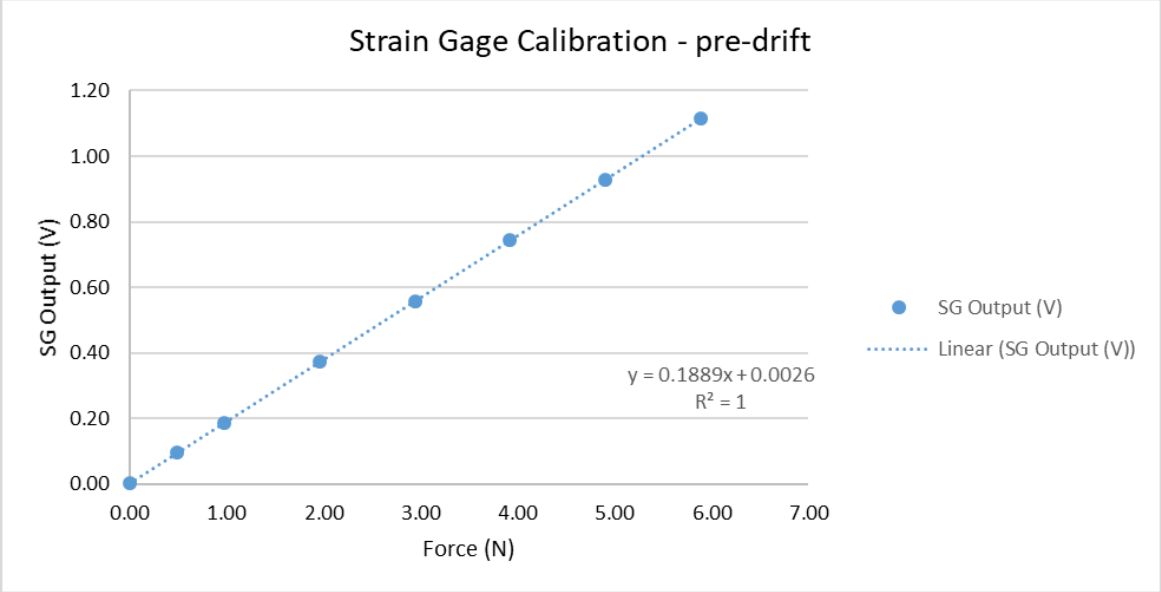

Figure D.1. Representative calibration curve (Trial 1 shown).

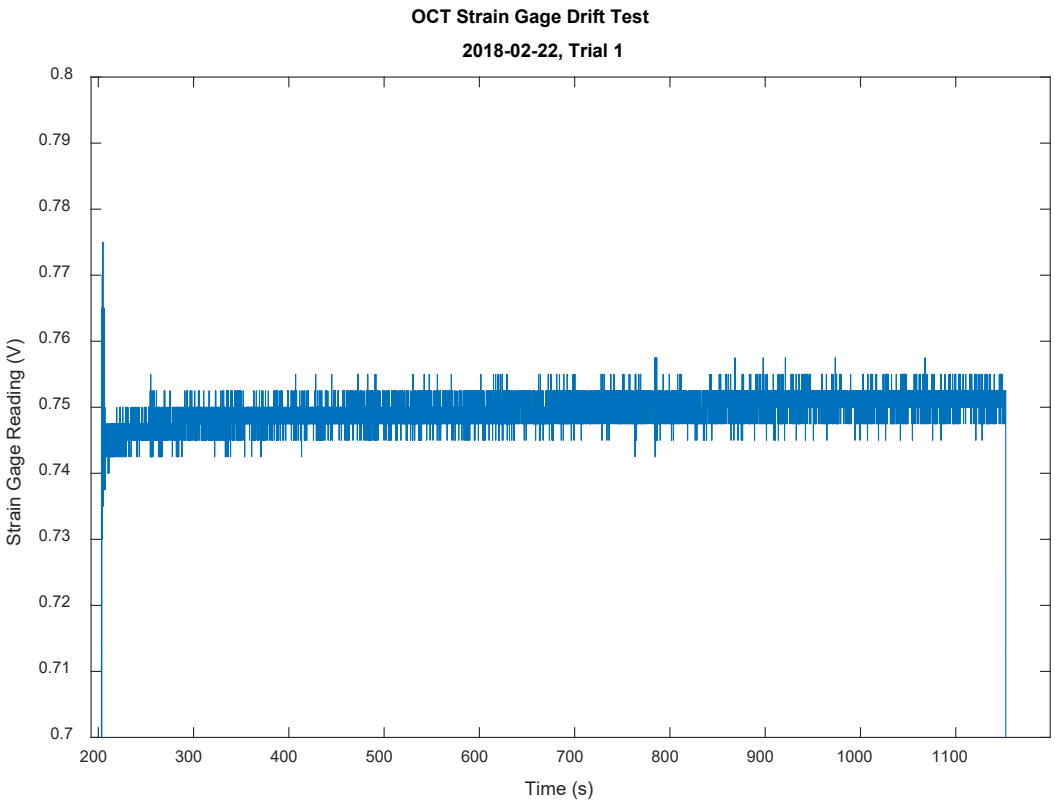

Figure D.2. Representative drift data. Strain gage beam loaded with 400 g for 15 min.

D.2. Resonance Test

Method summary

- Warm up strain gage for at least 30 min
- Tap end adapter to release any built-up charge
- After warming up, tap OCT probe piece at end of strain gaged beam to induce beam oscillations
- Calculate the mean period of the first 5 cycles
- Repeat 3 times

Result

- Resonant frequency was 98.1 Hz (SD ±1.2 Hz)

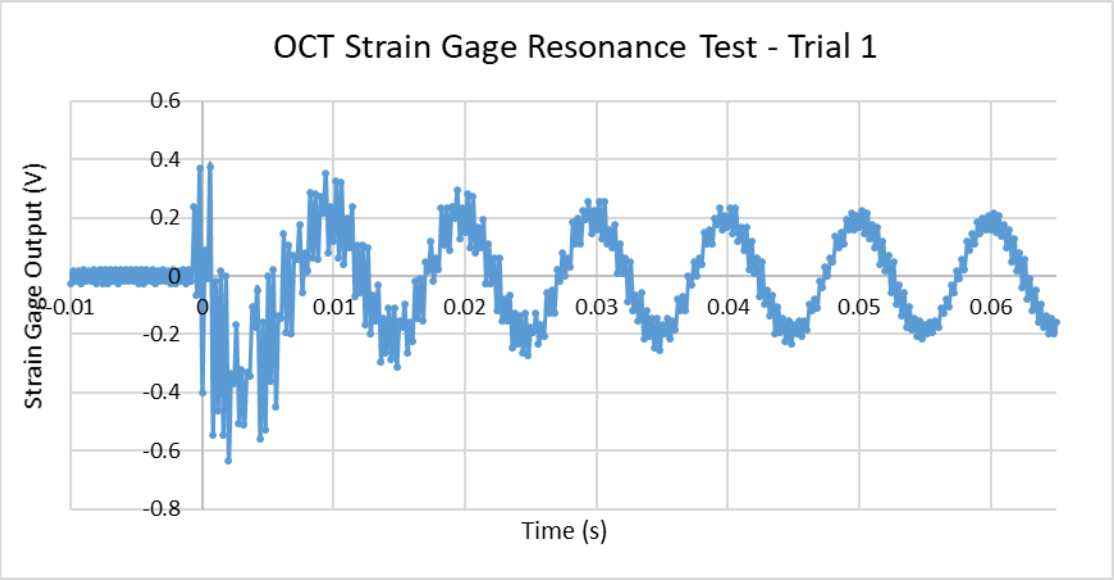

Figure D.3. Representative data from Resonance Test.

D.3. THERMAL TEST

Method summary

- Warm up strain gage for at least 30 min
- Tap end adapter to release any built-up charge
- Hang 400 g weight from OCT adapter at end of beam
- After 5 min load without heat, apply heat using warm lamp for 15 min, still loaded with 400 g
- Repeat 3 times

Result

- Temp increased from 23.9 C (SD ±0.2 C) to 27.6 C (SD ±1.2 C)
- Gage reading increased by 2.7 mV (SD ±0.4 mV)
    - Force equivalent: 0.014 N (SD ±0.002 N)
- This was within the drift seen during 15 min of 400 g load in the Drift Test.

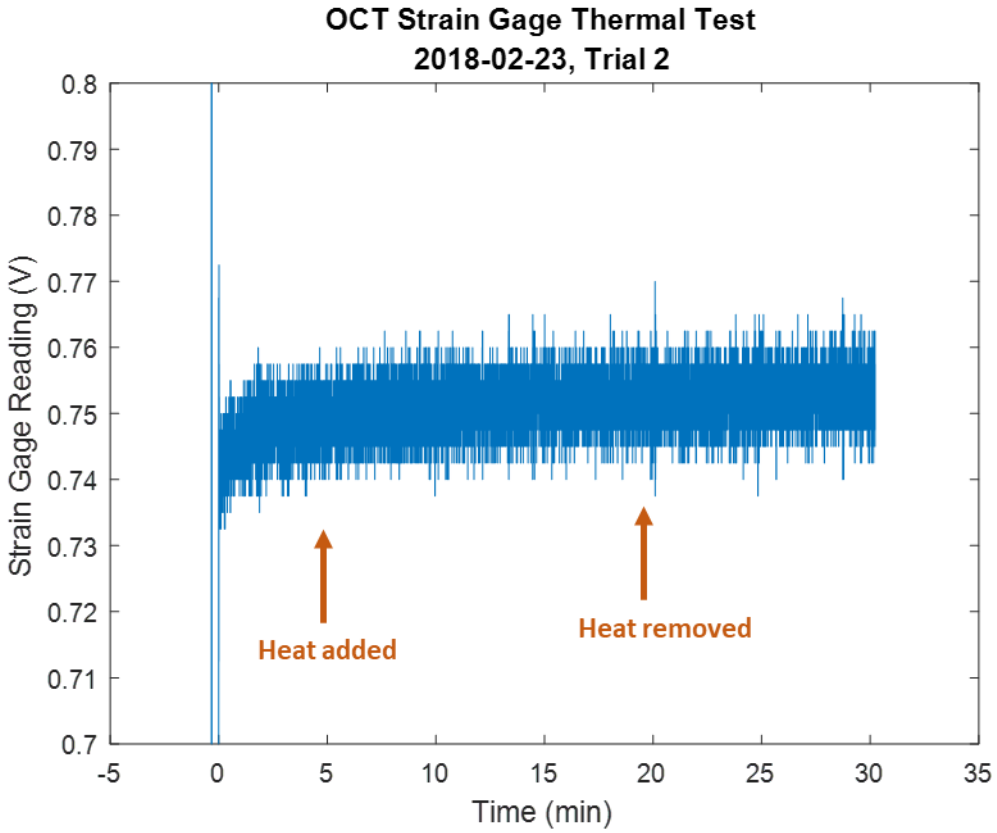

Figure D.4. Representative data from Thermal Test.

APPENDIX E. AIM 2 SUPPLEMENTARY FIGURES

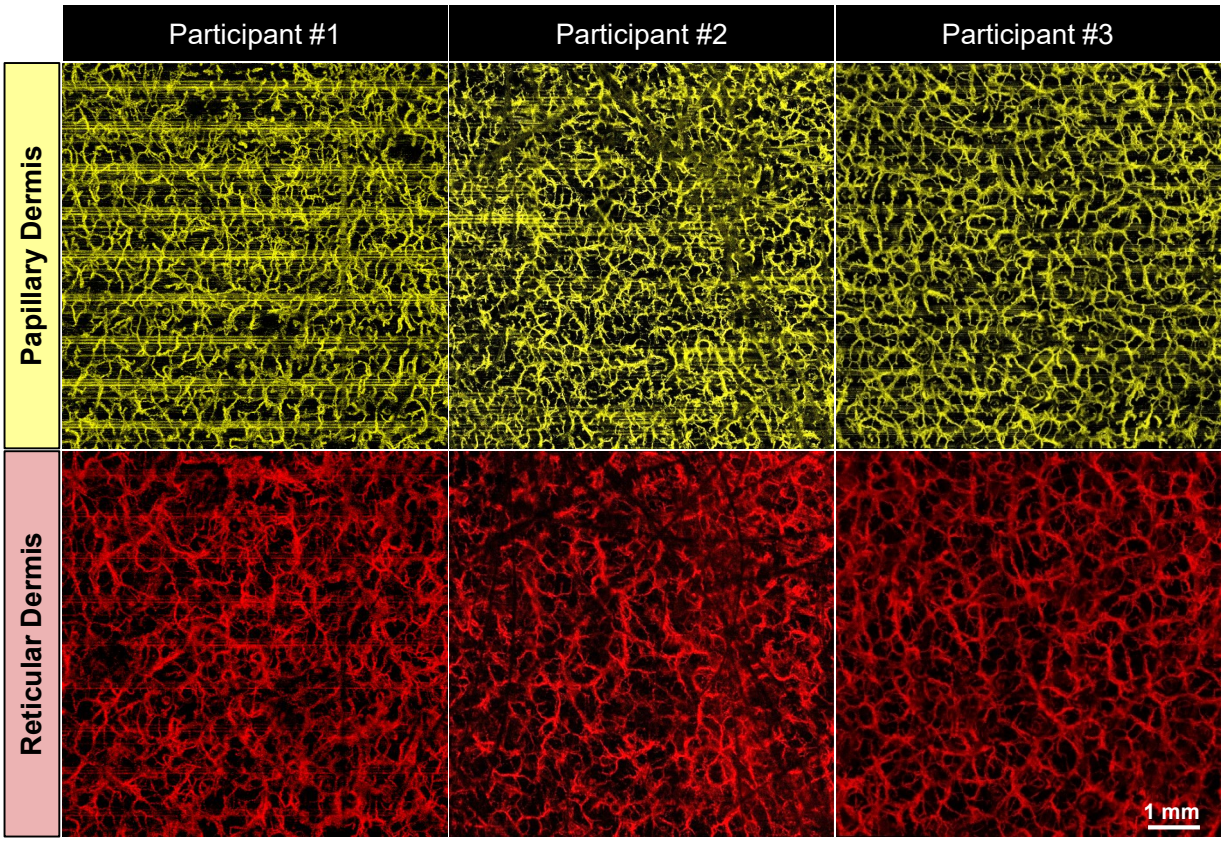

Figure E.1. Participants 1, 2, and 3 representative Maximum Dilation Test images at the test ROI.

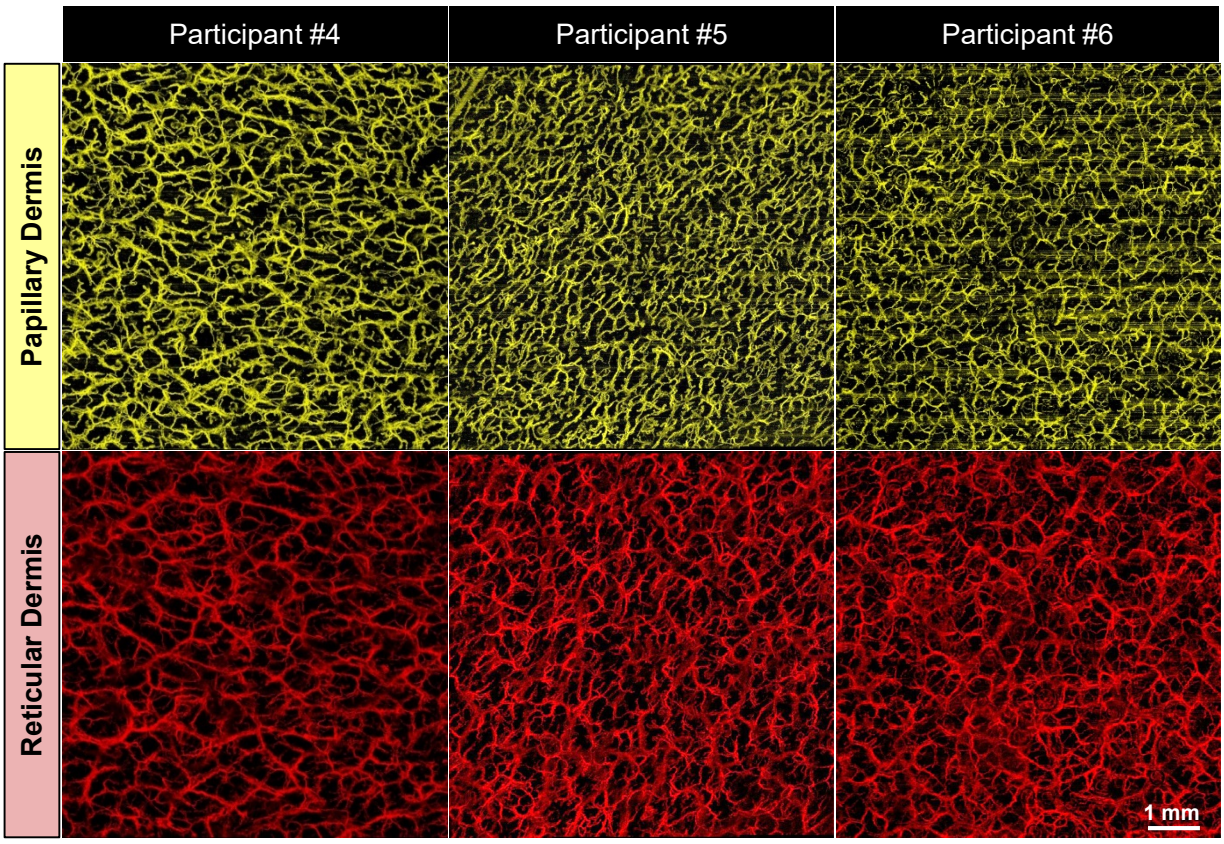

Figure E.2. Participants 4, 5, and 6 representative Maximum Dilation Test images at the test ROI.

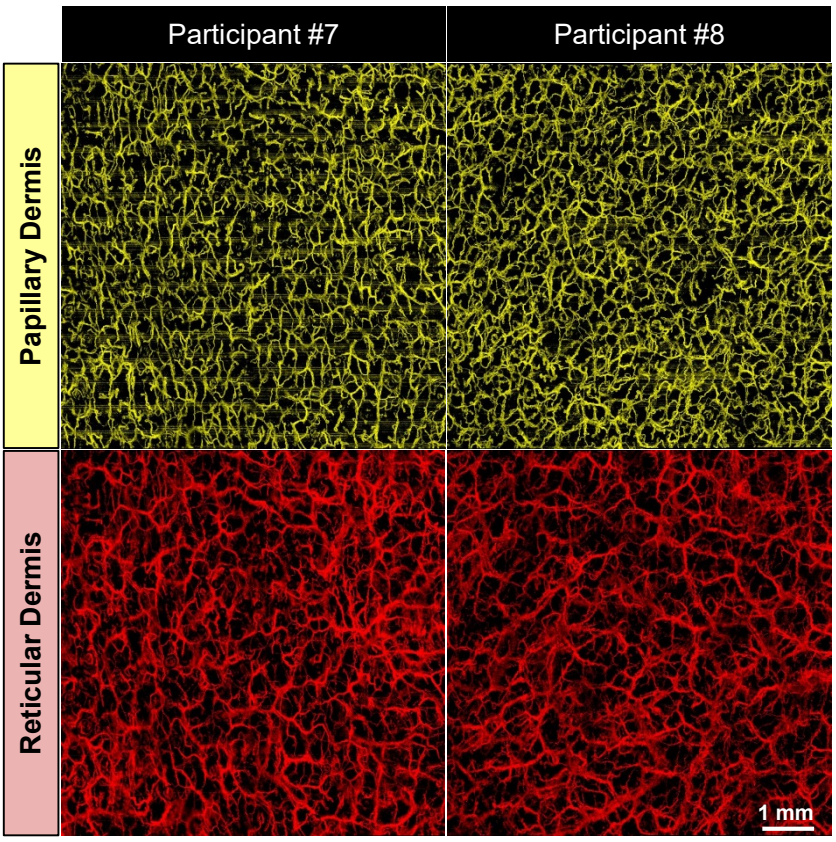

Figure E.3. Participants 7 and 8 representative Maximum Dilation Test images at the test ROI.

Week 1 vs Week 0 - Papillary Layer

Test Limb

Participant	VAD			Vessel Count			Mean Vessel Diameter		
	w1 larger	*w1 smaller*	*similar*	*w1 larger*	*w1 smaller*	*similar*	*w1 larger*	*w1 smaller*	*similar*
2	X					X			X
3		X			X			X	
4	X			X			X		
5	X					X			X
6			X			X			X
7		X			X			X	
8	X			X			X		

Control Limb

Participant	VAD			Vessel Count			Mean Vessel Diameter		
	w1 larger	*w1 smaller*	*similar*	*w1 larger*	*w1 smaller*	*similar*	*w1 larger*	*w1 smaller*	*similar*
2		X				X		X	
3			X	X				X	
4			X	X				X	
5	X					X	X		
6	X					X			X
7		X				X			X
8		X				X			X

Week 1 vs Week 0 - Reticular Layer

Test Limb

Participant	VAD			Vessel Count			Mean Vessel Diameter		
	w1 larger	*w1 smaller*	*similar*	*w1 larger*	*w1 smaller*	*similar*	*w1 larger*	*w1 smaller*	*similar*
2			X						
3	X								
4		X	X						
5	X								
6		X							
7			X						
8			X						

Control Limb

Participant	VAD			Vessel Count			Mean Vessel Diameter		
	w1 larger	*w1 smaller*	*similar*	*w1 larger*	*w1 smaller*	*similar*	*w1 larger*	*w1 smaller*	*similar*
2		X		X				X	
3			X			X			X
4			X			X			X
5			X			X			X
6			X			X			X
7			X			X			X
8		X			X				X

Figure E.4. Summary of trends seen in Maximum Dilation Test comparing week 1 to week 0. Comparisons of measurements from week 2 to week 0 for each ROI on each participant. A threshold of ±5% was used here as the threshold to determine if measurements were larger, smaller, or similar.